Making the Economic Case for Innovative HTLS Overhead Conductors

Final Project Report

Power Systems Engineering Research Center

Empowering Minds to Engineer
the Future Electric Energy System

Making the Economic Case for Innovative HTLS Overhead Conductors

Final Project Report

Project Team

Ravi Gorur, Project Leader
Gerald T. Heydt
Kory Hedman
Arizona State University

Robert Olsen
Washington State University

PSERC Publication 14-7

September 2014

For information about this project, contact

Ravi S. Gorur, Professor
School of Electrical, Computer and Energy Engineering
Arizona State University
PO Box 875706
Tempe, AZ 85287-5706
Telephone: 480 965 4894
Fax: 480 965 0745
Email: ravi.gorur@asu.edu

Power Systems Engineering Research Center

The Power Systems Engineering Research Center (PSERC) is a multi-university Center conducting research on challenges facing the electric power industry and educating the next generation of power engineers. More information about PSERC can be found at the Center's website: http://www.pserc.org.

For additional information, contact:

Power Systems Engineering Research Center
Arizona State University
527 Engineering Research Center
Tempe, Arizona 85287-5706
Phone: 480-965-1643
Fax: 480-965-0745

Notice Concerning Copyright Material

Acknowledgements

This is the final report for the Power Systems Engineering Research Center (PSERC) research project titled "Making the Economic Case for Innovative HTLS Overhead Conductors" (project T-47). We express our appreciation for the support provided by PSERC's industry members and by the National Science Foundation under the Industry / University Cooperative Research Center program.

The authors also thank the industry liaisons for this project: J. Fleeman (AEP), J. Hunt (SRP), R. Kondziolka (SRP), W. D. McLaughlin (Southern Co.), P. Myrda (EPRI), K. Cheung (Alstom Grid), J. Price (CAISO), A. Engelmann (Com Ed), S. Chen (PG&E), H. Chen (PJM), S. Ahmed (SCE), R. J. Beck (Southern Co.), A. Mander (Tri-State), and W. Timmons (WAPA) and D. Osborn (MISO). Several of the authors' colleagues and students at ASU provided useful comments especially Messrs. B. Pierre and X. Deng and Drs. G. Karady and L. Sankar, and Prof. R. G. Olsen, Washington State University.

One author, Askhat Tokombayev, wishes to express his thanks to his parents, Tulegen and Nailya, for their support and encouragement and to his brother Mirat who for inspiration to strive for continuous improvement. Another author K. Bannerjee wishes to thank his parents.

Executive Summary

Obtaining new right of ways for constructing transmission lines to handle increased demand for power is fraught with regulatory and legal issues and is extremely time consuming (> 10 years). The industry is interested in alternate methods for increasing power transfer using existing right of ways. High temperature, low sag overhead transmission conductors present an attractive option for high priority circuits as they replace existing conductors and carry higher current than conventional ASCR conductors. The impact of higher cost of construction and losses could be offset by power market enhancement. This project evaluates the effects of elevated temperature on conductor strength (Part I), systems (Part II), and economic impact (Part III) of HTLS conductors. Two types of composite cores, ACCR (aluminum conductor composite reinforced) and ACCC (aluminum conductor carbon composite) were evaluated.

The primary concern of the effect of high temperature is on the long-term mechanical strength of the core. The integrity of the core was determined from measurements that involved high temperature and mechanical stresses. It was shown that there are differences in the stability and tensile strength of the two types of composite cores over the temperature range of interest to users, however, the reduction in tension strength would not impact operation for the prescribed temperature range. A combination of diagnostic methods such as dynamic mechanical analysis (DMA), optical microscopy, tensile strength tests and temperature calculations were used to arrive at this conclusion.

The project evaluated the expenditures for transmission line reconductoring using HTLS and the consequent benefits obtained from the potential decrease in operating cost for thermally limited transmission systems. Studies performed considered the load growth and penetration of distributed renewable energy sources according to the renewable portfolio standards for power systems. An evaluation of payback period is suggested to assess the cost to benefit ratio of HTLS upgrades. An important point to make on the interpretation of results of this work, and conclusions, is that HTLS appears to be particularly suited for upgrade of existing transmission circuits.

The project also considered the probabilistic nature of transmission upgrades. The well-known Chebyshev inequality is discussed with an application to transmission upgrades. The Chebyshev inequality is proposed to calculate minimum payback period obtained from the upgrades of certain transmission lines. The cost to benefit evaluation of HTLS upgrades is performed using a 225 bus equivalent of the 2012 summer peak Arizona portion of the Western Electricity Coordinating Council (WECC). The results show that it is possible to justify the use of HTLS in this system in a coordinated expansion plan on the basis of operational cost reduction.

The project investigated the transmission expansion planning (TEP) model in order to make an economic case for the High Temperature Low Sag (HTLS) overhead conductors as one possible option to increase ampacity of the transmission system without having to obtain new right-of-ways (ROWs).

The proposed TEP model is formulated using mixed integer programming and the network model is approximated by the direct current optimal power flow (DCOPF) coordinated with the security constrained unit commitment (SCUC) problem and the piecewise linear loss approximation. The proposed TEP model is numerically tested on a modified IEEE 24-bus test system. It is shown on test cases that HTLS reconductoring is usually preferred when real power losses are ignored. On the other hand, parallel line addition option (with a traditional conductor) is favored when power losses are considered. As expected, system condition, such as overloading magnitude and frequency and the relative cost of each investment option, is shown to be key factors that may affect long-term optimal solution. The results thus demonstrate that when it is possible to add a parallel line in the same right of way, this seems to be a preferred option (with a traditional conductor like ACSR). On the other hand, when such options are not available, reconductoring a line with HTLS (replacing an older conductor with HTLS) seems to be a preferred way to increase the transfer capability within a network without having to acquire additional right-of-ways.

Project Publications:

Askhat Tokombayev, G. T. Heydt, "High temperature low sag (HTLS) technologies as upgrades for overhead transmission systems," Proc. North American Power Symposium, October 2013, Manhattan, KS, pp. 1 – 6.

Student Theses:

Koustubh Banerjee, "Making the case for high temperature low sag (HTLS) overhead transmission line conductors", MS Thesis, Arizona State University, 2014.

Askhat Tokombayev, "HTLS upgrades for power transmission expansion planning and operation," Masters Thesis, Arizona State University, May 2014.

Part I

Evaluating Critical Parameters of Composite Cores for High Temperature Low Sag Conductors for Power Delivery

Ravi Gorur, Faculty
Koustubh Bannerjee, Graduate Student

Arizona State University

For information about Part I, contact:

Ravi S. Gorur, Professor
School of Electrical, Computer and Energy Engineering
Arizona State University
PO Box 875706
Tempe, AZ 85287-5706
Telephone: 480 965 4894
Fax: 480 965 0745
Email: ravi.gorur@asu.edu

Power Systems Engineering Research Center

The Power Systems Engineering Research Center (PSERC) is a multi-university Center conducting research on challenges facing the electric power industry and educating the next generation of power engineers. More information about PSERC can be found at the Center's website: http://www.pserc.org.

For additional information, contact:

Power Systems Engineering Research Center
Arizona State University
527 Engineering Research Center
Tempe, AZ 85287-5706
Phone: 480-965-1643
Fax: 480-965-0745

Notice Concerning Copyright Material

Table of Contents

List of Figures

List of Tables

Nomenclature

A'	Projected area of the conductor per unit length
AAAC	All Aluminum Alloy Conductor
AAC	All Aluminum Conductor
ACCC	Aluminum Conductor Composite Core
ACCR	Aluminum Conductor Composite Reinforced
ACSR	Aluminum Conductor Steel Reinforced
ACSS	Aluminum Conductor Steel Supported
CFRP	Carbon Fiber Reinforced Plastic
CIGRE	International Council on Large Electric Systems (English)
CTC	Composites Technologies Corporation
CTE	Coefficient of thermal expansion
D	Conductor diameter
DMA	Dynamic Mechanical Analysis
DSC	Differential Scanning Calorimetry
E	Complex modulus of visco-elastic material
E'	Storage modulus of visco-elastic material
E''	Loss modulus of visco-elastic material
E'_T	Storage modulus of carbon fiber/epoxy composite at temperature T
E'_{To}	Storage modulus of carbon fiber/epoxy composite at temperature T_o
EHV	Extra High Voltage
G	Shear modulus of visco-elastic material
G	Shear modulus of CFRP at temperature T and time to relaxation t_r
G_g	Shear modulus of CFRP in the glassy region
GBIP	General Purpose Instrument Bus
GLS	Global Load Sharing
GTACSR	Gap Type Aluminum Conductor Steel Reinforced
H_c	Altitude of the sun
HTLS	High Temperature Low Sag

I	Conductor current
IEEE	Institute of Electrical and Electronic Engineers
k	Point of measurement
K_{angle}	Wind direction factor
K_f	Thermal conductivity of air at temperature T_f
L_o	Sample length at reference temperature
ΔL	Total change in length of sample
ΔL_o	Change in length of sample at reference temperature
ΔL_k	Change in length of sample at temperature T_k
L_{final}	Final length of sample
$L_{initial}$	Initial length of sample
LLS	Local Load Sharing
LVDT	Linear Variable Displacement Transducer
m	Weibull shape parameter
mcp	Conductor heat capacity
MMC	Metal Matrix Composite
N	Number of experiment test
NEETRAC	National Electric Energy Testing Research and Application Center
PMC	Polymer Matrix Composite
q_c	Convection heat loss
q_r	Radiation heat loss
q_s	Solar heat gain
Q_{se}	Total heat flux
R	Conductor resistance
ROW	Right of Ways
RT	Room Temperature
S.D	Standard Deviation
SM	Storage modulus
T_a	Ambient temperature

T_c	Conductor temperature
T_f	Thin film temperature around conductor
T_{final}	Final temperature of sample
T_g	Glass transition temperature
$T_{G\inf}$	Glass transition temperature of fully cured epoxy network
T_H	Conductor temperature at resistance $R(T_H)$
$T_{initial}$	Initial temperature of sample
T_k	Temperature at every measured point k
T_L	Conductor temperature at resistance $R(T_L)$
TMA	Thermal Mechanical Analysis
T_o	Reference temperature
t_r	Time to relaxation
t_s	Time to failure
v_w	Wind speed
Z_c	Azimuth angle of the sun
Z_l	Azimuth angle of transmission line
σ_s	Tensile strength of carbon conductor core at temperature T
σ_{To}	Tensile strength of carbon conductor core at temperature T_o
ν	Poisson's ratio
σ_g	Tensile strength of CFRP in glassy region
σ	Tensile strength of CFRP at temperature T and time to failure t_s
α	Coefficient of thermal expansion
α_{avg}	Average coefficient of thermal expansion
α_{avgi}	Average coefficient of thermal expansion of sample for particular test
α_{mean_avg}	The mean of average coefficients of thermal expansion of sample
ρ_f	Air density at temperature T_f
μ_f	Dynamic viscosity of air at temperature T_f
ϕ	Angle between the wind direction and conductor axis
β	Angle between the wind direction and perpendicular to the conductor axis

α_{ab}	Solar absorptivity
θ	Angle of incidence
ε	Emissivity

1. Introduction

1.1 Background

The electric power demand is increasing with each year. It is estimated that the growth in electric power demand will be approximately 28% by 2040 in the United States [1]. The current growth rate of electricity demand is 0.7% with an average growth of 0.9% per year [1]. The study findings given in reference [2] indicate that the utility industry will need new investments in generation infrastructure, with investment costs of billions of dollars, to supply the increasing demand. In order to meet the increasing power demand, significant investments in transmission and distribution infrastructure are necessary to keep pace with the increase in generation [2], [3]. The growth rate of electric power consumption in the mountain states of the U.S is highest at 1.52% per year [4]. Historically investment in transmission and distribution has been neglected for decades [3], [5]. This has led to congestion in the grid. The congestion in the grid can be attributed to other factors such as deregulation of the power industry, changing thermal limitations of transmission lines in existing right of ways (ROWs) and aging of power equipment [5]-[7]. Renewable portfolio standards, on the other hand, impose obligations on the utility industry to increase the penetration of renewable resource generation in the grid [8]. Renewable generation sites such as wind and solar tend to be far away from the load centers [3]. In order to transfer the generated power to customers, increase of present transmission capacity is required. However, as mentioned earlier, deterioration in transmission investment has occurred. To put things in perspective, transmission and distribution investment in the U.S. has decreased by 44% in 1980-99 [3]. The nation's grid infrastructure is also degrading and aging. This has led to brownouts and blackouts due to sag violations of traditional transmission conductors trying to supply increased power demand, especially during the summer months [5]. In brownouts, the system voltage drops for an amount of time in order to manage load during emergency. There are three solutions to overcome the problem of achieving increased power flow in the grid to meet the electricity demand [9]. These are:

1. Line compaction – As the name suggests, the distance between the phases of the transmission line are reduced. This has the effect of reducing the line reactance. Reduction in line reactance increases the power transfer capability and thus reduces congestion in the line [9].
2. Six phase transmission system – The six phase transmission system has the advantage of requiring lesser voltage level for the same amount of power transmission as compared to three phase power system [9]. Studies indicate that the ROWs requirement is also less due to smaller tower structures [9].
3. High Temperature Low Sag (HTLS) conductors – As the name suggests, these conductors have superior sag-temperature characteristics. HTLS conductors are generally used in thermally limited lines because replacing lines, which are limited by system stability limits, with HTLS conductors will not alleviate the problem [9], [10]. HTLS conductors are expected to operate at temperatures well above 100°C continuously with emergency temperatures of 200°C - 240°C [11], [12]. The power transfer capability can thus be increased in circuits containing HTLS conductors. The major advantage of increasing the power flow with the help of this method is

that construction of new supporting structures and development of new ROWs are not required [10].

Traditionally, the power system industry has responded to increase in power demand by increasing the system voltage levels [13], [14]. American Electric Power developed 765 kV Extra High Voltage (EHV) in 1960s to meet the increasing power demand [14]. Building new transmission lines entails acquiring and developing new ROWs by utility companies. This is a complex process, which involves easement contract and maintenance of ROWs [15], [16]. The use of HTLS conductors to increase the power transfer capability to meet the rising power demand ensures reduction in constructing new tower structures and development of new ROWs, since existing ROWs and supporting tower structures can be utilized for replacement of the traditional conductors by HTLS conductors [10], [17]. Thus, for thermally limited lines, one of the most attractive investments in transmission to increase the power flow is the use of HTLS conductors. Comparatively, little research has been conducted to study the capability of HTLS conductors to handle large current flow at elevated temperatures. This project focuses on the mechanical characterization of HTLS conductors with temperature. HTLS conductors consisting of metal matrix core (MMC) and carbon composite core or polymer matrix core (PMC) has been considered in this study. The following sections present the project objectives and previous relevant research on HTLS conductors and its constituent materials.

1.2 Project objectives

The main objective of the project is to quantify the loss of mechanical strength of HTLS conductors with temperature. High temperatures cause annealing of aluminum conductor wires and can cause degradation of the conductor core [17], [18]. Apart from the loss in strength of conductor, sagging of the line occurs at elevated temperatures. Sag dictates the power transfer capability of thermally limited transmission lines. The sag is dependent on the temperature of the line, which in turn depends on the amount of current flowing through the line [5]. Traditional conductors like Aluminum Conductor Steel Reinforced (ACSR) have a maximum operating temperature of 100°C [19]. HTLS conductors are designed to operate at temperatures up to 250°C without significant loss of strength. The HTLS conductors studied in this project are Aluminum Conductor Composite Reinforced (ACCR) and Aluminum Conductor Composite Core (ACCC). ACCR is manufactured by 3M Company and ACCC is manufactured by Composite Technologies Corporation (CTC) Global. There are other manufacturers of ACCC such as Midal Cables Ltd and Alcan Cable. ACCR have metal matrix core (MMC) and ACCC have carbon composite core/ polymer matrix core (PMC). In this project, carbon composite core and polymer matrix core (PMC) has been used interchangeably. The coefficient of thermal expansion of the HTLS conductor MMC and PMC cores are significantly less than that of ACSR steel cores [11], [12], [20]. HTLS conductors sag less than equivalent ACSR conductors due to low coefficient of thermal expansion.

Another important aspect that has been studied closely in this project is the temperature rise of HTLS conductors during fault currents. This study was performed using the guidelines outlined in IEEE 738-2006 standard [21]. C++ programs were written to simulate the temperature rise in metal matrix core and carbon composite core based HTLS

conductors during fault currents. The effects on the HTLS conductors were deduced from the results of the simulation. The objectives of the project can be summarized below:

1. Obtain and quantify mechanical strength variation of HTLS conductors with temperature.
2. Investigate the coefficient of thermal expansion of the HTLS conductor core.
3. Study the temperature rise in the HTLS conductor due to fault currents and obtain current temperature relationships.

1.3 HTLS conductors and relevant research reviews

The power transfer capability can be increased with the help of HTLS conductors in thermally limited lines. Traditionally heterogeneous conductors like ACSR were introduced to improve sag-temperature characteristics and thermal ratings over homogenous conductors like All Aluminum Conductor (AAC) and All Aluminum Alloy Conductor (AAAC) [22]. However, over the years, electric power demand has increased but the investment in new transmission lines have not kept pace. Thus, as mentioned before, congestion in the grid has increased. Presently, the trends have shifted to large investment in new transmission infrastructure. This includes introduction of HTLS conductors for existing transmission lines that are thermally limited [10]. HTLS conductors make it possible to have a power flow increase of 2-3 times over traditional ACSR conductors in existing transmission corridors. For example, DRAKE ACSR have a current carrying capacity of 1000 A at 100°C, whereas equivalent carbon composite based HTLS conductor have a current carrying capacity of over 1600 A at 180°C [21]. This translates into a power flow increase by at least a factor of 2.5 in lines replaced by carbon composite based HTLS conductors.

ACSR conductor, which is widely used for transmission lines, is a concentrically stranded conductor. It is consists of a relatively non-conducting steel core. The steel core is galvanized to prevent corrosion. The aluminum wires which covers the steel core is a hard drawn 1350 aluminum wire with H19 temper [22]. The maximum operating temperature of ACSR conductors is 100°C [19]. Above this temperature, annealing of the aluminum wires takes place which results in rapid degradation of tensile strength of the conductor. Morgan [18] and Harvey [23] have investigated the loss of tensile strength of overhead transmission conductors due to annealing. Both provide empirical formulas to calculate the loss of strength for ACSR conductors with temperature and time.

Due to increase in power demand, aging of grid infrastructure and thermal limitations, it is difficult to ramp up power flow through existing ACSR lines. This has led to the introduction of conductors that have better sag-temperature characteristics and higher ampacity [13]. These conductors are known as HTLS conductors. Recent introduction of HTLS conductors include ACCC and ACCR. Other types of HTLS conductors are –

1. ACSS – Aluminum Conductor Steel Supported
2. GTACSR – Gap type Aluminum Conductor Steel Reinforced
3. ZTACIR – Zirconium Type Aluminum Conductor Invar Steel Reinforced

This project focuses on HTLS conductors with metal matrix core and carbon composite cores. In particular, samples from ACCR and ACCC have been used for the study.

The carbon composite core or PMC based HTLS conductor consists of glass-carbon fiber/ epoxy matrix core. The core is organic in nature due to the epoxy matrix. The glass fiber/epoxy shell encases the carbon fiber/epoxy section. The function of the glass fiber/ epoxy shell is to isolate electrically the conducting carbon fiber/epoxy section of the core [6]. Thus, the glass fiber/epoxy acts like a dielectric medium and prevents galvanic corrosion between carbon fibers and aluminum wires. The core is not stranded; it is a single piece of rod running through the entire length of the conductor. The conductor wires, which surrounds the core, are fully annealed 1350 – O tempered aluminum [5], [11]. The conductor core is produced by pultrusion process [24]. The aluminum wires are arranged in trapezoidal configuration. The advantages of HTLS conductor with carbon composite cores are manifold. It offers large cross section area for the aluminum conductors, which consequently increases the ampacity compared to equivalent ACSR, a high strength to weight ratio, superior sag-temperature characteristics, extremely low coefficient of thermal expansion of the core and high tensile strength [5]. Fig 1.1 shows the picture of ACCC, which is a carbon composite core based HTLS conductor.

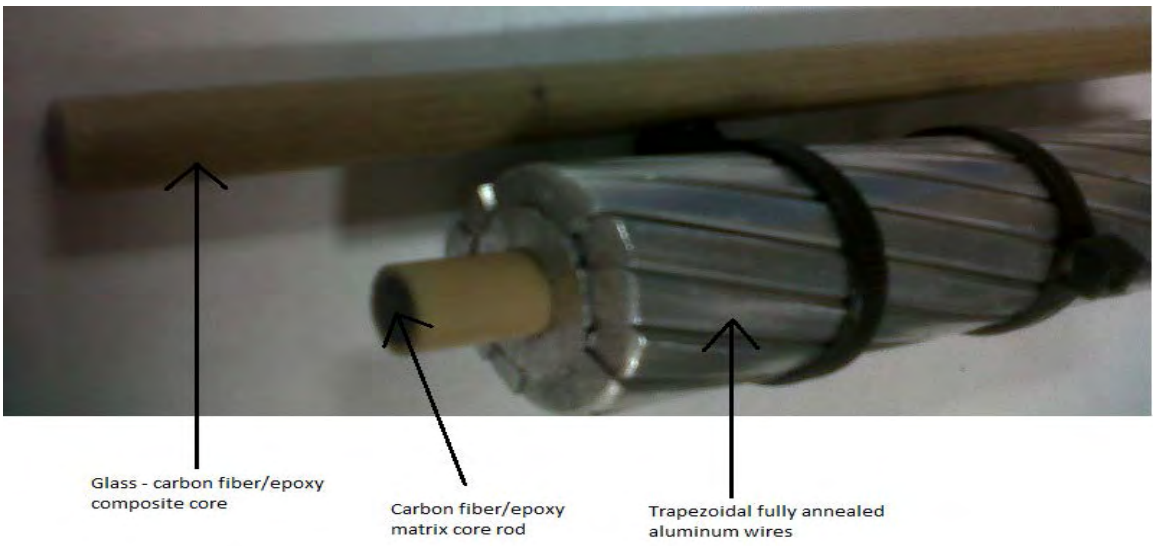

Figure 1.1: Photograph of Aluminum Conductor Composite Core (ACCC)

The metal matrix core (MMC) based HTLS conductor is designed to have significant property improvements over traditional ACSR conductors. These conductors have alumina fiber/aluminum matrix strands in the core. The aluminum matrix contains high purity aluminum. The alumina fibers are micrometer sized and are embedded in the aluminum matrix. The core consists of several alumina fiber/aluminum matrix strands and it is surrounded by high temperature aluminum –zirconium alloy wires. These wires can resist annealing up to temperatures of 210°C [25]. The aluminum zirconium wires provide added strength to the conductor and can be arranged in round wire or trapezoidal configurations [25]. The key features of this conductor are high tensile strength, high conductivity and high strength to weight ratio [25]. Compared to ACSR, it can retain its tensile strength at

temperatures above 100°C and sags less at high temperature due to low coefficient of thermal expansion [10], [12], [18], [20], [23], [25]. Fig 1.2 shows the picture of ACCR, which is a MMC based HTLS conductor.

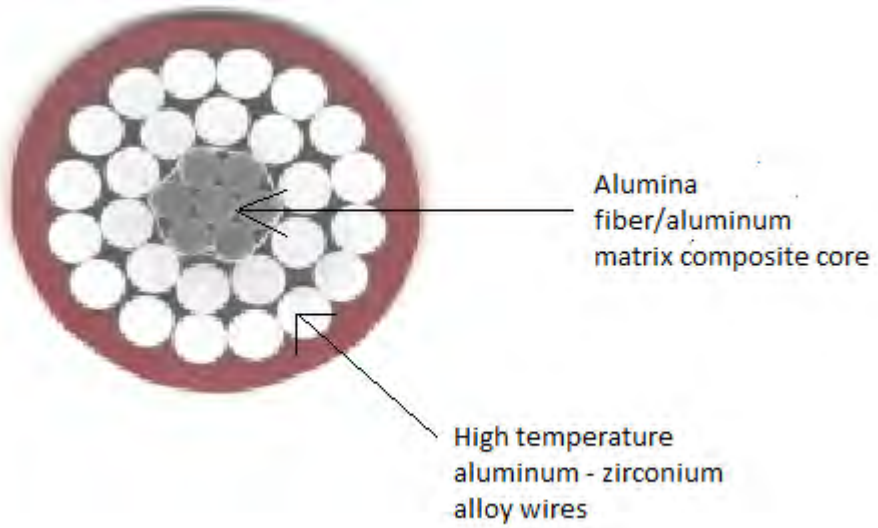

Figure 1.1: Diagram of Aluminum conductor composite reinforced (ACCR) [12]

HTLS conductor technology is comparatively new. The utilities do not have enough confidence in the performance of these conductors. To familiarize with the operation and handling of HTLS conductors like ACCC and ACCR, various field trials of the conductors were undertaken by Arizona Public Service, San Diego Gas & Electric and other utilities [10], [26]. Arizona Public Service have tested 1020 kcmil ACCC DRAKE equivalent at 69 kV transmission system in Phoenix, Arizona. The conductors were installed between four spans in 2005 with a total length of 956 ft. San Diego Gas & Electric have field-tested ACCR conductor of 795 kcmil which replaced ACSR conductor of 636 kcmil in a 69 kV transmission circuit in Oceanside, California. The conductors covered four spans of total length of 902 ft. The conductors were installed in 2005. These field tests monitored the conductor loading, sag -tension, corona and electric and magnetic fields continuously. According to the results of these field tests, the conductors performed as expected with all the parameters normal. In addition to these field tests, 3M Company have conducted their own outdoor tests on ACCR in Oak Ridge National Laboratory (ORNL) [27], [28]. The ACCR conductors were thermally cycled and exposed to various weather conditions. The conductors were then tested for residual tensile strength and stress-strain behavior. The results indicated that the conductors did not show any appreciable loss of tensile strength from clean conductor samples. Apart from field trails, manufacturing companies for ACCC and ACCR have tested the conductors for sag performance, fatigue, creep, aileron vibrations and stress strain relationships [12], [29]. Utilities and transmission operators around the world have successfully deployed ACCC and ACCR conductors commercially in various environments like heavy ice and marine installation, densely populated areas, etc. [29], [30].

Coefficient of thermal expansion of a transmission line is an important parameter. It indirectly determines the sag of a conductor, thus dictating thermal rating of the line. Various researches have been conducted to determine the coefficient of thermal expansion of the constituent materials of HTLS conductor. The coefficient of thermal expansion for carbon fibers and carbon fiber/epoxy composites has been extensively and experimentally determined in references [31]-[33]. The coefficient of thermal expansion for carbon fiber/epoxy composite range from $-0.6\times10^{-6}/K$ to $-0.001\times10^{-6}/K$ in the direction of the carbon fibers in the composite. Burks, Armentrout and Kumosa [34] used the axial and transverse coefficient of thermal expansion of the carbon composite core in ACCC to develop finite element models to predict the axial and transverse stresses in the core due to thermal mismatch between the carbon fibers, glass fibers and epoxy matrix. National Electric Energy Testing Research and Applications Center (NEETRAC) performed coefficient of thermal expansion measurements for ACCR and it was noted that the difference or mismatch in thermal expansion characteristics between the metal matrix core and the aluminum conductor wires caused complex behavior of the conductor [35]. Thermal kneepoint of a conductor plays an important role in determining the thermal expansion of the conductor [36]. Below the thermal kneepoint, the coefficient of thermal expansion of a conductor is due to both aluminum wires and the core. Above the thermal kneepoint, the core carries the load almost entirely and consequently the coefficient of thermal expansion of the conductor reflects that of the core. Since HTLS conductors cores of ACCR and ACCC have very low coefficient of thermal expansion as compared to ACSR, HTLS conductors sag less at high temperatures than ACSR. In fact, above the thermal kneepoint, ACCC shows the unique feature of almost flat sag temperature characteristics [37]. The thermal kneepoint for HTLS conductors like ACCR and ACCC occurs at lower temperatures than that of ACSR [10].

Bosze [38] showed that there is a correlation between the loss of tensile strength of carbon composite core of HTLS conductor and loss of storage modulus of the carbon-fiber/epoxy section of the core. Dynamic Mechanical Analysis (DMA) was used to determine the loss of storage modulus with temperature. The normalized curve of loss in storage modulus is equivalent to the normalized curve of loss in tensile strength. The correlation is given by equation 1.1:

$$\sigma_s(T) = \sigma_{To}\left[\frac{E'_T}{E'_{To}}\right] \tag{1.1}$$

where:

σ_s is the tensile strength at temperature T

σ_{To} is the tensile strength at temperature T_o

E'_T is the storage modulus at temperature T

E'_{To} is the storage modulus at temperature T_o

In DMA, a sinusoidal stress force is applied to visco-elastic material such as carbon fiber/epoxy composite [39], [40]. The strain response of the material is also sinusoidal but

lags the stress by an angle. This phase difference is due the energy absorbed in the material without performing any deformation. This is analogous to a response of an R-L circuit to a sinusoidal voltage. This leads to the concept of complex modulus in viscoelastic materials. The complex modulus is given by equation (1.2):

$$E = E^{'} + iE^{"} \tag{1.2}$$

where:
E is the complex modulus
$E^{'}$ is the storage modulus
$E^{"}$ is the loss modulus.

The storage modulus is related to the shear modulus by equation (1.3):

$$E^{'} = 2G(1+\upsilon) \tag{1.3}$$

where:
G is the shear modulus
υ is the Poisson's ratio.

Mathematically, the relationship of between shear modulus and tensile strength of a carbon fiber reinforced plastic (CFRP) is given by equation (1.4) [41]:

$$\frac{\sigma(t_s,T)}{\sigma_g} = \left(\frac{G(t_r,T)}{G_g}\right)^{\left(\frac{1}{2m}\right)} \tag{1.4}$$

where:
σ_g is the tensile strength at the glassy region
σ is the tensile strength at temperature T and time to failure t_s.
G_g is the shear modulus at the glassy region
G is the shear modulus at temperature T and time to relaxation t_r.
m is the Weibull shape parameter.

Glass transition temperature (T_g) is an important property of visco-elastic material. It is the temperature at which the material changes from glass state to amorphous state [40]. The change is associated with the loss of stiffness of the visco-elastic material. Glass transition temperature can be determined with the help of various techniques such as Differential Scanning Calorimetry (DSC), Thermal Mechanical Analysis (TMA) and DMA where DMA is considered the most sensitive technique to measure T_g [42]. There are several methods to determine glass transition temperature in DMA analysis [43]. Tan delta peak is used in the DMA of ACCC carbon core as the glass transition temperature. This method reflects the midpoint between the glassy and rubbery states of the material [43].

Rossoll [44] predicted the failure mechanism of ACCR metal matrix core under tensile load. In this research, local load sharing (LLS) mechanism and global load sharing (GLS) mechanism were applied to the failure of the conductor core. The predicted tensile strength values of the conductor core at different temperatures by the LLS mechanism were in good agreement with the experimental values. The strength of the core decreased by 4% from room temperature to 200°C. The loss of tensile strength of the core at 300°C was 10%. At 600°C, the loss of tensile strength was 30%. The melting point of the aluminum in the metal matrix is 650°C.

Thermal aging experiments on HTLS conductors provide insight on the mechanical response of the conductors to stress due to heat. Thermal aging of carbon composite cores presented in references [45]-[47] shows that the cores retain its tensile strength at room temperature. It also reveals that the glass fiber layer of the core protects the carbon fiber layer from oxidation. Thermal aging at different temperatures and lifetime modeling of aluminum zirconium alloy wires and alumina/aluminum matrix core used in ACCR were carried out by 3M Company [48], [49]. The core samples were aged at up to 500°C for a maximum of 2000 hours whereas the aluminum-zirconium alloy wire samples were aged at up to 400°C for a maximum of 1000 hours. The studies concluded that that there is statistically insignificant variation in the tensile strength of the aged core samples at room temperature and the aged samples retained their tensile strength. Lifetime modeling based on thermal aging of the aluminum-zirconium alloy wires concluded that the wires would lose 10% of its strength in 40 years when exposed continuously to 240°C.

1.4 Steady state and transient thermal ratings of overhead transmission conductors

Every overhead transmission line has a maximum operating temperature, which determines the thermal rating of the line. The thermal rating depends on the ambient weather parameters, conductor characteristics and conductivity [21], [47]. The passage of current through the conductor produces heat and along with solar radiation absorbed by the conductor balances the heat loss through convection and radiation [5], [21]. Traditionally, thermal ratings of overhead conductors are determined by assuming conservative values of ambient weather parameters such as 0.61 ft/s wind speed and high ambient temperature of 40°C [21]. The conductor characteristics include emissivity and absorptivity, which are usually taken as 0.5 [21]. CIGRE and IEEE have standardized the process of calculating the thermal ratings of overhead transmission lines [21], [50]. The latest IEEE standard for calculating the current temperature relationship of overhead bare conductors is the IEEE 738-2006 [21].

Thermal ratings indirectly provide the ampacity of the conductor. Ampacity is the maximum amount of current that a conductor can carry at the maximum allowable temperature under a certain set of weather parameters and conductor characteristics [47]. The maximum allowable temperature or the design temperature of the conductor depends on the sag and loss of tensile strength of the conductor with temperature. The thermal rating of the line depends on the aging of the line since the conductor characteristics changes with

time [21]. These factors have to be taken into account when estimating the current carrying capacity of the line over its lifetime.

The steady state thermal rating of the line is calculated when the line is in thermal equilibrium. Whereas, the transient thermal rating of the line provides the rate of temperature rise to its steady state value when there is a step increase in the current flowing though the conductor. The rate of temperature rise depends on the conductor's overall heat capacity [21]. The temperature of the conductor will rise slowly if the heat capacity of the conductor is high and vice versa. In transient thermal rating calculations due to fault currents, the heat capacity of the conductor core is generally neglected for fault duration of less than 60 seconds [21]. The thermal time constant for transient thermal rating calculations depends on the ac resistance of the conductor, heat capacity and difference between the square of the final and initial current magnitudes [21].

1.5 Report organization

In chapter 2, thermal aging experiments of carbon composite cores are presented. The carbon fiber/epoxy samples from ACCC is used for the experiments. The physical changes of the carbon composite cores due to heat exposure are observed with the help of an optical microscope and are described in this chapter. An explanation of the observed physical changes is also given.

Chapter 3 describes the TMA experiments for obtaining the coefficient of thermal expansion of the composite conductor cores. Detailed analysis of the experimental results is discussed. The mean and standard deviation of the thermal expansion coefficient of both metal matrix core and carbon composite core is established.

In chapter 4, DMA of carbon composite cores is presented and loss of storage modulus of the carbon core with temperature is obtained. Analysis of the loss of storage modulus of the cores is described. Percentage loss of tensile strength of the conductor core is estimated with the help of the loss of storage modulus of the carbon cores.

In chapter 5, the tensile testing of metal matrix core is described. Development of new custom grips for the tensile testing is discussed. Stress – strain relationship of the core is established from the load – displacement curve obtained from the tensile test.

Chapter 6 describes the calculation of current temperature relationships and temperature rise due to fault currents for the composite core conductors with the help of IEEE 738-2006 standard. The chapter also discusses the C++ programs written to simulate the temperature rise due to steady state currents and transient fault currents. The effect of the temperature rise due to fault currents on the structure of the composite cores has been discussed.

Chapter 7 provides the conclusion on the study of HTLS conductors with composite cores. It also presents the future work based on this present study.

2. Heat Treatment of Carbon Composite Cores

This chapter describes the heat treatment or thermal ageing of carbon composite cores of HTLS conductors. The maximum continuous operating temperature for these types of HTLS conductors is 180°C, with an emergency maximum temperature of 200°C [11]. The epoxy matrix of the carbon composite core is an organic material and organic materials are susceptible to degradation at high temperatures [17], [47]. Thus, degradation of the carbon composite core may occur due to heat treatment. Heat treatment of the carbon composite cores at various temperatures was performed in order to observe the degradation of the carbon fiber/epoxy matrix section as well as the glass fiber/epoxy matrix shell of the carbon composite.

2.1 Test setup

The test setup consists of high temperature Muffle Furnace. The muffle furnace is of Barnstead/Thermolyne Corporation make [51]. These are general purpose laboratory furnace and has a temperature range of 25°C - 1700°C. The maximum ramp rate as detailed in its user manual is 100°C/min. The muffle furnace consists of abrasive heating elements made up of alumina and silica. The thermocouple is made from a precious metal. The current controller of the furnace compares the temperature in the furnace chamber with the temperature set point and provides the appropriate current to its heating elements. In case of overheating due to overcurrents, relays and circuit breakers are provided.

The temperature of the heat treatment of the samples is programmed into the furnace. Samples were kept in isothermal zones of 125°C, 175°C, 200°C, 250°C and 300°C for 24 hours each. Some samples were kept for 40 hours at 125°C. The environment inside the muffle furnace chamber were the samples were kept was air. The test setup is shown in Fig 2.1.

Figure 2.1: Muffle furnace used for the heat-treatment of the carbon composite cores

2.2 Sample description

The samples used in this experiment were sectioned out from the ACCC carbon core. The ACCC carbon core consists of concentric glass fiber/epoxy matrix shell covering the carbon fiber/epoxy matrix rod. The samples were 1-2 cm in length and had a diameter of 9.53 cm, which is the diameter of the core in DRAKE sized ACCC. Fig 2.2 shows the cross section of an untreated sample. The samples were cut from the ACCC core rod with the help of carbide cutting tool. The difference in the coefficient of thermal expansion of the components of the core such as glass fiber/epoxy and carbon fiber epoxy can contribute to thermal stresses during thermal aging [34]. There are two types of interfaces present in the sample [34]:

1. Fiber matrix microscopic interface
2. Composite – Composite macroscopic interface (e.g. glass fiber/epoxy – carbon fiber/epoxy).

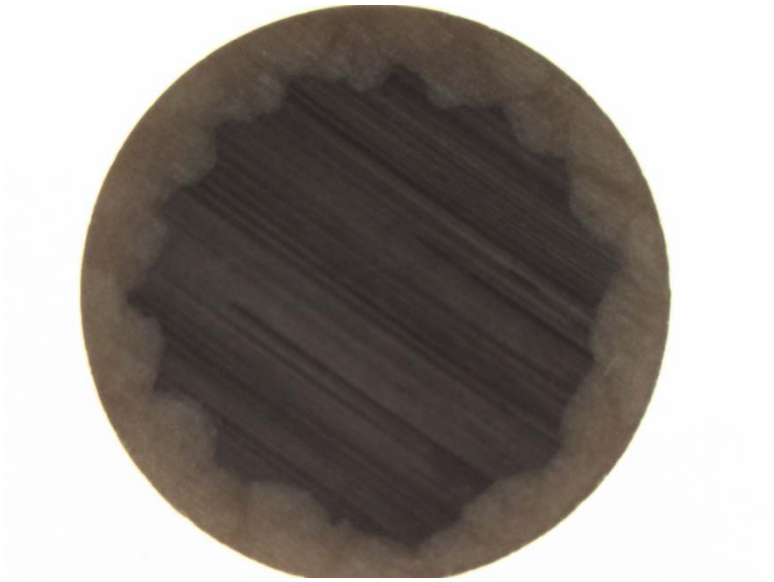

Figure 2.2: Cross section view of untreated carbon composite core

2.3 Results and discussion

The thermal aging of samples heat treated at different temperatures are shown in the Fig 2.3 – 2.7. Fig 2.3 shows the cross section of the sample heat – treated at 125°C for 24 hours. It can be seen that there are no cracks on the cross section of the sample. Fig 2.4 shows the sample heat – treated at 150°C for 24 hours. Radial cracks on the cross section of the sample can be seen. Fig 2.5 shows the cross section of the sample kept at 200°C for 24 hours. Similarly, Fig 2.6 and 2.7 shows the cross section of the sample for 250°C and 300°C.

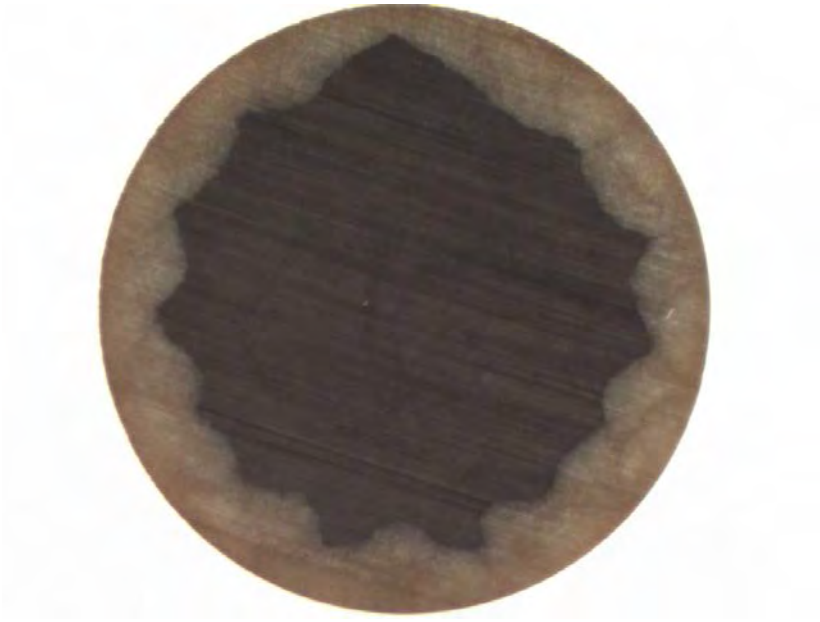

Figure 2.3: Cross section of the sample heat-treated at 125°C for 24 hours

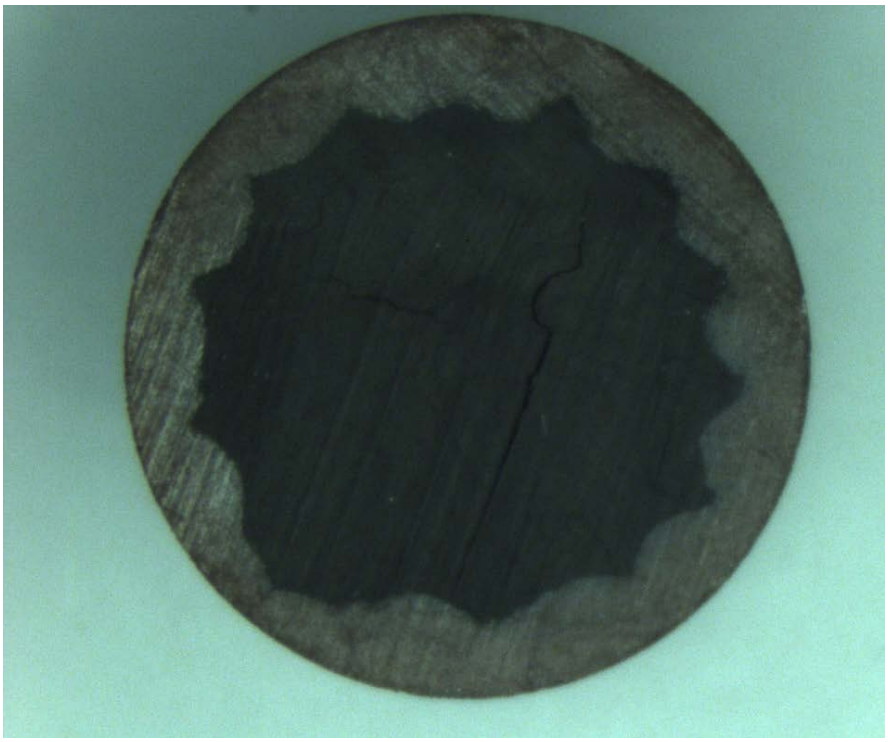

Figure 2.4: Cross section of sample heat treated at 150°C for 24 hours

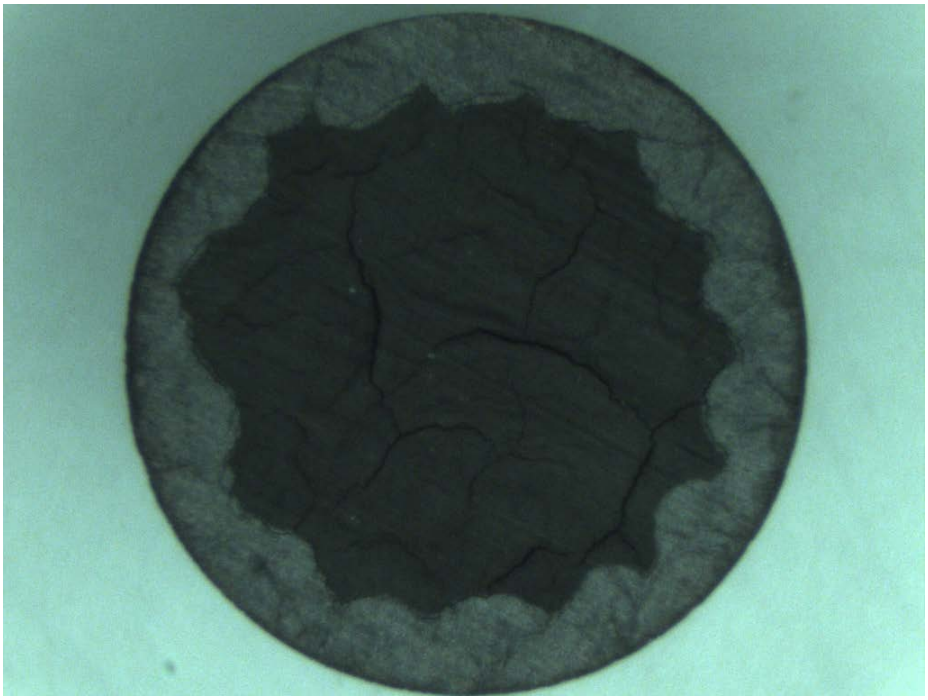

Figure 2.5: Cross section of the sample heat – treated at 200°C for 24 hours

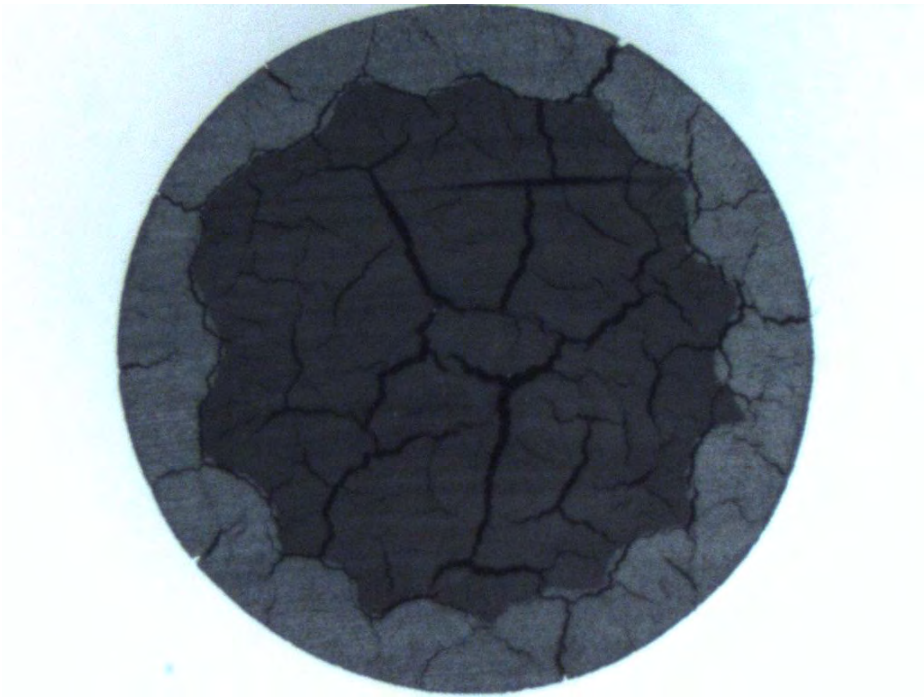

Figure 2.6: Cross section of the sample heat – treated at 250°C for 24 hours

Figure 2.7: Cross section of the sample heat – treated at 300°C for 24 hours

The sample became heavily degraded due to thermal aging after 24 hours at 250°C and 300°C. Numerous radial cracks on the carbon fiber/epoxy section as well as on the glass fiber/epoxy section appeared. Some of the cracks covered the entire width of the core sample. Fig 2.8 – 2.11 shows the cracks on the macroscopic interface between the glass

fiber/ epoxy and carbon fiber/epoxy of the sample kept at 150°C, 200°C, 250°C and 300°C for 24 hours respectively. The cracks on the interface increased in width with the increase in degree of heat – treatment of the sample. The cracks can be attributed to the difference in the thermal expansion coefficients of the glass fibers, carbon fibers and the epoxy matrix. At high temperatures, these materials expand differently at different rates. This causes development of thermal stress both between the fiber-matrix and glass fiber/epoxy – carbon fiber/epoxy [34]. Thus, it leads to cracking of the epoxy matrix and the macroscopic interface.

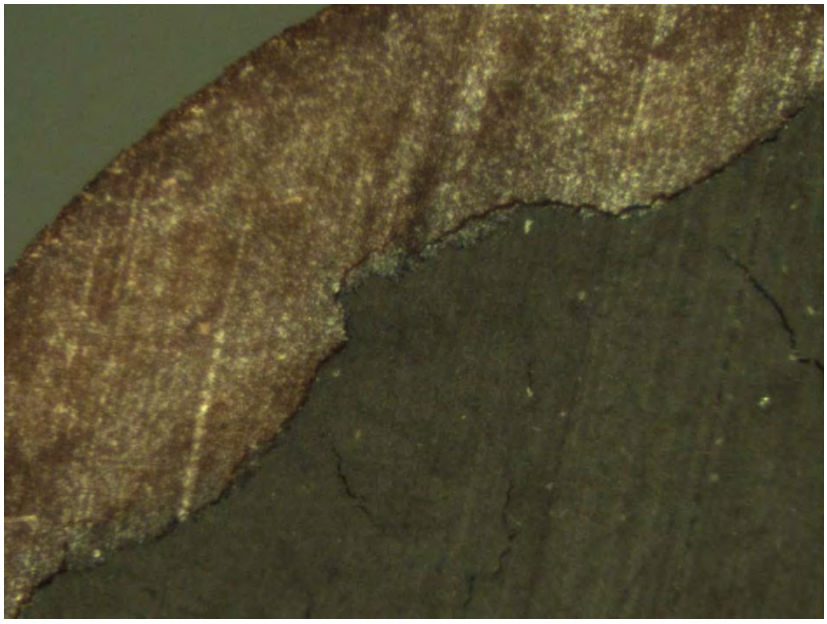

Figure 2.8: Macroscopic interface of the sample heat treated at 150°C for 24 hours

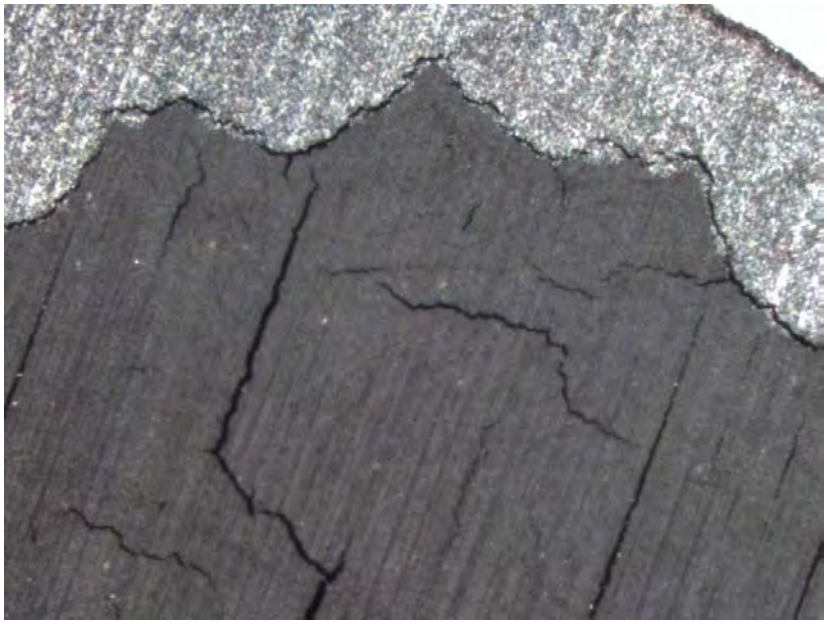

Figure 2.9: Macroscopic interface of the sample heat treated at 150°C for 24 hours

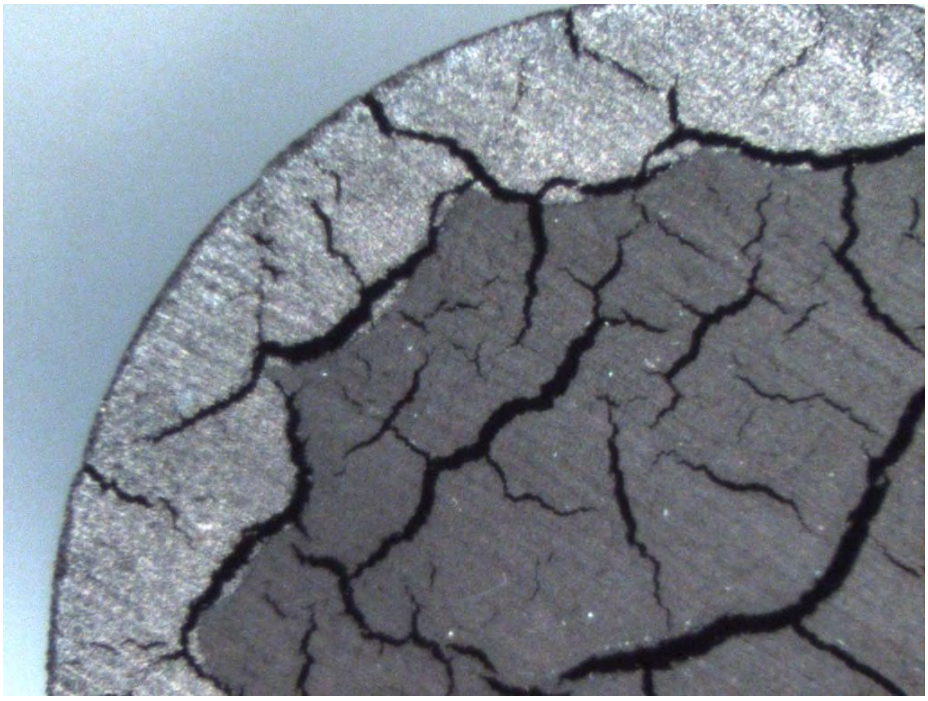

Figure 2.10: Macroscopic interface of the sample heat treated at 250°C for 24 hours

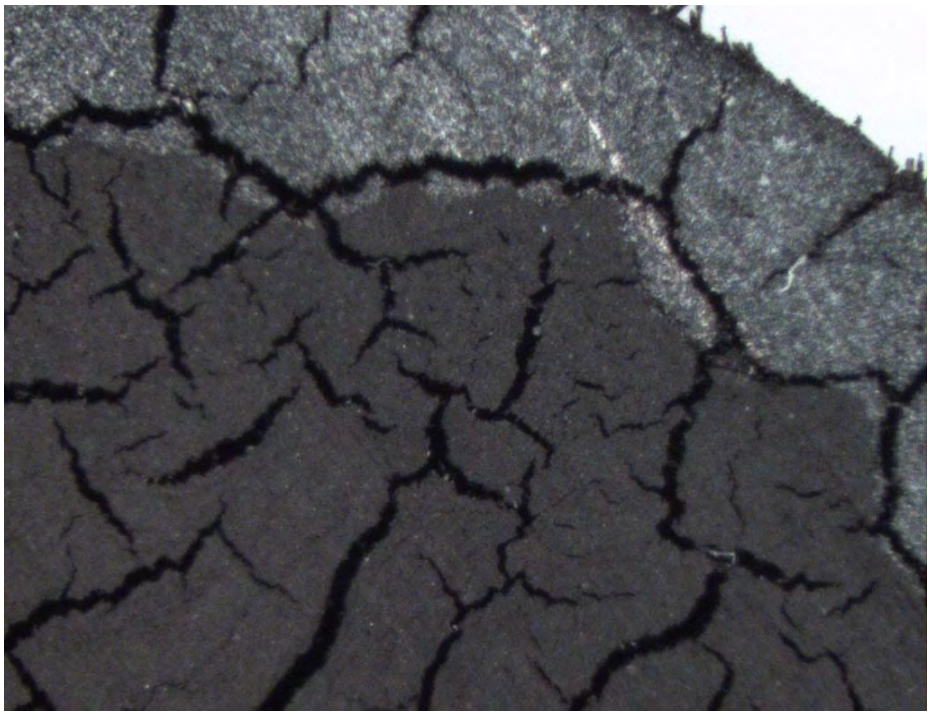

Figure 2.11: Macroscopic interface of the sample heat treated at 300°C for 24 hours

From the heat treatment of the carbon composite cores the following points were noted –

1. ACCC conductor core samples withstood sustained temperature of 125°C without any development of cracks on the cross section.
2. Cracks across the composite-composite interface and across carbon fiber/epoxy section were observed at 150°C and above. These cracks are due to mismatch of coefficient of thermal expansion between glass fibers, carbon fibers and epoxy.
3. At temperatures at or above 250°C, the width of the cracks and fissures across the core and the glass fiber/epoxy – carbon fiber/epoxy increased as compared to the cracks at lower temperatures. Radial cracks from the glass fiber/epoxy –carbon fiber/epoxy boundary across the glass fiber/epoxy section were observed. This radial cracks may expose the carbon fiber/epoxy portion to the atmosphere which will cause accelerated ageing [45], [46].

3. Thermal Mechanical Analysis of HTLS Conductor Cores

Coefficient of thermal expansion of a material is an important mechanical property. It provides an insight on the material response to temperature exposures. The sag of a transmission conductor is dependent on its coefficient of thermal expansion [20]. At the thermal kneepoint, most of the load on the conductor shifts to its core and thus the core controls the expansion of the conductor after the kneepoint [10], [36], [37]. HTLS conductor cores consist of multiple components such as carbon fiber in epoxy matrix for composite cores and alumina fibers in aluminum matrix. The mismatch of coefficient of thermal expansion between these materials can create micro and meso stresses [34]. In this chapter, thermal mechanical analysis (TMA) on carbon composite and metal matrix cores to obtain the respective coefficient of thermal expansions has been addressed. The results obtained from TMA of HTLS cores were analyzed to get the average coefficient of thermal expansion of the cores in the temperature range of room temperature - 300°C.

3.1 Thermal mechanical analysis

Thermal mechanical analysis detects dimensional changes in a material in response to change in temperature. Coefficient of thermal expansion can be calculated from the dimensional changes such as change in length of the material. In case of the carbon composite core and metal matrix cores of HTLS conductors, coefficient of thermal expansion in the longitudinal direction is of primary concern. The TMA system calculates thermal expansion coefficient is calculated by with the help of the following equation:

$$\alpha(k) = \frac{1}{L_o} * \frac{\Delta L_k - \Delta L_o}{T_k - T_0} \qquad \text{(k = 1..n)} \tag{3.1}$$

where:

α is the coefficient of thermal expansion of the sample

L_o is the sample length at reference temperature

ΔL_o is the change in length at reference temperature

ΔL_k is the change in length at temperature T_k

T_o is the reference temperature

The TMA system gathers the data points corresponding to α_k for every measured point k. An important consequence of equation (3.1) is TMA system can track variation in coefficient of thermal expansion of a material with temperature. The average coefficient of thermal expansion (α_{avg}) of a material in a certain temperature range is given by the following equation:

$$\alpha_{avg} = \frac{L_{final} - L_{initial}}{L_{initial} * (T_{final} - T_{initial})} \tag{3.2}$$

where:

L_{final} is the final length of the material

$L_{initial}$ is the initial length of the material

T_{final} is the final temperature of the material

$T_{initial}$ is the reference temperature

The software section of the TMA system applies signal correction procedures after the collection of data from the sample material under study. The three important signal correction procedures are [52]:

1. Zero correction – In this type of correction, the difference between the expansion of the piston and the sample holder is subtracted from the expansion curve of the sample. The curve signifying the difference between the expansion of the piston and the sample holder is called the zero curve.
2. Piston correction – The piston correction determines the change in length of the piston during the test and compensates this elongation by applying the coefficient of thermal expansion of the piston to the data curve to get an accurate expansion curve of the sample.
3. X-axis smoothening – This helps in smoothening the data curve over the investigated temperature range.

The accuracy of TMA measurements decreases when the coefficient of thermal expansion of the sample is much lower than the coefficient of thermal expansion of the sample holder [52]. In order to make the measurements more accurate, the sample holder should have a low coefficient of thermal expansion and the ramp rate of the temperature used in such tests should be limited to 2-5 K/min [52].

3.2 Test details

Linseis TMA/DMA L77 system was used to perform thermal mechanical analysis of the carbon composite core and the metal matrix core. Fig 3.1 shows the Linseis TMA/DMA L77 system. It consists of three parts in the hardware design [53]. The upper part of the system houses the LVDT sensor, its control circuits, amplifier, thermocouples and the thermostat. The measuring head, which contains the piston and the sample holder, is connected to the LVDT sensor. The expansion of the sample causes the piston to move and this motion is converted into electrical signal by the LVDT. The control circuits control the linear motor that applies static or dynamic force on the sample. The system provides a cylindrical furnace, which can completely cover the glass tube housing the sample holder and piston to provide uniform heating. The thermostat controls the temperature. The whole system is interfaced with a PC with MS-Windows running Linseis data acquisition and evaluation software. TMA/DMA L77 is very sensitive to vibrations, which can distort the data signals. In order to overcome this problem to a certain extent, the legs of the machine are kept on a material, which can absorb those materials.

Figure 3.1: Thermal mechanical analysis (TMA) test system

Linseis data analysis software consists of three sections [53].

Data acquisition section – In this section, the system acquires the dimensional change data from the TMA tests and stores it in the memory. The system also records the information about the sample and initial test conditions in this section.

Evaluation section – The data acquired from the system is analyzed and evaluated. This section also performs corrections on the data, if needed. Various parameters like coefficient of thermal expansion, relative and absolute change in length of the sample are calculated from the acquired data.

Programming section – This section is concerned with the programming of the number of temperature cycles, its ramp rate and dwell time for the TMA tests.

The following Table 3.1 lists out the test details for the evaluation of the coefficient of thermal expansion of the carbon composite core and metal matrix core of HTLS conductors.

Table 3.1: Test details for thermal mechanical analysis of the HTLS conductors

Type of core samples	Sample length (mm)	Sample diameter (mm)	No. of tests	Temperature range (°C)	Temperature ramp rate (°C/min)
ACCR	10.1	2.5	6	RT-300	5
ACCC	9.89	7.0	5	RT-300	5

Six tests were performed on ACCR metal matrix core sample and five tests were performed on ACCC carbon composite core sample. The length of the metal matrix core sample was 10.1 mm and the length of carbon composite core sample was 9.89 mm. The temperature was ramped from ambient to 300°C and a temperature ramp rate of 5°C/min was chosen.

3.3 Sample description

The samples used in the experiments were carbon fiber/epoxy matrix and alumina fiber/ aluminum matrix cylindrical rods with smooth flat surface at the top and bottom. A smooth surface profile is important because the piston tip contacts the sample on the top and an uneven surface might cause the piston tip to slip introducing error in the signal for change of length of the sample. The carbon fiber/epoxy matrix rod was obtained from the core of ACCC after stripping off the outer glass fiber/epoxy matrix shell. The alumina fiber/aluminum matrix rod was sectioned out from ACCR core.

3.4 Experimental procedure

Thermal mechanical analysis is a non-destructive testing method. The samples do not require special preparation for the testing. The following lists out the procedure undertaken to perform CTE tests for ACCR and ACCC core samples –

1. The sample was mounted on the sample holder and the tip of the piston, connected to the LVDT, was made to touch the sample on its flat surface.
2. A protective outer glass tube was used to cover the assembly.
3. The furnace was then introduced to cover the sample.
4. Initial test conditions were entered in the Linseis TMA/DMA L77 software. A static force of 0 mN was chosen in order to obtain the thermal expansion data. The temperature ramp rate for the tests was 5°C/min.
5. The temperature was ramped from ambient to 300 °C
6. Once the software had gathered the data for the thermal expansion of the sample, zero measurement correction and piston correction were applied to the acquired signal in order to take care of the thermal expansion of the piston and the sample holder.

7. The resultant thermal expansion data were then analyzed to obtain the mean of the coefficient of thermal expansion from the tests.

3.5 Results

The Linseis data analysis software captured the thermal expansion data from the experiments for ambient - 300°C. Fig 3.2 shows the result from the thermal expansion tests on ACCR core sample. It can be seen that the change in length with temperature over the range of ambient - 300°C for ACCR core sample was approximately 16 µm. Correspondingly, the coefficient of thermal expansion of the samples increased from approximately $5\times10^{-6}/K$ to $6\times10^{-6}/K$ with temperature. The sudden variations in the curve for change in length and coefficient of thermal expansion with temperature observed in few tests were due to noise in the data signals introduced by stray vibrations.

Fig 3.3 shows the results obtained from the thermal expansion tests on the carbon fiber/epoxy part of ACCC core sample. The tests for ACCC carbon core show that the final change in length of the sample with temperature was -2.5µm. Consequently, the coefficient of thermal expansion of the ACCC core sample decrease from $0.5\times10^{-6}/K$ at initial temperature to $-0.5\times10^{-6}/K$ at final temperature. The coefficient of thermal expansion of the carbon fiber/epoxy sample becomes negative since the thermal expansion coefficient of the constituent carbon fibers is negative and it dominates the mechanical properties in the axial direction.

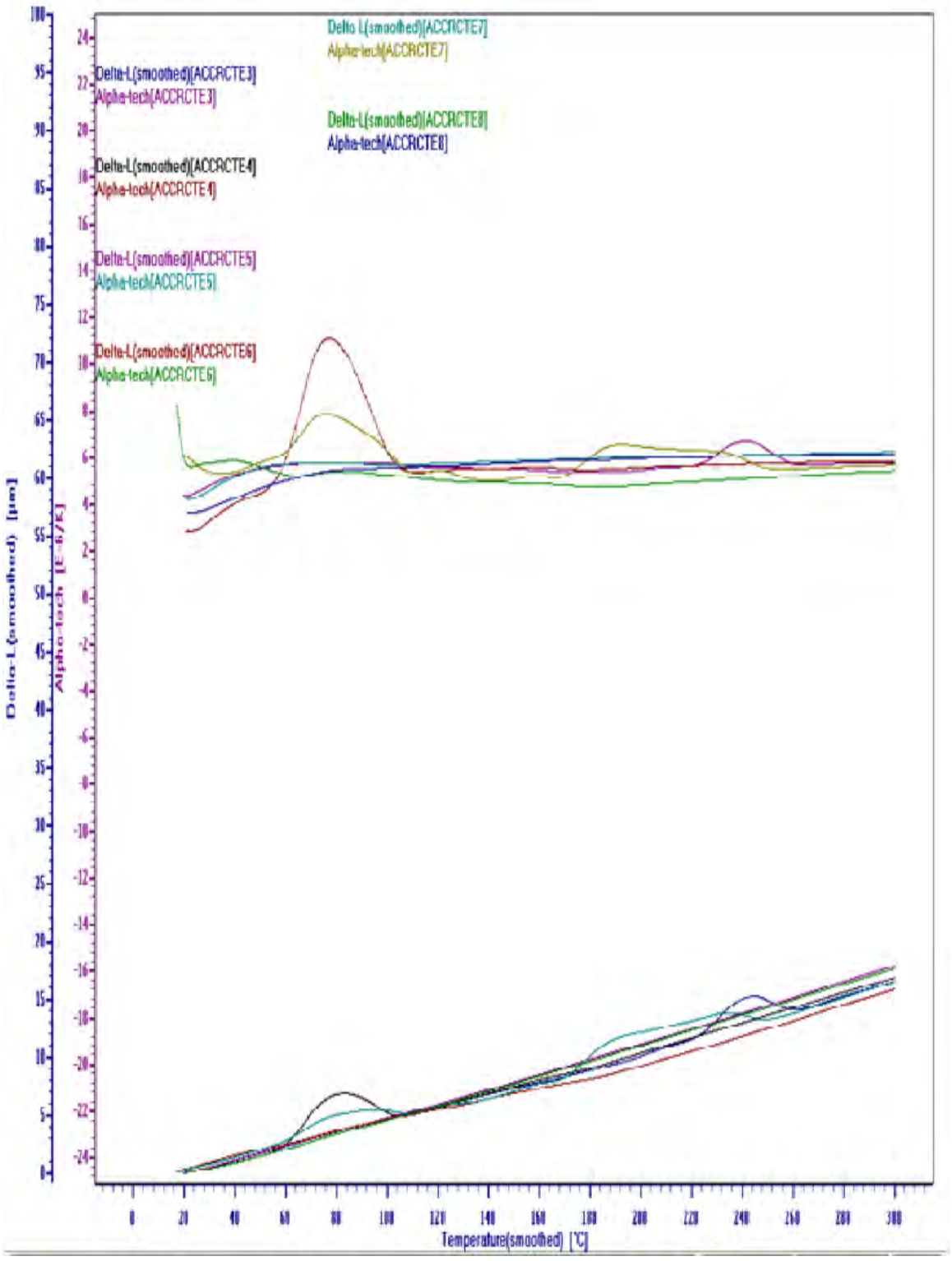

Figure 3.2: Comparison of change in length and coefficient of thermal expansion for ACCR core samples

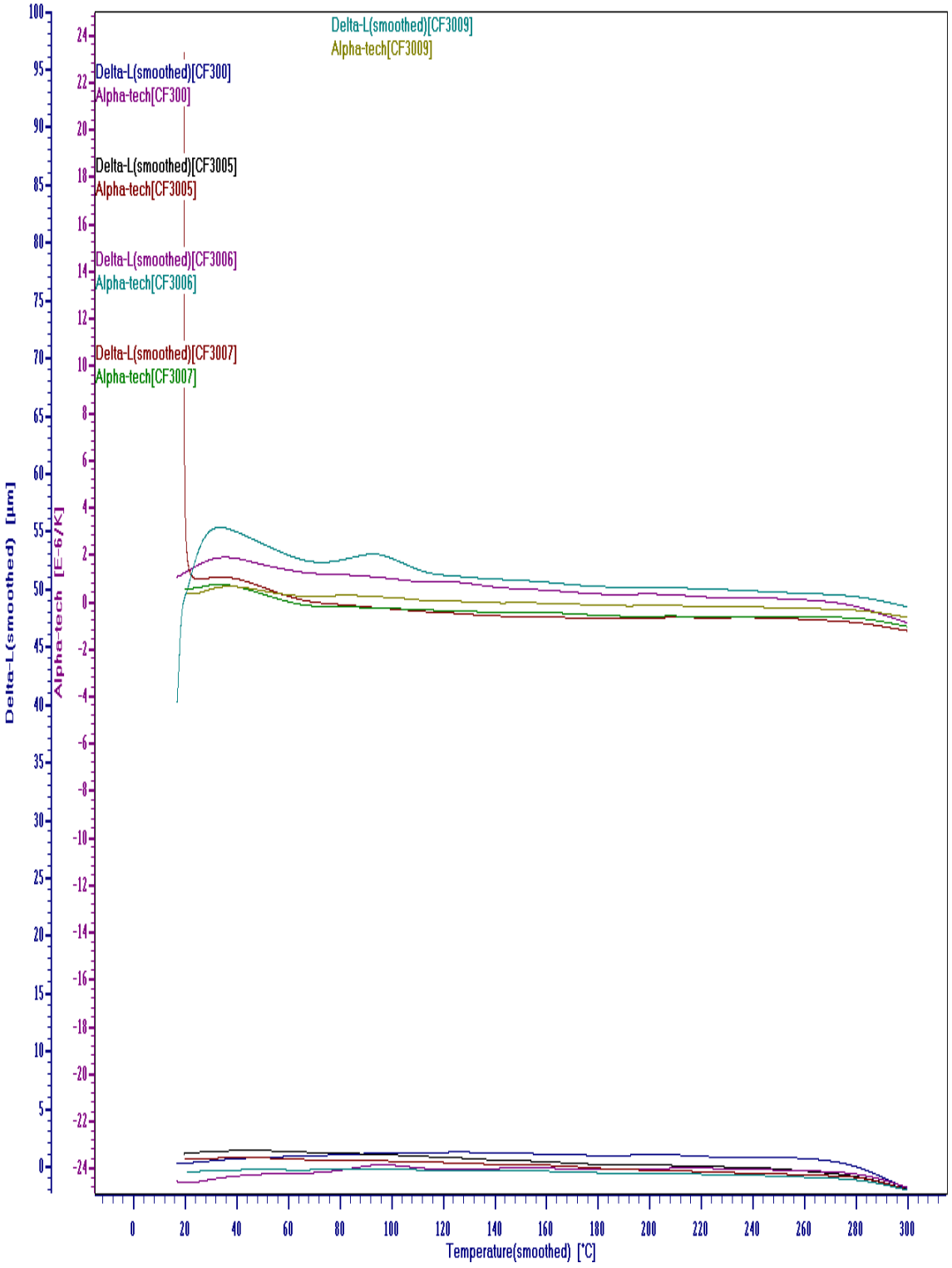

Figure 3.3: Comparison of change in length and coefficient of thermal expansion for ACCC core samples

3.6 Analysis of TMA test results

The data analysis section of the TMA software was employed to analyze the coefficient of thermal expansion curves obtained in the tests for ACCR and ACCC core samples. The mean, maximum and minimum of the coefficient of thermal expansion curves obtained from different tests on ACCR core sample is given in Fig 3.4.

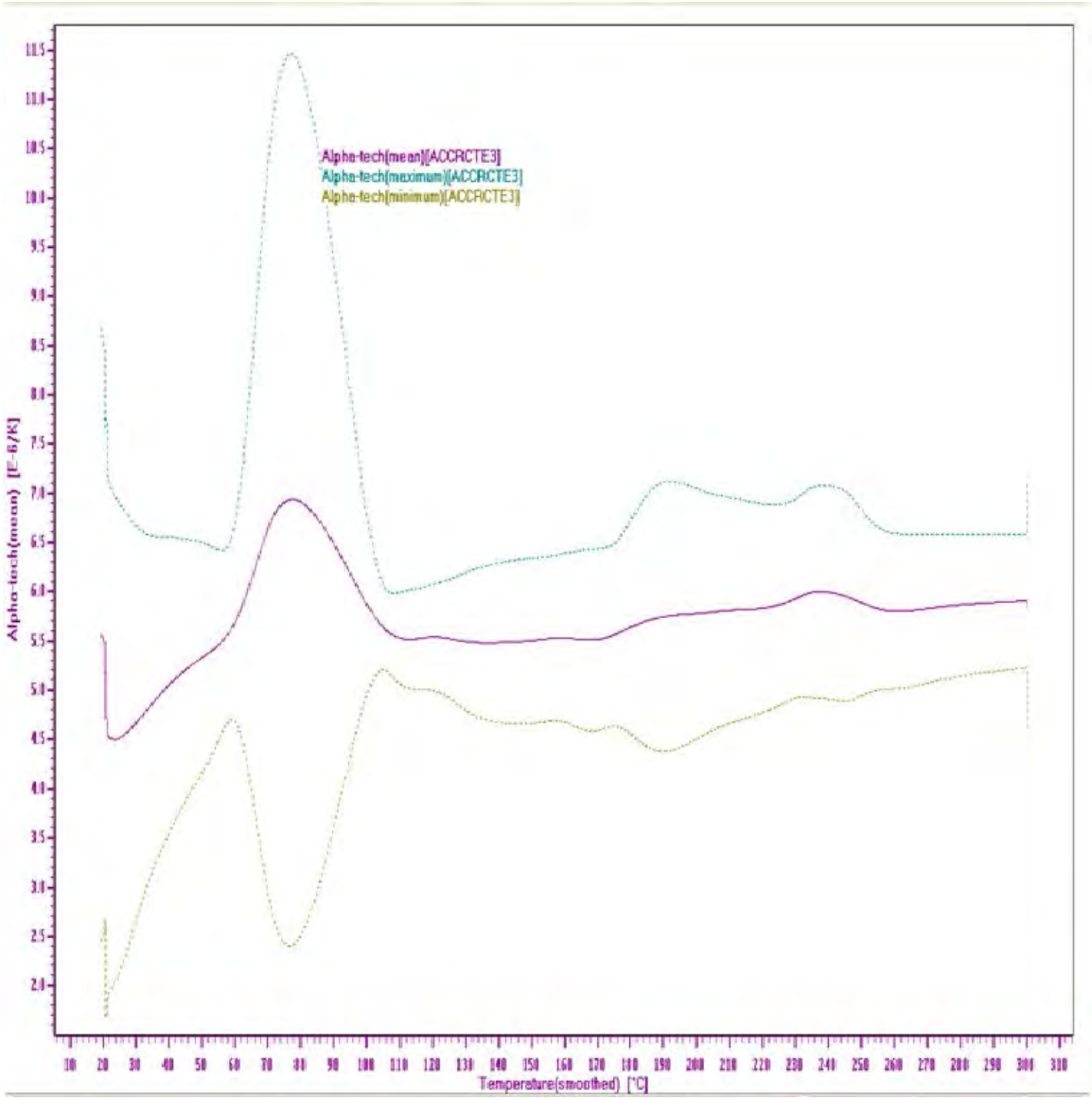

Figure 3.4: Maximum, minimum and mean of coefficient of thermal expansion curves for ACCR core samples

Fig 3.4 indicates that the coefficient of thermal expansion of the metal matrix core lies between $4.5\times10^{-6}/K$ and $6.5\times10^{-6}/K$ in the temperature range of 130°C - 300°C. The mean, maximum and minimum of the coefficient of thermal expansion curves obtained from different tests on ACCC carbon fiber/epoxy core sample is given in Fig 3.5.

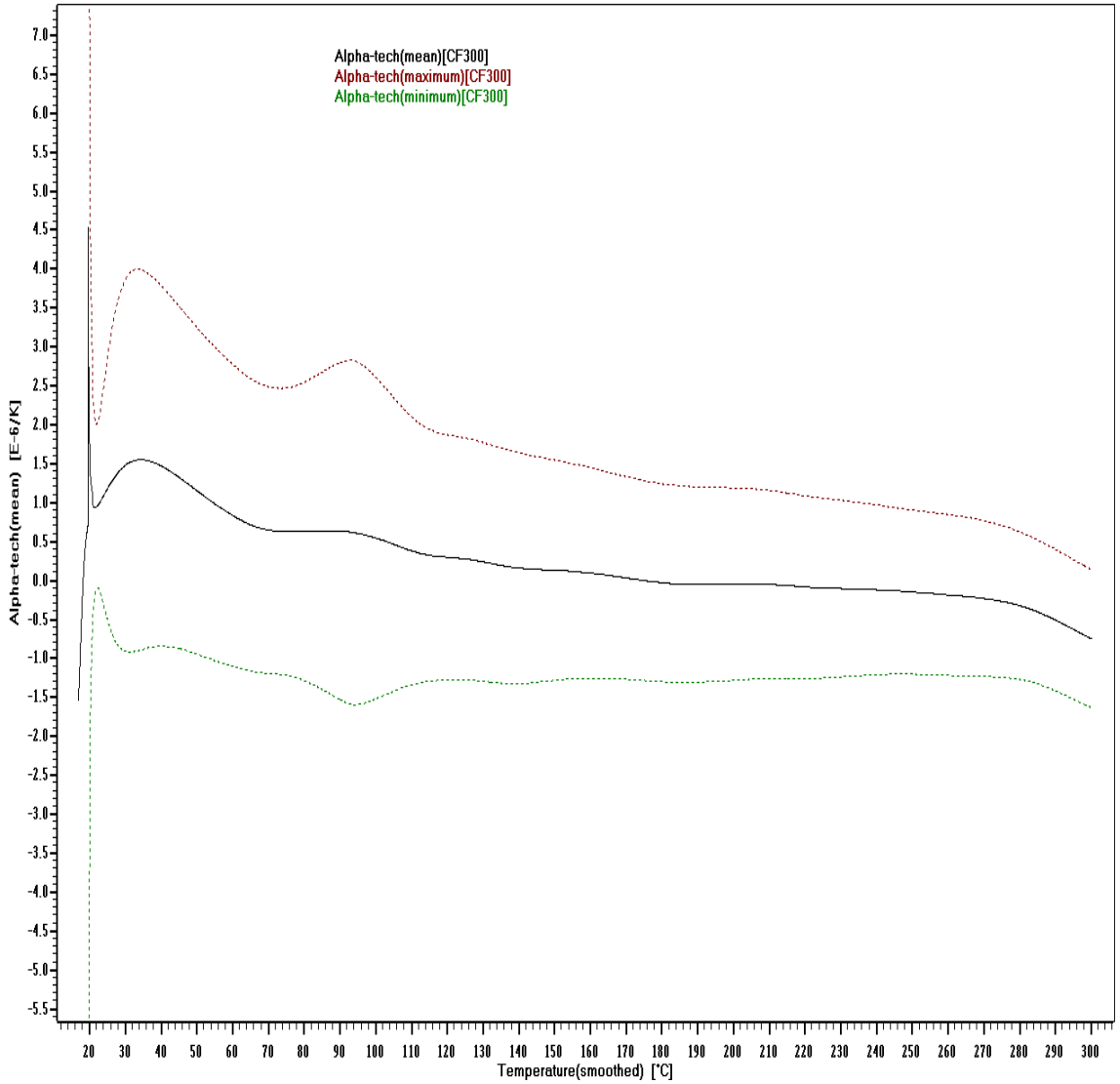

Figure 3.5: Maximum, minimum and mean of coefficient of thermal expansion curves for ACCC core samples

Fig 3.5 indicates that the coefficient of thermal expansion of the metal matrix core lies between $-1.0\times10^{-6}/K$ and $2\times10^{-6}/K$ for temperatures above 120°C. The average coefficient of thermal expansion α_{avg} of the ACCR core sample and the ACCC carbon finer/epoxy core sample in each test was calculated with the help of equation (3.2). The calculations are summarized in Tables 3.2 and 3.3.

Table 3.2: Summary of the average coefficient of thermal expansion (α_{avg}) calculations for the ACCR core sample

Test no	Change in length (μm)	Change in temperature (°C)	α_{avg} (10^{-6}/K)
1	16.52	280.5	5.837
2	16.72	279.2	5.923
3	17.78	279.8	6.293
4	15.81	283	5.534
5	16.4	282	5.756
6	17.58	279	6.243

The mean of the average coefficients of thermal expansion (α_{mean_avg}) of ACCR core sample calculated in each test were obtained with the help of the following equation (ambient - 300°C) –

$$\alpha_{mean\_avg(MMC)} = \frac{\alpha_{avg1} + \alpha_{avg2} + \alpha_{avg3} + \alpha_{avg4} + \alpha_{avg5} + \alpha_{avg6}}{6} \tag{3.3}$$

$$\alpha_{mean\_avg(MMC)} = 5.931 \times 10^{-6} / K \tag{3.4}$$

The standard deviation is:

$$S.D = \sqrt{\frac{\sum_{i=1}^{N} (\alpha_{avgi} - \alpha_{mean\_avg(MMC)})^2}{N}} \tag{3.5}$$

where:
N = 6

$$S.D = 2.663 \times 10^{-7} / K \tag{3.6}$$

Thus, the average coefficient of thermal expansion of ACCR metal matrix core in the temperature range of ambient - 300°C is $5.931 \times 10^{-6} / K$ according to the thermal mechanical analysis.

Table 3.3: Summary of the average coefficient of thermal expansion (α_{avg}) calculations for the ACCC CF/epoxy core sample

Test no	Change in length (μm)	Change in temperature (°C)	α_{avg} (10-6/K)
1	-2.23	283	-0.799
2	-3.05	280.2	-1.102
3	-0.54	283	-0.193
4	-2.7	280.2	-0.974
5	-1.61	279.4	-0.584

The mean of the average coefficients of thermal expansion (α_{avg}) of ACCC carbon fiber/epoxy core sample calculated in each test (ambient - 300°C) –

$$\alpha_{mean\_avg(CF/epoxy)} = \frac{\alpha_{avg1} + \alpha_{avg2} + \alpha_{avg3} + \alpha_{avg4} + \alpha_{avg5}}{5} \tag{3.7}$$

$$\alpha_{mean\_avg(CF/epoxy)} = -0.731 \times 10^{-6} / K \tag{3.8}$$

The standard deviation is:

$$S.D = \sqrt{\frac{\sum_{i=1}^{N} (\alpha_{avgi} - \alpha_{mean\_avg(CF/epoxy)})^2}{N}} \tag{3.9}$$

where:
N = 5

$$S.D = 3.202 \times 10^{-7} / K \tag{3.10}$$

Thus, the average coefficient of thermal expansion of ACCC carbon fiber/epoxy core in the temperature range of ambient - 300°C according to the thermal mechanical analysis is $-0.731 \times 10^{-6} / K$. The negative coefficient of thermal expansion of carbon fiber/epoxy and positive coefficient of glass fiber/epoxy in the ACCC composite core may cause significant thermal stress at the glass-carbon interface at elevated temperatures [34].

4. Dynamic Mechanical Analysis of Carbon Composite Cores

Dynamic mechanical analysis (DMA) is a thermal analysis technique that is employed to determine the stiffness of a visco-elastic material [39], [40], [42]. It provides important information on the storage modulus, loss modulus and tan delta of the material. The carbon composite core of HTLS conductors is a visco-elastic material because of the presence of epoxy. It has been shown that the tensile strength of a unidirectional hybrid glass fiber-carbon fiber/epoxy matrix rod has a correlation to the storage modulus of the unidirectional carbon fiber/epoxy part of the rod [38]. This correlation indicates that the normalized values of storage modulus with temperature are equal to the normalized values of the tensile strength with temperature of the hybrid composite. Thus, DMA can be applied to the carbon composite cores of HTLS conductors to determine the variation of storage modulus with temperature. This will then give an estimate on the variation of the tensile strength of the HTLS carbon composite core. In this chapter, DMA of carbon fiber/epoxy matrix samples from ACCC core is described and the results and analysis is presented.

4.1 TA instruments DMA Q800

TA instruments DMA Q800 [54] was used for dynamic mechanical analysis of the carbon fiber/epoxy core of ACCC. The machine consists of a non-contact drive motor, which applies sinusoidal force for the sample deformation, a drive shaft for force guidance and optical encoder displacement sensor. A furnace provides temperature control with the help of two thermocouples. The thermocouples are located close to the clamps that hold the sample. The clamps have high stiffness and low mass. The clamp consists of fixed and movable part. The moveable part is connected to the drive shaft. There are three different types of clamps depending on the mode of deformation. These modes of deformation are [54]:

1. Single/Dual cantilever bending mode – In this mode, the sample is clamped down at either ends or a single end by fixed clamps. A movable clamp applies the bending force at the center of the sample.
2. Tension mode – In this mode, the sample is placed in tension between a fixed and a moveable clamp. Thin films are particularly suited for this type of mode.
3. Compression mode – The sample is placed in compression between a fixed and a moveable plate.
4. Shear mode – Two pieces of the same sample is secured between two fixed plates and a moveable plate.
5. 3-Point bending mode – In this mode, the sample is supported at both ends and the moveable clamp applies the bending force.

Samples with rectangular geometry are suitable for single/dual cantilever or 3-point bending mode. The DMA Q800 can deliver a maximum force of 18 N and have a frequency range of 0.001 to 200 Hz. The temperature range in which it can operate is -150^{o}C to 600^{o}C. Special gas cooling accessory is required for sub ambient operation. DMA Q800 is capable of providing various modes of operation such as multi-frequency, multi-stress/strain, isostrain, creep/stress relaxation and controlled force/strain rate [54]. The system is

connected to a computer that runs TA instruments DMA software. The DMA software has the capability to control, acquire and analyze the data from the experiments. Fig 4.1 shows the TA instrument DMA Q800 system.

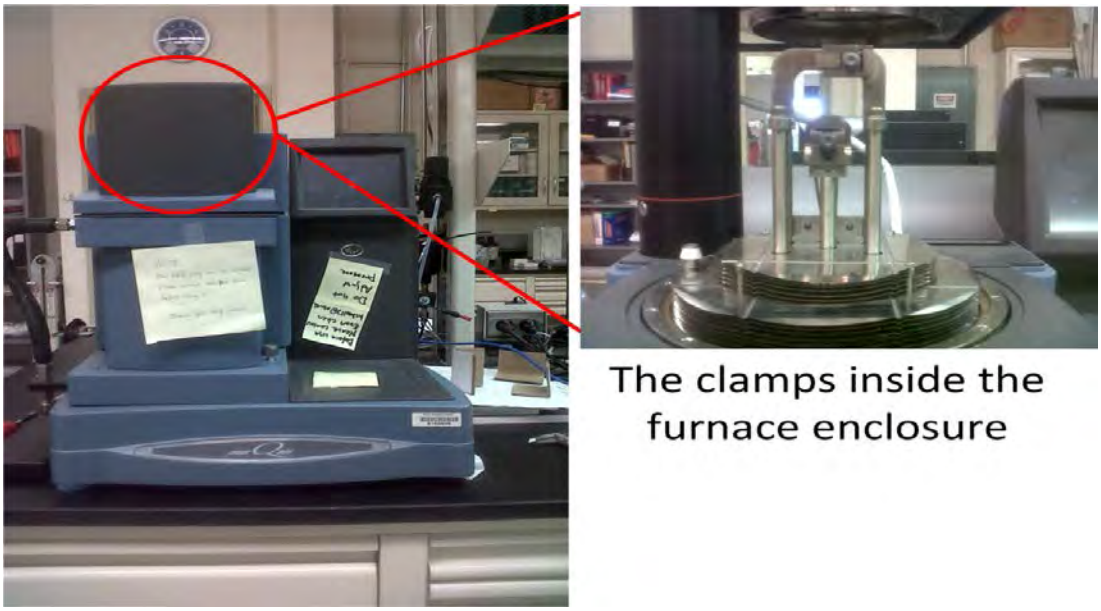

Figure 4.1: The dynamic mechanical analysis test system

4.2 Test details and procedure

DMA was performed on the samples with the help of TA instruments DMA Q800. The objective was to quantify the reduction in storage modulus with temperature and determine glass transition temperature of the samples. The mode of deformation chosen was the dual cantilever bending mode and dual cantilever clamps were installed. The samples were secured by the clamps with the help of a torque wrench set at 9 in-lbs. The mode of operation was multi-frequency mode at fixed frequency. An oscillating force of fixed frequency and amplitude 1 Hz and 20 µm respectively was applied perpendicular to the direction of the carbon fibers in the sample. A furnace covering the stage area holding the clamps achieved the heating of samples. The samples were heated from Ambient - 300^{o}C with a temperature ramp rate of 5^{o}C/min. The instrument and the clamps were calibrated in order to ensure accuracy of the data collected. The instrument and clamp calibration report is given in the Table 4.1 and 4.2 respectively. Several samples, prior to the DMA experiments, were heat treated at 125^{o}C, 175^{o}C and 250^{o}C for 120 hours in a muffle furnace. Data analysis was done with the help of TA instruments DMA software.

Table 4.1: DMA instrument calibration report

Type	Residual
Electronics	0.00007
Force	0.0029
Dynamic	0.0068
Position	Calibrated

Table 4.2: Clamp calibration report

Type	Mass	Offset	Compliance	Size
Dual Cantilever	29.5 gm	0.00 mm	0.181 µm/N	35 mm

1. DMA of untreated/ virgin samples - DMA with the conditions discussed above were performed on three untreated samples. The storage modulus and glass transition temperature of untreated samples were taken as the average of the three samples. One virgin sample was sent to Cambridge Polymer Group, Boston for DMA to determine the storage modulus variation with temperature of the sample. The result was received and is reproduced in appendix B.
2. DMA of heat treated samples – Twelve heat treated samples, with four samples in each heat treated batch (125^{o}C, 175^{o}C and 250^{o}C), were subjected to DMA with the above conditions. The storage modulus and the glass transition temperature values obtained for 125^{o}C, 175^{o}C and 250^{o}C heat treated samples were averaged from the values of the four samples in each heat treated batch.

The data files gathered from the experiment were loaded into excel sheets and relevant graphs were plotted in MATLAB software. The data file includes information about storage modulus, loss modulus, temperature, and tan delta values. Fig 4.2 shows the experimental setup.

Figure 4.2: DMA experimental setup

4.3 Sample description

Samples were machined out from the carbon fiber/epoxy composite part of DRAKE size ACCC core and had rectangular dimensions. It measured 60 mm in length, 4 mm in width and 1.6 mm in height. Samples were checked for any surface defects prior to the experiments. The samples consist of unidirectional carbon fibers embedded in epoxy matrix. Fig 4.3 shows a carbon fiber fiber/epoxy composite sample from ACCC core.

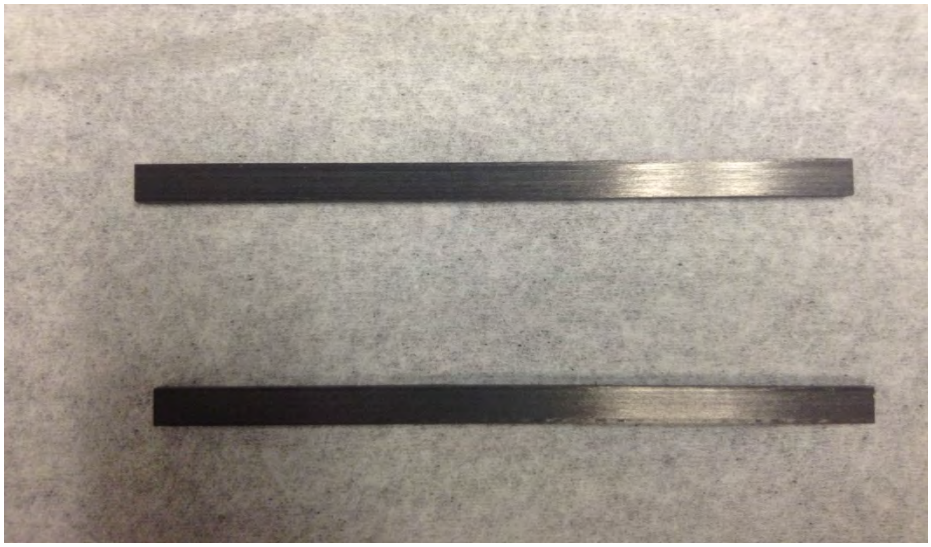

Figure 4.3: Carbon fiber/epoxy matrix samples from ACCC core

4.4 Results

Dynamic mechanical analysis provides the loss of storage modulus of ACCC carbon fiber/epoxy core with temperature. The loss in tensile strength of the ACCC carbon core from room temperature can be estimated from the storage modulus curve with temperature [38]. The error in the values between normalized storage modulus and normalized tensile strength of the conductor is normally less than 10% [38]. The peak of tan delta curve characterizes the glass transition temperature (T_g) of the sample. Fig 4.4 shows the loss in storage modulus and tan delta for the untreated samples. The graph shows the average values of storage modulus and tan delta of the three untreated samples. Similarly, the results of DMA on heat-treated samples are shown in Fig 4.5 – 4.7. Fig 4.8 compares the loss in storage modulus with temperature and the glass transition temperature (characterized by the peak of the tan delta curve) of the untreated and heat-treated samples.

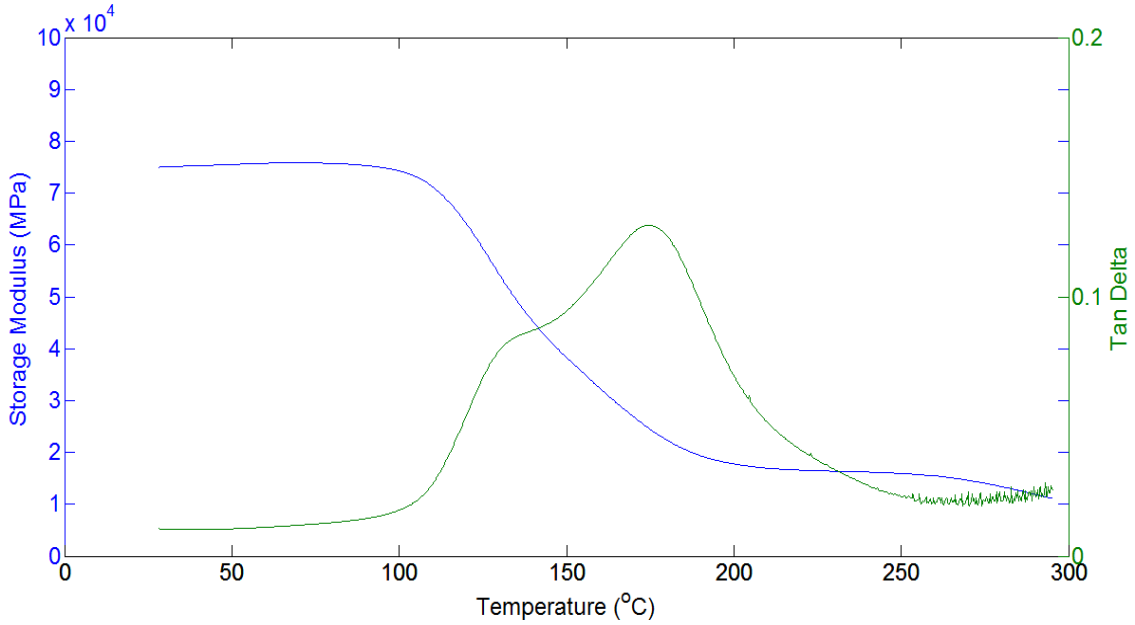

Figure 4.4: Storage modulus and tan delta of virgin samples

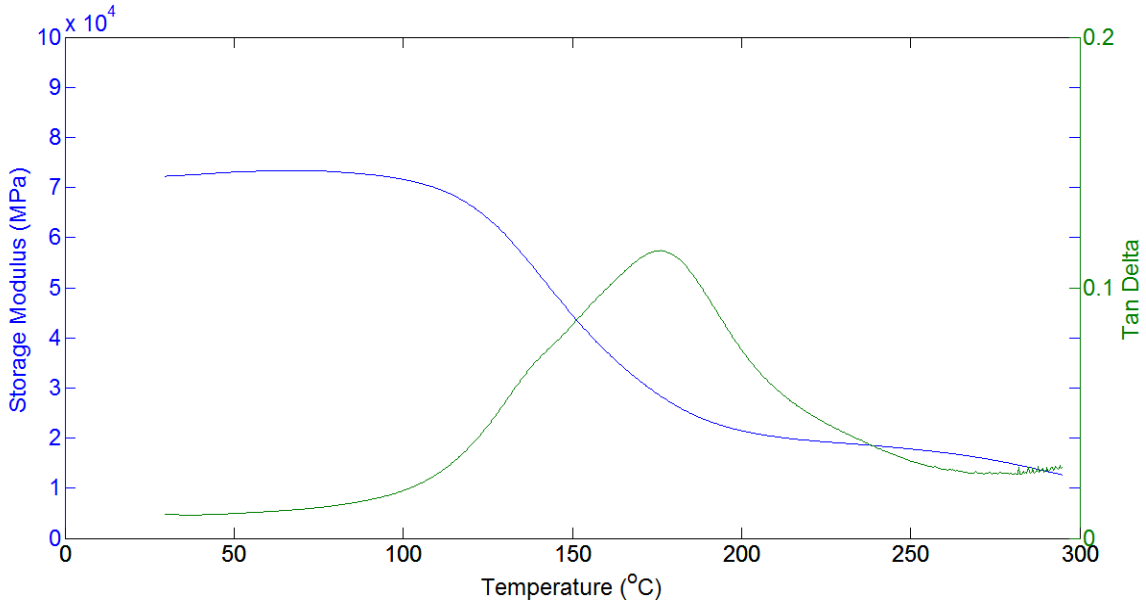

Figure 4.5: Storage modulus and tan delta of samples heat treated at 125°C

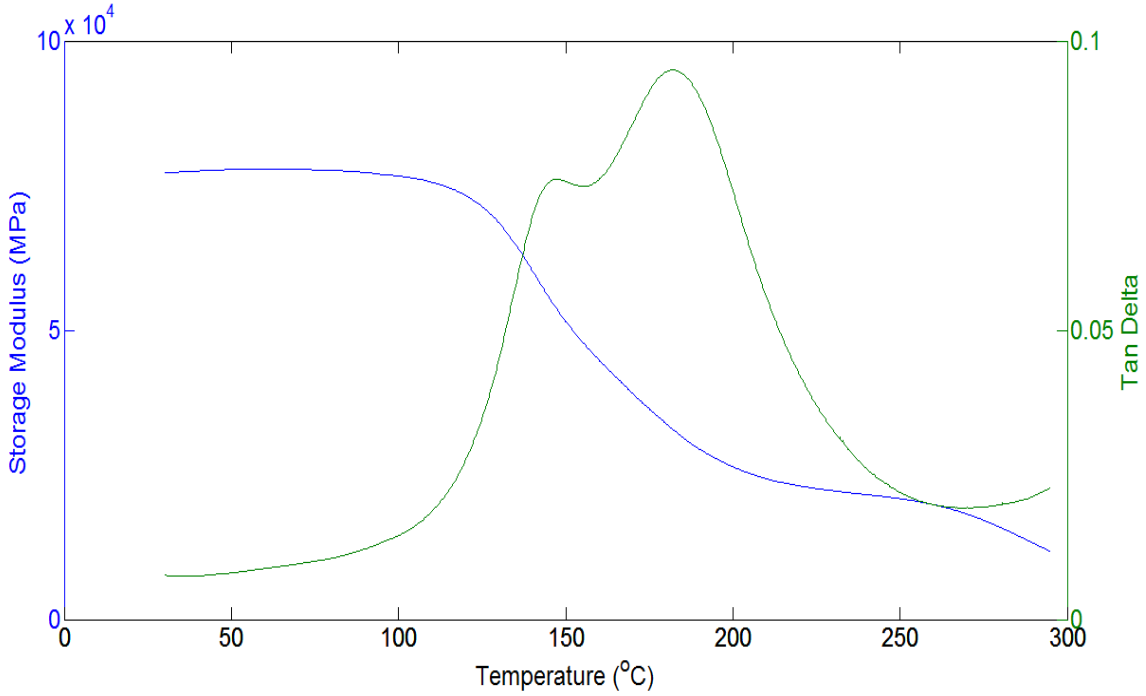

Figure 4.6: Storage modulus and tan delta of samples heat treated at 175°C

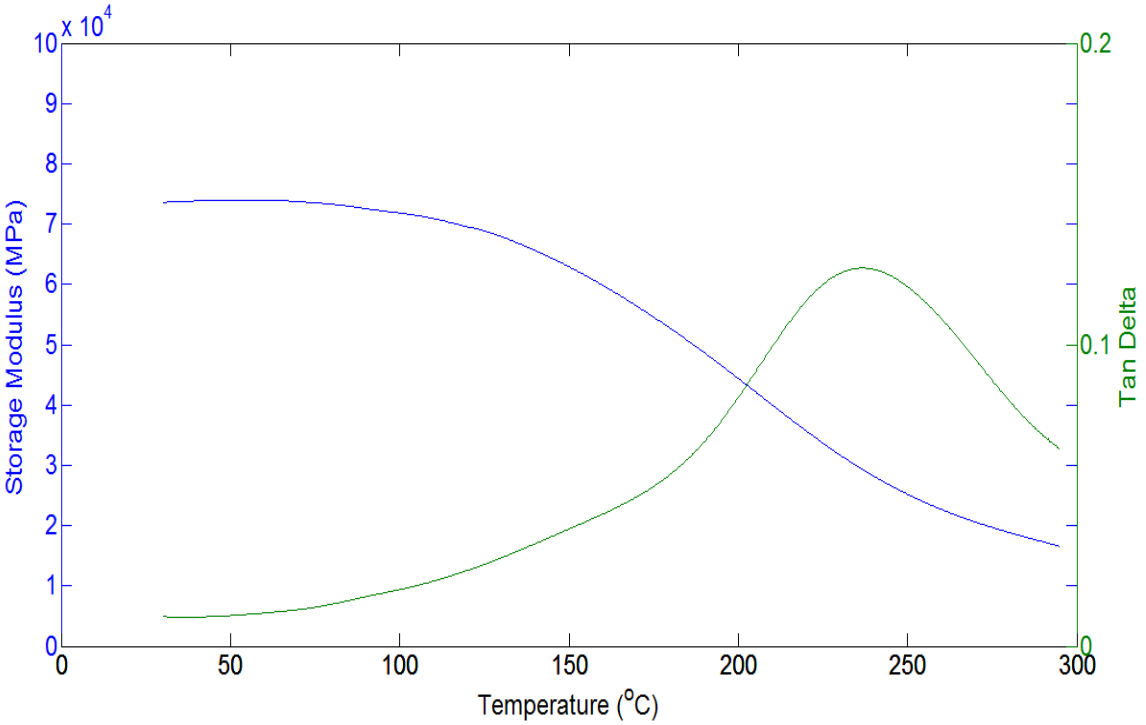

Figure 4.7: Storage modulus and tan delta of samples heat treated at 175°C

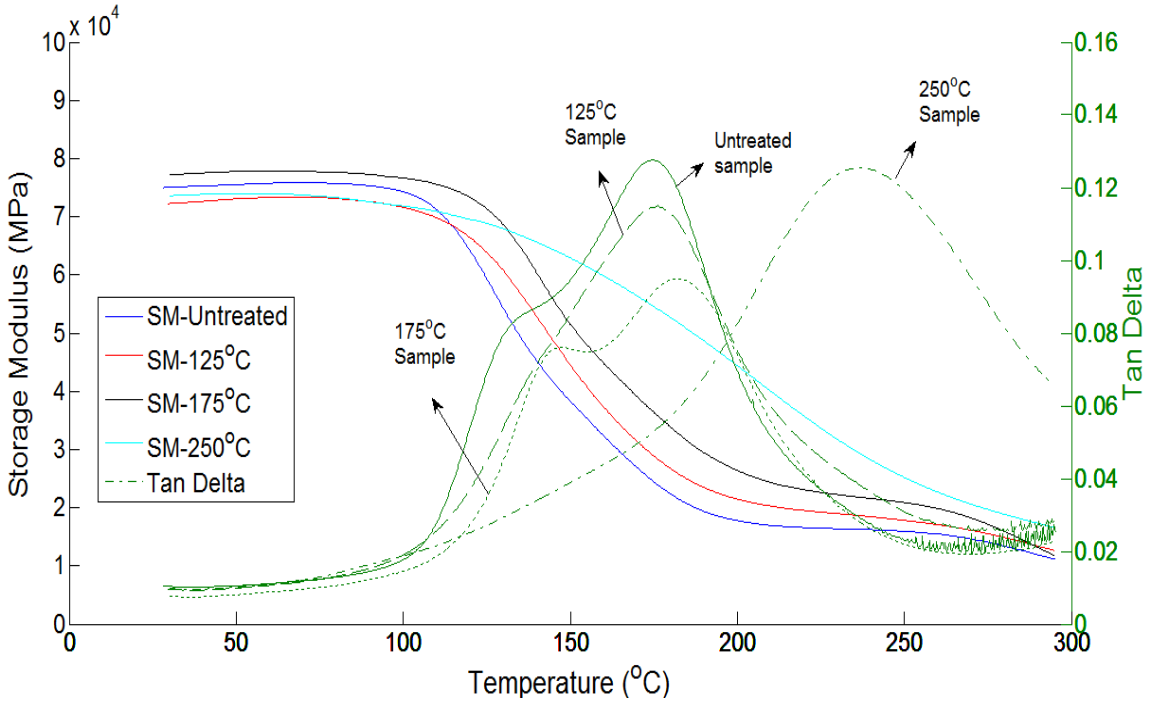

Figure 4.8: Comparison of DMA of untreated and heat – treated samples

DMA results of both untreated and heat treated samples, except 250°C heat-treated samples, indicate that the samples retain their storage modulus until 110°C -120°C. This is followed by a rapid drop in storage modulus in the temperature range of 120°C - 200°C. The storage modulus plateaus after 200°C, which is followed by another drop in storage modulus after 250°C. For the 250°C heat-treated samples, the storage modulus is retained until 130°C. The decline of storage modulus for 250°C heat-treated samples is gentler compared to untreated and other heat treated samples. Fig 4.8 indicates that the slope of decline in storage modulus is the sharpest for the untreated samples and decreases progressively as the degree of heat-treatment of the samples increases. Fig 4.8 also show that the glass transition temperatures shift towards higher temperatures with increasing order of heat treatment of the samples. The observed shift in the glass transition temperature can be explained by considering that the epoxy matrix of the untreated sample is not fully cured. Heat treatment of the samples increased the cross linked density of the matrix which raises the glass transition temperature. This is called post curing of epoxy [46], [55], [56]. Here, the heat treatment caused post curing of the epoxy matrix in the sample.

The glass transition temperature reflects the cure temperature if the cure temperature is less than the glass transition temperature of the fully cured network [56]. The cure plot of epoxy is available in reference [56]. However, if the cure temperature is greater than the glass transition temperature of the fully cured network of epoxy matrix, then the observed glass transition temperature would be less than the cure temperature [56]. Thus, three cases for the epoxy matrix, having a fully cured glass transition temperature of T_{Ginf}, cured or heat treated at T_o are described:

1. T_o less than T_{Ginf} – In this case, Tg becomes equal to To. As To increases, the Tg of the network correspondingly increases.
2. To equal to TGinf – In this case, Tg becomes equal to TGinf.
3. To is greater than TGinf – In this case, Tg is less than To. As To increases, the Tg of the network correspondingly decreases and vice versa. Degradation of the cross-link of the epoxy matrix takes place.

It is important to note here that the cross-linked network of epoxy eventually reaches full cure in a long time at ambient conditions [56]. Cure temperatures accelerate the process [55], [56]. The fact that the glass transition temperature increases after heat treatment of the samples shows that the epoxy matrix in the samples was not fully cured. From Fig 4.4, it can be seen the untreated samples had two tan delta peaks at around 132°C and 174°C. This indicates two polymerization reactions. For 125°C heat-treated samples, the glass transition temperature was 176°C approximately. This is almost equal to the glass transition temperature of the untreated samples. The glass transition temperature was 182°C for 175°C heat-treated samples. The glass transition temperature for 175°C heat-treated samples was greater than 175°C because of a small amount of additional post curing induced due to temperature scan until 300°C during DMA. However, for 250°C heat-treated samples, the glass transition temperature was 238°C, which is less than the post cure temperature (250°C). This shows that the heat treatment temperature of 250°C was more than the glass transition temperature of the fully cured network for epoxy matrix. Since the glass transition temperature of 250°C heat-treated samples was close to the temperature of heat treatment (250°C), the glass transition temperature of the fully cured network of the epoxy matrix of the samples was approximately 250°C.

4.5 Analysis

The results obtained from the DMA experiments were analyzed to quantify the loss of storage modulus (hence tensile strength of the ACCC composite core) with temperature. Table 4.3 summarizes the results for the DMA experiments and provides the loss of storage modulus (hence tensile strength) of the untreated and heat-treated samples at 125°C, 175°C and 250°C. The heat-treated samples retained their storage modulus (hence tensile strength) at ambient conditions after the heat treatment. The loss of storage modulus for untreated samples operating at 125°C, 175°C and 250°C were more than heat-treated samples. Heat treatment (post curing) of samples at or above 125°C improved the storage modulus (hence tensile strength) characteristics, which can be attributed to increased cross-link density of the polymer due to post curing [55], [56].

Table 4.3: Summary of the DMA results

Tempera-ture (°C)	Storage Modulus (°C)				Reduction in Storage Modulus (%)			
	Untreated Sample	Heat Treated Samples			Untreated Samples	Heat Treated Samples		
		125°C	175°C	250°C		125°C	175°C	250°C
Ambient	74977	72237	77209	73584	-	-	-	-
125°C	59163	63768	71375	68827	21	11	7	6
175°C	24356	28865	36318	54563	67	60	53	25
250°C	15935	17813	20873	25185	78	75	73	65

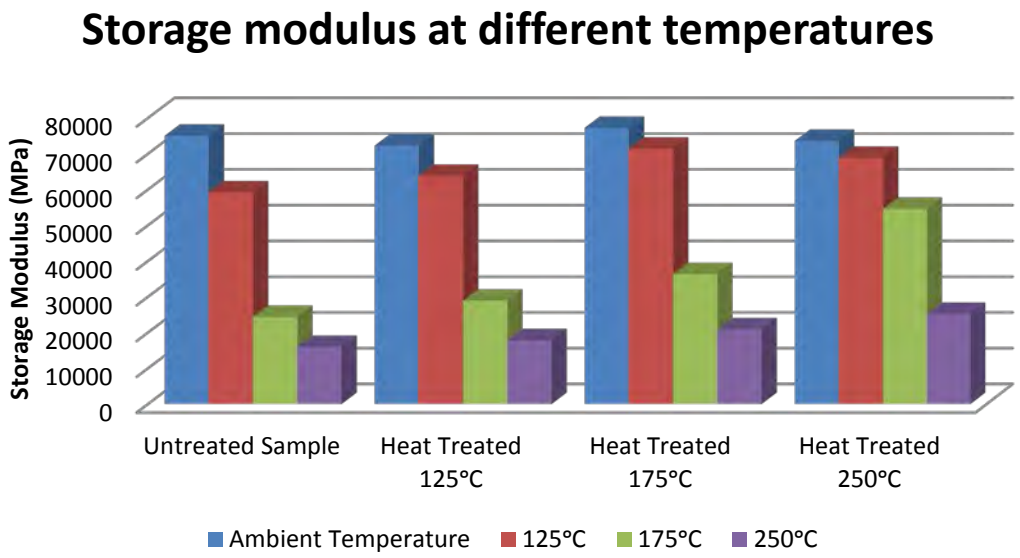

Figure 4.9: Graph showing storage modulus at different temperatures for the untreated and heat – treated samples

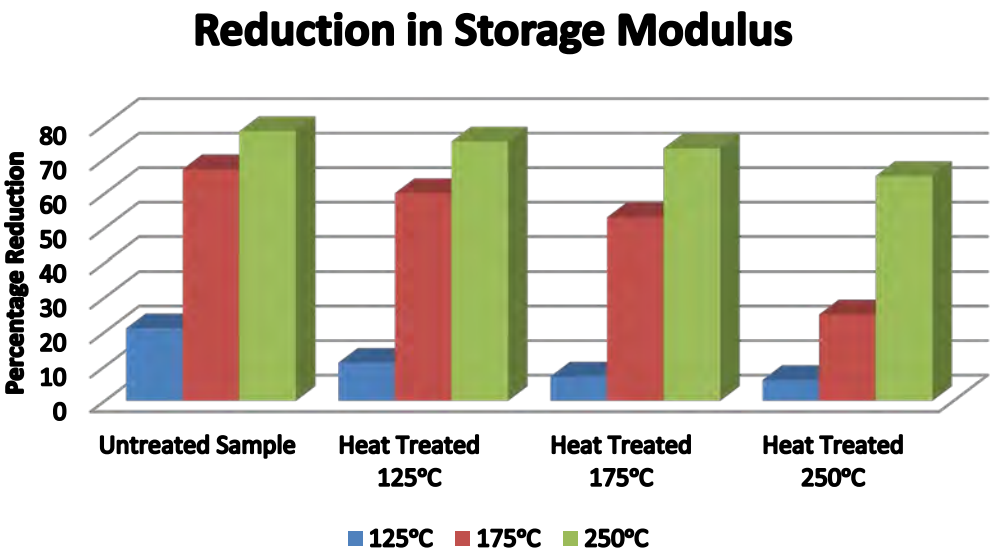

Figure 4.10: Graph showing reduction in storage modulus (hence tensile strength) at different temperatures for the samples

Equation (1.1) gives the relationship between the storage modulus of the carbon fiber/epoxy core and the tensile strength of the hybrid core of glass-carbon fiber/epoxy. The tensile strength of DRAKE size ACCC carbon core is 153.8 kN [11]. Thus, according to Table 4.3, the tensile strength of the DRAKE size ACCC carbon core will be around 81.5 kN, if the conductor is continuously operating at 175°C without any previous history of the conductor being subjected to temperatures above 175°C. This is a reduction around 50%. Lastly, the results indicate that the glass transition temperature of fully cured epoxy matrix (T_{Ginf}) lies around 250°C. If the conductor is subjected to temperatures above T_{Ginf} for a long period (>120 hrs), then permanent degradation of fiber-epoxy interface may occur reducing the tensile strength of the conductor permanently.

5. Tensile Testing of Metal Matrix Cores

This chapter describes the tensile testing of ACCR metal matrix core. In order to understand the loss of tensile strength of ACCR core with temperature in laboratory, it is important to first test the loading of the core with appropriate gripping fixtures successfully. Custom grips were developed for the tensile testing of the ACCR core strand. Stress strain curve was also calculated from the load displacement curve of the metal matrix core specimen.

5.1 Development of custom gripping fixtures

A custom-made gripping fixture was developed for the tensile testing of the metal matrix core. The new grips work on the principle of friction force. It consists of three parts. The 3-D model of the custom grip is shown in Fig 5.1.

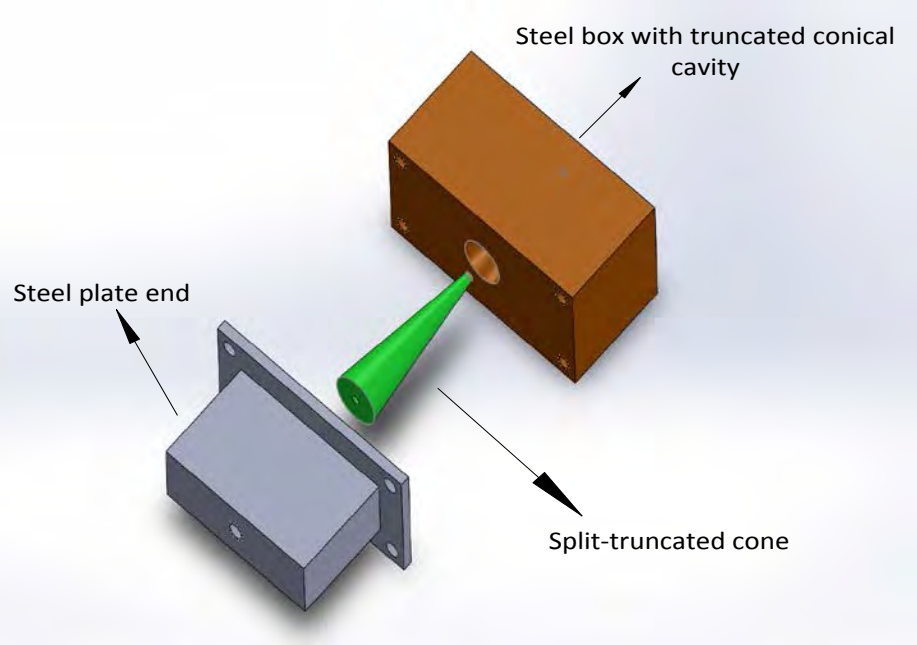

Figure 5.1: 3-D model of the custom grip

The first part is made up of a steel box of dimensions 80 mm x 40 mm x 40 mm with a truncated cone cavity in the middle of the steel box. The diameter of the smaller circle of the truncated cone cavity is 3 mm and is at the top face of the steel box. The angle of the cavity is approximately 10 degrees. Four to eight female portion of screw connectors of size/thread 10-32 were drilled at the bottom of the steel box. The second part consists of truncated cone split into two halves along its diameter. The smaller mouth has an inner diameter of 2.8 mm and the outer diameter of 3 mm. The angle of the truncated cone is 10 degrees. The interior portion of the two halves of truncated cone have semi cylindrical cavity of diameter 2.8 mm. This is shown in Fig 5.2.

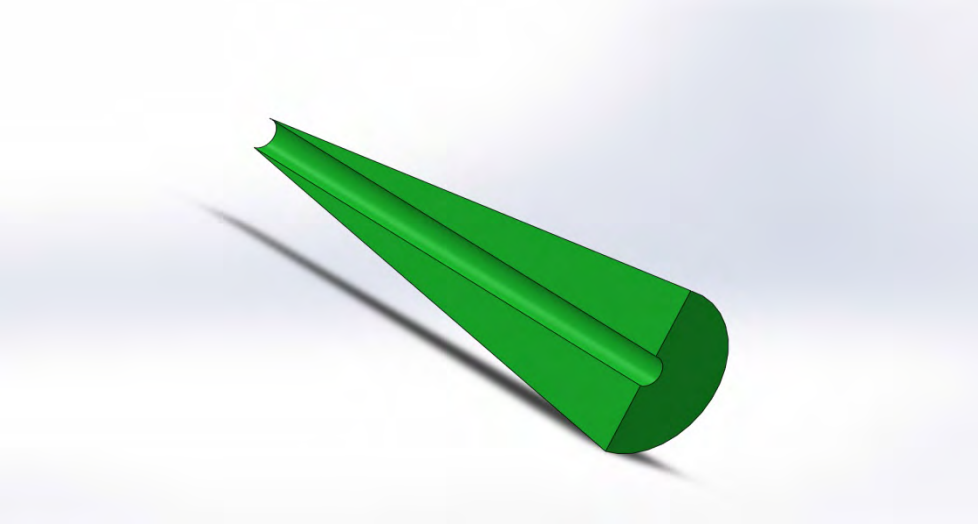

Figure 5.2: 3-D model of split truncated cone

The split-truncated cone wraps around and holds one end of the specimen. The third part consists of a steel plate of dimension 8cm x 4 cm x 0.35 cm with rectangular steel back of dimensions 60 m x 40 mm x 36.5 mm. The steel back contains the female portion of screw connector of size/thread ¼ - 20 that helps in connecting the gripping fixture to the load frame. The steel plate has eight clearance holes for screw size/thread 10-32. The two halves of the truncated cone with one end of the specimen fit together in the cavity of the steel box with a portion of the split-truncated cone protruding about 5 mm out from the bottom of the steel box. It is secured in the place by the steel plate pushing from the bottom with the help of four or eight screw size/thread 10-32. The force exerted by the steel plate on the split-truncated cone allows tight gripping of the specimen by compressing the top ends of the split truncated cones. The friction force between the specimen and the interior of the truncated cone holds the specimen in place.

5.2 Sample description

Specimens were alumina fiber/aluminum matrix composite rods obtained from the metal matrix core of ACCR composite conductor. The specimen rod was 2.3 mm in diameter and 127 mm long. The ultimate tensile strength of these metal matrix composite rods is approximately 1400 MPa [44]. Fig 5.3 shows the sample with the custom grips.

Figure 5.3: ACCR core strand sample held by the custom grips

5.3 Experimental setup

Tensile test on the metal matrix core strand was performed at room temperature using the INSTRON 4411 MTS test system [57]. The system consists of a load frame and a control console. The load frame provides tension or compression force to the specimen mounted on it. Control console performs calibration and controls the test with the help of feedback control systems. The test setup conditions are inputted through the front panel attached to the load frame. The load frame have cross-head drive motor, which applies tension or compression by moving the crosshead upwards or downwards. A load transducer measures the applied load on the specimen. A general purpose instrument bus (GBIP) provides for data connection with a personal computer. The GBIP conforms to the IEEE 488 interface standard. The schematic diagram of the experimental setup is shown in Fig 5.4.

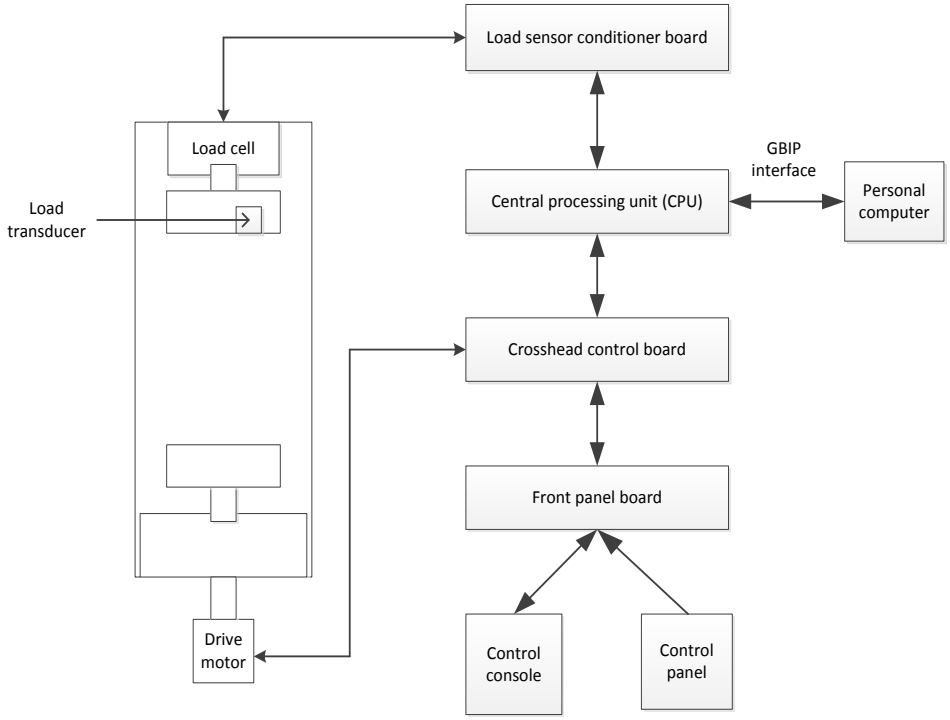

Figure 5.4: Schematic diagram of the INSTRON 4411 test system

Figure 5.5: The INSTRON 4411 MTS system interfaced to a personal computer

5.4 Test details and procedure

Tensile test of ACCR metal matrix core was performed using INSTRON testing machine with 5 kN load cell at room temperature. The specimen was loaded in the custom gripping fixture that was then secured to the load frame and is shown in Fig 5.6. The gauge length

of the specimen was 1.89 inches. The crosshead speed was set at 2 mm/min and a data rate of 5 pts/sec was enabled by the machine's data acquisition system. The test was carried out until the machine reached its maximum load limit of 5 kN. The load – displacement results was used to calculate the stress-strain curves of the specimens. The initial test was conducted with the grips having only four screws on each fixture. This lead to reduced friction between the sample and the grips since the force on the truncated cones by the steel plate was not enough. The result was slippage of the sample inside the gripping fixtures.

Figure 5.6: Specimen mounted on the load frame with the custom grips

Figure 5.7: Specimen loaded at 5 kN with the help of the custom gripping fixtures on the test frame

The custom grips were fitted with four more screws in order to increase the force on the truncated cone by the steel plate. This increased the friction force between the specimen and the interior of the truncated cone. In the subsequent test, the specimen was successfully loaded to 5 kN. Fig 5.7 shows the metal matrix core specimen successfully loaded to 5kN.

5.5 Results

Load displacement graphs were obtained from the tensile tests. The load displacement plots are given in Fig 5.8 and 5.9. In the first test, slippage of the specimen occurred inside the gripping fixture. This problem was addressed by introducing another four new screw connectors between the steel box and the plate in order to increase the force on the truncated cone. Thus, the total number of screw connectors for the grips in the second test was eight. This resulted in increase of friction force on the specimen. The tensile test data for the two tests are given below in Table 5.1.

Table 5.1: Tensile test data for ACCR core strand specimen

Parameter	Test 1	Test 2
Maximum load, kN	3.48	5
Maximum displacement, mm	26.03	2.13
Modulus of elasticity, GPa	-	62.34

5.6 Analysis

The test data were analyzed to produce the stress-strain plot for the test 2, in which the specimen was successfully loaded to 5 kN. The stress strain plot for test 2 is given in the Fig 5.10.

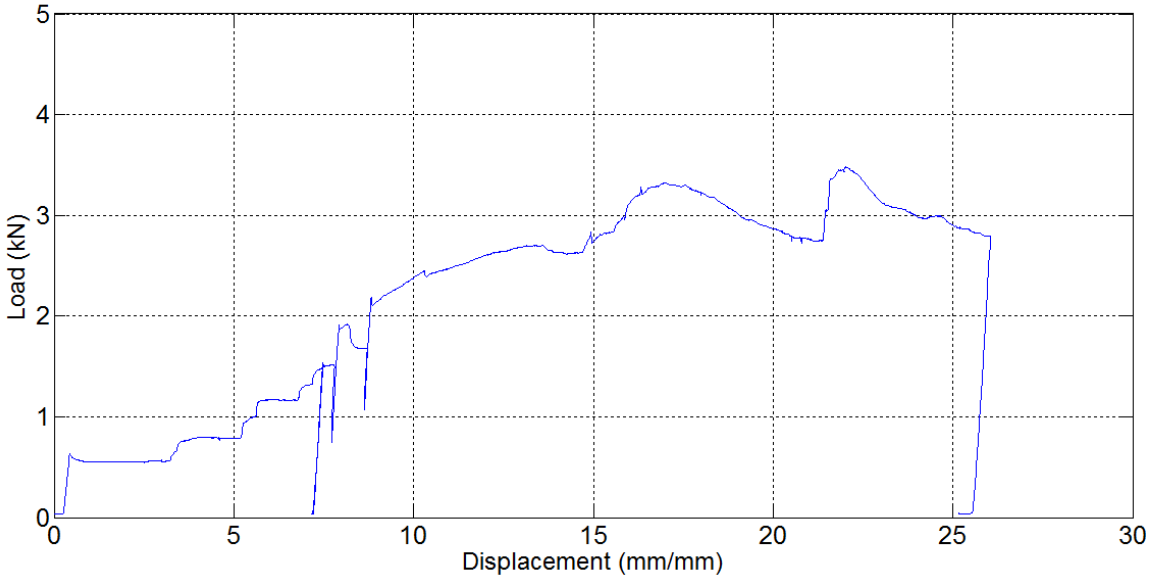

Figure 5.8: Load –Displacement plot for test 1

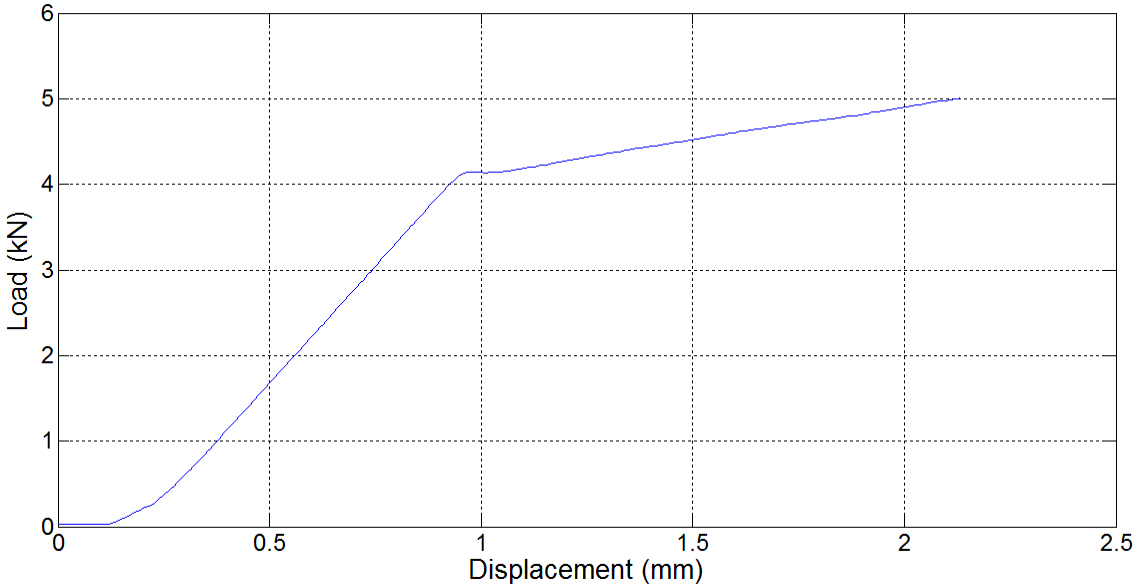

Figure 5.9: Load-Displacement plot for test 2

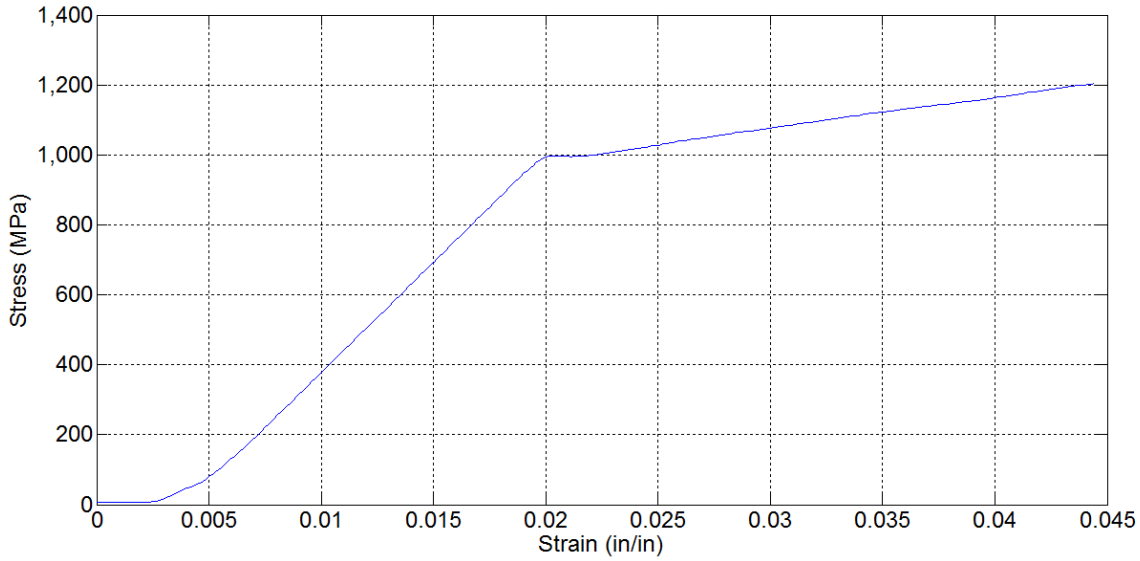

Figure 5.10: Stress-Strain plot for ACCR metal matrix core strand specimen in test 2

It is important to note that the stress vector is obtained by dividing the load vector with the cross sectional area of the specimen and the strain vector is obtained by dividing the displacement vector with the gauge length of the specimen. In literature, the reported value of tensile strength of ACCR metal matrix core strand at room temperature is approximately 1400 MPa [44]. The specimen was successfully loaded up to 1200 MPa. This corresponded to the maximum machine capability of 5 kN. Thus, further loading of the specimen was not possible. The elastic modulus of the ACCR metal matrix core strand was calculated as 62.34 GPa.

It can be seen from the stress strain plot that the slope changes at a strain of 0.02 mm/mm and corresponding to a stress of 1000 MPa. This change of slope can be due to the physical changes in aluminum matrix, which is a ductile material. Ductile material exhibits a yield point as opposed to brittle material [58]. The alumina fibers in the conductor are brittle material and the aluminum matrix is ductile. The change of slope may thus represent the yield point of the specimen. At the yield point, microplasticity occurs in the matrix that can be characterized by stress concentration in the matrix near sharp ends of the fiber [59]. However, the change of slope can also be explained by a small amount of slippage of the specimen in the gripping fixtures. Slippage of the specimen can be remedied with the help of an abrasive material such as silicon carbide gel between the specimen and the interior of the truncated cone. This will increase the friction force and may prevent slippage.

6. Thermal Ratings and Current Temperature Relationship of HTLS Conductors

Current flowing through a conductor causes its temperature to rise. Temperature rise after a certain limit can cause thermal degradation of the conductor and may compromise its operation. Temperature rise affects the resistance, mechanical strength and thermal expansion of the conductor [20], [21]. Increased sag is a direct consequence of the temperature rise of the conductor due to increased power flow in the line. High temperatures can cause a conductor to sag below its sagging limit. The annealing of the conductor due to high temperatures causes loss of tensile strength [18]. In case of carbon composite core of HTLS conductors, high temperatures can cause degradation of the core, which may lead to loss of tensile strength of the conductor. Thus, the continuous current that a conductor can carry should be calculated so that the operating temperature it produces should not cause significant annealing or loss in tensile strength and sagging limits are not violated. Conservative ambient weather conditions is used in order to calculate the steady state thermal rating which allows for increased power flow during emergency conditions [21]. The conductor temperature depends on various other parameters, apart from heat loss due to current flow, such as convection heat loss, radiation heat loss and solar heat gain. Ambient weather parameters and conductor electrical resistance also play an important role in determining the conductor operating temperature. The conductor heat capacity contributes to the rate of rise of conductor temperature during transient conditions. In this chapter, IEEE 738-2006 [21] has been utilized to calculate the steady-state thermal rating and current temperature relationship of HTLS conductors. Transient operation of HTLS conductors has been studied with the help of IEEE 738 standard and fault current temperature relationships have been developed for ACCC and ACCR.

6.1 Steady-state thermal calculations

The steady state heat balance operation results in a steady operating temperature for the conductor at a given operating current assuming that the ambient weather parameters remain constant. The steady state heat balance operation depends on various heat loss and gain rates [21]. This has been described in the subsequent subsections.

6.1.1 Steady-state heat balance

The steady state heat balance equation shows that the sum of heat loss due to current flow and solar heat gain of the conductor balances the conductor heat loss due to convection and radiation. The convection heat loss depends on forced convection and natural convection. The steady-state heat balance equation for a conductor carrying a current I (A) and having a resistance R (Ω/m) at temperature T_c (°C) is given below:

$$q_c + q_r = q_s + I^2 R(T_c) \tag{6.1}$$

where:

q_c is the convection heat loss in W/m

q_r is the radiation heat loss in W/m

q_s is the solar heat gain in W/m

$I^2R(T_c)$ is the ohmic heat gain in W/m.

From equation (6.1), the current in the conductor is:

$$I = \sqrt{\frac{q_c + q_r - q_s}{R(T_c)}} \tag{6.2}$$

6.1.2 Forced convection heat loss

Convective heat loss is one of the major sources of heat loss from the conductor. Forced convection heat loss occurs when wind flow is present on the conductor. There are two equations which address the convection heat loss produced due to high and low wind speeds. For low wind speed the equation for the forced convection heat loss rate is:

$$q_{c1} = \left[1.01 + 0.0372\left(\frac{D\rho_f V_w}{\mu_f}\right)^{0.52}\right] k_f K_{angle}\left(T_c - T_a\right) \tag{6.3}$$

The equation for high wind speed is:

$$q_{c2} = \left[0.0119\left(\frac{D\rho_f V_w}{\mu_f}\right)^{0.6}\right] k_f K_{angle}\left(T_c - T_a\right) \tag{6.4}$$

where:

q_c is convection heat loss rate in W/m

D is the conductor diameter in mm

ρ_f is the air density in kg/m^3 at temperature T_f

V_w is the wind speed in m/s

μ_f is the dynamic viscosity of air in Pa-s at temperature T_f

k_f is the thermal conductivity of air in W/(m-°C) at temperature T_f

K_{angle} is the wind direction factor

T_c is the conductor temperature in °C

T_a is the ambient temperature in °C.

The temperature T_f, in degrees, is given by:

$$T_f = \frac{T_c + T_a}{2} \tag{6.5}$$

This is the temperature of the thin film around the conductor. The wind direction factor is given by:

$$K_{angle} = 1.194 - \cos(\phi) + 0.194\cos(2\phi) + 0.368\sin(2\phi) \tag{6.6}$$

where:
ϕ is the angle between the wind direction and the conductor axis, in degrees.

The wind direction factor can also be expressed in terms of the compliment of the angle between wind direction and the conductor axis.

$$K_{angle} = 1.194 - \sin(\beta) - 0.194\cos(2\beta) + 0.368\sin(2\beta) \tag{6.7}$$

where:
β is the angle between the wind direction and perpendicular to the conductor axis, in degrees.

6.1.3 Natural convection heat loss

The natural convection heat loss is shown below:

$$q_{cn} = 0.0205\rho_f^{0.5} D^{0.75}\left(T_c - T_a\right)^{1.25} \tag{6.8}$$

where:
D is the conductor diameter in mm
ρ_f is the air density in kg/m^3 at temperature T_f
T_c is the conductor temperature in °C
T_a is the ambient temperature in °C.

Natural convection occurs when there is no wind flowing around the conductor. The IEEE current-temperature standard [21] recommends using the higher value of convection heat loss obtained from forced convection heat loss equation and natural convection heat loss equation for conservative calculations. Vector sum of forced convection and natural convection values can be used but it is not conservative.

6.1.4 Solar heat gain

The solar heat gain imparts heat to the conductor and consequently raises its temperature. The solar heat gain rate depends on the angle of incidence of the sun, the projected area of the conductor, the absorptivity and the total heat flux received by the conductor. For conservative calculations, the angle of incidence is taken as 90 degrees. The solar heat gain is:

$$q_s = \alpha_{ab} Q_{se} \sin(\theta) A' \tag{6.9}$$

where:
α_{ab} is solar absorptivity
Q_{se} is total heat flux received in W/m^2

θ is the angle of incidence in degrees
A' is the projected area of the conductor per unit length.

The angle of incidence is calculated with the help of the following equation:

$$\theta = \arccos[\cos(H_c)\cos(Z_c - Z_L)] \tag{6.10}$$

where:
H_c is the altitude of the sun in degrees
Z_c is the azimuth of the sun in degrees
Z_L is the azimuth of the transmission line in degrees.

The azimuth of the transmission line is 90° or 270° for a line running in the east – west direction, whereas it is 0° or 180° for a line running in the north south direction [21].

6.1.5 Radiation heat loss

The conductor also loses heat through radiation, although to a lesser extent as compared to convection heat loss. The radiation heat loss is:

$$q_r = 0.0178 D \varepsilon \left[\left(\frac{T_c + 273}{100} \right)^4 - \left(\frac{T_a + 273}{100} \right)^4 \right] \tag{6.11}$$

where:
D is the conductor diameter in mm
ε is the emissivity
T_c is the conductor temperature in °C
T_a is the ambient temperature in °C.

6.1.6 Conductor resistance

For calculation of thermal ratings of the conductor, a linear function of the electrical resistance with temperature is considered. This is given in equation (6.12):

$$R(T_c) = \left[\left(\frac{R(T_H) - R(T_L)}{T_H - T_L} \right) \right] (T_c - T_L) + R(T_L) \tag{6.12}$$

where:
$R(T_c)$ is the resistance of the conductor at temperature T_c, in Ω
$R(T_H)$ is the resistance of the conductor at temperature T_H, in Ω
$R(T_L)$ is the resistance of the conductor at temperature T_L, in Ω
T_c is the conductor temperature in which new resistance is being calculated, in °C
T_H is the conductor temperature in which resistance $R(T_H)$ is given, in °C

T_L is the conductor temperature in which resistance $R(T_L)$ is given, in °C.

The function calculates AC electrical resistance. It is known that the electrical resistivity of common metals like aluminum increases in a non-linear fashion with temperature [21]. If the conductor temperature at which the resistance is desired lies between T_H and T_L, then the calculated resistance will higher than the actual resistance and thus will result in a conservative calculation. However, in most cases the error will be negligible. If conductor temperature, at which the resistance is desired, is higher than T_H, then the calculated resistance value would be lower than the actual resistance at that temperature. According to IEEE 738 standard [21], the resistance value for 1350 H19 aluminum strand at 500°C calculated from equation (6.12) is 5% lower than the actual value, when the resistance of the aluminum strand is given at 25°C (T_L) and 75°C (T_H).

6.1.7 Steady state ampacity rating for HTLS conductors

In this section, steady state thermal/ampacity ratings for HTLS conductors have been calculated with the help of a C++ program developed in Microsoft Visual Studio. The program employed the IEEE 738-2006 standard [21] for calculating the thermal steady state ratings. Table 6.1 outlines the input conditions for the program. The results for steady state ampacity rating of ACCR and ACCC for the conditions described in Table 6.1 is given in Table 6.2.

Table 6.1: Input parameters for thermal steady state rating

Input Parameters	ACCR	ACCC
Wind speed (m/s)	0.61	0.61
Conductor elevation (m)	0	0
Emissivity	0.5	0.5
Solar absorptivity	0.5	0.5
Ambient temperature (°C)	40	40
Maximum temperature (°C)	210/240	180/200
Latitude (°)	43	43
Conductor diameter (mm)	28.12	28.12
Angle between conductor axis and wind direction (°)	90	90
Day number	161	161
Solar hour	14	14
AC resistance at 25°C (Ω/mile)	0.112	0.089
AC resistance at 75°C (Ω/mile)	0.134	0.106

Table 6.2: Steady state ampacity rating of ACCR and ACCC conductors

Conductor type (DRAKE)	Steady state ampacity rating	
	Continuous operation	Emergency operation
ACCR	1645 A	1770 A
ACCC	1700 A	1820 A

The continuous operating temperature of ACCR is 210°C and of ACCC is 180°C. The emergency temperature of ACCR is 240°C and of ACCC is 200°C. It can be seen from Table 6.2 that the ampacity of ACCC is greater than ACCR at both continuous operating temperature and emergency temperature, even though the continuous operating and emergency temperatures of ACCC is lower than ACCR.

6.1.8 Current – temperature relationship of HTLS conductors

A C++ program was developed to compute the current-temperature relationship of ACCC and ACCR conductors. The program also calculated ACSR conductor current temperature relationship, which was plotted with the HTLS conductors for comparison. The approach prescribed in IEEE 738 standard [21] was followed in the program. Data of current temperature relationship of ACSR, ACCC and ACCR obtained from C++ program are plotted between percent current on x-axis and temperature on y-axis. The base current in the plots is the current rating of equivalent ACSR at 100°C. Different conductor sizes have been considered namely DRAKE, LAPWING and BLUEBIRD. The assumptions for the calculation of data are following.

1. Clear atmosphere is assumed.
2. Angle of incidence of the sun is taken as 90 degrees for conservative calculations.

The general input parameters are given in Table 6.3. Specific input parameters for DRAKE, LAPWING and BLUEBIRD size conductors are given in Table 6.4 -6.6. The current temperature relationships for these conductors are given in Fig 6.1-6.3.

Table 6.3: Input parameters for current-temperature relationship

Input Parameters	Value
Wind speed (m/s)	0.61
Conductor elevation (m)	0
Emissivity	0.5
Solar absorptivity	0.5
Ambient temperature (°C)	40
Latitude (°)	43
Angle between conductor axis and wind direction (°)	90
Day number	161
Solar hour	14

Table 6.4: Conductor specific (DRAKE) input parameters for current temperature relationship

Input parameters	ACSR	ACCR	ACCC
Conductor diameter (mm)	28.1	28.1	28.1
AC resistance at 25°C (Ω/mile)	0.117	0.112	0.089
AC resistance at 75°C (Ω/mile)	0.139	0.134	0.106

Table 6.5: Conductor specific (LAPWING) input parameters for current temperature relationship

Input parameters	ACSR	ACCR	ACCC
Conductor diameter (mm)	38.2	38.9	38.2
AC resistance at 25°C (Ω/mile)	0.0617	0.0576	0.0507
AC resistance at 75°C (Ω/mile)	0.0728	0.069	0.0595

Table 6.6: Conductor specific (BLUEBIRD) input parameters for current temperature relationship

Input Parameter	ACSR	ACCC
Conductor diameter (mm)	44.75	44.75
AC resistance at 25°C (Ω/mile)	0.0475	0.0387
AC resistance at 75°C (Ω/mile)	0.0554	0.0447

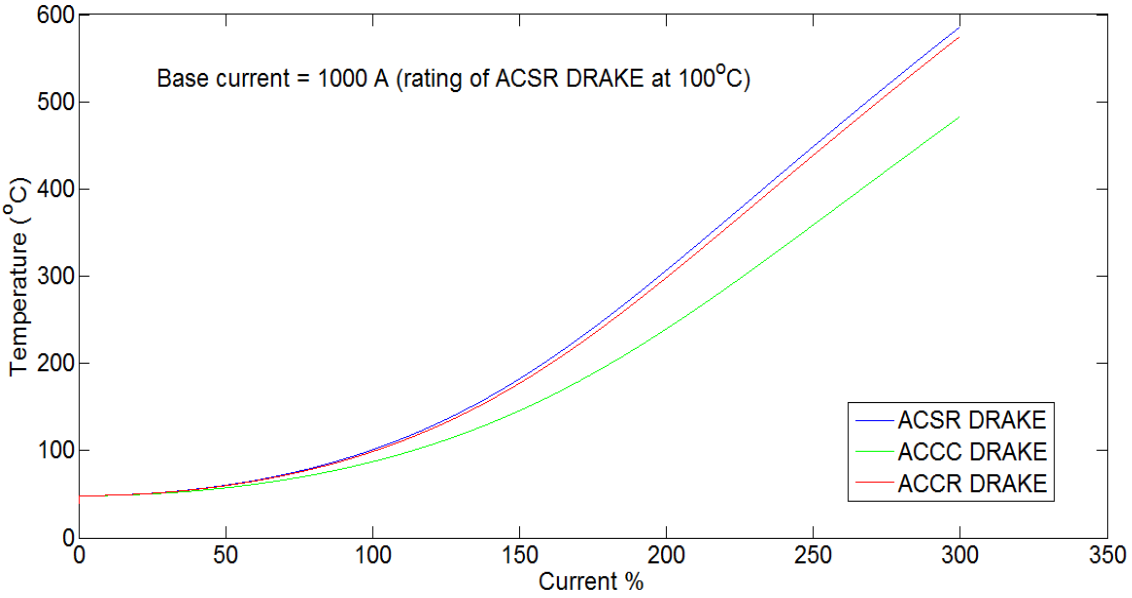

Figure 6.1: Current-temperature relationship of DRAKE sized conductors

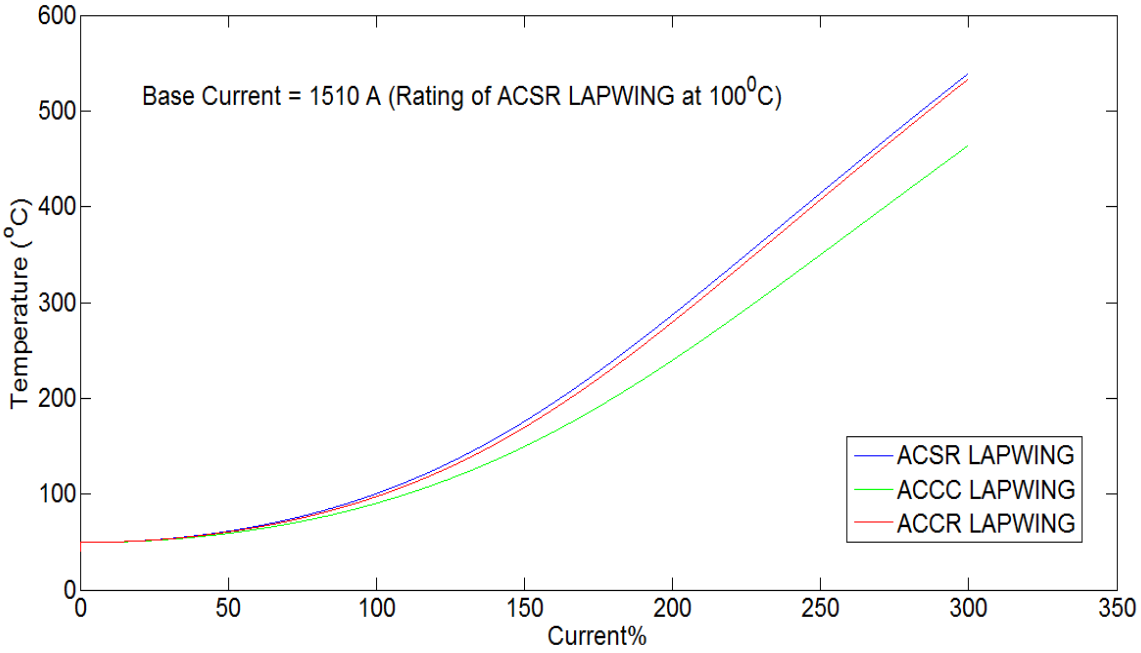

Figure 6.2: Current-temperature relationship of LAPWING sized conductors

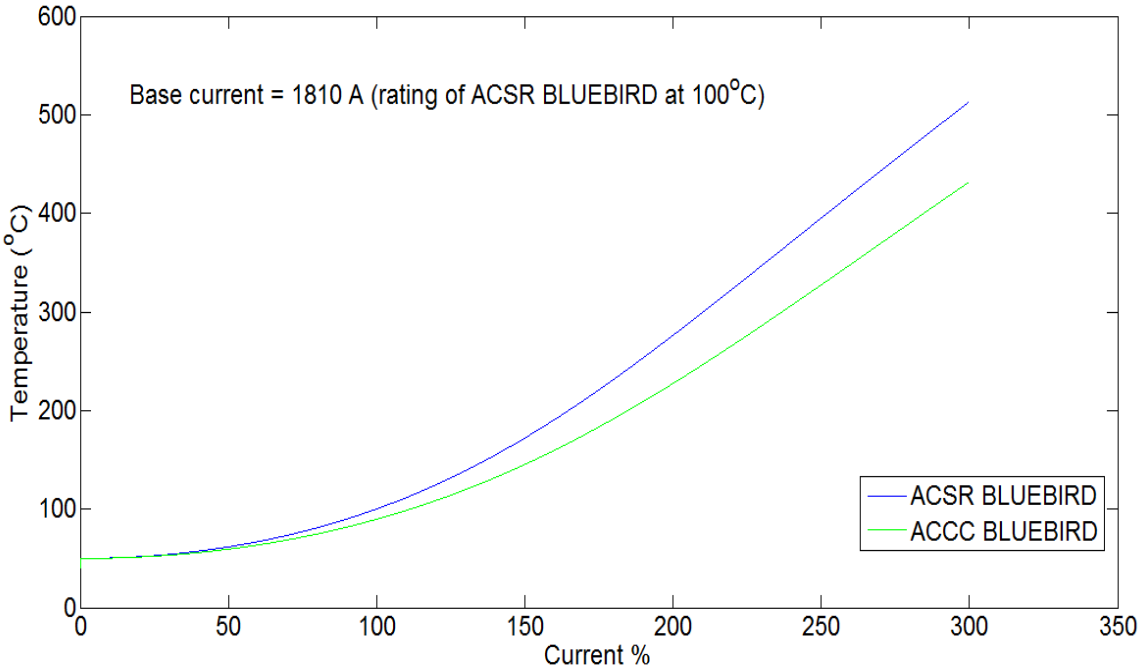

Figure 6.3: Current-temperature relationship of BLUEBIRD sized conductors

The current temperature relationship of the conductors reveals that in ACCC the temperature rise is low compared ACSR and ACCC at high temperatures in all the conductor sizes studied. ACCC has a superior current temperature relationship. The current

temperature curves for ACSR and ACCR is similar but ACSR is thermally limited to 100°C whereas ACCR can operate continuously until 210°C. Thus, ACCR can carry more current than equivalent ACSR conductor can.

6.2 Transient thermal calculations

Transient thermal calculations were used to obtain the fault current – temperature curves of ACCC and ACCR conductors. The methodology for obtaining transient conductor temperature outlined in the IEEE 738 standard [21] was followed. A C++ program in Microsoft Visual Studio was developed to achieve the fault current – temperature calculations. The effect of fault currents of the order of 10 kA – 80 kA on the conductors was studied.

6.2.1 Non-steady-state heat balance

The non-steady-state heat balance equation is used to model the conductor temperature change in response to a step change of current flowing through the conductor [21]. For fault currents, this step increase is very large from initial operating current to final fault current. The ambient weather conditions are assumed to remain constant during the process of temperature change due to step change in the current. The conductor heat capacity influences the rate of temperature change. Equation (6.13) gives the non-steady state heat balance equation for a conductor carrying a transient current I (A) and having a resistance R (Ω/m) at temperature T_c (°C):

$$q_c + q_r + mC_p \frac{dT_c}{dt} = q_s + I^2 R(T_c) \tag{6.13}$$

where:

q_c is the convection heat loss in W/m

q_r is the radiation heat loss in W/m

q_s is the solar heat gain in W/m

$I^2 R(T_c)$ is the ohmic heat gain in W/m.

mC_p is the conductor heat capacity in W-s/(m-°C)

From equation (6.13), the rate of change of conductor temperature can be calculated as:

$$\frac{dT_c}{dt} = \frac{1}{mC_p}\left(q_s + I^2 R(T_c) - q_c - q_r\right) \tag{6.14}$$

The total heat capacity of the conductor is taken as the sum of the heat capacities of its constituent material. The product of its specific heat and the mass per unit length gives the heat capacity of the constituent materials of the conductor. However, for fault current calculations, the heat capacity of the core of the conductor is generally neglected for fault durations less than 60 seconds [21].

6.2.2 Fault current – temperature relationship of carbon composite core based conductors

Fault currents flowing through a conductor can quickly raise its temperature beyond permissible limits. Generally, fault currents are cleared in 3 – 5 cycles by the primary protection of the system. However, if the primary protection fails, then the backup protection operates in 0.2 – 0.5 seconds [60]. As described above, a C++ program was developed for obtaining the temperature rise of conductors subjected to fault currents for any duration. This program was employed to give the temperature rise for DRAKE ACCC for fault currents of duration up to 5 seconds. The ambient weather conditions and the conductor material characteristics for DRAKE ACCC are given in Table 6.7.

Table 6.7: Input parameters for fault current-temperature relationship of DRAKE ACCC conductor

Input parameters	Values
Wind Speed (m/s)	0.61
Elevation (m)	0
Emissivity	0.5
Solar Absoptivity	0.5
Ambient Temperature (°C)	40
Latitude (°)	43
Conductor diameter (mm)	28.1
Angle between conductor axis and wind direction (°)	90
Day number	161
Solar hour	14
AC resistance at 25°C (Ω/mile)	0.089
AC resistance at 75°C (Ω/mile)	0.106
Heat capacity of aluminum conductor (W-s/m-°C)	1289.34

The aluminum conductor of ACCC is produced from 1350 O – tempered aluminum [11]. The mass per unit length of the aluminum in DRAKE ACCC conductor is 1.4326 kg/km [61]. This gives a heat capacity of 1289.34 J/(m-°C) for the calculations. The heat capacity of the core was neglected since the applied fault durations were less than 60 seconds in the simulation. Fault currents of 10 kA, 50 kA and 80 kA and duration up to 5 seconds were considered on DRAKE ACCC conductor operating initially at 125°C, 175°C and 200°C. The initial operating currents of the conductor are given in Table 6.8.

Table 6.8: Initial operating currents for DRAKE ACCC conductor

Temperature	Initial operating current
125°C	1354.08 A
175°C	1679.6 A
200°C	1813.33 A

Table 6.9 summarizes the results of the temperature rise on DRAKE ACCC conductor due to fault currents of 10 kA, 50 kA and 80 kA at different fault clearance times. Fig 6.4 gives the temperature rise for DRAKE ACCC conductor operating initially at 125°C, 175°C and 200°C under a fault current of 50 kA cleared in 0.55 seconds by backup protection. From the fault current – temperature relationship of DRAKE ACCC conductors, it can be concluded that:

1. If the fault current, of the order of 50 kA, is eventually cleared by the backup protection system, then the temperature in the conductor might rise above 250°C.
2. The temperatures (≥250°C) exceed the glass transition temperature of the fully cured network of the epoxy matrix (T_{Ginf}), thus damaging to the fiber-matrix interface and permanently degrading the tensile strength of the conductor.

Table 6.9: Summary of temperature rise of DRAKE ACCC under different fault currents

Fault current (kA)	Initial operating temperature (°C)	Temperature at fault clearance times (°C)				
		3 cycles	5 cycles	0.583 s	1 s	5 s
10	125	125.3	125.5	128.5	131	155
	175	175.4	175.5	178.8	182	210
	200	200.4	200.6	204	206	235
50	125	132.5	137.5	222.5	310	2490
	175	185.5	189.3	286.5	384	2820
	200	209.1	215.1	318	420	2981
80	125	144	158	430.2	792	7897
	175	197.5	213	525	940	7898
	200	223.8	240.3	574	1004	7898

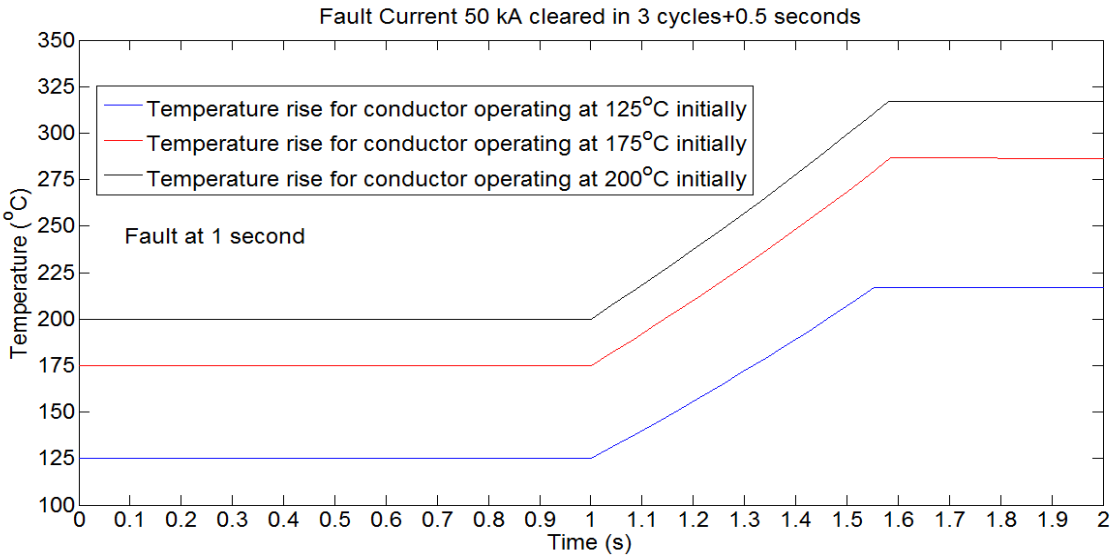

Figure 6.4: Fault current-temperature curves for DRAKE ACCC conductor

6.2.3 Fault current – temperature relationship of metal matrix core based conductors

Similar to the previous section, the temperature rise of metal matrix core based ACCR conductor due to fault currents was studied with the help of the developed C++ program. Ambient weather conditions and conductor characteristics, except the AC resistances and heat capacity of the aluminum conductor, given in Table 6.7 were considered. The value of AC resistance and heat capacity for DRAKE ACCR conductor considered in the calculations are given in Table 6.10. The initial operating currents of the conductor are given in Table 6.11.

Table 6.10: AC resistances and heat capacity of DRAKE ACCR conductor

AC resistance at 25°C (Ω/mile)	AC resistance at 25°C (Ω/mile)	Heat capacity of aluminum conductor (W-s/m-°C)
0.1126	0.1349	1062

Table 6.11: Initial operating currents for DRAKE ACCR conductor

Temperature	Initial operating current
125°C	1201.14 A
175°C	1488.47A
200°C	1606.36 A
240°C	1770 A

Table 6.12 summarizes the result of temperature rise on DRAKE ACCR conductor under fault currents of 10 kA, 50 kA and 80 kA of duration up to 10 seconds.

Table 6.12: Summary of temperature rise of DRAKE ACCR under different fault currents

Fault current (kA)	Initial operating temperature (°C)	Temperature at fault clearance times (°C)				
		3 cycles	5 cycles	0.583 s	1 s	10 s
10	125	125.4	125.7	131	135	227
	175	175.4	175.8	180.9	186	292
	200	200.5	200.9	206	210	257
	240	240.56	240.95	246	251	373
50	125	136.56	145	288	452	6225.7
	175	188.2	197	359	541	6225.7
	200	215	224	394	598.5	6225.7
	240	255	267	454	688.8	6225.7
80	125	155.4	177	700	1629.2	8626.8
	175	209	237	830	1888.6	8626.8
	200	237	261.5	893	1997.6	8626.8
	240	280	308	996	2209.3	8626.8

The conductor temperature reaches steady state within 10 seconds when exposed to a fault current of 50 kA or higher. Fig 6.5 gives the temperature rise for DRAKE ACCR conductor operating initially at 125°C, 175°C, 200°C and 240°C under a fault current of 50 kA cleared in 0.55 seconds by backup protection.

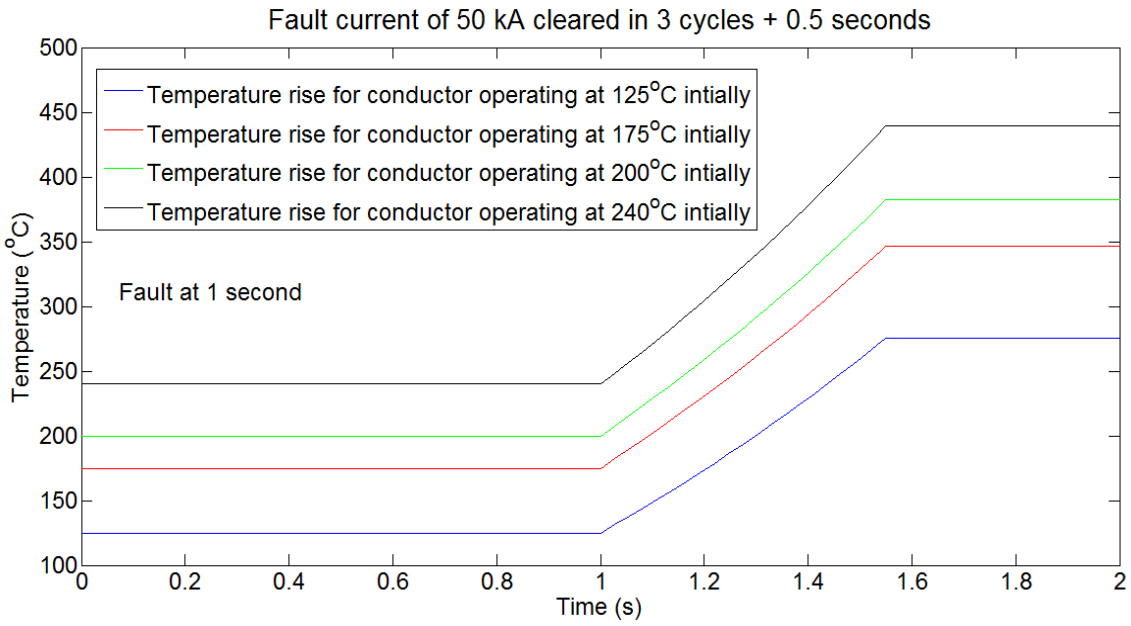

Figure 6.5: Fault current-temperature curves for DRAKE ACCR conductor

It can be seen from Table 6.12, the fault currents of the order of 80 kA can raise the temperature of DRAKE ACCR conductors above 650°C if the fault is cleared by backup protection in 0.583 seconds. The melting point of the aluminum matrix of ACCR is 650°C [59]. The alumina fibers of ACCCR conductor do not degrade in molten aluminum matrix since no chemical reaction occurs between alumina fibers and molten aluminum matrix [59]. However, it is important to investigate the residual strength of the conductor when the molten matrix solidifies after the clearance of the fault.

7. Conclusion and Future Work

7.1 Conclusions

The objective of this research is to characterize the mechanical properties of HTLS conductors with respect to temperature. HTLS conductors with carbon composite cores and metal matrix cores have been considered for the study. The work focused on the carbon composite core based conductors. Heat treatment of these conductor cores was performed to gauge the changes in its physical appearance and evolution of cracks with temperatures. Thermal mechanical analysis of the HTLS conductor cores provided information of its coefficient of thermal expansion. The loss of storage modulus (hence loss of tensile strength) of carbon composite cores with temperature was obtained with the help of the dynamic mechanical analysis. Dynamic mechanical analysis procedure provides a quick alternative to tensile testing of conductor at different temperatures to estimate the loss in tensile strength with temperature. The stress-strain behavior of metal matrix core was captured by conducting tensile testing. The current temperature relationships including fault currents for the HTLS conductors were developed using the IEEE 738-2006 standard. The programs were developed in C++ language in Microsoft Visual Studio suite. The calculations from these programs helped understand the set of conditions under which the conductors might accrue damage to its structure.

Chapter 2 described the heat treatment of carbon composite core based conductors. ACCC conductor core samples were exposed to isothermal environment at 125°C, 150°C, 200°C, 250°C and 300°C. The results of this experiment showed that the ACCC conductor core can operate continuously at 125°C without the development of cracks either on carbon fiber/epoxy matrix and also on the glass-carbon fiber/epoxy interface. No cracking on the glass fiber/epoxy was observed. Isothermal environment at 150°C and above led to cracks on the carbon fiber/epoxy as well as fracture of the glass-carbon interface. The cracks and fractures increased in severity at temperatures 250°C and above. Radial cracks extending from the edge of the glass fiber/epoxy matrix section of the core to the glass-carbon interface were observed at this temperature. The ACCC conductor is designed to operate continuously at a maximum temperature of 180 °C with an emergency temperature of 200°C. However, cracks and fractures on the core are present from at least 150°C.

In chapter 3, the coefficients of thermal expansion of the metal matrix and carbon composite core of HTLS conductors were evaluated with the help of thermal mechanical analysis. The variations of the coefficient of thermal expansion of the cores with temperature were studied. The average coefficients of thermal expansion were also calculated in the temperature range of RT- 300°C. The average coefficient of thermal expansion of the metal matrix core was calculated to be $6\times10^{-6}/K$. The average coefficient of thermal expansion of carbon fiber/epoxy section of the carbon composite core was calculated to be $(-0.731)\times10^{-6}/K$. The thermal expansion coefficient of the metal matrix core is much higher than that of carbon composite core.

In chapter 4, dynamic mechanical analysis of the carbon fiber/epoxy samples sectioned from ACCC core were performed. Several samples were heat treated prior to the experiments. The results indicated that the storage modulus (hence tensile strength) of the conductor core decreased about 65-70 % at 250 °C. Samples which were heat treated retained their storage modulus at room temperature after the heat treatment. The storage modulus characteristics improved with the degree of heat treatment of the samples, that is the rate of loss of storage modulus (hence tensile strength) with temperature decreased. This can be attributed to increased cross linked density of the epoxy matrix. However, the results showed that, the heat treatment at 250°C is just above the glass transition temperature of the fully cured network of the epoxy matrix. Thus, temperatures above 250°C will cause thermal degradation of the carbon composite core and reduce its mechanical strength by permanently damaging the fiber matrix interface.

In chapter 5, the tensile testing of metal matrix core was performed. The specimen, ACCC core strand was loaded successfully at 5 kN with the help of new custom grips. The custom gripping fixtures developed grips the sample with the help of friction force between the grips and the specimen. This friction occurs when the steel plate pushes on the split truncated cone, housing one end of the specimen, while it is inside the conical cavity of the steel box which compresses the upper end of the split truncated cone. This causes the split truncated cone to contact the specimen tightly and locks it down with the help of friction force. The stress strain curve of the metal matrix cone was also developed from the load displacement plot. The result indicated a presence of a yield point on the stress strain curve for the metal matrix core. The modulus of elasticity was calculated to be.

In chapter 6, the steady state thermal operation and transient thermal operation of metal matrix and carbon composite core based HTLS conductors were studied with the help of IEEE 738-2006 standard [21]. C++ programs were written in Microsoft Visual Studio to perform the calculations. The steady state thermal calculation yielded the current temperature relationships of the HTLS conductor and the transient thermal calculation provided the fault current temperature relationship. The current temperature relationship indicates that ACCC conductor have superior current temperature characteristics than ACSR and ACCR conductors. The fault current temperature relationships reveal that for DRAKE ACCC, the temperature can rise above 250°C for fault current of the order of 50 kA cleared in 0.58 seconds by the backup protection. This can cause thermal degradation and permanent damage to the matrix and fiber matrix interface. On the other hand, the temperature rise for DRAKE ACCR is above 650°C for fault currents of the order of 80 kA cleared by the backup protection in 0.58 seconds. This will cause melting of the aluminum matrix of the conductor core. This may affect the residual tensile strength of the conductor after the core cools.

7.2 Future work

The work done in this project focuses on the carbon composite core based HTLS conductors. Preliminary work has been done on the metal matrix core based conductor. Thus, much of the future research should be done in characterizing the metal matrix core based HTLS conductors. In this work loss of tensile strength of carbon composite core was

estimated with the help of dynamic mechanical analysis indirectly through storage modulus. Tensile testing of the carbon composite core should be performed in order to validate the results from the dynamic mechanical analysis of the core. More research is required to perform tensile testing of metal matrix core at different temperatures to quantify the loss of tensile of the core with temperature.

References

[1] U.S Energy Information Administration. *Annual energy outlook 2013 with projections to 2040*. April 2013, available at: http://www.eia.gov/forecasts/aeo/pdf/0383(2013).pdf.

[2] Chupka, M. W.; R. Earle, P. Fox-Penner and R. Hledik. *Transforming America's power industry: The investment challenge 2010-2030*. Nov. 2008, available at: http://www.eei.org/ourissues/finance/Documents/Transforming_Americas_Power_Industry_Exec_Summary.pdf.

[3] Harris Williams & Co. *Transmission & distribution infrastructure*. White Paper, Summer 2010, available at: http://www.harriswilliams.com/sites/default/files/industry_reports/final%20TD.pdf.

[4] Huntington, H. *Electricity demand outlook: Now and in the future*. Energy Modeling Forum Stanford University, December 2009, available at: http://www.ncsl.org/documents/energy/HHuntington1209.pdf.

[5] Alawar, A.; E. J. Bosze and S. R. Nutt. *A composite core conductor for low sag at high temperatures*. IEEE Transactions on Power Delivery, vol. 20, no. 3, pp. 2193-2199, July 2005.

[6] Lobry, J.; and D. Guery. *Theoretical study of dielectric breakdown in a new composite core HTLS conductor*. IEEE Transactions on Power Delivery, vol. 7, issue 4, pp. 1862-1867, October 2012.

[7] Torre, W. *Dynamic circuit thermal line rating*. October 1999, available at: http://www.energy.ca.gov/reports/2002-01-10_600-00-036.pdf.

[8] Cory, K. S.; and B. G. Swezey. *Renewable portfolio standards in the States: Balancing goals and implementation strategies*. Technical Report, NREL, December 2007, available at: http://www.nrel.gov/docs/fy08osti/41409.pdf.

[9] Dave, K.; N. Mohan, D. Xianda, R. Gorur and R. Olsen. *Analyzing techniques for increasing power transfer in the electric grid*. North American Power Symposium (NAPS), pp. 1-6, September 2012.

[10] Electric Power Research Institute. *Demonstration of advanced conductors for transmission lines*. Final Project Report, July 2008, available at: http://www.energy.ca.gov/2013publications/CEC-500-2013-030/CEC-500-2013-030.pdf.

[11] CTC Global. *ASTM conductor spec-sheets*. Available at: http://www.ctcglobal.com/images/uploads/main/ASTM_Conductor_Spec_Sheets.pdf.

[12] 3M Company. *Aluminum conductor composite reinforced technical notebook (795 kcmil family): Conductor and accessory testing*. Available at: http://multimedia.3m.com/mws/mediawebserver?mwsId=66666UuZjcFSLXTtN8Tt4xfEEVuQEcuZgVs6E%20Vs6E666666.

[13] Holman, J. *Increasing transmission capacity*. January 2011. Available at: http://windsystemsmag.com/article/detail/191/increasing-transmission-capacity.

[14] American Electric Power. *Notes on transmission facts*. Available at: http://www.aep.com/about/transmission/docs/transmission-facts.pdf.

[15] Public Service Commission of Wisconsin. *Notes on right-of-ways and easement for electric facility construction*. Available at: http://psc.wi.gov/thelibrary/publications/electric/electric02.pdf.

[16] Bonneville Power Authority. *Notes on project components and construction, operation and maintenance activities*. Available at: http://www.bpa.gov/Projects/Projects/I-5/draftEIS/DEIS%20Volume%201/Chapter%203%20Project%20Components.pdf.

[17] Gorur, R. S.; N. Chawla, J. Hunt and M. Dyer. *Mechanical and electrical issues concerning the use of composite materials for supporting core in transmission line conductors*. IEEE Conference on Electrical Insulation and Dielectric Phenomena, pp. 501-504, October 2006.

[18] Morgan, V. T. *Effect of elevated temperature operation on the tensile strength of overhead conductor*. IEEE Transactions on Power Delivery, vol. 11, issue 1, pp. 345-352, January 1996.

[19] General Cable. *Notes on TransPower® ACSR/TW bare overhead conductor*. Available at: http://www.stabiloy.com/NR/rdonlyres/5263D5D3-D512-4934-9F2F-5B0DE99F41BC/0/GC_pg114120_TransPwr_ACSR_TW.pdf.

[20] Douglass, D. A.; and R. Thrash. *Sag and tension of conductor*. In Electric Power Generation, Transmission and Distribution, L. L. Grigsby, Ed. Boca Raton: CRC Press, Ch. 14, pp. 1-42, 2012.

[21] IEEE Standard 738-2006. *IEEE standard for calculating the current – temperature of bare overhead conductors*. January 2007.

[22] Thrash, F. R. *Transmission conductors – a review of the design and selection criteria*. Available at: http://www.southwire.com/support/TransmissionConductoraReviewOfTheDesignandSelectionCriteria.htm.

[23] Harvey, J. R. *Effect of elevated temperature operation on the strength of aluminum conductors*. IEEE Transactions on Power Apparatus and Systems, vol. PAS-91, issue 5, pp. 1769-1772, September 1972.

[24] Bogner, B. R.; W. V. Breitigam, M. Woodward and K. L. Forsdyke. *Thermoset resins for pultrusion*. In Pultrusion for Engineers, T. F. Starr, Ed. Boca Raton: CRC Press, Ch. 4, pp. 97-174, 2000.

[25] Johnson, D. J.; T. L. Anderson and H. E. Deve. *A new generation of high performance conductors*. Power Engineering Society Summer Meeting, vol. 1, pp. 175-179, July 2001.

[26] Hunt, J.; et al. *Composite conductor field trial summary report: ACCR 795-SRP-Phoenix, AZ field trial*. 3M Company, 2006, available at:

http://multimedia.3m.com/mws/mediawebserver?mwsId=SSSSSufSevTsZxtUnx29ox_vevUqevTSevTSevTSeSSSSSS--&fn=ACCR795SRPFieldHED6-20-06.pdf.

[27] Springer, P. *477-kcmil 3M brand composite conductor evaluation of materials from ORNL field test*. 3M Company, 2004, available at: http://multimedia.3m.com/mws/mediawebserver?mwsId=66666UF6EVsSyXTtOxT6NXTcEVtQEVs6EVs6EVs6E666666--&fn=72%20-%20477%20ACCR%20Post%20ORNL.pdf.

[28] Springer, P. *1272-kcmil 3M™ composite conductor (ACCR) evaluation of materials from ORNL field test*. 3M Company, 2006, available at: http://multimedia.3m.com/mws/mediawebserver?mwsId=SSSSSuH8gc7nZxtUo8tSm8_1evUqe17zHvTSevTSeSSSSSS--&fn=69%20-%201272%20Post-ORNL.pdf.

[29] Hill, T. *Experience and benefits of using high temperature low sag (HTLS) overhead conductors*. 24th AMEU Technical Convention, October 2013.

[30] 3M Company. *Notes on customer installations*. Available at: http://solutions.3m.com/wps/portal/3M/en_US/EMD_ACCR/ACCR_Home/CustomerInstall/CustomerInstall/.

[31] Ishikawa, T.; K. Koyama and S. Kobayashi. Thermal expansion coefficients of unidirectional composites. Journal of Composite Materials, vol. 12, no. 2, pp.153-168, July 1978.

[32] Bowles, D. E.; and S. S. Tompkins. *Prediction of coefficients of thermal expansion for unidirectional composites*. Journal of Composite Materials, vol. 23, no. 4, pp. 370-388, April 1989.

[33] Kulkarni, R.; and O. Ochoa. *Transverse and longitudinal CTE measurements of carbon fibers and their impact on interfacial residual stresses in composites*. Journal of Composite Materials, vol. 40, no. 8, pp. 733-754, April 2006.

[34] Burks, B.; D. L. Armentrout and M. Kumosa. *Failure prediction analysis of an ACCC conductor subjected to thermal and mechanical stresses*. IEEE Transactions on Dielectrics and Electrical Insulation, vol. 17, issue 2, pp. 588-596, April 2010.

[35] McCullough, C. *Coefficient of thermal expansion for 477-T16 ACCR*. 3M Company, 2010, available at: http://multimedia.3m.com/mws/mediawebserver?mwsId=SSSSSufSevTsZxtUOY_UNxtvevUqevTSevTSevTSeSSSSSS--&fn=477%20Coeff%20of%20Thermal%20Expan.pdf.

[36] Kavanagh, T.; and O. Armstrong. *An evaluation of high temperature low sag conductors for uprating the 220 kV transmission network in Ireland*. 45th International Universities Power Engineering Conference (UPEC), pp. 1-5, September 2010.

[37] Composite Technology Corporation. *Development of stress – strain polynomials and creep parameters for ACCC/TW conductors*. February 2007, available at: http://www.powline.com/files/cables/ctc_conductors.pdf.

[38] Bosze, E. J.; A. Alawar, O. Bertschger, Yun-I. Tsai and S. R. Nutt. *High temperature strength and storage modulus in unidirectional hybrid composites*. Composite Science and Technology, vol. 66, issue 13, pp. 1963-1969, October 2006.

[39] Foreman, J. *Dynamic mechanical analysis of polymers*. American Laboratory, January 1997, available at: http://www.tainstruments.com/pdf/literature/TA236.pdf.

[40] Menard, K. P. *Dynamic mechanical analysis: A practical introduction*. Boca Raton: CRC Press, 2008.

[41] Nakada, M.; Y. Miyano, M. Kinoshita, R. Koga, T. Okuya and R. Muki. *Time-temperature dependence of tensile strength of unidirectional CFRP*. Journal of Composite Materials, vol. 36, no. 22, pp. 2567-2581, November 2002.

[42] CMS Resources. *Notes on dynamic mechanical analysis: a beginner's guide, Perkin Elmer*. Available at: http://www.perkinelmer.com/CMSResources/Images/44-74546GDE_IntroductionToDMA.pdf.

[43] TA Instruments. *Notes on measurement of the glass transition temperature using dynamic mechanical analysis*. Available at: http://www.tainstruments.com/pdf/literature/TS64.pdf.

[44] Rossoll, A.; B. Moser and A, Mortensen. *Tensile strength of axially loaded unidirectional Nextel 610™ reinforced aluminum: a case study in local load sharing between randomly distributed fibers*. Composites Part A: Applied Science and Manufacturing, vol. 43, issue 1, pp. 129-137, January 2012.

[45] Kar, N. K.; Y. I. Tsai, E. Barjasteh, E. J. Bosze and S. R. Nutt. *Accelerated aging and durability of composite rods for power transmission lines*. Available at: http://www.iccm-central.org/Proceedings/ICCM17proceedings/Themes/Industry/OTHER%20APPLICATIONS/A6.4%20Nutt.pdf.

[46] Barjasteh, E.; E. J. Bosze, Y. I. Tsai and S. R. Nutt. *Thermal aging of fiberglass/carbon-fiber hybrid composites*. Composites Part A: Applied Science and Manufacturing, vol. 40, issue 12, pp. 2038-2045, December 2009.

[47] Gorur, R.; B. Mobasher and R. Olsen. *Characterization of composite cores for high temperature low sag (HTLS) conductors*. PSERC Publication 09-05, July 2009.

[48] McCullough, C. *Thermal aging behavior and lifetime modeling for aluminum-zirconium alloy used in ACCR*. 3M Company, 2006, available at: http://multimedia.3m.com/mws/mediawebserver?mwsId=66666UgxGCuNyXTtOxT6Mxf_EVtQEcuZgVs6EVs6E666666--&fn=86%20-Aging%20StudyforAl-ZrWis.pdf.

[49] McCullough, C. *Accelerated thermal aging behavior for aluminum-matrix composite wire used in the core for ACCR*. 3M Company, 2006, available at: http://multimedia.3m.com/mws/mediawebserver?mwsId=66666UF6EVsSyXTtOxT6MxMtEVtQEVs6EVs6EVs6E666666--&fn=99%20-%20Accelerated%20Aging%20Study.pdf.

[50] Staszewski, L.; and W. Rebizant. *The differences between IEEE and CIGRE heat balance concepts for line ampacity considerations*. Proceedings of the International Symposium Modern Electric Power Systems (MEPS), pp. 1-4, September 2010.

[51] Barnstead Thermolyne Corporation. *High temperature muffle furnace operation manual and parts list*. Available at: http://www.nist.gov/ncnr/upload/E133thermolyne.pdf.

[52] Linseis Inc. *Thermal analysis dilatometer- and TMA- evaluation with MS-Windows*. Princeton Junction, NJ, January 1998.

[53] Linseis Inc. *Notes on Linseis – TMA/DMA L77*. Available at: http://www.linseis.net/html_en/thermal/tma/pdf/TMA_ENGISH.pdf.

[54] TA Instruments. *Q800 dynamic mechanical analysis brochure*. Available at: http://www.tainstruments.com/pdf/brochure/dma.pdf.

[55] Strong, A. B. *Understanding epoxies*. Brigham Young University, available at: http://strong.groups.et.byu.net/pages/articles/articles/epoxies.pdf.

[56] Carbas, R. J. C.; L. F. M. da Silva, E. A. S. Marques and A. M. Lopes. *Effect of post cure on the glass transition temperature and mechanical properties of epoxy adhesives*. Journal of Adhesion Science and Technology, vol. 27, issue 23, pp. 2542-2557, April 2013.

[57] Instron. *Instron model 4400 universal testing system user manual*. Available at: http://fab.cba.mit.edu/content/tools/instron/M10-94400-1.pdf.

[58] OptoMech. *Notes on stress-strain relationships, OPTI 222 Mechanical Design in Optical Engineering*. Available at: http://fp.optics.arizona.edu/optomech/references/OPTI_222/OPTI_222_W4.pdf.

[59] Chawla, N.; and K. K. Chawla. *Metal matrix composites*. New York: Springer, 2006.

[60] Glover, J. D.; M. S. Sarma and T. J. Overbye. *Power system analysis & design*. 5th ed. Delhi, India: Cengage Learning, 2012.

[61] Davies, J. R. *Aluminum and aluminum alloys*. J. R. Davies & Associates, ASM International, 1993.

Appendix 1: Thermal Mechanical Analysis Results

A.1 Calculations for coefficient of thermal expansion of ACCR metal matrix core.

The average coefficients of thermal expansion (CTE) for ACCR metal matrix core were calculated for each of the six tests. The change in length of the sample from room temperature to 300°C is also given. The calculations are given below:
Average CTE calculation for test 1:

$\Delta L = 16.52$ μm $\quad T_{ini} = 19.5$°C $\quad T_{final} = 300$°C

$$\alpha_1 = \frac{\Delta L}{L \Delta T} = \frac{16.52 \times 10^{-6}}{10.1 \times 10^{-3} \times 280.5} = 5.837 \times 10^{-6} / K \qquad \text{(A.1.1)}$$

Average CTE calculation for test 2:

$\Delta L = 16.72$ μm $\quad T_{ini} = 20.8$°C $\quad T_{final} = 300$°C

$$\alpha_2 = \frac{\Delta L}{L \Delta T} = \frac{16.72 \times 10^{-6}}{10.1 \times 10^{-3} \times 279.2} = 5.923 \times 10^{-6} / K \qquad \text{(A.1.2)}$$

Average CTE calculation for test 3:

$\Delta L = 17.78$ μm $\quad T_{ini} = 20.2$°C $\quad T_{final} = 300$°C

$$\alpha_3 = \frac{\Delta L}{L \Delta T} = \frac{17.78 \times 10^{-6}}{10.1 \times 10^{-3} \times 279.8} = 6.293 \times 10^{-6} / K \qquad \text{(A.1.3)}$$

Average CTE calculation for test 4:

$\Delta L = 15.81$ μm $\quad T_{ini} = 17$°C $\quad T_{final} = 300$°C

$$\alpha_4 = \frac{\Delta L}{L \Delta T} = \frac{15.81 \times 10^{-6}}{10.1 \times 10^{-3} \times 283} = 5.534 \times 10^{-6} / K \qquad \text{(A.1.4)}$$

Average CTE calculation for test 5:

$\Delta L = 16.4$ μm $\quad T_{ini} = 18$°C $\quad T_{final} = 300$°C

$$\alpha_5 = \frac{\Delta L}{L \Delta T} = \frac{16.4 \times 10^{-6}}{10.1 \times 10^{-3} \times 282} = 5.756 \times 10^{-6} / K \qquad \text{(A.1.5)}$$

Average CTE calculation for test 6:

$\Delta L = 17.58$ μm $\quad T_{ini} = 21$°C $\quad T_{final} = 300$°C

$$\alpha_6 = \frac{\Delta L}{L \Delta T} = \frac{17.58 \times 10^{-6}}{10.1 \times 10^{-3} \times 279} = 6.243 \times 10^{-6} / K \qquad \text{(A.1.6)}$$

A.2 Calculations for coefficient of thermal expansion of ACCC carbon composite core

3. The average coefficients of thermal expansion (CTE) for ACCC carbon composite core were calculated for each of the six tests. The change in length of the sample from room temperature to 300°C is also given. The calculations are given below:

Average CTE calculation for test 1:

ΔL = -2.23 μm T_{ini} = 17°C T_{final} = 300°C

$$\alpha_1 = \frac{\Delta L}{L\Delta T} = \frac{-2.23\times10^{-6}}{9.89\times10^{-3}\times283} = -0.799\times10^{-6}/K \qquad \text{(A.2.1)}$$

Average CTE calculation for test 2:

ΔL = -3.05 μm T_{ini} = 19.8°C T_{final} = 300°C

$$\alpha_2 = \frac{\Delta L}{L\Delta T} = \frac{-3.05\times10^{-6}}{9.89\times10^{-3}\times280.2} = -1.102\times10^{-6}/K \qquad \text{(A.2.2)}$$

Average CTE calculation for test 3:

ΔL = -0.54 μm T_{ini} = 17°C T_{final} = 300°C

$$\alpha_3 = \frac{\Delta L}{L\Delta T} = \frac{-0.54\times10^{-6}}{9.89\times10^{-3}\times283} = -0.193\times10^{-6}/K \qquad \text{(A.2.3)}$$

Average CTE calculation for test 4:

ΔL = -2.7 μm T_{ini} = 19.8°C T_{final} = 300°C

$$\alpha_4 = \frac{\Delta L}{L\Delta T} = \frac{-2.7\times10^{-6}}{9.89\times10^{-3}\times280.2} = -0.9744\times10^{-6}/K \qquad \text{(A.2.4)}$$

Average CTE calculation for test 5:

ΔL = -1.61 μm T_{ini} = 20.6°C T_{final} = 300°C

$$\alpha_5 = \frac{\Delta L}{L\Delta T} = \frac{-1.61\times10^{-6}}{9.89\times10^{-3}\times279.4} = -0.5836\times10^{-6}/K \qquad \text{(A.2.5)}$$

Appendix 2: Dynamic Mechanical Analysis Results

B.1 Cambridge polymer DMA results

Several carbon fiber/epoxy matrix samples sectioned out from the ACCC carbon core were sent to Cambridge polymer Inc. for DMA testing. The temperature ramp rate for the DMA testing was 5°C/min and dual cantilever clamps were employed. The torque wrench used to secure the clamps with the sample was set to 9 in-lb. The amplitude and frequency of the oscillating force were 20 µm and 1 Hz respectively. The temperature range under investigation was room temperature - 300°C. The storage modulus, loss modulus and the tan delta curve of the sample as a function of the temperature is given in Fig B.1.1. Table B.1.1 presents some corresponding data points for the curves.

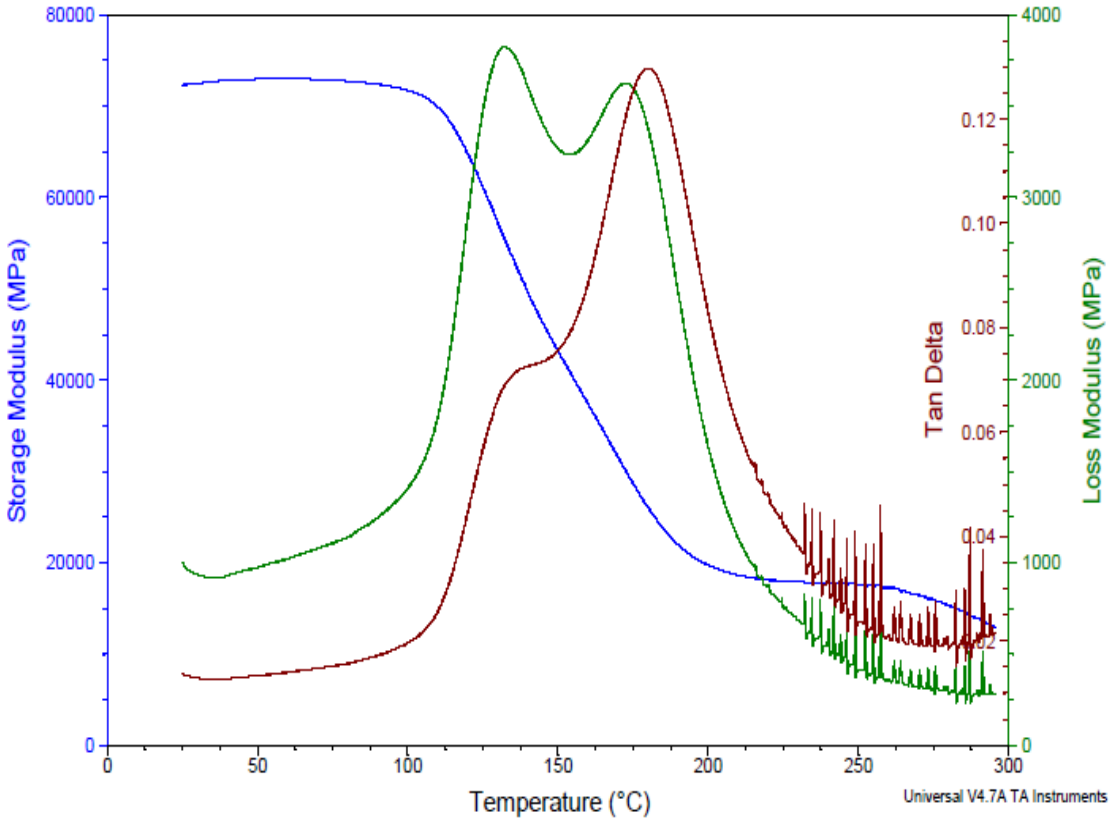

Figure B.1.1: Storage modulus, loss modulus and tan delta curves with temperature for untreated ACCC carbon fiber/epoxy sample

Table B.1.1: Storage modulus, loss modulus and tan delta at various temperatures

Temperature (°C)	Storage modulus (MPa)	Loss modulus (MPa)	Tan delta
75.05	72833	1108	0.02
132.12	55568	3825	0.07
172.60	30048	3625	0.12
250.12	17591	416	0.02

B.2 Standard deviation, relative standard deviation for storage modulus curves and tan delta values

The maximum, minimum and average standard deviation of the storage modulus curves obtained in the DMA tests for virgin and heat treated samples were calculated. The relative standard deviation of the storage modulus curves from these tests from the mean storage modulus curve is also presented. Similarly, the standard deviation and relative standard deviation of the values of tan delta peak gathered from the experiments is given here. Table B.2.1 and table B.2.2 provides the standard deviation and relative standard deviation values.

Table B.2.1: Minimum, maximum, average and relative standard deviation of the storage modulus curves

Type of sample	Minimum S.D (MPa)	Maximum S.D (MPa)	Temperature at minimum S.D (°C)	Temperature at maximum S.D (°C)	Average S.D (MPa)	Relative S.D (%)
Virgin sample	674	4485	295	139	2164.2	8.15
125°C sample	962.34	6405.8	294	30	3908.6	13.18
175°C sample	1510.9	5344	295	157	3076.1	9.1
250°C sample	1187.4	3964.7	295	145	3076	7.33

Table B.2.2: Tan delta mean, standard deviation and relative standard deviation of the tan delta values

Type of sample	Tan delta mean	Standard deviation	Relative standard deviation (%)
Virgin sample	0.1275	0.0023	1.8
125°C sample	0.1151	0.0087	7.56
175°C sample	0.095	0.0059	6.21
250°C sample	0.1254	0.0064	5.1

Intentionally Blank

Part II

The Economic Case for HTLS Overhead Conductor Designs

Gerald T. Heydt, Faculty
Askhat Tokombayev, Graduate Student

Arizona State University

For information about Part II, contact:

Gerald T. Heydt, Regents' Professor
School of Electrical, Computer and Energy Engineering
Arizona State University
PO Box 875706
Tempe, AZ 85287-5706
Telephone: 480 965 8307
Fax: 480 965 0745
Email: heydt@asu.edu

Power Systems Engineering Research Center

The Power Systems Engineering Research Center (PSERC) is a multi-university Center conducting research on challenges facing the electric power industry and educating the next generation of power engineers. More information about PSERC can be found at the Center's website: http://www.pserc.org.

For additional information, contact:

Power Systems Engineering Research Center
Arizona State University
527 Engineering Research Center
Tempe, AZ 85287-5706
Phone: 480-965-1643
Fax: 480-965-0745

Notice Concerning Copyright Material

Table of Contents

List of Figures

List of Tables

Nomenclature

ACCC	Aluminum Conductor Composite Core
ACCR	Aluminum Conductor Composite Reinforced
ACSR	Aluminum Conductor Steel Reinforced
C_i	Generation cost at i^{th} generator
$C'_{Operating}$	Operating cost after transmission upgrades
$C_{Operating}$	Operating cost before transmission upgrades
$C_{Project}$	Upgrade cost
CR_i	Expectation of operational cost reduction
CSP	Concentrated solar power
$F(t)$	Probability distribution function
$f(t)$	Probability density function
FC	Fuel cost
FERC	Federal Energy Regulatory Commission
HTLS	High Temperature Low Sag
MW	Megawatt
MVAr	Megavar
OPF	Optimal power flow
P_i	Active power output at generator i
$P_{i\,min}$, $P_{i\,max}$	Minimum and maximum active power outputs at generator i
$P_{line\,k}$	Active power flow at line k
PV	Photovoltaic
Q_i	Reactive power output at generator i
$Q_{i\,min}$, $Q_{i\,max}$	Minimum and maximum reactive power outputs at generator i
$Q_{line\,k}$	Reactive power flow at line k
PV	Photovoltaic
Q_i	Reactive power output at generator i

$Q_{i\,min}$, $Q_{i\,max}$	Minimum and maximum reactive power outputs at generator i
$Q_{line\,k}$	Reactive power flow at line k
R	Resistance of transmission lines
RES	Renewable energy sources
RPS	Renewable Portfolio Standards
$S_{line\,k}$	Thermal rating of k^{th} transmission line
SCOPF	Security constrained optimal power flow
$V_{i\,min}$, $V_{i\,max}$	Minimum and maximum voltages value at bus i
$\|Vi\|$	Voltage magnitude at bus i
VO&M	Variable operation and maintenance (cost)
WECC	Western electricity coordinating council
X	Reactance of transmission line
δ_i	Bus voltage angle at bus i
δ_{max}	Maximum voltage angle deviation across the line
Π	Payback period
μ_x	Mean value of variable x
σ_x	Standard deviation of variable x

1. Introduction to HTLS Conductors

1.1 Final Project Report Overview

This is Part II of the final documentation of the PSERC research project "Making the Economic Case for Innovative HTLS Overhead Conductors." Part II focuses on the use of operational cost reduction as a result of reconductoring upgrades using HTLS technologies. The application is in transmission expansion.

An important point to make on the interpretation of results of this work, and conclusions, is that HTLS appears to be particularly suited for upgrade of existing transmission circuits. This is the approach take in this work, namely that the emphasis is on upgrading existing overhead circuits to HTLS.

1.2 Project Motivation

High temperature, low sag overhead transmission conductors are proposed for high voltage transmission for high priority circuits. The HTLS conductors would result in lower right of way for a given energy transfer. The impact of higher cost is offset by power market enhancement. This project evaluates the systems and economic impact of HTLS conductors.

1.3 An Overview of HTLS Technologies

Transmission expansion in electric power system is a procedure by which large scale transmission system is designed to be reliable and feasible for future system loads. The problem of transmission expansion is complex due to the large number of variables, for example:

- Future load scenario;
- Availability of the rights-of-way;
- Future generation resource scenarios;
- Conductor types utilized;
- Technologies used (e.g., DC, AC, overhead, underground);
- Project cost.

Progressive penetration of distributed renewable energy sources has a positive influence on power transmission problem-solving. In the U.S. grids with competitive electricity markets, transmission congestion can become one of the impediment to possible electric power cost reduction. Progress in the smart grid development and integration of the distributed renewable sources can flatten the peak value of system load demand, thereby decrease electric power generation cost. Present costs of distributed renewable energy sources technology require excessive investment making impossible to attain the height of the renewable energy utilization. As a result, penetration of the renewable sources cannot facilitate transmission congestion problem significantly.

In terms of transmission expansion, in the United States, the main goal of the Federal Energy Regulatory Commission (FERC) is a promotion of electric power supply reliability and providing lower electricity cost for the costumers by reducing transmission congestions. Therefore, a well-considered transmission expansion should take into account possible operating cost reduction during upcoming operating period.

There are several factors that can impact transmission expansion:

Load growth
Load growth is a one of the main incentives for the transmission expansion. According to load growth forecast total electric energy consumption in U.S. will increase by 28% from 2011 to 2040 [1]. Development of the transmission infrastructure is an indispensable measure to meet the requirements for providing all the consumers with the sufficient electric power.

Renewable energy sources (RES) integrations
Integration of the renewable energy sources makes a great impact to the existing power grid. The Renewable Portfolio Standards (RPS) issued by DoE [2] requires the total power of at least 10% in 30 states to be generated by the renewable energy sources beginning from 2015. Installation of a high quantity of the renewable sources and ecological restrictions can force to shut down a significant portion of the conventional (coal, natural gas) power plants. Dislocation of the generation units can require an increase in transmission capability at certain parts of the system, particularly at the area where new generation units to be located.

Proximity to the sources of raw materials
Compared to the transportation of the fuel, transmission of the electric power is less expensive. Therefore, close location of the power plant to the fuel source can reduce electric power generation cost. Possible unbalanced distribution of the generation units and system loads can also be a reason of transmission congestion which requires system transmission expansion.

Obsolescence of existing transmission facilities
The existing transmission system has been built starting from the beginning of 20^{th} century. The progressive electric power consumption and forecast on the upcoming load growth can require upgrades and improvement of the existing transmission system. The life span of typical transmission lines is 35-40 years [3]. By the end of the exploitation period, the transmission capabilities of these transmission lines often do not satisfy the increased load requirements.

All factors above stimulate the transmission system development. As a result higher investments and land are involved to increase transmission system capabilities. This report focuses on the revealing the circumstances favorable for High Temperature Low Sag (HTLS) conductor implementation and consequent economic benefits.

This chapter introduces the background of existing transmission systems, disadvantages of each type of conventional transmission expansion options and introduces comparatively new technology, known as HTLS conductors which can become a possible measure to increase transmission capability. A brief introduction of HTLS conductor features and implementations are provided.

1.4 Properties of HTLS Conductors

The HTLS conductors, such as Aluminum Conductor Composite Core (ACCC) and Aluminum Conductor Composite Reinforced (ACCR), are designed to operate at the temperatures as high as 200^{o}C, more than two times higher, comparing with conventional Aluminum Conductor Steel Reinforced (ACSR) conductors, which normally operate at 75^{o}C. The composite core of the HTLS provides additional strength to the conductor, which reduces the sag of the transmission line during the operation at high temperatures. Typically, such conductors are capable to conduct the current as high as 2 to 3 times comparing with conventional ACSR conductors of comparable cross-sectional area [4]. There is little difference in weight and diameter between HTLS and conventional ACSR conductors. The electrical features, namely per mile resistance and reactance, are comparable with ACSR. The transmission lines which can often become congested can be good candidates for HTLS implementation, since no upgrades of towers are required for the reconductoring. Another feature of the HTLS conductors is higher corrosion resistance, which can increase a life span for the upgraded transmission lines [5]. Additional disadvantages of HTLS upgrading include outage time, required for the upgrades; and a lower level of experience with HTLS as compared with conventional conductors.

The main disadvantage of the HTLS conductors is its high cost which varies from two to six times compared to comparable conventional ACSR conductors [6]. However, due to the similarity in physical supporting requirements, the reconductoring using HTLS does not usually require reinforcement of the towers, insulators or other equipment. This feature of lower or comparable weight of HTLS conductors may allow significant cost reduction for upgrading of existing transmission lines. Comparing with other types of transmission upgrades, a rapid reconductoring using HTLS conductors usually does not require long term line outage. In the research for this work, this advantage of HTLS technologies was mentioned by several U.S. transmission companies. The short time required for reconductoring allows for the facilitation of possible consequences of a long term outage. The typical transmission upgrades methods and their advantages and disadvantages are shown in Table 1.1.

Table 1.1: Comparison of different transmission upgrades methods

Upgrade Method	Advantages	Additional Expenses and Disadvantages
Parallel single circuit line	Possibility of operation during new line construction	Rights-of-way availability
Parallel line on existing towers	Lower transmission losses due to decrease in equivalent line resistance	Expenses for long duration of line outage Towers usually do not have appropriate design to carry parallel circuit
Voltage level increase	Lower transmission losses due to high voltage, low current operation	Line outage duration expenses Right-of-way availability Transformer cost
Reconductoring with HTLS	No upgrades in towers and insulators facilitates upgrade	Cannot increase security rating

As seen from Table 1.1, compared with conventional transmission upgrades, HTLS reconductoring may be a good option for increased thermal rating. Parallel single circuit construction and installation of a new parallel line on existing towers can also increase security rating of the transmission line due to decreased equivalent line impedance. A significant alternative is often redesign of an existing circuit utilizing a higher transmission voltage. The voltage increase method is also capable of increasing the security rating. However such types of upgrades often require additional rights-of-way which can be hard to attain. Of course, higher transmission voltage requires total replacement of transformers and adjacent equipment. For short transmission lines, security limitation is usually not a limiting factor. As illustrations, for the research for this report, most HTLS implementations were found to be of length less than 50 miles, and many were found to be less than 25 miles. For such lines reconductoring using the HTLS conductors can be a good option for transmission upgrades.

1.5 State of the Art for HTLS Conductor Applications

HTLS conductors are a comparatively new technology introduced in transmission engineering. A number of performed studies are based on revealing the advantages and disadvantages and the possibility of HTLS conductors implementation. A sampling appears below.

Reference [6] stated that during long term operation at high temperatures, the resistance of the conductor increases. In long heavily loaded transmission lines high ratio of the conductor resistance to reactance R/X can lead to transmission security limitation. The increased resistance may also require additional reactive power support on the receiving buses to keep the voltage level within acceptable ranges. On the contrary, the HTLS manufacturer Southwire data, reference [7], shows insignificant increase in resistance at high circuit currents.

Reference [8] stated that the increase in thermal rating of a reconductored transmission line can necessitate the upgrade of the subsequent transmission lines if they are not capable to meet higher power transmission requirements. The simulation results in [8] suggest that the effect of the transmission capability increase by the upgrading only one line is not significant.

Studies performed in [9] describe the impact of the magnetic field due to increased current in the conductor in HTLS lines. Even though in the U.S. in normal conditions, the conductor does not operate at high current permanently, contradiction with magnetic field requirements can be a barrier for HTLS utilization. The comparison of the initial installation cost and difference in sag at maximum operating temperatures are provided in [8].

According to [9], the ruling span method for calculating the sag of the transmission line gives unacceptable error if the conductor (including HTLS conductors) operates at high temperatures. A new method of computation of the conductors sag and tension provided in [10] for high temperature conductors. This study is particularly important when transmission line sag becomes a limiting factor for electric power transmission.

According to [11], there are generally three ways of transmission capability increase: application of *dynamic rating* which can increase thermal rating by 5-20%; conductor re-tensioning, with 20-50% increase in transmission capabilities; reconductoring using HTLS conductors with over 50 percent increase in thermal rating. In [8] Kopsidas et al. mentioned that the method of conductors retention has already been applied for most thermally limited conductors; therefore such method can hardly be applicable for contemporary transmission lines.

In [11] and [12], Kavanagh, Armstrong, Geary and Condon proposed the implementation of the HTLS conductors as an option to increase the transmission capability in order to meet the requirements of attaining 40% of Irish energy generation from renewable energy sources. When the rights-of way become difficult to attain, implementation of HTLS can become a suitable option.

The industry implementation of the HTLS conductors is described in [13]. The thermal rating of reconductored transmission lines is increased by over 100%. In the "Leon Creek to Pleasanton" project, the system wide transmission losses were *decreased* due to HTLS conductor application.

The model of the integration of the conductor ampacity monitoring and HTLS conductor implementation is developed in [14]. This model allows the evaluation of conductor sag at different circumstances to optimize the usage the conductor full thermal rating potential. Note that real time sag is often the ultimate limit of ampacity.

According to [15], the transmission capability in specific implementation was increased from 170 MVA to 450 MVA (+164%) after reconductoring conventional ACSS conductor 230 kV transmission line by HTLS. The short term emergency rating was increased to 500 MVA with duration up to 30 minutes for the upgraded transmission line.

1.6 Scope of the Report and Contributions

Part II focuses on the comparison of the existing transmission expansion methods with implementation of HTLS conductors. The method of identification of congested transmission lines and beneficial economic conditions for HTLS conductor implementation is shown. The cost-benefit analysis of HTLS upgrades is performed.

Due to renewable energy sources integration, a portion of conventional generation units are likely to be retired or redispatched to lower operative levels. Therefore, the increase of transmission capabilities may be needed to accommodate these generation changes. Implementation of HTLS conductors should be considered in cases with high level of renewable energy resource integration. In this study, the change in transmission upgrades scenario is shown for cases with distributed energy resource integration.

The result of the studies provides useful information for transmission planning and cost-benefit assessment from the transmission lines upgraded using HTLS. The possible decrease in operating cost after a transmission line upgrade is studied, and the payback periods for the upgraded transmission lines are calculated.

A probabilistic model of the load growth is used in the report. The expectation of total transmission upgrade expenses is calculated in terms of the load growth forecast. The research is based on the reconductoring of existing transmission lines using HTLS conductors to assess its full potential as a transmission upgrade method.

1.7 Part II Outline

Five additional chapters and appendix form Part II of the project report. Chapter 2 provides descriptions of the methods which are used to identify the transmission lines – candidates for upgrade. Such lines are most likely to become overloaded beyond thermal rating. The thermally limited lines present active constraints in economic dispatch.

Chapter 3 proposes a method to calculate the minimum payback period for the transmission expansion projects. The evaluation of minimum payback period is based on Chebyshev's inequality. The advantage of proposed method is an accuracy irrespective of system load distribution. The only values required are the forecasted load mean value and the standard deviation.

In Chapter 4 the simulation of the Arizona portion of the Western Electricity Coordinating Council (WECC) system with a summer peak load of 2012 is described. The transmission lines candidates for upgrades are identified. The decrease in operating cost and potential payback period are calculated for the identified transmission lines to provide the economic benefit resulting from the HTLS conductor implementation.

Chapter 5 represents the possibility of transmission upgrades using HTLS technology, considering penetration of renewable energy sources on the distribution level of power system. The results show the effect of transmission lines loading due to integration of RES in power system.

In Chapter 6 a summary of the main results of the report and suggestions of the future work is provided. Appendix A describes the Arizona portion of WECC system parameters.

2. Identification of Transmission Lines for Upgrade

2.1 Transmission Expansion Considerations

The ability of transmission lines to carry bulk power depends on different factors such as thermal and security limits, conductor sag, voltage and transient stability. The thermal rating indicates a maximum current that can be transferred through a transmission line with no violation in sag. Security limits refer to maximum voltage phase angle difference across the transmission line to maintain synchronous operation of the system. The violation of security limits can lead to severe consequences during normal operation and especially in emergencies. Voltage stability refers to ability of the system to maintain voltages in a prescribed operations range at all buses in the system after being subjected to a disturbance from a given initial operating condition. The outage of a heavily loaded transmission line can be a reason for system stability loss. Therefore, the compliance with security constraints is necessary for a valid transmission expansion planning. Fig. 2.1 is a simple pictorial of their considerations. In this chapter, the aforementioned issues are integrated to identify those transmission circuits that should be upgraded.

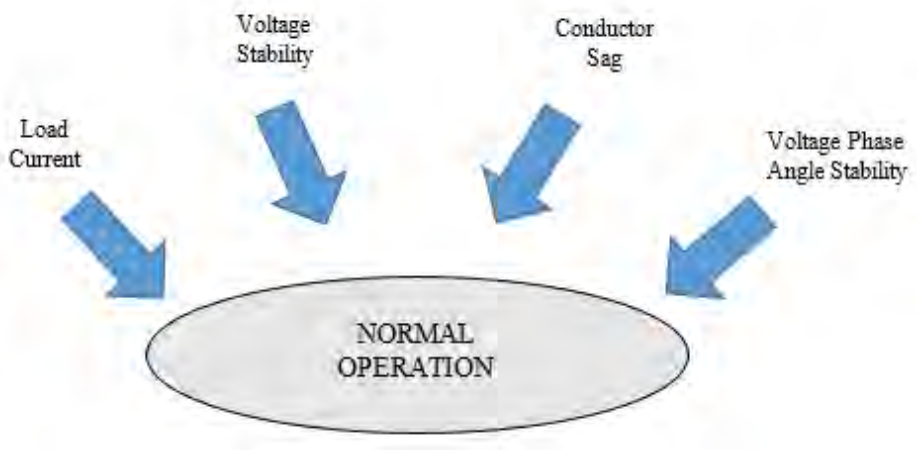

Figure 2.1: A pictorial of nominal operation of a transmission circuit

2.2 Methods of Transmission Capability Increase

Load growth, system deregulation, power marketing can be a motivation for power transmission expansion. Different methods of transmission expansion have their advantages and disadvantages. Followed by system reliability, the cost of transmission expansion becomes the most important factor for selecting an appropriate philosophy of transmission expansion. The main methods of transmission expansion increase are listed below with a brief description of these technologies:

Construction of new AC or DC transmission lines. This option requires high investments for transmission equipment and rights-of-way. New construction is especially suitable for long-term transmission expansion planning. The overhead construction of DC transmission lines is reasonable mainly for comparatively long lines due to inverter and rectifier construction expenses. In [16], the authors cite 500 km beyond which DC is often favored over AC. Reference [17] discusses advantages and disadvantages of DC transmission lines over AC.

Construction of the new transmission lines can also include utilization of underground cables. This option is suitable in urban areas where construction of the overhead transmission lines is complicated. Comparing with overhead transmission lines, underground cables offer a better protection against temporary outages. However, if the outage occurs, time required to locate the fault and repair underground cable requires more time and labor. Comparatively high cost of underground cables is also a significant impediment for its widespread implementation.

Reconductoring of existing transmission lines using conductors with higher thermal rating (including HTLS conductors). This method is suitable for those parts of the system where the thermal rating or the sag of existing transmission lines is a limiting factor of transmitted power. Usually, the use of higher ampacity conductors entails additional tower construction or modification. HTLS conductors, on the other hand, often do not require tower modifications. Reconductoring with no upgrades in towers and insulators reduces expenses for transmission upgrade. The high speed of upgrade is an advantage in HTLS designs since extended outages of key circuits may sometimes be avoided. The main negative aspect of HTLS upgrades related to the high cost of this technology. Reference [8] discusses the advantages and disadvantages of HTLS solutions.

High phase order systems. High phase order is a complicated technology that requires many unusual transmission engineering approaches such as: special and unusual transformer connections; protective relaying considerations; tower design; three phase to *N*-phase conversion ($N > 3$) and engineering expertise in this technology [18].

Voltage level increase. The advantage of this straightforward option is reduction in transmission losses. This option may be divided into two voltage upgrade ranges, for example increase of up to +15%, and increase of (usually substantially) more than +15%. For upgrade of operating voltage of up to +10% relatively few special considerations are needed. For example, in the Western U.S., 500 kV circuits are often operated at +10% high voltage. However, when simple operating policies are not enough to obtain the higher transmission capability that is needed planers may consider substantial increase in circuit voltages (e.g., converting a 138 kV circuit to 220 kV). High investments are required for increasing voltage level due to the installation of new transmission equipment and substation construction. Acquisition of rights-of-way for higher voltage level can be a problem in urban areas.

For congested transmission lines with comparatively low transmission capability, construction of new AC transmission lines or reconductoring of existing lines are usually applicable. A thorough analysis is required to identify the best option of system transmission capability increase in each particular case.

2.3 Method of Identification of the Transmission Lines to be Upgraded

The main purpose of transmission expansion is the increase of transmission capability and possibly reducing system operation cost. The main factors that have the largest impact on the transmission expansion decisions are system reliability improvement, economical effect (can be estimated as a payback period from new line construction or existing line upgrade), right-of-way availability, and public opinion. Among these factors, economic benefit is one of the most important indicators in

selecting the optimal solution. This observation is the core concept since power engineering is often cost-to-benefit driven. Fig. 2.2 shows a rough comparison of time horizons for planning and operation in power engineering. The approach taken here is to perform transmission expansion at some time *T* in the future. And, the approach is to minimize the constrained operation cost at time *T*. In other words, the operating constraints and economic dispatch are done in operating real time at all points in the planning horizon.

During system operation, optimal generation dispatch can be limited by thermal rating of some transmission lines. However, operation can be improved by upgrading those transmission paths whose thermal ratings are the active limiting constraints during generation redispatch. Increase in thermal rating of such transmission lines alleviates thermal rating constraints, therefore allows better solution of the OPF.

Upgrades can be performed by a wide range of transmission expansion strategies. In this discussion, implementation of HTLS technologies is used to replace conventional ACSR conductors. That is, the focus is completely on the potential use of HTLS solutions.

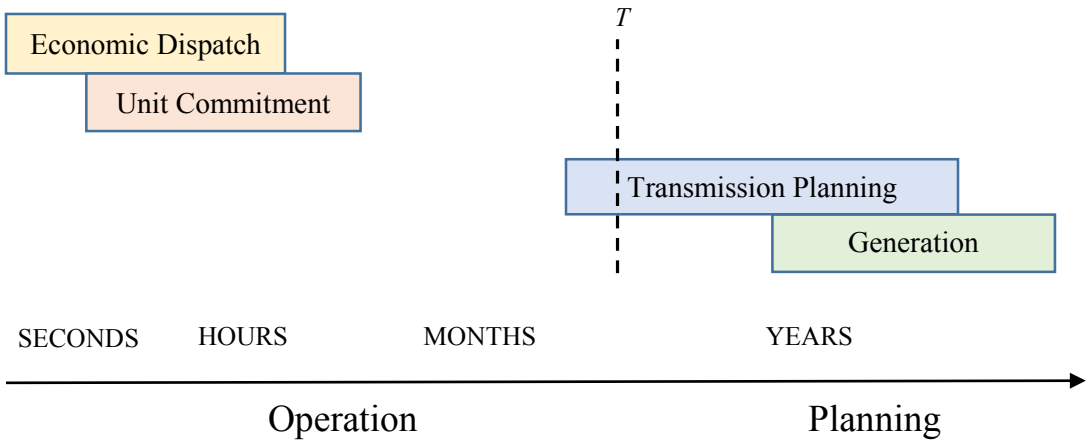

Figure 2.2: A pictorial of operating and planning time horizons

2.4 The Transmission Expansion Approach

For purposes of estimation of economic benefits afforded by HTLS implementation, define a payback period as an integrated period required to return the investment for reconductoring of an existing transmission line using HTLS technology. The payback period can be estimated by dividing the total investment spent for transmission upgrade by the decrease in system operation cost ($/h). The calculation of system operating cost decrease is carried out by the calculation of the difference between the operation cost before and after reconductoring,

$$\Pi = Payback\ period$$

$$= \frac{Project\ investments}{New\ operating\ cost - Old\ operating\ cost}$$

$$= \frac{C_{Project}}{C^{l}_{Operating} - C_{Operating}}$$

where $C_{project}$ is in dollars and $C^{l}_{Operating}$ and $C_{Operating}$ are in dollars per hour.

According to security requirements, all the system components should operate within their safe operating margins after the outage of any single component, i.e., it should be compliant with *N*-1 contingency requirements [19].

To calculate the decrease in operating cost resulting from a transmission upgrade, employ the following method: for an interconnected power system, the formulation of the AC OPF is

$$\min_{P_i} \sum C_i(P_i)$$

subject to

$$P_{i\,min} \le P_i \le P_{i\,max} \quad (2.1)$$
$$Q_{i\,min} \le Q_i \le Q_{i\,max} \quad (2.2)$$
$$|V_{i\,\min}| \le |V_i| \le |V_{i\,max}| \quad (2.3)$$
$$|P_{line\,k} + jQ_{line\,k}| \le S_{line\,k} \quad (2.4)$$
$$|\delta_m\text{-}\delta_n| \le \delta_{max} \quad (2.5)$$

where inequalities (2.1) and (2.2) represent requirements for active and reactive power generation at all generators *i*, inequality (2.3) represents bus voltage magnitude limits at any bus *m*, and (2.4) represents requirements for the thermal rating of all lines *k*. Note that $S_{line\,k}$ is the thermal rating of line *k* [20]. Inequality (2.5) represents the limits of voltage angle deviation across the transmission line for the purpose of system secure operation.

If a limiting factor of the OPF solution is (2.4). In this expression, the upgrade of the corresponding transmission line allows the alleviation of the active constraint, therefore providing a better solution of the OPF.

The following strategy is used for identification of those transmission lines that should be upgraded. The candidate lines for reconductoring should be identified as set Ω using a security constrained optimal power flow (SCOPF) technique. This yields a per hour operating cost. Then employing an SCOPF once more, allow the violation of one transmission line thermal rating in Ω under *N*-1 conditions. If the solution is found with no violation of any transmission line thermal rating, then, at the given system wide loading condition, the system economic optimal operation is possible with no line upgrades (no reconductoring). Otherwise (i.e., violations are found), define those

transmission lines in Ω as candidates for reconductoring and perform reconductoring using HTLS. Again, note that the focus here is on HTLS and no other alternatives are considered. For purposes of this study, the resulting upgrade in the thermal ratings is by factor of two. This is the usual case because the ampacity of ACSR and comparable HTLS conductors are typically in the ratio 1:2, [4]. Subsequently, perform an SCOPF again. The process is repeated until there are no further limitations in thermal ratings. After each reconductoring, calculate the per hour generation cost. The process of defining candidate transmission lines for upgrading is shown in Fig. 2.3.

The decrease in operating cost is a key factor for the payback period calculation. Assume that the total cost of reconductoring for a certain line is known. Then the payback period can be estimated dividing the expenses for transmission line reconductoring by the decrease in per hour operating cost and load duration time.

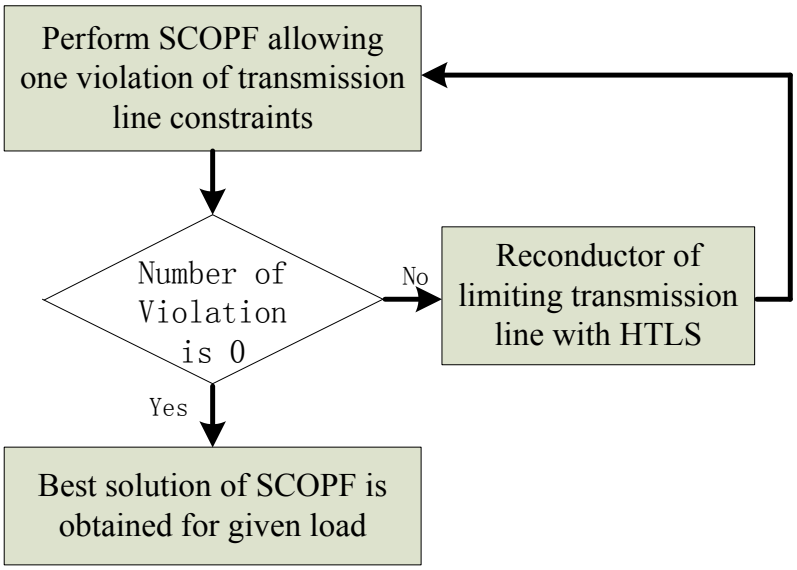

Figure 2.3: Basic strategy for the determination of transmission lines to upgrade

A quadratic cost approximation was used to estimate the cost of power generation. The operation cost adds up to the cost of power generation at all system generation buses. The objective is a minimization of system operating cost. Assume a quadratic cost approximation for power generation. The cost of generation power P at unit i is calculated using,

$$C_i = (A + BP_i + CP_i^2) \times FC + VO\&M \times P_i \qquad (2.6)$$

where C_i is total generation cost in \$/h at generation unit i; P_i is the power generated at bus i in MW; A, B and C are cost coefficients or multipliers; FC is a fuel cost and $VO\&M$ is Variable Operations and Maintenance. The values of the multipliers are dependent on the generator type and were evaluated using historical data from the generating units. Table 2.1 presents the values of the coefficients for different generator types that are used in this work [21].

Table 2.1: Cost function multipliers for different generation types (From [21])

Generation Type	A	B	C	Fuel Cost ($/Mbtu)	VO&M ($/MWh)
Coal fired	0	20	0.01	4.945	1.442
Nuclear	0	20	0.01	1.286	2.285
Natural Gas (Gas Turbine)	0	12.17	0.01	6.062	2.357
Natural Gas (Steam Turbine)	0	11.27	0.01	6.072	1.195
Natural Gas (Combined Cycle)	0	12.193	0.01	6.062	0.827
Hydro	0	10	0	1.00	1.287

2.5 Summary

This chapter discusses the methods of identification of the transmission lines targeted for reconductoring. The objective of transmission upgrade performance is the decrease in system operational expenses. The payback period is suggested to assess the effectiveness of HTLS technology implementation,

$$Payback\ period = \frac{Project\ cost}{New\ operating\ cost - Old\ operating\ cost}$$

The proposed transmission lines upgrade involve HTLS technology which can have benefit for both reduction of system operational cost (real-time operation) and a minimum cost solution of the transmission expansion problem (long term planning).

A basic strategy for the determination of transmission lines to upgrade has been proposed. This strategy based on three mail calculations:

- The SCOPF to identify transmission line constraints
- Reconductoring critical lines and assessment of performance
- Identification of the optimal solution.

Note that the analysis shown evaluates HTLS solutions only. Other transmission expansion strategies may give better results.

3. Payback Assessment Using Chebyshev's Inequality

3.1 Chebyshev's Inequality

In probability theory, the Chebyshev's inequality relates to the dispersion of variants. The inequality guarantees that no more than $1/k^2$ fraction of the variant's values can be greater than k. The uniqueness of this inequality is that it holds true irrespective of the random variable probability distribution type. The original citation to Chebyshev's widely acclaimed work is [22].

This chapter proposes a method of assessment of transmission expansion based on Chebyshev's inequality. References [23] and [24] are small sampling of the literature that contains a discussion of Chebyshev's inequality, and [25] – [26], give examples of application.

3.2 Application to Transmission Expansion

One of the main incentives for the transmission expansion is system operation cost reduction. Load growth uncertainty is an important factor which should be considered during the transmission expansion planning. Due to the uncertainty, error in the power demand forecast can lead to significant deviation from the expected savings resulting from the transmission upgrades. Discovery of a method to estimate the shortest payback period obtained from transmission system upgrades is important for the evaluation of the transmission planning overall.

Due to uncertainty in load forecast, the load growth forecast problem is usually represented as a probabilistic model. Application of the probabilistic model based on Chebyshev's inequality may be suitable for the assessment of the economic efficiency obtained after upgrades regardless of the load distribution.

Chebyshev's inequality gives an upper bound for the probability that a random variable is greater than a certain value. The advantage of Chebyshev's inequality is the accuracy of the model irrespective of the distribution that random variable. A disadvantage is that the Chebyshev's inequality can only give the upper bound of the cited probability, but not its exact value. In this application, the random variable considered is the system-wide effective peak demand. Let X denote that peak demand. Since the forecasted load usually has unknown probability distribution, the model based on Chebyshev's inequality cannot guarantee the accuracy of the results. Implementation of a proposed model allows the estimation of the shortest expected payback period from a selected transmission upgrade method.

According to Chebyshev [22], for any random variable X with mean value μ_x and variance σ_x^2, the following inequality holds,

$$P\{|X - \mu_x| \geq t\} \leq \frac{\sigma_x^2}{t^2} \tag{3.1}$$

where t$\geq \sigma_x$. The Inequality (3.1) holds for any probability distribution function. Standardization of the random variable allows setting the mean value of the variable to be zero, and standard deviation to be one (i.e., standardized measure). As a result, (3.1) can be represented as

$$P\{|X'| \le t\} = P\{-t \le X' \le t\} \ge 1 - \frac{1}{t^2} \tag{3.2}$$

where $X' = \frac{X-\mu_x}{\sigma}$.
In terms of the probability density function, Inequality (3.2) can be expressed as:

$$\int_{-t}^{t} f(x)dx \ge 1 - \frac{1}{t^2} \tag{3.3}$$

The value of the left hand part of (3.3) is the area below the curve of the probability density function *f(x)* between *–t* and *t* as shown in Fig. 3.1.

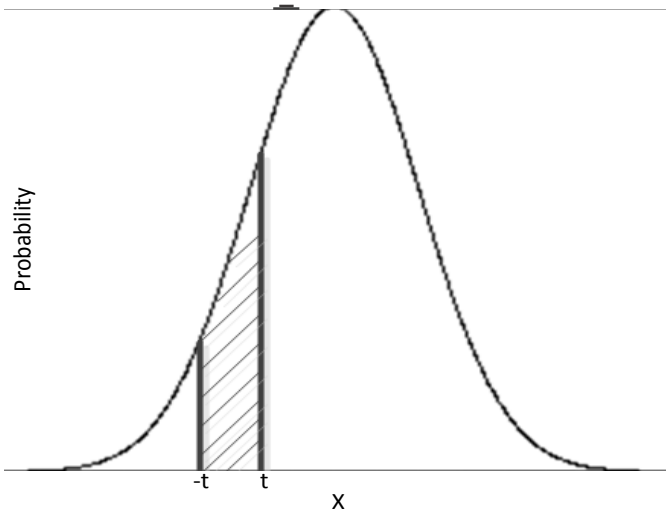

Figure 3.1: Probability density function. Value of (3.3) for a normally distributed variable

In general, the value of the function *f(x)* integrated from *–t* to 0 is not equal to the value of *f(x)* integrated from 0 to *t*, i.e.,

$$S_1 = \int_{-t}^{0} f(x)dx \ne \int_{0}^{t} f(x)dx = S_2$$

Let S_1-S_2 = ε. Then (3.3) becomes,

$$2[F(t) - F(0)] \ge 1 - \xi - \frac{1}{t^2} \tag{3.4}$$

where *F(t)* is a probability distribution function of *f(x)* for the load $x = t$. For most cases, probability distribution function at $x = 0$ is not equal to 0.5. Define β as a deviation, i.e., the value of *F(t)* at $t = 0$ is equal to $0.5+\beta$. Hence (3.4) becomes,

$$2[F(t) - 0.5 - \beta] \ge 1 - \xi - \frac{1}{t^2} \tag{3.5}$$

or

$$F(t) \geq \frac{2+\lambda}{2} - \frac{1}{2t^2} \tag{3.6}$$

where $2\beta - \varepsilon = \lambda$. A similar expression is derived for the left part of probability distribution function,

$$F(-t) \leq \frac{-\lambda}{2} + \frac{1}{2t^2}. \tag{3.7}$$

Expressions (3.6) and (3.7) show the upper and lower bounds of probability distribution model based on Chebyshev's inequality, for $t < 0$ and $t > 0$ respectively.

Assuming a symmetric probability distribution where $\varepsilon = 0$ and $\beta = 0$, Inequalities (3.6) and (3.7) become,

$$\begin{aligned} F(t) &\geq 1 - \frac{1}{2t^2} \quad (t \geq 1) \\ F(-t) &\leq \frac{1}{2t^2} \quad (t \geq 1) \end{aligned} \tag{3.8}$$

According to the Inequalities in (3.8), the function $P\{|X'| \geq t\}$ can be expressed as shown in Fig. 3.2.

With reference to (3.8), Fig. 3.2 shows the probability distribution function of the random variable which takes the value greater than parameter t. The Chebyshev's inequality bounds are shown as dash-dot line. According to Chebyshev's inequality, the probability distribution function curve for any kind of distribution lies between Chebyshev's bounds. That is, the distribution of a random variable x lies below the dash-dot line for $t \leq -1$; and the distribution of x is above the dash-dot line for $t \geq 1$. The dashed line on the plot is a probability distribution function for a normally distributed random variable, and the solid line is for normalized load data (i.e., standardized measure), taken from the actual demand at the PJM interconnection for 2012 [27].

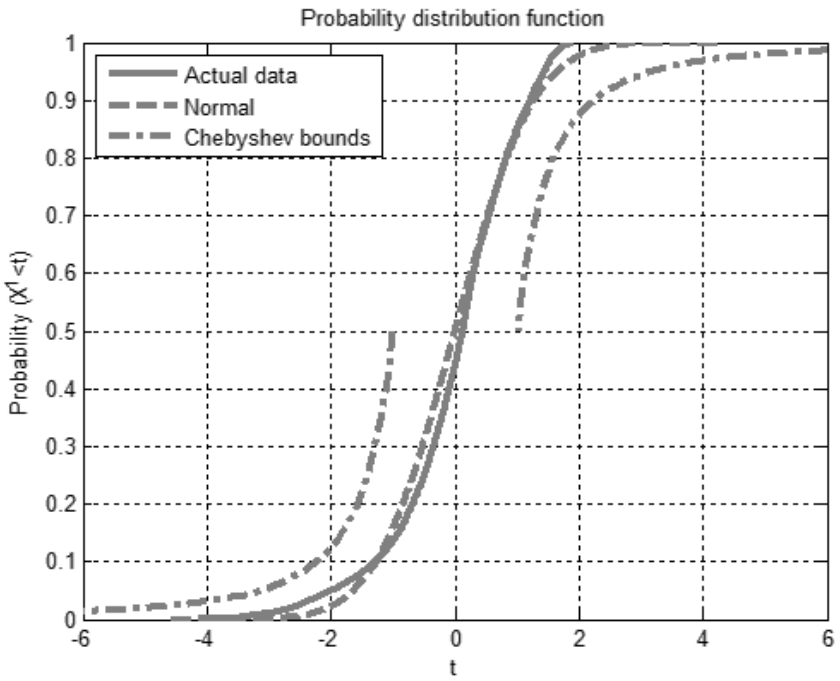

Figure 3.2: Probability distribution graph illustrating (3.8)

The method of expected payback period assessment is used to evaluate the economic effect from transmission upgrades. The operational cost reduction after performing the transmission system upgrades is a function of the load. For a normal distribution of the peak demand, probability density function is known. For Chebyshev's inequality bounds, probability distribution function curve is shown. The probability density function can be found by differentiation of the probability distribution curve.

For a random variable with given probability distribution, the probability distribution curve can be approximated as a piecewise linear function. Let random variable X be the system peak load. The operating cost reduction c(x) at load X = x is a function of x. The expectation of the operation cost reduction can be found by

$$\int_{-\infty}^{\infty} c(x) f(x) dx = c(x)F(x)\,|_{-\infty}^{\infty} - \int_{-\infty}^{\infty} F(x) dc(x) \tag{3.9}$$

where *f(x)* is probability density function, *F(x)* is probability distribution function expressed as a piecewise linear function and $c(x)F(x)|_{-\infty}^{\infty}$ is $c(\infty)F(\infty)$-$c(-\infty)F(-\infty)$.

The system operation cost increases with the load. Therefore, the higher the system load, the higher the cost reduction after performing transmission upgrades. The expectation of system operation cost reduction calculated using Chebyshev's inequality gives the highest cost reduction, i.e., the expected time for payback period is lowest. Therefore, the expected payback period assuming the Chebyshev's inequality bounds can be used as a reference for the shortest expected payback period from the transmission upgrades.

The value of Chebyshev type calculations of bound on payback period will be assessed further in Chapter 4 in which representative data will be used.

3.3 Summary

This chapter proposes a method of assessment of transmission upgrades. Having found the payback period according to the method described in Chapter 2, Chebyshev's inequality can further be used to estimate the minimum payback period for any upgraded transmission line. Transmission upgrades can be considered economically efficient if the payback period is close to the value obtained from Chebyshev's inequality. In practice, the payback period cannot be as short as a value obtained by Chebyshev's inequality since the Chebyshev value is the shortest *theoretical* payback duration. Knowledge of minimum payback period gives information on the adequacy of the investments to transmission system, therefore provided method can be a valuable tool for transmission expansion projects evaluation.

4. Upgrade Case Studies Utilizing an Actual Transmission System as a Test Bed

4.1 HTLS Technology Implementation for the Arizona Transmission System

This chapter presents illustrative results achieved from implementation of the transmission upgrades method discussed in Chapter 2. The effectiveness of the method is based on the theoretical material described in Chapter 3. A 225 bus Arizona portion of the WECC system was used as a test bed to analyze the effectiveness of HTLS reconductoring. The 2012 summer peak load case was used as a base case with some system data "tuning" to insure that the base case is *N*-1 compliant. The data tuning was needed to avoid inaccuracy due to the equivalency of the actual southwest WECC system (e.g., equivalence of circuits below 100 kV, and omission of certain out-of-area interconnections). The base case studied was a reduced load case to insure *N*-1 compliance. A load growth study was performed to evaluate the reasonableness of HTLS implementation. No detail of the dynamic stability of the resultant system was considered except that the steady state line voltage phase angle differences were constrained to 30^{o}. The simulation was performed using PowerWorld software.

For the cited Arizona test bed, the load variation with time was not available. In order to obtain a realistic test, hour by hour actual load data from the PJM interconnection were used. To create a realistic scenario, the PJM data were scaled so that the annual peak value was identical to the 2020 forecast Arizona peak demand.

4.2 Cost Comparison of Transmission Upgrades

Expenses restrictions and difficulty in acquisition of new rights-of-way make transmission expansion a costly endeavor. The problem of rights-of-way acquisition becomes especially acute within urban areas. The use of HTLS offers an attractive uprating option since reconductoring of the lines on the existing towers does not require lengthy line outages. In many cases, the duration of the line outage during transmission reconfiguration is a key factor because the line outage can only be tolerated for certain system operating conditions. However, there are some conditions for which reconductoring with new tower placement may be a better option (e.g., according to WECC transmission capital cost studies [28], the transmission line per mile reconductoring cost with HTLS transmission lines is higher than construction of new lines). Table 4.1 illustrates this point. Note that in Table 4.1 and all subsequent tabular results, the Arizona transmission system is used as a test bed.

Table 4.1: WECC estimates of per mile costs for 230, 345 and 500 kV

Voltage	230 kV		345 kV		500 kV		
Equipment	single circuit	double circuit	single circuit	double circuit	single circuit	double circuit	HVDC bipolar
Base cost $/mi	$927K	$1484K	1298K	2077K	1854K	2965K	1484K
Multipliers							
Conductor							
ACSR	1.00	1.00	1.00	1.00	1.00	1.00	1.00
ACSS	1.08	1.08	1.08	1.08	1.08	1.08	1.08
HTLS	3.60	3.60	3.60	3.60	3.60	3.60	3.60
Structure							
Lattice	0.90	0.90	1.00	1.00	1.00	1.00	1.00
Tubular steel	1.00	1.00	1.30	1.30	1.50	1.50	1.50
Length							
> 10 mi	1.00	1.00	1.00	1.00	1.00	1.00	1.00
3 – 10 mi	1.20	1.20	1.20	1.20	1.20	1.20	1.20
< 3 mi	1.50	1.50	1.50	1.50	1.50	1.50	1.50
Age							
New	1.00	1.00	1.00	1.00	1.00	1.00	1.00
Reconductor	0.35	0.45	0.45	0.55	0.55	0.65	0.55

K=1000

According to Table 4.1, calculate the different methods of transmission upgrade for selected transmission lines. The transmission upgrades cost comparison is shown in Table 4.2. Cost comparison of the three basic upgrade methods, i.e., HTLS reconductoring, new parallel line construction and new double circuit line construction, are provided. The transmission lines selected as candidates for upgrade are identified according to the method described in Section 2.3.

Table 4.2 illustrates that the reconductoring using HTLS technology is not the cheapest upgrade solution. Construction of new parallel single line is usually less expensive upgrade method. However, this upgrade method is infeasible due to the problems with rights-of-way availability.

Table 4.2: Upgrade cost for the selected transmission lines

Line name	Voltage level (kV)	Length (miles)	Transmission line upgrade cost (10^6 $)		
			HTLS Reconductoring	New parallel single line construction	New double circuit line construction
LCS – CNT	230	7.0	9.811	7.008	11.219
SAT – TRS	230	6.1	7.709	6.107	3.555
AFI-GLL	230	2.1	3.311	2.628	4.207
RRD-OOE	230	4.0	5.045	4.005	6.411
MMK-SSL	230	5.5	6.937	5.506	8.815
GLL-GDL	230	1.6	2.522	2.002	3.205

4.3 Effectiveness of HTLS Reconductoring

In this report, the evaluation of the of the transmission upgrades effectiveness methods is based on payback period. During load growth, there are certain transmission lines whose upgrade becomes necessary due to system topology. These upgrades do not impact on system operational cost even after reconductoring. An example of such reconductoring can be two parallel transmission lines

supplying a load bus, as shown in Fig 4.1. Assume both Line 1 and Line 2 have similar thermal rating. If Line 1 becomes congested during the outage of Line 2, reconductoring of any (or both) of those lines will not decrease system operation cost since reconductoring does not affect the generation optimal dispatch. Calculation of the payback period for such transmission lines is not viable using provided method. Operation cost decrease is usually possible for those lines, which are located centrally in the interconnection.

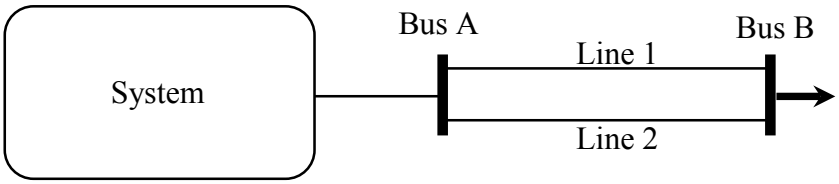

Figure 4.1: Example of the transmission line upgrade for which the calculation of payback period is not viable

According to the method discussed at Section 2.3, during the load growth study, perform a SCOPF allowing violation in thermal rating of only one transmission line during *N*-1 operation conditions and calculate the decrease in operating cost after reconductoring that transmission line. The decrease in operating cost and payback period are shown in Table 4.3, assuming a constant system wide load value. The payback period, however, can be shortened significantly if the system operates at higher loads. For the reconductoring of those transmission lines which do not improve the solution of the SCOPF, assume that there is no. Such lines are not of research interest (e.g., Apache – Adams, Tucson – DelBac, DelBac – Nogales shown in Table 4.3).

Table 4.3: Transmission line reconductoring cost, reduction in operating cost at different peak periods

System load peak period (GW)	Transmission line and voltage level	Possible to avoid line overloading by redispatch	HTLS recond. cost ($10^6$$)	Reduce in operating cost ($/hour)	Payback period (years)
10.09	YVP –VRD (230 kV)	No	45.82	–	–
10.77	APC – ADM (115 kV)	No	–	–	–
10.87	LCS – CNT (230 kV)	Yes	9.811	149.48	7.492
11.26	TSS– DLS (115 kV) CLA –LLP (230 kV)	No No	– 66.739	– –	– –
11.56	DLC – NLS (115 kV)	No	–	–	–
12.15	LLP – CCC (230 kV)	No	61.48	–	–
12.44	SAT – TRS (230 kV) AFI – GLL (230 kV) RRD – OOE (230 kV)	Yes Yes Yes	7.709 3.311 5.045	38.03 52.01 82.96	23.14 7.26 6.94
12.54	MMK – SSL (230 kV)	Yes	6.937	42.87	18.47
13.22	GLL – GDL (230 kV)	Yes	2.522	9.15	31.46

In this study, reconductoring of transmission lines is performed when one of the lines becomes congested during *N*-1 contingency analysis, i.e., operates at 100% of its long term thermal rating. Test cases indicate that for a large scale system, upgrade of only one line does not change generation dispatch significantly. As a result, the impact from the reconductoring is low and the

payback period is long. If load growth is considered, the impact from reconductoring may become significant. Reduction in operating cost and payback period at higher load levels for the indicated WECC test bed are shown in Table 4.4. Note that in Table 4.4, the peak load period is accounted as either the full day (24 h) or a fraction of a day (namely 2 h for this study): this calculation is shown in the rows of the table separated by a solidus (i.e., a slash, /). For example, operational cost reduction achieved after reconductoring of transmission line LCS – CNT is 149.5 $/hour, if the system wide load is 10.87 GW (111% of base case), and 2351 $/hour, if the system wide load is 11.26 GW (115% of base case). The payback period shown in Table 4.4 is achieved assuming the system wide load increase right after reconductoring (i.e., static load growth study). For precise evaluation purposes, the dynamic load growth model is described in Section 4.4.

A typical transmission line life is 35-40 years [3]. Assuming that the peak load of the system is only two hours per day, the economic benefit becomes evident from Table 4.4. The benefits from decreased operating cost at non-peak load conditions are not considered. However, decrease in operating cost during non-peak load periods can also reduce the payback period further than those indicated in Table 4.4.

4.4 Transmission Upgrades Project Payback Period Evaluation

The benefits obtained from transmission upgrades often depend on system load forecast. Uncertainty in load forecast may cause the error in estimation of economic benefit achieved from the transmission upgrades. According to the method proposed by Section 3.3, economical assessment of the project by calculation of minimum payback period becomes possible. Knowledge on the project minimum payback period can also be desired to evaluate the adequacy of the investments to the transmission system.

Power system load growth is usually a probabilistic model. Transmission expansion planning engineers frequently use a normal distribution model to forecast system load. However, such models usually do not represent system future load precisely and may cause an error in the evaluation of economical aspect of the project. As an example, the difference between the real load distribution at PJM interconnection and normal distribution is shown in Fig. 4.2. In Fig. 4.2, the horizontal scale is the standard deviation.

Table 4.4: Reconductored transmission lines and payback period

Transmission line		System wide load (GW)						
		10.87	11.26	11.55	12.44	12.54	13.22	13.91
LCS – CNT	Savings $/hour	149.5	2351	3705	5218		31116	
	Payback period (years)*	7.49/89.9	0.48/5.71	0.30/3.62	0.22/2.58		0.04 /0.432	
SAT – TRS	Savings $/hour				38.03		3641	
	Payback period (years)*				23.1/278		0.24/2.90	
AFI – GLL	Savings $/hour				52.01		9505	
	Payback period (years)*				7.3/87.2		0.04/0.48	
RRD – OOE	Savings $/hour				82.96		1842	
	Payback period (years)*				6.9/83.3		0.31/3.74	
MMK – SSL	Savings $/hour					42.87	13736	14233
	Payback period (years)*					18.5/221.7	0.06/0.69	0.06/0.67
GLL – GDL	Savings $/hour						9.15	5816
	Payback period (years)*						31.5/377.5	0.05/0.60

*(Note: 7.49/89.9 means that the payback period is 7.49 years if the peak demand period is two hours (for every day) and the payback period is 89.9 years if the peak demand period exists for 12 hours each day)

A dynamic load growth model is used for evaluation of the transmission system upgrade project. The peak demand in 2012 is 16.32 GW and the mean value of the forecasted load in 2020 is 20GW [29], i.e., 1.28 times higher comparing with system peak load in 2012. To keep the system reliable operation and correspondence with N-1 contingency requirements, system load is decreased by 40%. For research purposes, the standard deviation for the forecasted load is set to 5%.

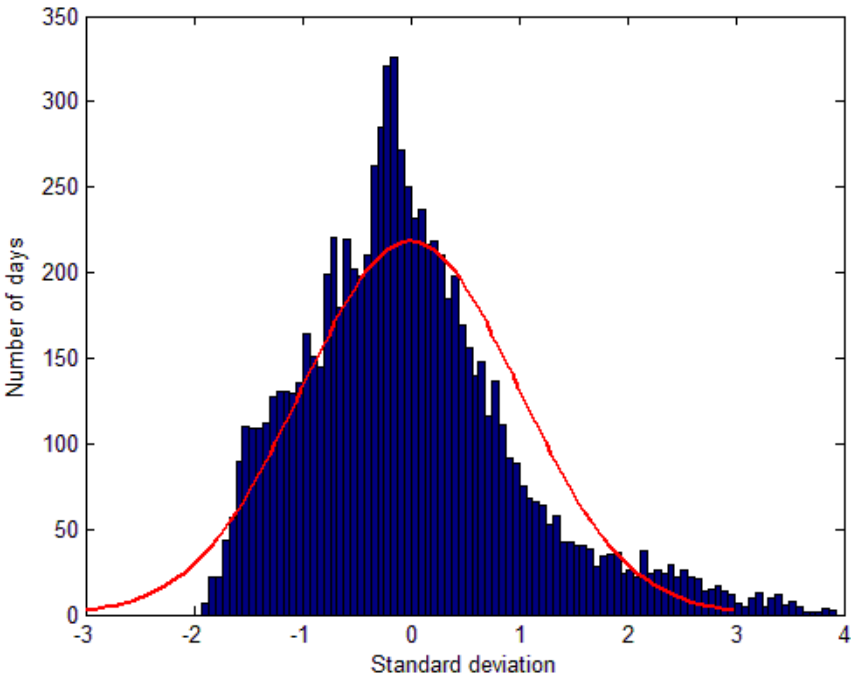

Figure 4.2: PJM system load (standardized), 2012

The assumption of equal load growth within even periods is appropriate for dynamic load growth modeling. Figure 4.3 shows the time when the reconductoring of identified transmission lines should be performed. According to Table 4.4, at system wide load equal to 10.87 GW, reconductoring of the transmission line LCS – CNT results in decrease of system operational cost. The system wide load with the mean value 10.87 GW is expected to be during the years 2014 to 2016. Therefore, to meet the system transmission requirements, reconductoring of this transmission lines should be performed before the end of 2014. Similarly, reconductoring of the other lines is performed before 2018 or 2020, depending on when the reconductoring would afford system operational cost decrease.

For calculation of the expected payback period, use the function of cost reduction in terms of system load, and system load growth probability density function. Then, the expectation of cost reduction for each upgraded transmission line can be calculated according to (4.1),

$$CR_i = \int_{-\infty}^{\infty} c_i(x) f(x) dx \qquad (4.1)$$

where CR_i is the expectation of operational cost reduction for the transmission line i, $c_i(x)$ is a function of the operational cost reduction after reconductoring in terms of system load, $f(x)$ is a system load probability density function and x is a system wide load. For calculation simplicity, the function of operational cost reduction is expressed as a piecewise linear function. It can be obtained by calculating operational cost reduction at different system wide load level according to Section 4.2. Part of the values can be seen in

Table 4.4. For the comparison purposes, three different models of load distribution are used:

- Normal distribution;

- Chebyshev's inequality model;
- PJM system 2012 year real load distribution model (assuming system load distribution change insignificantly yearly).

The probability density function for normal distribution is known. For the Chebyshev inequality and real load distribution models, analytical expression of probability density function is unknown. Therefore, for these two models, (4.1) can be calculated as,

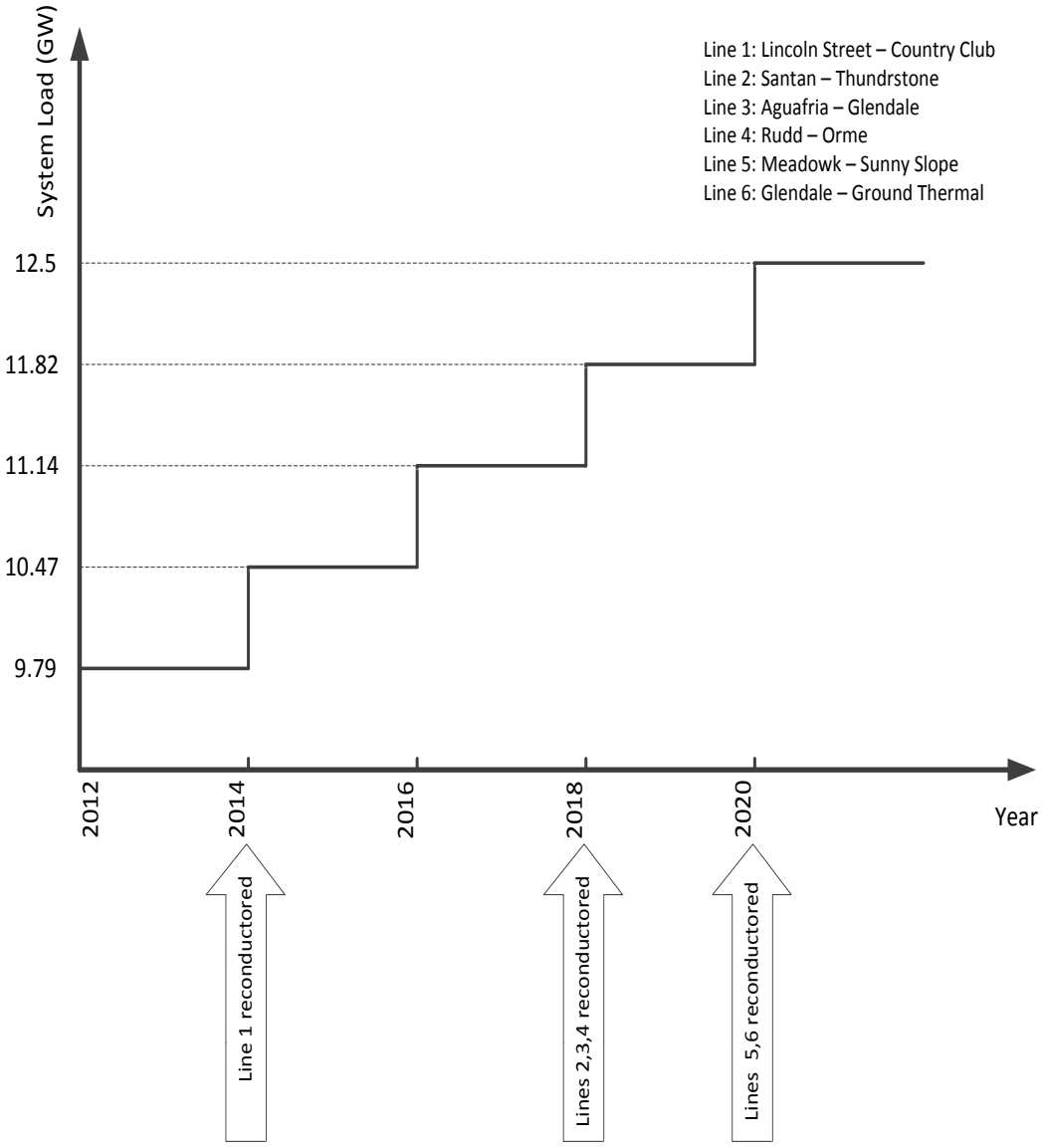

Figure 4.3: Transmission line reconductoring time during system load growth

$$CR_i = \int_{-\infty}^{\infty} c(x) f(x) dx = c(x)F(x)\,|_{-\infty}^{\infty} - \int_{-\infty}^{\infty} F(x) dc(x) \qquad (4.2)$$

where *F(x)* is a probability distribution function. For real load distribution model, *F(x)* is known from the real data, and for Chebyshev's inequality model *F(x)* can be found according to (3.8).

For the proposed transmission upgrade project, six transmission lines are targeted for reconductoring. The cost reduction is supposed to begin immediately after performing the reconductoring of the first transmission line. Transmission line LCS – CNT becomes reconductored by the end of 2014. Therefore the payback period for the project begins from the year 2014. Since the system load increases gradually, the system operating cost also increases following the system load.

To estimate the payback period of the project, the calculation of the operational cost decrease afforded by each upgraded transmission line is required. Assume that the load growth is equal within two even time periods. Knowing the system peak load of 2012 and 2020, the estimation of the system load during each year during this period is possible. However, the system peak load during each year between 2012 and 2020 is uncertain due to the forecast error. Therefore it (i.e., system peak load) can be handled as a probabilistic model. The system peak load mean values for these years are shown in Tables 4.5, 4.6 and 4.7.

The calculation of the operational cost reduction allows estimation of expected revenue achieved from the transmission upgrades during these years. For instance, the mean value of system peak load in 2014 is 10.47 GW with 5% (0.524 GW) standard deviation. Having known probability density function *f(x)* or probability distribution function *F(x)* and operational cost decrease *c(x)*, calculation of the expected operational cost reduction for the upgraded lines becomes possible using (4.2). Sum up the expected operational cost reductions achieved by the upgraded transmission lines (in this case, before 2014 only one transmission line, i.e., LCS – CNT was upgraded), obtain the expected system operational cost reduction for 2014. Assume that the system operates at the peak load conditions 2 hours daily (730 hours per year). Multiply the expected operational cost reductions by number of hours operated during one year (730 hours) to calculate the revenue obtained from reconductoring during this year.

Similarly, the expected cost reduction and total revenue achieved from the transmission lines upgrades can be calculated for each year. The results for the 2014-2020 are shown in Tables 4.5 (calculations based on normal distribution load model), 4.6 (calculations based on Chebyshev distribution load model) and 4.7 (calculations based on real data distribution load model).

According to the Table 4.3, the total investments for the aforementioned six transmission lines upgrade is equal to 35.335 million dollars. The expected revenue achieved from the transmission upgrades during 2014 to 2019 for different types of load distribution are shown in Tables 4.3, 4.4 and 4.5. The expected revenue obtained before all the transmission lines become reconductored (2014 – 2019), and the non-recovered part of the investment is the difference between the total investments and revenue achieved during the years 2014 – 2019. The results are shown in Table 4.8.

Table 4.5: Expected operational cost reduction and total revenue
(Based on normal distribution load model)

Time period (Year)		2014	2015	2016	2017	2018	2019	2020
Load Mean Value (GW)		10.47	10.81	11.14	11.49	11.82	12.16	12.5
Expected operational cost reduction ($/h)	LCS – CNT	619	1144	1915	3262	5152	8278	12810
	SAT – TRS	—	—	—	—	204	556	1135
	AFI – GLL	—	—	—	—	528	1444	2956
	RRD – OOE	—	—	—	—	109	292	590
	MMK – SSL	—	—	—	—	—	—	3901
	GLL – GDL	—	—	—	—	—	—	304
	All upgraded transmission lines	619	1144	1915	3262	5993	10570	21696
Total revenue (10^6 $)		0.452	0.835	1.398	2.381	4.375	7.716	15.838

Table 4.6: Expected operational cost reduction and total revenue
(Based on Chebyshev distribution load model)

Time period (Year)		2014	2015	2016	2017	2018	2019	2020
Load Mean Value (GW)		10.47	10.81	11.14	11.49	11.82	12.16	12.5
Expected operational cost reduction ($/h)	LCS – CNT	1918	3094	3379	5225	8157	13294	16875
	SAT – TRS	—	—	—	—	742	1363	1790
	AFI – GLL	—	—	—	—	1925	2649	4672
	RRD – OOE	—	—	—	—	391	697	908
	MMK – SSL	—	—	—	—	—	—	6782
	GLL – GDL	—	—	—	—	—	—	1119
	All upgraded transmission lines	1918	3094	3379	5225	8215	18003	32146
Total revenue (10^6 $)		1.40	2.259	2.467	3.814	5.997	13.142	23.466

Table 4.7: Expected operational cost reduction and total revenue
(Based on real distribution load model)

Time period (Year)		2014	2015	2016	2017	2018	2019	2020
Load Mean Value (GW)		10.47	10.81	11.14	11.49	11.82	12.16	12.5
Expected operational cost reduction ($/h)	LCS – CNT	602	1137	1794	3188	5097	8155	12300
	SAT – TRS	—	—	—	—	181	524	1060
	AFI – GLL	—	—	—	—	469	1424	2758
	RRD – OOE	—	—	—	—	165	290	547
	MMK – SSL	—	—	—	—	—	—	3573
	GLL – GDL	—	—	—	—	—	—	446
	All upgraded transmission lines	602	1137	1794	3188	5912	10383	20684
Total revenue (10^6 $)		0.439	0.83	1.310	2.327	4.316	7.580	15.100

Assuming that the maximum system mean load is 12.5 GW, according to the payback period definition, divide non-refunded investment by the system operation cost reduction in 2020, obtain the system operation time left to achieve total payback. By adding 6 years (i.e., the years 2014-2019 which are the previous years of system operation) to the obtained value, one calculates the total payback period for the proposed transmission upgrade project. The calculated expected project payback period is shown in Table 4.8.

The results in Table 4.8 show that the minimum payback period calculated using Chebyshev's inequality is 16.6% shorter compared with the payback period calculated using the actual data distribution. However, system load distribution function depends on many factors, i.e., load distribution, generation availability, and climatic factors. The Chebyshev model guarantees that the payback period cannot be shorter than the value, calculated using the Chebyshev model irrespective to all these factors.

Table 4.8: Expected operation cost reduction and expected period
for the transmission upgrade project

	Normal distribution model	Chebyshev model	Actual data distribution
Revenue during 2014-2019 ($10^6$$)	17.155	29.079	16.802
Non-refunded investments ($10^6$$)	18.18	6.256	18.533
System operation time left to achieve total payback	1.15 years	0.27 years	1.23 years
Expected project payback period	7.15 years	6.27 years	7.23 years

4.5 Active Power Losses in HTLS Transmission Lines

The high losses of HTLS transmission lines are a disadvantage, but it can only be an issue if conductors operate at high temperatures permanently. At the operating condition described in Section 4.3, HTLS conductors are used only to increase the emergency rating, but not for operating at high temperatures permanently. As a result, the overall increase of system losses is negligible.

In the United States, according to general operating policies, new HTLS transmission lines are not operated at high temperatures in long term operating scenarios, but only during emergency cases (e.g., line outage). Therefore, high losses are generally not an issue for HTLS conductors under this operating policy.

Based on the example provided in Section 4.4, in the system with total of 248 transmission lines, reconductoring of only six transmission lines increased the available transmission capability of the system by almost 50%. After performing the upgrades, the power flow mainly changes in the upgraded transmission lines, but not in the lines, located electrically far from them. Thus, at the given load value, the increase in losses caused by generation redispatch and transmission lines upgrades is insignificant.

As an example, at total system wide load of 1.11 times the base 9.7944 GW, during *N*-1contingency analysis, the 230 kV LCS – CNT transmission line becomes congested, i.e., runs 100% of its 607 MVA thermal rating. When the total system load is 1.35 times the base of 9.7944 GW, this upgraded transmission line with thermal rating 1214 MVA runs at 51.2% of its thermal rating. At the worst *N*-1 transmission outage case, the difference in the current is 2.04%. That infers that during the *N*-1 outage case, active power losses in LCS – CNT increase only by 4.12%. Note that the *N*-1 outage case cited results are relatively small increase in system-wide active power losses. And the increase in active power losses is temporary. The high losses disadvantage of HTLS does not apply in this case.

4.6 Summary

The analysis based on Arizona transmission system shows the feasibility of system operational cost reduction after performing the reconductoring using HTLS technology. Among the six upgraded transmission lines, some are located in the urban area where the new rights-of-way are not attainable. Therefore the other methods of upgrades become unattractive due to higher cost or impossibility of implementation (such as parallel line construction).

The payback period for the cited upgrade overall is 7.23 years (assuming load forecast based on previous years data). However, depending on the real load distribution, the payback period may be shortened to 6.27 years. The shortest payback period is valuable information for the final decision of transmission upgrades performance. The estimated short payback period is an advantage in favor to the proposed method of HTLS technology implementation. There is, however, a possibility that the mean value of the real load distribution is significantly lower than forecasted load. Such a case can significantly extend the payback period, and the transmission upgrades performed according to the proposed method become ineffective.

This chapter also addresses the operational issue of active power losses caused by the HTLS utilization. Operationally, using present U. S. operating policy, the higher current in HTLS conductors does not cause significant system active power loss increase. The reason is that in the proposed upgrade method, only a few transmission lines are suggested for reconductoring (e.g., in the given example, only six of 248 transmission lines are upgraded). Therefore in scope of the system overall, increase in active power loss may be insignificant. Further, the use of HTLS conductors to their substantially higher current rating is effectuated only for a few hours per year: this is a consequence of the use of the higher current paths only as *N*-1 considerations so require. Therefore, again, one concludes that under the applications envisioned, excess active power losses may not be a significant factor.

5. HTLS Technology and Renewable Energy Sources Integration

5.1 Analysis of the Impact of Distributed Energy Sources Integration on Transmission

In concordance with the renewable portfolio standards, 15% of the total generation in Arizona should be produced from renewable energy sources by 2025 [2]. As a result, a large amount of energy is expected to be generated from photovoltaic (PV) and concentrated solar power (CSP) plants. CSP generation is likely to be in the 280 MW range, (e.g., near Yuma, the Solana plant is at or near completion) [30]. A large number of smaller PV installations are also expected. Since PV generation units are also adopted through low voltage distribution systems, an interface is needed to connect to the transmission grid. Large central station, utility scale PV and CSP as well as residential scale PV result in changed use of the transmission system. This fact suggests a reassessment of the transmission system loading. Integration of renewable generation in the given system may require an upgrade of part of the transmission system. In either case, CSP or PV energy may require substantial transmission expansion or upgrading. Note that large central station fossil fuel plants are often located far from load centers. The development of PV resources is expected to be distributed at the load center itself. This change in location of generation is a reason for focusing on specialized needs in transmission expansion. This chapter introduces the possibility of HTLS technology utilization at the circumstances with the penetration of a large amount of renewable energy sources.

In this study, the impact of widely dispersed residential PV generation is studied. Note that CSP generation is basically the same topologically as fossil fuel generation. That is, this is concentrated generation. It is possible that new transmission resources will be needed to accomplish CSP plants, but the transmission engineering procedures are not really different from these utilized to accommodate coal plants. For this reason, CSP resources are not considered further. Rather, PV generation is assumed to be located near load buses.

5.2 Integration of Renewable Energy Resources

The Arizona transmission system introduced in Chapter 4 is used as a test bed. The solar PV is assumed to be only in the Phoenix metropolitan area – mainly residential roof top PV. The PV generation is assumed to be collected at substation buses. The power level of the applied PV generators on each bus is selected proportional to the total load at that bus. To keep the system total load unchanged, traditional generation of an equal amount to the added PV power must be reduced or decommitted. For illustration purposes, the Four Corners coal generation has been chosen to be decommitted since the three units at Four Corners, or about 1540 MW are expected to be closed by 2014 [31].

In the illustrative example shown in this chapter, four cases have been reviewed: a total generation of 560 MW, 750 MW and 1310 MW at the Four Corners power plant is replaced by distributed generation units connected through the 230 kV buses in the Phoenix metropolitan area. Note that there is no intended implication that centralized solar plants are unimportant, but the focus of this study is strictly on roof top PV. For this reason, the test beds indicated are designed as stated above.

5.3 A Comparison of Transmission Expansion Using Conventional Overhead Conductors

Among the solutions to increase system transmission capability is the construction of parallel lines to complement existing lines. A further alternative is the construction of new towers which are capable of supporting two parallel circuits. Both of these solutions require supplementary conditions: the first option requires attainable right-of-way, the second option will require temporary outage of the line intended to be upgraded. If both of these requirements cannot be fulfilled, HTLS reconductoring can become a viable solution. A further option is the increase of voltage level of the existing transmission path. However, in terms of economic efficiency, and the intended focus on HTLS, this option is not considered in this study.

In the performed studies, the distributed energy resources are located near the load buses. A significant portion of generated power at these buses is not required to be transferred to the other parts of the system but consumed locally. As a result, distributed location of low power energy resources can lead to transmission loss reduction and decreased loading of some transmission lines. If these transmission lines were targeted for upgrade with no consideration of future power generation units, the objectivity of the upgrades can be doubtful because the penetration of distributed energy sources may affect transmission upgrades planning significantly. This section analyzes the reasonableness of the performing transmission upgrades taking into account high penetration of renewable energy sources.

For these studies the load growth is assumed. The same studies as described in Chapter 4 are performed. The only difference is that the portion of the generating units at Four Corners (coal power plant) is substituted by renewable energy sources (PV) with no assumed change in operating cost.

At this point, the cases of committing a total of 560, 750, 1310 MW of solar generation, and decommission of the same generation capacity at Four Corners are described. Table 5.1 shows the upgrade cost and the system load at which the upgrades are performed. The results are also depicted in the step diagram in Fig. 5.1.

The transmission lines indicated in Table 5.1 are recommended to be upgraded using HTLS conductors due to comparatively low cost and close location to the urban area. As mentioned in Chapter 4, these upgrades can reduce system operating cost and the payback period can be calculated. The transmission lines that do not decrease system operating cost are more likely to be upgraded utilizing different upgrade techniques. Such a decision can make the upgrade expenses lower compared to the reconductoring using HTLS technology. For the example test bed cases, the load growth in all considered cases is identical. The transmission lines that do not decrease system operating cost should be upgraded at the same system wide load value (e.g., as shown in Table 4.3, transmission line YVP –VRD should be upgraded when system wide load reaches the value 10.09 GW. The load value at which YVP –VRD should be upgraded is the same for the base case as well as for the cases with distributed energy sources penetration). Such transmission lines are of no interest in this report. The transmission upgrades cost versus system wide load is shown on Fig. 5.2. Only transmission lines that may have “payback period” are considered.

Table 5.1: Upgrade cost for the cases with substitution of traditional steam generators by distributed generator units

Peak system load (GW)	Total power of generation units at Four Corners substituted by PV generation units			
	Base case (No PV)	560 MW	750 MW	1310 MW
	Upgrade cost (10^6\$)	Upgrade cost (10^6\$)	Upgrade cost (10^6\$)	Upgrade cost (10^6\$)
10.87	9.81			
10.97		7.71		
11.26			7.71	
11.75			9.81	7.71
11.95				11.95
12.25		9.81		
12.44	7.71 3.31 5.05			
12.54	6.94			
12.63		3.31		
13.22	2.52	6.94	6.94 3.31	9.81
13.81		2.52		
13.91	4.49			
Total upgrade cost (10^{6} \$)	39.83	30.29	27.77	29.47

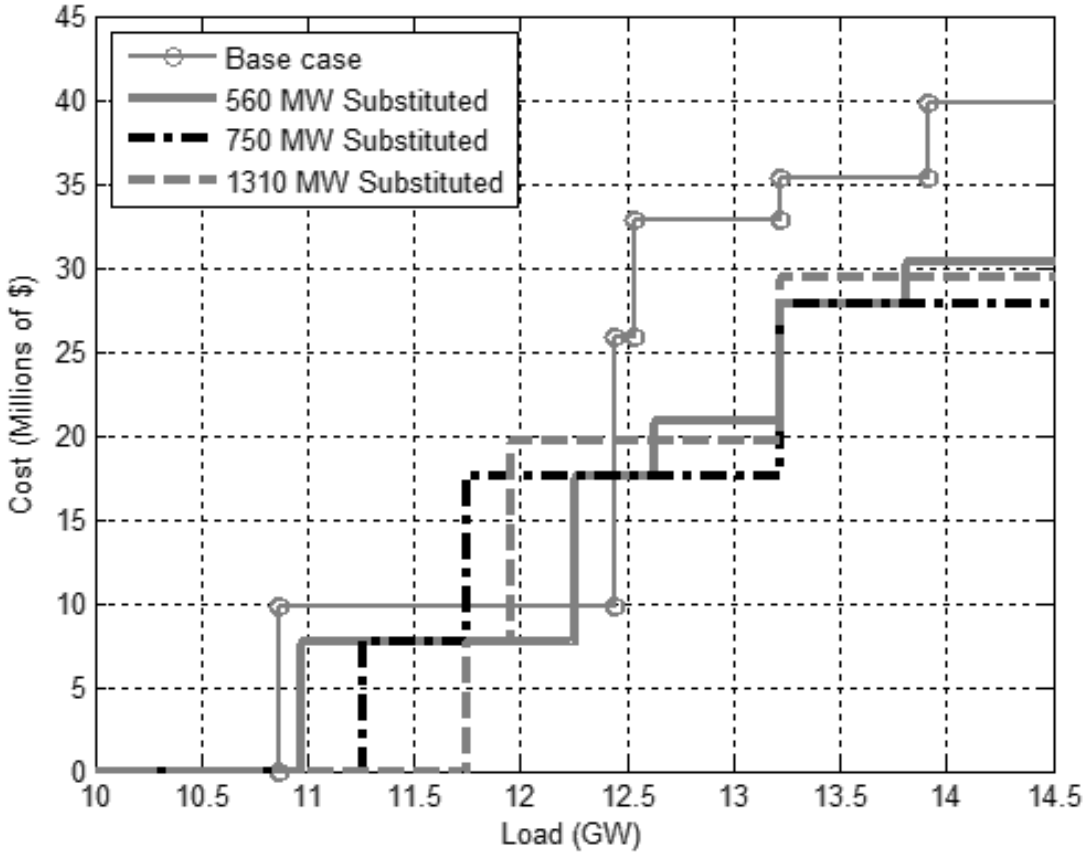

Figure 5.1: Pictorial of investments required for transmission upgrades

The results in Table 5.1 show that the transmission lines targeted for the upgrades can vary significantly depending on the capacity of distributed energy sources. A higher capacity of the distributed energy sources does not necessarily lead to less expenses required for the transmission upgrades. In addition, in the cases with the distributed PV generation units considered, the integrated payback period for the transmission upgrade project can be short. This is the case since the system wide load at which the first transmission line becomes upgraded is significantly higher than in the base case with no PV generation considered. That means that integration of distributed energy resources can afford operation at higher system wide load without transmission upgrades.

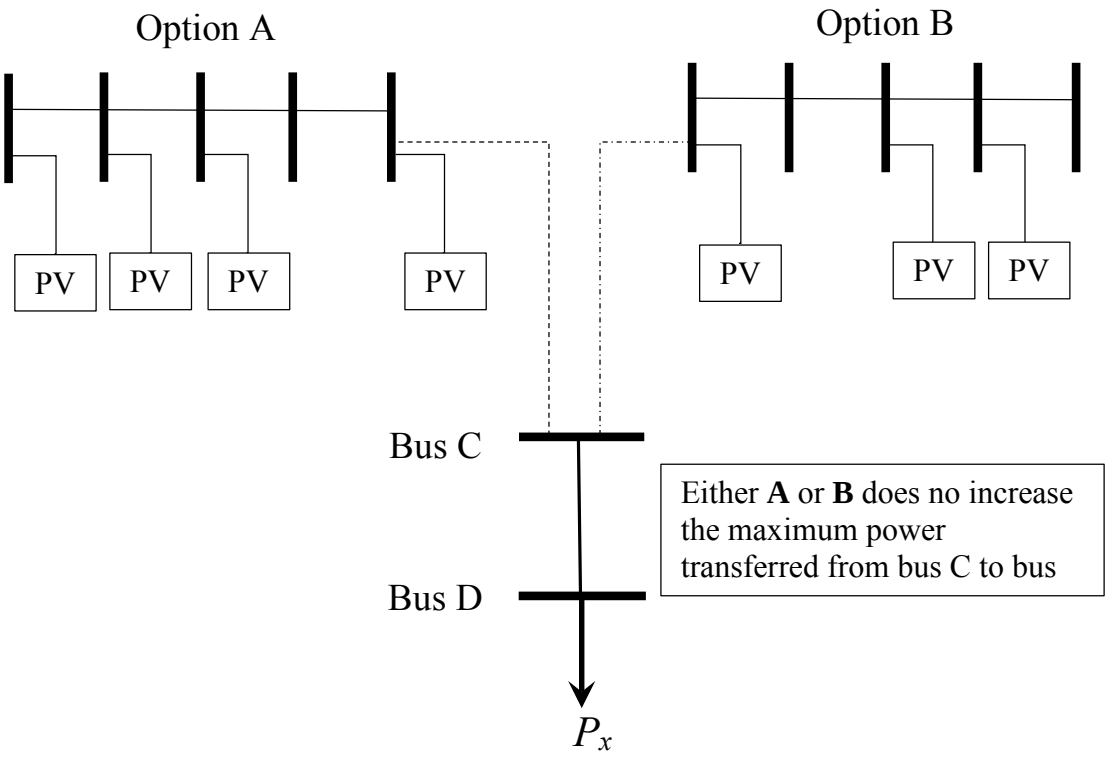

Figure 5.2: A pictorial of the addition of PV remote from the load center

5.4 Summary

This chapter describes the effect of the penetration of distributed renewable energy sources on transmission systems. The simulation results show that high expected amount of distributed energy sources may have a significant effect on transmission upgrades. The upgrade of some transmission lines becomes unnecessary due to the decreased line loading. The rescheduling and redistribution of generation as a result of integrating renewable generating resources may require transmission upgrades and these upgrades may require less expenses than generation rescheduling.

Since distributed generation units are installed at a comparatively low voltage level, and the generated power mainly is consumed locally, the need for upgrading high voltage transmission lines may not materialize.

Consideration of generation and load in transmission expansion engineering are examples of date and assumption embedded with uncertainty. The entire transmission expansion process involves multiple objectives and many requirements. Therefore, for minimization of the investments on transmission upgrades, every specific feature of the system (e.g., rights-of-way availability, maximum duration of line outages) and the benefits obtained from the system upgrade (e.g., system reliability, economic efficiency) should be carefully assessed.

6. Conclusions

6.1 Main Conclusions

This report suggests a method of identification of transmission lines which should be upgraded using HTLS conductors in compliance with system secure operation requirements. Implementation of HTLS upgrades may decrease the operational cost of the system under recommended operation conditions. This is a consequence of the alleviation of transmission loading constraints. Reconductoring with HTLS can be reasonable for those cases where the thermal rating of existing transmission lines is a limiting factor of the security constrained optimal power flow. The reasonableness of the reconductoring, estimated as a payback period, varies depending on the system load growth and existing system transmission line loading.

The utilization of Chebyshev's inequality was proposed to evaluate the economical aspect of the transmission expansion projects. The results show that the minimum payback period estimated using Chebyshev's inequality does not significantly deviate from the payback period, estimated using real load data distribution. The advantage of proposed model is the accuracy of minimum payback period estimation regardless of system load distribution.

The main advantages of HTLS technology are the reduced right-of-way requirement and the short duration of transmission upgrade projects. Capability of HTLS to operate at higher currents can significantly decrease system operational cost and surpass the negative effect from high one-time expenses required for HTLS conductors. Even though HTLS can conduct higher currents, if the nominal operation of the transmission system does not utilize the additional ampacity of the HTLS upgrades, there will be no expected increase in transmission losses. This is the usual operating strategy in North America. The higher ampacity ratings of HTLS, under suggested system operation, are used only for operation during contingencies.

Utilization of HTLS for reconductoring of single transmission line located centrally in the interconnection not likely to allow permanent operation at high current (e.g., 200^{o}C). The reason is that the loss of a heavily loaded HTLS line can lead to the overloading of nearby lines.

The upgrade cost of the existing transmission lines using HTLS can be lower than the construction of some types of new transmission lines. The supplementary requirements for HTLS reconductoring are often less intrusive than for other transmission expansion alternatives.

This work analyzed HTLS conductor utilization assuming high penetration of distributed renewable energy sources. Location of the distributed RES at residential level may decrease the loading of some transmission lines and increase the loading of the others. Installation of RES at low voltage buses may decrease the loading of some high voltage (e.g., 345 kV) long transmission lines so that the upgrade of these lines becomes unnecessary. Instead, the lower voltage level transmission lines (e.g., 115 kV, 230 kV) may become overloaded. Since such transmission lines require less investments for the upgrades, HTLS becomes a viable option for the transmission investments.

6.2 Recommendations for Future Work

This report is focused on the economic analysis of HTLS implementation in AC transmission systems for the purpose of decreasing system operating cost. The following studies could be performed to fully evaluate the possibilities of further implementation of HTLS conductors:

- Consideration of conductor degradation and effect on generation dispatch;
- Impact of power storage on transmission loading;
- Investigate the possibility of HTLS to afford loading at *N*-1-1 contingency cases;
- Studying the effect of HTLS conductors on system stability due to the increased resistance at high temperatures;
- Possibilities of HTLS implementation in DC circuits and high-phase order transmission systems;
- Comparison of magnetic field with conventional conductors and evaluation of the effect on environment due to high currents.

References

[1] U.S. Energy Information Administration. *Annual Energy Outlook 2013 with Projections to 2040*. Office of Integrated and International Energy Analysis, U.S. Department of Energy, April 2013. http://www.eia.gov/forecasts/aeo/pdf/0383(2013).pdf.

[2] Arizona Corporation Commission. *Commissioners Approve Rules Requiring 15 Percent of Energy from Renewables by 2015*. Public Information Office, Phoenix, AZ, November 1, 2006.

[3] Acres International Corporation. *Update of Life-Cycle Cost Studies for Overhead and Underground Electric Transmission Lines – 1996*. State of Connecticut, Connecticut Siting Council, Hartford, CT, May 2001.

[4] Sterlite Technologies Limited. *High Temperature Conductors*. Annual Report 2010-2011.

[5] Pierre, B. J.; G. T. Heydt. *Increased Ratings of Overhead Transmission Circuits Using HTLS and Compact Designs*. North American Power Symposium, pp. 1-6, 2012.

[6] Exposito, A. G.; J. R Santos, P. C. Romero. *Planning and Operational Issues Arising from the Widespread Use of HTLS Conductors*. IEEE Transactions on Power Systems, vol. 22, no. 4, pp. 1446-1455.

[7] Southwire Company. *Aluminum Conductor, Steel Supported. Trapezoidal Shaped Aluminum Strands*. Carrollton, GA.

[8] Kopsidas, K.; S. M. Rowland. *Evaluation of Potentially Effective Ways for Increasing Power Capacity of Existing Overhead Lines*. International Conference on Sustainable Power Generation and Supply, pp 1-7, 2009.

[9] Mateescu, E.; D. Marginean, G. Florea, Gal St. I. A., C. Matea. *Reconductoring Using HTLS Conductors. Case Study for a 220 kV Double Circuit Transmission LINE in Romania*. IEEE PES International Conference on Transmission and Distribution, Construction, Operation and Live-Line Maintenance (ESMO), pp. 1-7, 2011.

[10] Pereira, A. A.; J. Mauricio. *A Model for Uprating Transmission Lines by Using HTLS Conductors*. IEEE Transactions on Power Delivery, vol.26, no. 4, pp. 2180-2188.

[11] Kavanagh, T.; O. Armstrong. *An Evaluation of High Temperature Low Sag Conductors for Uprating the 220 kV Transmission Network in Ireland*. 45th International Universities Power Engineering Conference, 2010.

[12] Geary, R.; T. Condon, T. Kavanagh., O. Armstrong, J. Doyle. Introduction of High Temperature Low Sag Conductors to the Irish Transmission Grid. CIGRE 2012, Accessed at www.cigre.org.

[13] Avery, P. *High Capacity/ Low Sag Conductor for the Power Industry*. CTC Cable Corporation, WIA, November 9, 2010. Accessed at http://wyia.org/wp-content/uploads/2010/11/pat-avery.pdf.

[14] Fernandez, E.; I. Albizu, M. T. Bedialauneta, S. Arriba, A. J. Mazon. *System for Ampacity Monitoring and Low Sag Overhead Conductor Evaluation*. 16th IEEE Mediterranean Electrotechnical Conference, pp. 237-240, 2012.

[15] Western Area Power Administration. *Project Profile*. Accessed at http://www.southwire.com/transmission/project-profile-western-area-power-admin.htm.

[16] Siemens AG. *High Voltage Direct Current Transmission – Proven Technology for Power Exchange*. Energy Sector, Germany. Accessed at http://www.siemens.com/sustainability/pool/en/environmental-portfolio/products-solutions/power-transmission-distribution/hvdc_proven_technology.pdf.

[17] Michael, P.E. *HVDC Transmission. An Economical Complement to AC Transmission*. ABB Grid Systems, WECC Transmission Planning Seminar, February 2009.

[18] Willems, J. L. *The Analysis of High-Phase-Order Power Transmission Systems*. IEEE Transactions on Circuits and Systems, vol. 29, no. 11, pp. 786 -789, .November 1982.

[19] North American Electric Reliability Corporation. *Reliability Concepts. Version 1.0.2*. December 19, 2007. Accessed at http://www.nerc.com/files/concepts_v1.0.2.pdf.

[20] Cain, M. B.; R. P. O'Neil, A. Castillo. *History of Optimal Power Flow and Formulations*. December 2012, Accessed at: http://www.ferc.gov/industries/electric/indus-act/market-planning/opf-papers/acopf-1-history-formulation-testing.pdf.

[21] Eftekharnejad S. *The Impact of Increased Penetration of Photovoltaic Generation on Smart Grids*. PhD. dissertation, Arizona State University, Tempe, AZ, December 2012.

[22] Chebyshev, P. (П. Чебышев). *Des valeurs moyennes*. Journal de Mathematiques Pures et Appliquées, v. 2, no. 12, pp. 177-184, 1867.

[23] Hogg, R. V.; A. T. Craig. *Introduction to Mathematical Statistics*. 4th edition, Macmillan Publishing Co., New York.

[24] Encyclopedia of Mathematics. *Chebyshev inequality in probability theory*. Accessed at http://www.encyclopediaofmath.org/index.php/Chebyshev_inequality_in_probability_theory.

[25] G. Hu; Y. Zhang, M. Jing, Y. Tang, B. Gu. *Credibility Test for Blind Processing Results of Sinusoidal Using Chebyshev's Inequality*. School of Electronic and Information Engineering, Nanjing College of Information Technology.

[26] Stoikova, L.S. *Generalized Chebyshev Inequalities and Their Application in the Mathematical Theory of Reliability*. Cybernetics and System Analysis, vol. 46, no.3, 2010.

[27] PJM Interconnection. *Hourly Load Data for 2012*. Accessed at http://www.pjm.com/markets-and-operations/energy/real-time/loadhryr.aspx.

[28] Western Electricity Coordinating Council. *TEPPC - Capital Costs for Transmission and Substations – Recommendations for WECC Transmission Expansion Planning*. Engineering report by Black and Veatch, 2012.

[29] G. Barbose G. State *Adjusted Load Forecast: Arizona*. Lawrence Berkeley National Laboratory, TEPPC DSM Task Force Conference Call, August, 2010.

[30] National Renewable Energy Laboratory. *Solana Generating Station Project*. Accessed at http://www.nrel.gov/csp/solarpaces/project_detail.cfm/projectID=23.

[31] The Farmington Daily Times. *APS plans to shut down 3 unites at Four Corners Power Plant by end of year*. Farmington NM, October 4, 2012. Accessed at http://www.daily-times.com/ci_21688249/aps-plans-shut-down-3-units-at-four.

Appendix A - Test Bed Data

Table A.1: Generator records (bus 1-109)

Number of Bus	ID	Status	Set Volt	AGC	AVR	Min MW	Max MW	Min MVAr	Max MVAr
1	1	Closed	1.05	YES	YES	0	885	-342	480
2	1	Closed	1.05	YES	YES	0	750	-280	395
4	1	Closed	1.05	YES	YES	0	2415	-600	1050
8	1	Closed	1.05	YES	YES	150	950	-600	540
9	1	Closed	1.05	YES	YES	0	984	-600	700
11	1	Closed	1.05	YES	YES	0	750	-280	500
17	1	Closed	1.05	YES	YES	0	110	-42	50
23	1	Closed	1.05	YES	YES	0	560	-200	280
41	1	Closed	1.05	YES	YES	0	360	-110	258
46	1	Closed	1.05	YES	YES	0	639.6	-315	430.5
56	1	Closed	1.05	YES	YES	0	244.5	-85	150
57	1	Closed	1.05	YES	YES	0	153.5	-59	95
61	1	Closed	1.05	YES	YES	90	646	-283	401
62	1	Closed	1.07	YES	YES	0	1352	-310	800
63	1	Closed	1.07	YES	YES	0	1444	-310	800
64	1	Closed	1.07	YES	YES	0	1352	-310	800
65	1	Closed	1.05	YES	YES	0	862	-300	380
87	1	Closed	1.05	YES	YES	0	126	-19.5	47.5
94	1	Closed	1.05	YES	YES	0	58	-16	22
109	1	Closed	1.05	YES	YES	0	1382	-828	860

Table A.2: Generator records (bus 112-214)

Number of Bus	ID	Status	Set Volt	AGC	AVR	Min MW	Max MW	Min MVAr	Max MVAr
112	1	Closed	1.05	YES	YES	74	637	-84	269
123	1	Closed	1.05	YES	YES	200	976	-322	495
138	1	Closed	1.05	YES	YES	200	840	-240	430
146	1	Closed	1.05	YES	YES	0	75	-30	140
147	1	Closed	1.05	YES	YES	0	350	-140	200
177	1	Closed	1.05	YES	YES	0	212	-29	45
179	1	Closed	1.05	YES	YES	-12	30.4	-20	16
195	1	Closed	1.05	YES	YES	0	314	-82	92
196	1	Closed	1.05	YES	YES	0	330	-94	100
204	1	Closed	1	YES	YES	0	0	-9999	9999
205	1	Closed	1	YES	YES	0	0	-9999	9999
206	1	Closed	1	YES	YES	0	0	-9999	9999
207	1	Closed	1	YES	YES	0	0	-9999	9999
208	1	Closed	1	YES	YES	0	0	-9999	9999
209	1	Closed	1	YES	YES	0	0	-9999	9999
210	1	Closed	1	YES	YES	0	0	-9999	9999
211	1	Closed	1	YES	YES	0	0	-9999	9999
212	1	Closed	1	YES	YES	0	0	-9999	9999
213	1	Closed	1	YES	YES	0	0	-9999	9999
214	1	Closed	1	YES	YES	0	0	-9999	9999

Table A.3: Switched shunt records

Number of Bus	ID	Reg Bus Num	Status	Control Mode	Volt High	Volt Low	Nominal MVAr
11	1	11	Closed	Fixed	1.1	0.95	-90.00
26	1	26	Closed	Fixed	1.1	0.95	35.00
29	1	29	Closed	Fixed	1.1	0.95	300.00
31	1	31	Closed	Fixed	1.1	0.95	153.00
35	1	35	Closed	Fixed	1.1	0.95	43.20
55	1	55	Closed	Fixed	1.1	0.95	49.20
57	1	57	Closed	Fixed	1.1	0.95	15.60
76	1	77	Closed	Fixed	1.1	0.95	28.80
82	1	83	Closed	Fixed	1.1	0.95	27.00
92	1	93	Closed	Fixed	1.1	0.95	27.00
93	1	94	Closed	Fixed	1.1	0.95	40.00
112	1	113	Closed	Fixed	1.1	0.95	150.00
130	1	131	Closed	Fixed	1.1	0.95	40.00
137	1	138	Closed	Fixed	1.1	0.95	39.60
139	1	140	Closed	Fixed	1.1	0.95	33.10
157	1	158	Closed	Fixed	1.1	0.95	38.90
163	1	164	Closed	Fixed	1.1	0.95	200.00
186	1	187	Closed	Fixed	1.1	0.95	165.00
189	1	190	Closed	Fixed	1.1	0.95	240.00

Table A.4: Transmission line records (lines 1-27)

From Number	To Number	Circuit	Xfrmr	*R*	*X*	*B*	Lim A MVA
1	5	1	No	0.00218	0.04901	3.73739	2017.80
1	65	1	No	0.00074	0.01743	1.32274	1732.00
2	3	1	No	0.00177	0.04189	3.34000	1732.10
3	4	1	No	0.00077	0.01804	1.39842	2147.70
3	7	1	No	0.00098	0.02319	1.85366	2017.80
4	6	1	No	0.00241	0.05865	4.86560	2017.80
5	132	1	No	0.00003	0.00030	0.00000	1093.00
5	133	1	No	0.00003	0.00030	0.00000	1093.00
6	7	1	No	0.00081	0.01925	1.53854	2017.80
6	67	1	No	0.00040	0.00960	0.90380	2598.00
6	67	2	No	0.00040	0.00960	0.90380	2598.00
6	70	1	No	0.00000	0.00100	0.00000	1732.00
8	75	1	No	0.00020	0.00440	0.41670	2598.00
8	75	2	No	0.00020	0.00440	0.41670	2598.00
9	76	1	No	0.00000	0.00050	0.00000	3000.00
9	76	2	No	0.00000	0.00050	0.00000	3000.00
10	11	1	No	0.00855	0.08218	0.00000	687.20
10	11	2	No	0.00860	0.08270	0.00000	687.20
10	12	1	No	0.00361	0.06736	1.02994	597.60
10	13	1	No	0.00364	0.03474	0.53082	597.60
11	201	1	No	0.00030	0.00420	0.07150	1200.00
12	13	1	No	0.00340	0.03262	0.49913	597.60
14	164	1	No	0.00090	0.00970	0.01864	468.00
15	29	1	No	0.00330	0.02510	0.05860	370.90
15	31	1	No	0.00240	0.01870	0.04500	370.90
16	33	1	No	0.00800	0.07200	0.15120	435.00
16	61	1	No	0.00038	0.00281	0.00260	527.80

Table A.5: Transmission line records (lines 28-54)

From Number	To Number	Circuit	Xfrmr	*R*	*X*	*B*	Lim A MVA
17	25	1	No	0.01180	0.06900	0.14400	280.90
18	25	1	No	0.00850	0.05400	0.09800	280.90
18	38	1	No	0.00770	0.04490	0.09000	211.00
19	26	1	No	0.00035	0.00143	0.31160	462.10
19	28	1	No	0.00020	0.00070	0.17000	518.00
19	52	1	No	0.00030	0.00100	0.06148	509.90
20	39	1	No	0.00190	0.01714	0.05932	720.00
20	113	1	No	0.00096	0.00832	0.03008	720.00
20	121	1	No	0.00161	0.01460	0.05006	720.30
21	159	1	No	0.00830	0.08790	0.16934	239.00
21	164	1	No	0.00840	0.08870	0.17078	468.00
22	36	1	No	0.00090	0.00930	0.03660	637.40
22	40	1	No	0.00085	0.00837	0.00000	733.00
22	112	1	No	0.00081	0.00781	0.02100	435.00
24	52	1	No	0.00100	0.01010	0.22772	457.00
24	112	1	No	0.00040	0.00400	0.00720	457.00
26	29	1	No	0.00210	0.01680	0.03400	313.00
26	46	1	No	0.00135	0.00746	0.01031	750.00
27	30	1	No	0.00050	0.00501	0.01877	733.00
27	31	1	No	0.00158	0.01515	0.03154	437.00
27	35	1	No	0.00089	0.00887	0.02000	457.70
28	35	1	No	0.00053	0.00220	0.53400	324.70
29	31	1	No	0.00480	0.03720	0.07200	370.90
29	44	1	No	0.00388	0.02936	0.06164	309.10
30	31	1	No	0.00073	0.00721	0.02591	733.00
31	121	1	No	0.00015	0.00130	0.00000	286.80
31	121	2	No	0.00015	0.00130	0.00000	286.80
31	170	1	No	0.00001	0.00030	0.00000	637.00

Table A.6: Transmission line records (lines 55-81)

From Number	To Number	Circuit	Xfrmr	*R*	*X*	*B*	Lim A MVA
32	48	1	No	0.01370	0.09600	0.16740	334.60
32	51	1	No	0.00000	0.00030	0.00000	268.10
32	189	1	No	0.01580	0.10970	0.19112	259.00
33	37	1	No	0.00666	0.04868	0.09270	286.80
34	37	1	No	0.00582	0.04254	0.08200	286.80
34	61	1	No	0.00266	0.01981	0.04460	796.70
34	129	1	No	0.00483	0.02824	0.06230	1164.80
34	175	1	No	0.00000	0.00200	0.00000	200.00
36	39	1	No	0.00080	0.00900	0.03540	720.20
38	42	1	No	0.00361	0.02105	0.04218	211.00
39	49	1	No	0.00133	0.01054	0.01916	374.00
39	112	1	No	0.00213	0.01867	0.06788	797.00
39	164	1	No	0.00397	0.03480	0.12662	637.40
39	170	1	No	0.00272	0.02740	0.13488	733.00
40	46	1	No	0.00197	0.01540	0.05855	717.00
40	131	1	No	0.00074	0.00580	0.01937	1195.00
41	131	1	No	0.00182	0.01419	0.03918	1195.00
42	50	1	No	0.00420	0.02600	0.04890	306.00
43	45	1	No	0.00090	0.00860	0.01880	437.40
44	118	1	No	0.00000	0.00030	0.00000	804.70
44	129	1	No	0.00083	0.00470	0.01005	1170.00
45	164	1	No	0.00710	0.06470	0.14380	437.40
47	113	1	No	0.00000	0.00030	0.00000	750.00
48	170	1	No	0.00300	0.02130	0.03710	334.60
49	179	1	No	0.00067	0.00526	0.00956	374.00
50	51	1	No	0.00000	0.00030	0.00000	796.70
53	60	1	No	0.02710	0.12160	0.01664	47.80
53	146	1	No	0.01530	0.09430	0.01314	120.00

Table A.7: Transmission line records (lines 82-108)

From Number	To Number	Circuit	Xfrmr	*R*	*X*	*B*	Lim A MVA
53	183	1	No	0.03800	0.23370	0.03264	120.00
54	82	1	No	0.00000	0.00030	0.00000	142.00
56	57	1	No	0.00010	0.00030	0.00000	598.00
56	152	1	No	0.01060	0.06490	0.00904	167.00
56	168	1	No	0.01710	0.10530	0.01470	120.00
56	180	1	No	0.00270	0.01660	0.00232	120.00
57	58	1	No	0.03091	0.25063	0.02980	159.30
57	163	1	No	0.03480	0.14890	0.01976	100.00
57	174	1	No	0.01540	0.09480	0.01322	120.00
58	168	1	No	0.02960	0.12340	0.01630	145.40
59	160	1	No	0.01370	0.03790	0.00448	80.10
59	168	1	No	0.08820	0.24420	0.02622	80.10
65	72	1	No	0.00176	0.04189	3.32630	1732.00
66	73	1	No	0.00026	0.00382	0.41947	1732.00
66	75	1	No	0.00048	0.01091	1.06576	1732.00
67	74	1	No	0.00034	0.00724	0.68725	1732.10
67	76	1	No	0.00003	0.00069	0.64820	1732.00
67	76	2	No	0.00003	0.00067	0.62620	2598.00
67	76	3	No	0.00003	0.00071	0.53580	1299.00
68	70	1	No	0.00000	0.00010	0.00000	1238.00
69	70	1	No	0.00000	0.00010	0.00000	1238.00
71	158	1	No	0.00182	0.05144	4.89200	1238.00
72	73	1	No	0.00046	0.00874	0.70448	1732.00
75	76	1	No	0.00020	0.00428	0.40122	1732.00
76	77	1	No	0.00000	0.00050	0.00000	3000.00
76	78	1	No	0.00020	0.00550	0.51350	3000.00
76	79	1	No	0.00000	0.00050	0.00000	3000.00
80	81	1	No	0.00135	0.00236	0.00014	73.70

Table A.8: Transmission line records (lines 109-135)

From Number	To Number	Circuit	Xfrmr	*R*	*X*	*B*	Lim A MVA
81	82	1	No	0.06184	0.18458	0.01192	119.50
81	86	1	No	0.00056	0.00168	0.00011	95.20
82	160	1	No	0.02706	0.08076	0.00521	139.40
83	107	1	No	0.00030	0.00130	0.00020	83.60
84	87	1	No	0.02469	0.11702	0.01640	159.30
84	92	1	No	0.03040	0.14536	0.01996	119.50
84	108	1	No	0.00901	0.01407	0.00144	39.80
85	87	1	No	0.01739	0.09977	0.01360	181.20
85	94	1	No	0.00988	0.04722	0.00648	159.30
85	103	1	No	0.01327	0.03312	0.00762	167.30
85	104	1	No	0.03472	0.06072	0.00714	73.70
86	89	1	No	0.01742	0.05146	0.00337	95.20
86	146	1	No	0.01319	0.11675	0.01592	123.50
86	146	1	No	0.11333	0.39946	0.05064	123.50
87	94	1	No	0.01282	0.06033	0.00856	159.30
88	89	1	No	0.00004	0.00017	0.00000	22.90
89	93	1	No	0.01617	0.47870	0.00313	119.50
90	93	1	No	0.00178	0.00587	0.00040	119.50
90	98	1	No	0.00321	0.01013	0.00067	119.50
91	96	1	No	0.00549	0.01724	0.00234	139.40
91	97	1	No	0.01218	0.04139	0.00732	119.50
91	107	1	No	0.00160	0.00730	0.00110	161.30
92	96	1	No	0.00711	0.03321	0.00468	119.50
92	106	1	No	0.00117	0.00222	0.00026	83.60
95	102	1	No	0.00290	0.01385	0.00190	161.30
95	105	1	No	0.00430	0.02030	0.00290	119.50
96	102	1	No	0.01638	0.07814	0.01080	172.10
97	101	1	No	0.01000	0.03120	0.00630	172.10

Table A.9: Transmission line records (lines 136-162)

From Number	To Number	Circuit	Xfrmr	*R*	*X*	*B*	Lim A MVA
98	105	1	No	0.01422	0.06811	0.00466	164.30
99	106	1	No	0.00119	0.00225	0.00013	39.80
100	102	1	No	0.00046	0.00292	0.00094	328.60
101	105	1	No	0.00888	0.02131	0.00964	164.30
103	105	1	No	0.03392	0.10392	0.02028	181.20
106	107	1	No	0.00040	0.00200	0.00030	164.30
110	176	1	No	0.00000	0.00050	0.00000	120.00
111	174	1	No	0.00000	0.00050	0.00000	145.40
112	113	1	No	0.00120	0.00988	0.04042	725.00
112	128	1	No	0.00141	0.01238	0.04502	725.00
114	118	1	No	0.00136	0.00845	0.06192	725.00
114	119	1	No	0.00110	0.00671	0.05070	725.00
115	118	1	No	0.00101	0.00877	0.03218	637.40
115	120	1	No	0.00067	0.00584	0.02142	637.40
115	121	1	No	0.00610	0.03608	0.07322	363.00
115	121	2	No	0.00611	0.03614	0.07334	363.00
115	127	1	No	0.00031	0.00185	0.00374	358.50
115	127	2	No	0.00031	0.00185	0.00374	358.50
116	118	1	No	0.00082	0.00716	0.02604	637.00
116	123	1	No	0.00080	0.00730	0.02660	598.00
117	125	1	No	0.00948	0.05145	0.10522	458.00
117	126	1	No	0.00237	0.01409	0.02852	363.00
117	126	2	No	0.00237	0.01409	0.02852	363.00
118	120	1	No	0.00123	0.01072	0.03912	796.70
118	124	1	No	0.00314	0.01778	0.04698	450.10
119	131	1	No	0.00109	0.00941	0.03512	637.00
119	164	1	No	0.00249	0.02143	0.08008	498.00
120	121	1	No	0.00385	0.02510	0.17054	717.00

Table A.10: Transmission line records (lines 163-189)

From Number	To Number	Circuit	Xfrmr	*R*	*X*	*B*	Lim A MVA
121	170	1	No	0.00003	0.00030	0.00000	637.00
121	170	2	No	0.00002	0.00030	0.00000	637.00
122	126	1	No	0.00187	0.01103	0.02236	362.50
122	190	1	No	0.00000	0.00050	0.00000	399.00
122	190	2	No	0.00000	0.00050	0.00000	399.00
123	124	1	No	0.00229	0.01096	0.08382	788.00
123	126	1	No	0.00148	0.01296	0.04742	363.00
123	130	1	No	0.00315	0.01386	0.01562	788.00
128	131	1	No	0.00050	0.00435	0.01582	725.00
131	164	1	No	0.00157	0.01274	0.04801	894.00
134	138	1	No	0.00101	0.01057	0.19400	755.00
135	138	1	No	0.00511	0.05386	0.96200	925.00
135	142	1	No	0.00407	0.04244	0.77763	925.00
135	151	1	No	0.00002	0.00021	0.00379	818.70
136	138	1	No	0.00498	0.05195	0.95080	925.00
136	138	2	No	0.00491	0.05135	0.94180	925.00
137	139	1	No	0.00063	0.00663	0.12300	925.00
137	141	1	No	0.00817	0.08550	1.60340	925.00
138	140	1	No	0.00508	0.04856	1.07680	717.00
138	140	2	No	0.00592	0.06168	1.13960	717.00
139	142	1	No	0.00185	0.01929	0.35347	925.00
139	149	1	No	0.00108	0.01185	0.19640	818.70
143	144	1	No	0.04330	0.23308	0.00000	9997.00
143	145	1	No	0.01090	0.06078	0.00000	9997.00
143	214	1	No	0.00000	0.11142	0.00000	9997.00
144	145	1	No	0.01340	0.07974	0.00000	9997.00
144	213	1	No	0.00000	0.10983	0.00000	9997.00
145	212	1	No	0.00000	0.04913	0.00000	9997.00

Table A.11: Transmission line records (lines 190-216)

From Number	To Number	Circuit	Xfrmr	*R*	*X*	*B*	Lim A MVA
146	211	1	No	0.00000	0.12131	0.00000	9997.00
147	148	1	No	0.02090	0.12609	0.00000	9997.00
147	150	1	No	0.01550	0.14199	0.00000	9997.00
147	153	1	No	0.00330	0.02919	0.06369	438.20
148	152	1	No	0.15360	0.42814	0.00000	9997.00
152	171	1	No	0.02140	0.13140	0.00000	9997.00
154	155	1	No	0.00290	0.02317	0.00000	9997.00
154	155	1	No	0.00000	0.00760	0.00000	1593.00
154	156	1	No	0.01370	0.09500	0.16600	319.00
154	210	1	No	0.00000	0.04921	0.00000	9997.00
155	156	1	No	0.02210	0.19372	0.00000	9997.00
155	159	1	No	0.02280	0.16653	0.00000	9997.00
155	177	1	No	0.00457	0.03292	0.06020	358.00
155	209	1	No	0.00000	0.01000	0.00000	9997.00
156	159	1	No	0.00330	0.02916	0.00000	9997.00
156	185	1	No	0.00830	0.06278	0.00000	9997.00
156	208	1	No	0.00000	0.01144	0.00000	9997.00
157	186	1	No	0.00307	0.04261	0.69365	1171.20
159	178	1	No	0.00620	0.06590	0.12680	239.00
159	207	1	No	0.00000	0.05233	0.00000	9997.00
160	172	1	No	0.01040	0.06380	0.00890	120.00
160	173	1	No	0.01670	0.04690	0.00568	135.00
160	191	1	No	0.00000	0.00050	0.00000	135.00
161	181	1	No	0.00740	0.05120	0.08892	319.00
161	187	1	No	0.00200	0.01510	0.03030	451.00
161	187	2	No	0.00200	0.01510	0.03030	451.00
162	171	1	No	0.00900	0.05550	0.00774	120.00

Table A.12: Transmission line records (lines 217-243)

From Number	To Number	Circuit	Xfrmr	*R*	*X*	*B*	Lim A MVA
162	183	1	No	0.00950	0.05820	0.00812	120.00
163	184	1	No	0.03640	0.10210	0.01240	120.00
164	167	1	No	0.00800	0.06350	0.10920	451.00
164	169	1	No	0.00430	0.03230	0.06678	319.00
164	188	1	No	0.00290	0.03020	0.05792	335.00
165	186	1	No	0.00563	0.07809	1.27136	1171.20
167	169	1	No	0.01820	0.11740	0.01510	120.00
167	175	1	No	0.02200	0.11840	0.01470	102.00
167	187	1	No	0.00740	0.05810	0.11940	451.00
168	171	1	No	0.04590	0.14990	0.01814	120.00
168	192	1	No	0.00000	0.00050	0.00000	145.40
170	190	1	No	0.00420	0.03190	0.06480	438.00
170	190	2	No	0.00420	0.03190	0.06480	438.00
172	173	1	No	0.00840	0.05160	0.00720	120.00
172	176	1	No	0.00840	0.05160	0.00720	120.00
172	180	1	No	0.03100	0.19070	0.00000	9997.00
174	176	1	No	0.00830	0.05100	0.00712	120.00
175	182	1	No	0.00868	0.09030	0.01080	225.00
178	188	1	No	0.00770	0.00626	0.20440	334.00
181	190	1	No	0.00170	0.01150	0.01990	438.00
185	189	1	No	0.00475	0.03299	0.05726	335.00
185	206	1	No	0.00000	0.05620	0.00000	9997.00
187	205	1	No	0.00000	0.28985	0.00000	9997.00
193	196	1	No	0.00570	0.06500	1.00700	1100.00
193	196	2	No	0.00550	0.06540	1.00700	1100.00
193	198	1	No	0.00500	0.05950	0.91620	896.00
193	198	2	No	0.00490	0.05980	0.91080	1195.10

Table A.13: Transmission line records (lines 244-248)

From Number	To Number	Circuit	Xfrmr	*R*	*X*	*B*	Lim A MVA
194	202	1	No	0.00327	0.01100	0.06906	440.00
196	204	1	No	0.00000	0.02776	0.00000	9997.00
197	200	1	No	0.01620	0.16110	0.29490	440.00
197	203	1	No	0.00229	0.02277	0.04144	398.40
202	203	1	No	0.00660	0.06578	0.11970	398.40

Table A.14: Transformer records (transformer 1-27)

From Number	To Number	Circuit	Xfrmr	R	X	B	Lim A MVA	Tap Ratio
1	10	1	Yes	0.00040	0.03312	0	1000.0000	0.97951
2	11	1	Yes	0.00018	0.01060	0	840.0000	1.02375
5	55	1	Yes	0.00057	0.04562	0	725.0000	1.02435
5	56	1	Yes	0.00055	0.04589	0	725.0000	1.02435
6	39	1	Yes	0.00029	0.02534	0	4482.0000	0.98438
6	205	1	Yes	0.00003	0.01261	0	672.0000	1.05000
7	41	1	Yes	0.00093	0.08253	0	672.0000	0.99590
8	44	1	Yes	0.00040	0.03150	0	560.0000	1.05000
10	17	1	Yes	0.00111	0.04225	0	203.0000	1.00000
11	23	1	Yes	0.00057	0.02771	0	1250.0000	1.00000
12	31	1	Yes	0.00074	0.04122	0	1875.0000	0.97500
32	54	1	Yes	0.00658	0.16986	0	166.6000	0.97500
33	55	1	Yes	0.00107	0.03440	0	200.0000	1.00000
33	56	1	Yes	0.00085	0.03516	0	200.0000	1.00000
63	128	1	Yes	0.00018	0.01456	0	672.0000	1.02375
64	203	1	Yes	0.00006	0.00298	0	1233.0000	1.02380
64	204	1	Yes	0.00056	0.01153	0	1233.0000	1.02380
65	60	1	Yes	0.00011	0.00973	0	1533.0000	1.07763
65	61	1	Yes	0.00011	0.00964	0	1533.0000	1.07763
65	62	1	Yes	0.00011	0.00977	0	1533.0000	1.07763
69	66	1	Yes	0.00000	0.02000	0	650.0000	1.00000
69	67	1	Yes	0.00000	0.02000	0	650.0000	1.00000
70	202	1	Yes	0.00005	0.01308	0	1233.0000	1.02380
71	200	1	Yes	0.00056	0.01153	0	598.0000	1.05000
71	201	1	Yes	0.00056	0.01153	0	598.0000	1.05000
72	197	1	Yes	0.00015	0.01717	0	598.0000	1.05000
72	198	1	Yes	0.00015	0.01717	0	598.0000	1.05000

Table A.15: Transformer records (transformer 28-54)

From Number	To Number	Circuit	Xfrmr	R	X	B	Lim A MVA	Tap Ratio
72	199	1	Yes	0.00015	0.01717	0	598.0000	1.05000
75	103	1	Yes	0.00000	0.00280	0	1500.0000	1.05000
111	81	1	Yes	0.00000	0.08287	0	404.0000	1.02500
112	203	1	Yes	0.00006	0.00958	0	1233.0000	1.00000
112	204	1	Yes	0.00055	0.00012	0	1233.0000	1.00000
119	96	1	Yes	0.00000	0.03776	0	300.0000	1.00000
119	97	1	Yes	0.00000	0.03801	0	300.0000	1.00000
119	202	1	Yes	0.00006	0.00183	0	1233.0000	1.00000
124	200	1	Yes	0.00055	0.00012	0	598.0000	1.00000
124	201	1	Yes	0.00055	0.00012	0	598.0000	1.00000
125	197	1	Yes	0.00015	0.00553	0	598.0000	1.00000
125	198	1	Yes	0.00015	0.00553	0	598.0000	1.00000
125	199	1	Yes	0.00015	0.00553	0	598.0000	1.00000
131	196	1	Yes	0.00013	0.01194	0	672.0000	0.99526
133	195	1	Yes	0.00014	0.01249	0	672.0000	0.99526
134	139	1	Yes	0.00015	0.01614	0	672.0000	1.00000
135	205	1	Yes	0.00020	0.00011	0	672.0000	1.00000
136	147	1	Yes	0.00000	0.02827	0	375.0000	1.00000
137	196	1	Yes	0.00013	0.02844	0	672.0000	1.00000
138	126	1	Yes	0.00039	0.02550	0	672.0000	1.00000
138	127	1	Yes	0.00039	0.02550	0	672.0000	1.00000
139	195	1	Yes	0.00041	0.02927	0	672.0000	1.00000
141	140	1	Yes	0.00000	0.18200	0	200.0000	1.00000
143	142	1	Yes	0.00000	0.04433	0	150.0000	1.02500
145	144	1	Yes	0.00000	0.04444	0	150.0000	0.98040
151	148	1	Yes	0.00004	0.01420	0	600.0000	0.97510
152	148	1	Yes	0.00000	0.01514	0	1300.0000	1.07520

Table A.16: Transformer records (transformer 55-64)

From Number	To Number	Circuit	Xfrmr	R	X	B	Lim A MVA	Tap Ratio
155	154	1	Yes	0.00000	0.06000	0	500.0000	0.98040
158	159	1	Yes	0.00004	0.01420	0	600.0000	1.00000
159	157	1	Yes	0.00000	0.01586	0	500.0000	1.00000
173	175	1	Yes	0.00000	0.03000	0	167.0000	1.02500
177	176	1	Yes	0.00005	0.01795	0	650.0000	1.00000
185	186	1	Yes	0.00054	0.02695	0	350.0000	1.00000
187	186	1	Yes	0.00080	0.04540	0	700.0000	1.00000
189	163	1	Yes	0.00017	0.04872	0	1800.0000	0.97500
191	190	1	Yes	0.00100	0.04220	0	400.0000	1.00000
192	191	1	Yes	0.00000	0.02333	0	300.0000	1.00000

Table A.15: Load records (bus 2-60)

Number of Bus	ID	Status	S MW	S MVar
2	1	Closed	257.12	-4.84
3	1	Closed	505.80	-5.41
4	1	Closed	594.49	-27.79
10	1	Closed	72.72	8.28
11	1	Closed	13.20	0.00
13	1	Closed	39.36	0.00
14	1	Closed	36.72	7.80
15	1	Closed	201.00	56.94
16	1	Closed	40.44	6.06
17	1	Closed	44.70	5.34
18	1	Closed	129.36	14.22
19	1	Closed	154.98	70.62
20	1	Closed	295.20	86.04
21	1	Closed	19.62	31.68
22	1	Closed	186.00	68.40
23	1	Closed	14.04	1.98
23	2	Closed	65.63	-14.87
24	1	Closed	29.28	3.00
25	1	Closed	0.72	0.30
26	1	Closed	82.50	12.36
27	1	Closed	124.62	35.88
28	1	Closed	83.64	36.90
29	1	Closed	19.27	14.80
30	1	Closed	91.50	24.84
31	1	Closed	260.40	81.60
32	1	Closed	81.24	3.66
34	1	Closed	21.66	4.26
35	1	Closed	201.60	77.52
36	1	Closed	113.76	27.54
37	1	Closed	9.48	0.00
38	1	Closed	68.22	21.42
39	1	Closed	125.76	27.66
40	1	Closed	54.00	13.20
42	1	Closed	27.30	0.00
43	1	Closed	26.70	5.16
47	1	Closed	122.52	3.18
49	1	Closed	27.42	8.22
53	1	Closed	28.14	8.40
54	1	Closed	4.98	1.62
55	1	Closed	35.17	14.76
57	1	Closed	0.84	0.00
58	1	Closed	14.40	7.74
60	1	Closed	0.00	-1.15

Table A.18: Bus records (bus 62-144)

Number of Bus	ID	Status	S MW	S MVar
62	1	Closed	39.00	29.28
63	1	Closed	39.00	29.28
64	1	Closed	39.00	29.28
65	1	Closed	19.56	2.82
67	1	Closed	851.11	138.96
76	1	Closed	500.40	46.20
80	1	Closed	13.44	6.60
83	1	Closed	12.66	5.22
84	1	Closed	0.12	0.06
86	1	Closed	14.16	8.22
88	1	Closed	2.58	0.30
90	1	Closed	18.90	8.22
91	1	Closed	1.32	0.48
92	1	Closed	10.08	6.48
93	1	Closed	7.56	4.86
95	1	Closed	0.12	0.06
96	1	Closed	13.38	5.40
97	1	Closed	3.60	1.44
98	1	Closed	5.52	3.78
99	1	Closed	1.38	0.54
103	1	Closed	17.16	0.00
105	1	Closed	1.14	0.00
110	1	Closed	12.18	7.50
111	1	Closed	9.00	5.58
112	1	Closed	306.90	23.22
113	1	Closed	158.46	0.78
114	1	Closed	216.30	6.54
115	1	Closed	115.39	12.66
116	1	Closed	294.18	-1.45
118	1	Closed	75.24	9.26
119	1	Closed	214.98	4.93
120	1	Closed	243.72	2.34
122	1	Closed	227.16	-2.60
124	1	Closed	147.06	-14.41
126	1	Closed	434.76	-27.97
127	1	Closed	203.04	14.28
128	1	Closed	188.52	0.00
129	1	Closed	130.68	5.22
130	1	Closed	70.32	0.00
135	1	Closed	121.48	55.40
135	2	Closed	82.16	-37.70
136	1	Closed	-321.92	45.07
138	1	Closed	243.82	19.13
143	1	Closed	176.98	2.79
144	1	Closed	270.76	-4.08

Table A.16: Load records (bus 145-216)

Number of Bus	ID	Status	S MW	S MVar
145	1	Closed	366.48	4.48
146	1	Closed	-9.84	13.50
147	1	Closed	55.48	-1.18
148	1	Closed	44.69	0.38
150	1	Closed	24.24	-1.09
152	1	Closed	40.65	2.63
154	1	Closed	-54.64	10.72
154	2	Closed	279.17	33.39
155	1	Closed	206.87	-193.54
155	2	Closed	-381.63	216.25
156	1	Closed	-107.18	-3.46
158	1	Closed	11.18	199.80
159	1	Closed	9.52	-2.66
159	2	Closed	85.31	24.39
160	1	Closed	26.34	8.70
167	1	Closed	11.58	4.27
171	1	Closed	4.90	-0.97
172	1	Closed	9.95	1.67
173	1	Closed	1.38	0.48
175	1	Closed	14.41	1.90
178	1	Closed	10.44	0.00
180	1	Closed	4.40	-0.72
183	1	Closed	68.35	11.87
184	1	Closed	5.40	1.80
185	1	Closed	-18.33	18.05
187	1	Closed	-29.22	-0.34
188	1	Closed	17.88	0.00
189	1	Closed	11.88	-1.32
191	1	Closed	7.38	2.76
192	1	Closed	21.06	6.90
195	1	Closed	-49.33	-1.54
195	2	Closed	15.00	4.98
196	1	Closed	-229.88	40.92
197	1	Closed	18.66	6.18
199	1	Closed	13.22	3.38
199	2	Closed	-6.64	1.22
200	1	Closed	-78.62	15.32
201	1	Closed	-200.40	13.80
203	1	Closed	16.44	5.40
216	1	Closed	0.00	-4.99

Intentionally Blank

Part III

Investment Planning Model Considering HTLS Conductors

Kory W. Hedman, Faculty
Jonghwan Kwon, Graduate Student

Arizona State University

For information about this project, contact

Kory W. Hedman
Arizona State University
Department of Electrical Engineering
P.O. BOX 875706
Tempe, AZ 85287-5706
Phone: 480 965-1276
Fax: 480 965-0745
Email: kory.hedman@asu.edu

Power Systems Engineering Research Center

The Power Systems Engineering Research Center (PSERC) is a multi-university Center conducting research on challenges facing the electric power industry and educating the next generation of power engineers. More information about PSERC can be found at the Center's website: http://www.pserc.org.

For additional information, contact:

Power Systems Engineering Research Center
Arizona State University
527 Engineering Research Center
Tempe, Arizona 85287-5706
Phone: 480-965-1643
Fax: 480-965-0745

Notice Concerning Copyright Material

Table of Contents

List of Figures

List of Tables

Nomenclature

Indices and Sets

d	Index for day types, $d \in D$
g	Index for generators, $g \in G$
$g(n)$	Set of generators connected to node n
i	Index for segments, $i \in I$
k	Index of transmission lines, $k \in K$
$k(n,;)$	Set of lines specified as to node n
$k(;,n)$	Set of lines specified as from node n
n	Index for buses, $n \in N$
$st1, st2$	Index for sub problems
t	Index for time periods, $t \in T$
y	Index for years, $y \in Y$

Parameters

A	The AC resistance of a unit length conductor at $0\,^{o}C$
B	The temperature coefficient of resistance
B_k^O	Electrical susceptance of typical transmission line k
B_k^R	Electrical susceptance of HTLS transmission line k
B_k^A	Electrical susceptance of parallel transmission line k
B_k^{AH}	Electrical susceptance of HTLS parallel transmission line k
c_g	Operation cost of generator g ($/MWh)
c_g^{SU}	Startup cost of generator g
c_g^{SD}	Shutdown cost of generator g
$Cost^{\deg O}$	The end of service cost for typical conductor
$Cost^{\deg R}$	The end of service cost for HTLS conductor
$Cost^{\deg A}$	The end of service cost for parallel conductor
$Cost^{\deg AH}$	The end of service cost for HTLS parallel conductor
d	Strand diameter [in]
D	The conductor diameter
d_{nt}	Real power load at bus n in period t
D_d	Number of days in day type d
Deg_{kt}^T	The degradation effect due to the temperature T in period t
Deg_{Time}^T	The additional degradation effect due to the consecutive overheating operation
DT_g	Min down time for generator g
E	The linearize constant for the radiation heat loss rate

f	Flattening factor
G_k^O	Electrical conductance of typical transmission line k
G_k^R	Electrical conductance of HTLS transmission line k
G_k^A	Electrical conductance of parallel transmission line k
G_k^{AH}	Electrical conductance of HTLS parallel transmission line k
h	The convective heat transfer rate
ir	Interest rate
I^{HTLS}	Capital cost of HTLS line ($/Mile)
I^{Add}	Capital cost of parallel line ($/Mile)
I^{AH}	Capital cost of HTLS parallel line ($/Mile)
LS^b	The temperature effect term
LS^{time}	The additional effect term due to the consecutive operation
LS^{TempO}	Loss of strength effect by temperature of typical transmission line k
LS^{TempR}	Loss of strength effect by temperature of HTLS transmission line k
LS^{TempA}	Loss of strength effect by temperature of parallel transmission line k
LS^{TempAH}	Loss of strength effect by temperature of HTLS parallel transmission line k
LS^{timeO}	Additional loss of strength effect of typical transmission line k
LS^{timeR}	Additional loss of strength effect of HTLS transmission line k
LS^{timeA}	Additional loss of strength effect of parallel transmission line k
LS^{timeAH}	Additional loss of strength effect of HTLS parallel transmission line k
$Line_k^{mile}$	Length of transmission line (Mile)
M_k^1, M_k^2, M_k^3	Big M values
mC_P	Conductor heat capacity
NL_g	No-load cost of generator g
$P_k^{\max O}$	Thermal rating of typical transmission line k
$P_k^{\max R}$	Thermal rating of HTLS transmission line k
$P_k^{\max A}$	Thermal rating of parallel transmission line k
$P_k^{\max AH}$	Thermal rating of HTLS parallel transmission line k
$P_g^{\max}$	Max output and min output of generator g
P_g^{min}	Min output of generator g
Q_C	Forced convection hear loss rate
Q_R	Radiated heat loss rate
Q_S	Rate of solar heat gain
r_d	Reserve requirement (Percentage of total demend)
R	The reduction in cross-sectional area during wire drawing [%]
R_g^{hour}	Max ramp up and down rate for generator g

R_g^{SU} Max start up ramp rate for generator g

R_g^{SD} Max shutdown ramp rate for generator g

R_g^{10} 10-minuite ramp rate for generator g

RS_{1350} Residual aluminum (1350 alloy) strength as a percentage of initial strength [%]

S_i^L Slope of segment i for loss approximation

S_i^{TO} Slope of segment i for temperature calculation of typical transmission line

S_i^{TA} Slope of segment i for temperature calculation of HTLS transmission line

S_i^{TR} Slope of segment i for temperature calculation of parallel transmission line

S_i^{TAH} Slope of segment i for temperature calculation of HTLS parallel transmission line

STR_{1350} Calculated initial strength of the aluminum (1350 alloy) strands [N, Ibf]

STR_{ST} Calculated initial strength of the steel core [N, Ibf]

STR_T Calculated initial strength of the conductor [N, Ibf]

t Elapsed time [hours]

$T^{RatingO}$ Max temperature of typical transmission line

$T^{RatingR}$ Max temperature of HTLS transmission line

$T^{RatingA}$ Max temperature of parallel transmission line

$T^{RatingAH}$ Max temperature of HTLS parallel transmission line

T^{maxO} Length of temperature block of typical transmission line

$T^{\max R}$ Length of temperature block of HTLS transmission line

$T^{\max A}$ Length of temperature block of parallel transmission line

$T^{\max AH}$ Length of temperature block of HTLS parallel transmission line

UT_g Min up time for generator g

W The loss of strength [%]

W_a The loss of strength in the fully-annealed state [%]

$\grave{o}_s$ The emissivity of the conductor

θ^{max} Bus voltage angle difference limits

κ_y Salvage factor in year y

σ The Stefan-Boltzmann constant

Variables

ad_{ky} Binary variable indicating addition of parallel line decision (k, y)

ah_{ky} Binary variable indicating addition of HTLS parallel line decision (k, y)

ahs_{kdy}^{st1} HTLS parallel line addition status (k, d, y) in investment sub-problem

ahs_{kdy}^{st2} HTLS parallel line addition status (k, d, y) in production cost sub-problem

as_{kdy}^{st1} Parallel line addition status (k, d, y) in investment sub-problem

as_{kdy}^{st2}	Parallel line addition status (*k, d, y*) in production cost sub-problem
$C_{ktdy}^{\deg O}$	Loss of strength cost of typical transmission line (*k, t, d, y*)
$C_{ktdy}^{\deg R}$	Loss of strength cost of HTLS transmission line (*k, t, d, y*)
$C_{ktdy}^{\deg A}$	Loss of strength cost of parallel transmission line (*k, t, d, y*)
$C_{ktdy}^{\deg AH}$	Loss of strength cost of HTLS parallel transmission line (*k, t, d, y*)
C_{kt}^{deg}	The degradation cost for line *k* in period *t*
$Cost^{deg}$	The end of service cost for the conductor
Deg_{kt}	The degradation for line *k* in period *t*
$I^2R(T_C)$	Joule heating
LoS_{kt}	The loss of tensile strength for line *k* in period *t*
LoS_{ktdy}^{O}	Loss of strength of typical transmission line (*k, t, d, y*)
LoS_{ktdy}^{R}	Loss of strength of HTLS transmission line (*k, t, d, y*)
LoS_{ktdy}^{A}	Loss of strength of parallel transmission line (*k, t, d, y*)
LoS_{ktdy}^{AH}	Loss of strength of HTLS parallel transmission line (*k, t, d, y*)
P_{gtdy}	Real power output (*g, t, d, y*)
P_{ktdy}	Real power flow (*k, t, d, y*)
P_{ntdt}^{L}	Total losses on all lines connected to and delivering power to bus *n* (*n, t, d, y*)
P_{ntdt}^{L+}	Total losses on the line *k* and delivered to 'to bus' *n* (*n, t, d, y*)
P_{ntdt}^{L-}	Total losses on the line *k* and delivered to 'from bus' *n* (*n, t, d, y*)
P_{ktdy}^{over}	Slack variable for line overloading (*k, t, d, y*)
r_{gtdy}	Spinning reserve provided by generator (*g, t, d, y*)
re_{ky}	Binary variable indicating HTLS reconductoring decision (*k, y*)
rs_{kdy}^{st1}	HTLS reconductoring status (*k, d, y*) in investment sub-problem
rs_{kdy}^{st2}	HTLS reconductoring status (*k, d, y*) in production cost sub-problem
T_C	Conductor temperature [^oC]
T_∞	The room temperature
T_{ktdy}	Transmission line temperature (*k, t, d, y*)
T_{ktdy}^{b+}	Length of positive temperature block (*k, t, d, y*)
T_{ktdy}^{b-}	Length of negative temperature block (*k, t, d, y*)
u_{gtdy}	Binary unit commitment variable (*g, t, d, y*)
v_{gtdy}	Startup variable (*g, t, d, y*)
w_{gtdy}	Shutdown variable (*g, t, d, y*)

θ_{ntdy}	Bus voltage angle (*n, t, d, y*)
θ_{ktdti}^{k+}	Length of positive orthant segment (*k, t, d, y, i*)
θ_{ktdti}^{k-}	Length of negative orthant segment (*k, t, d, y, i*)

Terms

ACSR	Alloy Aluminum Conductor Steel Reinforced
HTLS	High Temperature Low Sag
ROW	Right of way
SCUC	Security Constraint Unit Commitment

Intentionally Blank

1. Introduction

1.1 Research Premise

Since it is, generally, not economical to store electricity, the power system always needs appropriate generation and transmission capacity to ensure a reliable and stable supply of electricity every second. For this reason, system operators need to conduct long-term power system expansion planning as well as short-term operation planning studies [1]. Transmission expansion planning (TEP) is one of the methods of long-term planning motivated by serving future forecasted demands and improving both the efficiency and the reliability of the power system [2]. TEP determines time, location, and size of new lines that should be installed in the power system [3]-[4]. However, political obstacles and environmental issues often impede construction of a new transmission line. As a result, recent academic studies, as well as those by utility companies, have given considerable attention to new means of transporting more power through existing transmission systems [5].

Another option to increase the transfer capability between points is to reconductor a path with a conductor that has a higher thermal capacity, such as a High Temperature Low Sag (HTLS) conductor. The structural modification and extended power outages during the construction are minimal. The HTLS conductors are developed to increase thermal limits by improving thermal expansion characteristic and tensile strength with temperature. The addition of a parallel line, when a tower structure has the ability to add another set of phases, is another way that one may consider. The advantage of this method is that resistance and power losses of the line are reduced. However, the transmission towers should be replaced since most of them do not support such parallel line installation, and it may take more out of service time than reconductoring [6]. Moreover, addition of an HTLS parallel line is another option that brings thermal rating increase over 200%, while take the advantage of parallel line addition option (with a traditional conductor), reduced power losses.

In addition to a physical structure modification, the Thermal Constraint Relaxation (TCR) is an operation-based option that allows the line flow exceeding steady state line ratings with a certain penalty price. However, the material tensile strength of conductors may decrease with consecutive operation at elevated temperature due to annealing, and such accumulated affects can reduce the expected service time of the conductor. Therefore, the penalty price in TCR should be at least as high as the degradation cost incurred due to the damage.

1.2 Report Scope

This report proposes the long-term TEP model considers HTLS reconductoring, parallel line addition, HTLS parallel line addition, and TCR as possible options to increase transmission capacity while preserving current ROWs. The proposed TEP model is formulated as a mixed integer programming problem and the network flow model is

approximated by the direct current optimal power flow (DCOPF) combined with a piecewise linear loss approximation model (to create a lossy DCOPF) and a security constrained unit commitment (SCUC) formulation. Lagrange Relaxation (LR) and a decomposition algorithm are applied to solve the proposed model based on a parallel computing environment.

This research also proposes the degradation model to capture the costs associated with overloading operation, which may incur loss of tensile strength and a reduction in the expected service life of the conductor. In addition, a piecewise linear approximation is applied to approximate the current-temperature relationship of the conductor. The degradation model is incorporated with the proposed TEP model.

1.3 Report Organization

This report is organized into six chapters. Chapter 2 provides background and technical details, which is helpful to understand later chapters. A concept of the transmission expansion planning (TEP) and alternative options that can be used in TEP while preserving current ROWs are presented first. Chapter 2 also provides current-temperature relationship of the conductor as well as the effect of elevated temperature operation. The characteristic of the HTLS conductors is briefly presented. Lastly, two technical details, piecewise loss approximation and LR, are introduced.

The focus in Chapter 3 is on the proposed degradation model. The chapter introduces the piecewise linearized temperature model to approximate line temperature in a linear manner. The chapter then presents the linearized degradation model along with its pros and cons. Monte Carlo simulations are conducted to compare the proposed method and IEEE standard equations in Chapter 3.

The mathematical optimization problem for the long-term TEP model is developed in Chapter 4. The formulation uses piecewise linear techniques to approximate real power losses and line temperatures. It is assumed that getting new ROWs is restricted. Also, HTLS reconductoring, parallel line addition, and HTLS parallel line addition are considered as investment options. The decomposition approach is applied to solve the model more efficiently.

The long-term TEP model developed in Chapter 4 is simulated using the IEEE 24 bus Reliability Test System (RTS) in Chapter 5. System modification and basic information of the simulation is presented. A traditional TEP model, which does not consider the degradation effect, is compared with the proposed model. Also, the impact due to considering line losses is evaluated.

Chapter 6 is a concluding chapter. It provides a summary of the work in this report and discusses future work.

2. Background

This chapter provides the background knowledge necessary to understand the technical details in the subsequent chapters. The information in this chapter also provides context for this report. The chapter describes the Transmission Expansion Planning concept in Section 2.1 and the means of increasing transmission system capacity in Section 2.2. HTLS conductors are introduced in Section 2.3. The conductor thermal behavior is presented in Section 2.4. The conductor degradation effect, due to high-temperature operation, is presented alongside a literature review of contemporary work in Section 2.5. Section 2.6 describes the piecewise linear approximation of line losses. Section 2.7 provides the LR and decomposition algorithm.

2.1 Transmission Expansion Planning

Since electricity cannot be economically stored, the power system always needs appropriate generation and transmission capacity to ensure a reliable and stable supply of electricity every second. For this reason, system operators need to conduct long-term power system expansion planning as well as short-term operation planning. Transmission expansion planning (TEP) is one of the methods of long-term planning motivated by serving future forecasted demands and improving both the delivery efficiency and the reliability of the power system [2]. TEP determines time, location, and size of new lines that should be installed in the power system [3]-[4].

From the planning time horizon point of view, TEP can be classified into static transmission expansion planning (STEP) and dynamic transmission expansion planning (DTEP) [5]. In STEP, all investments are considered within a single year; while in DTEP, the installation of the new line is planned in different time horizons. DTEP will provide a better planning solution, but is harder to solve [7].

Diverse models have been proposed to formulate TEP. Generally, the models can be classified into two groups by the assumptions or simplifications of the power flows. They are either formulated as alternating current optimal power flow (ACOPF) or as direct current optimal power flow (DCOPF), where the latter is a simplified and linearized model of the former one. The advantages and disadvantages of two models are discussed in [2].

Algorithms for solving TEP can be divided into two groups, mathematical programming (MP) and meta-heuristics (or heuristics) [2][5][8]. MP, such as dynamic programming (DP) [9], quadratic programming [10], non-linear programming [11], mixed integer programming (MIP) [12]-[13], have been frequently used and, depending on the class of the optimization problem that is being considered, these techniques are, at times, exact solution methods. Algorithms, such as interior point algorithm [14]-[15] and Benders' decomposition [16]-[17], have been also proposed to solve MP. On the other hand, meta-heuristics, such as genetic algorithm (GA) [18], greedy randomized adaptive search procedure (GRASP) [19], tabu search [20], and fuzzy set theory, [21], can solve the

problem relatively quickly but there is no general guarantee that the meta-heuristic will be effective at finding quality solutions nor can they guarantee a global solution.

Two main assessments for TEP are economic assessment and reliability assessment [22]. One of the methodologies of economic assessment is "Transmission Economic Assessment Methodology" (TEAM), which is developed by the California Independent System Operator (CAISO) [23]. The reliability assessment is directly related to the reliability standards, which are specified by the North American Reliability Corporation (NERC) [22].

2.2 Increasing Transmission System Ampacity

Political obstacles and environmental issues often impede construction of a new transmission line, especially when a new right of way is required. As a result, recent academic studies, as well as those by utility companies, have been given considerable attention to new means of transporting more power through existing transmission systems. In this section, power flow limits of the transmission system are investigated first, then diverse means to increase the transmission system ampacity, without needing new ROWs, are introduced [5].

The maximum allowable conductor temperature and the assumed "worst-case" conditions, such as ambient weather conditions or ground clearance requirements, typically determine the thermal rating of an overhead transmission line. The maximum allowable conductor temperature, which can be converted to the amount of power that can be transferred over the line, is specified to avoid excessive sag or loss of tensile strength. For example, the temperature limit on the Alloy Aluminum Conductor Steel Reinforced (ACSR) conductor ranges from 50°C to 150°C based on the maximum sags or loss of tensile strength in the aluminum strands [24].

In addition, non-thermal system restrictions, such as system stability problems, can also limit the maximum power flow. Generally, system modifications cannot resolve such problems. For example, the voltage drop limit requires a lower power flow for the longer overhead lines. Typically, the power flow is restricted by the thermal limit for shorter lines (up to 50 Mile). Longer lines (50 to 200 Mile) have voltage regulation and very long lines (more than 200 Mile) are limited by stability issues [26].

Note that the transmission system consists of electrical equipment, which is typically specified to have certain power flow limits for safe and reliable operation. The maximum allowable power flow over the whole transmission system may be limited by any one of the system elements, but especially by the transformer. Reference [27] shows that only 41% of the circuits were limited by the line thermal limits and 59% of the circuits were limited by other system elements.

There are several different means to increase transmission capability. The optimal way may depend on factors such as system structure, environmental concerns, and existing component conditions. In addition, it is necessary to know how much and how often one

needs in-creased capability. Diverse alternatives to increase transmission line capacity can be divided into two groups based on needs and conditions: investment options for modifying physical structures and operational options by improving control or monitoring of system status [28].

When the overloading magnitude and frequency is small, conductor retentioning may be a possible way to reduce sag at high temperatures and, therefore, increase the line rating. Increasing tower height may also be an efficient investment option. However, the corresponding increases in rating are modest. On the other hand, when overloading occurs frequently at high magnitude, a possible investment option is reconductoring with a conductor with a higher thermal capacity, such as a HTLS conductor. The corresponding rating may increase by more than 100%. All the options above preserve current system structure, with the exception of replaced conductors. Also, the environmental impact is normally low and extended out-of-service period for invested lines during construction are rare [28]-[31].

Parallel line addition is an alternative way that one may consider. The advantage of this method is a reduced resistance and power losses over the line. However, the transmission towers should be replaced, since most of them do not support parallel line installation. Also, it may need more out of service time than reconductoring option [28]. Moreover, HTLS parallel line addition is another option that brings a thermal rating increase over 200%, while take the advantage of parallel line addition option, reduced power losses.

Large transmission capacity increases, which require replacing the whole transmission line structure and increase both the voltage and current, would be the most dramatic option among other investment options. Also, this is the most expensive and time consuming process, but it only preserves the current ROWs [29].

In addition to system configuration changes by investment, there are operational based options available for increasing transmission line capability. Dynamic Line Rating (DLR) utilizes real time adjusted line rating based on the ampacity under ambient circumstances such as weather parameters and other conditions. Transmission systems are commonly operated at much less than their thermal capacity under steady state operation. Implementing DLR may allow the use of less conservative assumptions, i.e., the worst case. The real time rating can be determined by line temperature measurements along with line rating theory. Reference [29] studied different means to utilize DLR in Finland. Note that DLR is unlikely to change any non-thermal operating limits.

Thermal Constraint Relaxation (TCR) is another operational based option that allows the line flow to exceed the steady state line ratings for a certain penalty price. Typically, exceeding the steady state operating level is only allowed for emergency situations for a limited time in order to avoid load interruptions. Many ISOs implement similar constraint relaxations. For example, in CAISO's day-ahead market simulations, a penalty price for violating the steady state line rating is $5,000/MWh [32]. However, such constraint relaxations are generally implemented because of infeasibility or to enable price control, not for increasing transmission line capacity [33]. TCR in this study aims to increase the

line ampacity by utilizing the asset more flexibly. It is clear that there is a cost associated with flexible operations. For instance, exceeding the steady state operation level can cause the loss of tensile strength due to overheated line temperature. It may also reduce the lifespan of the asset. Therefore, the penalty price for overloading should be at least as high as the degradation cost incurred due to the damage. These high temperature effects on the conductor, as well as the degradation model for capturing the penalty price, are discussed in detail in Section 2.5 and Chapter 3, respectively.

2.3 Thermal Behavior of the Overhead Conductors

The fundamental parameter that specifies overhead conductor thermal limits is its maximum allowable temperature, as well as maximum sag and decreased conductor clearance from the ground [26]. Thus, the conductor temperature is an essential clue for determining thermal limits and it can be achieved from an investigation of the thermal behavior of the conductors. A combination of heating and cooling affect contributes to the conductor temperature. The main sources of conductor heating are current flowing on the line, radiation from the sun, and reflection from the surroundings. At a same time, the ambient air temperature, wind speed, and radiation of heat from the conductor incurs a cooling effect. These heating and cooling energies should be balanced all the times. A generic representation of the conductor thermal behavior is shown in Figure 2.1 [29], [34].

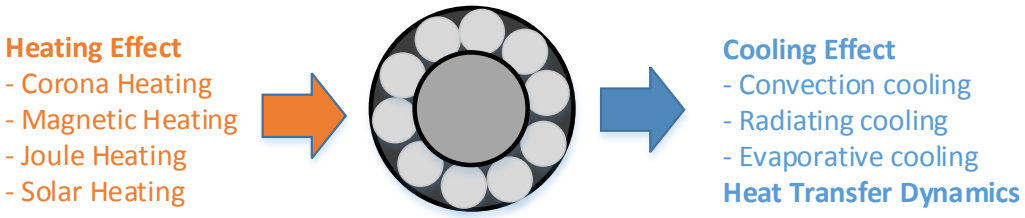

Figure 2.1 Generic representation of the conductor thermal behavior

However, such quantities vary along the transmission line and are difficult to measure or predict precisely due to the inherent nonlinearity of the conductor thermal dynamics. The IEEE and CIGRE working groups provide the conductor temperature prediction models, which utilize the conductor thermal balance characteristic on a unit length of conductor.
IEEE has published mathematical models to predict conductor temperature [35]. This model provides standard methods for calculating conductor temperature and the thermal capacity in the steady and dynamic states. In the IEEE Standard, the dynamic heat balance equation is expressed as follows,

$$Q_C + Q_R + mC_P \frac{dT_C}{dt} = Q_S + I^2 R(T_C) \tag{2.1}$$

The IEEE standard ignored the corona heating effect, magnetic heating effect, and evaporative cooling effect, which have little impact on the thermal behavior of the conductor. In addition, this equation normally requires repeated calculation due to its

inherent nonlinearity. Specific methods to calculate each term in (2.1) can be found in [35].

The CIGRE working group has also published on the thermal behavior of overhead conductors in [36], describing a calculation method for conductor thermal behavior. The CIGRE standard presents the more theoretically complete heat balance equation, but their approach to the calculation of the heat balance terms is different from the IEEE standard. Schmidt et al. [37] examined the differences between both standards, as well as its impact on the line rating determination.

In addition, W. Z. Black et al. [38] proposed a simplified conductor temperature model by approximation of the radiation term as a linear function of conductor temperature. A simple solution can be obtained by eliminating one of the nonlinearities in the conductor temperature equation. The simplified equations can be expressed as follows,

$$T - T_{\infty} = \frac{I^2(A + BT_{\infty}) + \alpha_s DQ_S}{\pi hD + \alpha_l D\sigma E - I^2 B} \tag{2.2}$$

2.4 Effect of High Temperature Operation on the Overhead Conductor

It is clear that operation of overhead conductors at elevated temperature can cause damage to the aluminum wires cumulatively and that prolonged high temperature operation will significantly reduce the expected service life of the conductor. As the current flowing through a conductor increases, a conductor elongates with the increased temperature. This elongation increases the sag of the conductor, which decreases the ground clearance. If the conductor temperature remains high for an extended and consecutive period of time, the tensile strength of the conductor may decrease [39]. Although the loss of strength is gradual, it accumulates over time and increases the probability of outages and blackouts [40]. Also, the effects of the elevated temperature operation on the aluminum conductor are irreversible, and the damages experienced by the conductor are also cumulative. Figure 2.2 shows the relationship between conductor sags and temperature for different conductors. Note that other factors that may incur negative changes in the conductor's mechanical and electrical properties, such as wind induced vibration and corrosion, are outside of the scope of this study [41]-[42].

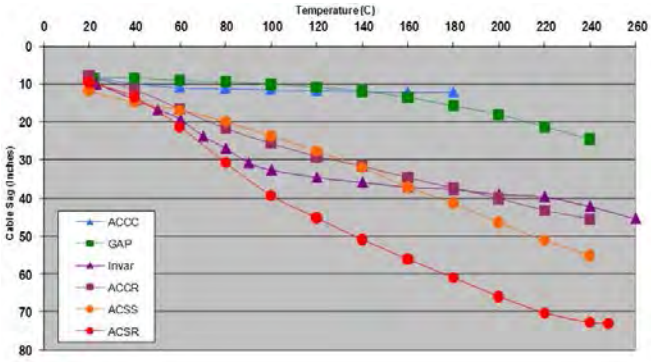

Figure 2.2 Conductor sags vs. Temperature [43]

The material tensile strength of aluminum and copper wires decreases with consecutive operation at temperatures above $75^{o}C$ and extended exposure at such high temperature can lead to tensile failures. The American Society for Testing and Materials (ASTM) and the International Engineering Consortium (IEC) standards specify the minimum tensile strength of aluminum and copper wires. Also, the National Electrical Safety Code (NESC) sets the minimum permissible clearance to ground and other features for aerial transmission lines [24].

The loss of tensile strength of a conductor is caused by annealing effect. Annealing is the metallurgical process where applied high temperature softens hardened metal resulting in a loss of tensile strength and is a function of both the magnitude of the temperature and the duration of the overheated time [35]. The loss of tensile strength of aluminum conductors, such as steel reinforced conductors (ACSR), is a function of the loss of strength of the aluminum strands compared to the rated strength of both the aluminum and steel wires. Typically, the steel wires will not anneal at temperatures used for ACSR steady state and even for emergency operation. Since the ACSR conductor derives about half of its strength from the steel wires and half from the aluminum wires, the degradation of the aluminum strands only partially impacts the overall conductor strength. The ACSR conductor can be operated such that the maximum loss of overall strength of the conductor is limited to about 10% [35].

Some conductors are designed to reduce the effect of annealing on conductor strength by increasing the strength percentage of steel core or using already annealed aluminum strands. For those conductors, however, the maximum temperature can be determined by the thermal capability of connectors, as well as by other accessories. The maximum operating temperature of different types of conductors can be found in [6].

The loss of strength due to annealing of the aluminum wires is a temperature and time dependent phenomenon. Predicting such loss requires a complex analysis of the metallurgical aspects of the conductor components as well as probability characteristic of ambient factors that may affect the conductor temperature. However, the key to approximate the loss of strength over the expected life of the conductor is to predict the time-temperature series that will result in annealing. These time-temperature patterns can be obtained by predicting weather conditions and making an assessment of the current-temperature calculation. The projected remaining strength of the conductor can be determined based on such information [6].

Harvey et al. [44] used experimental results to derive the residual strength predict equations, which were adopted in the IEEE standard for determining the effects of high temperature operation on conductors [45]. In the IEEE standard, the residual conductor strength predictor equations for high-temperature operation are expressed as follows,

$$RS_{1350} = (-0.24T + 134)t^{-(0.001T - 0.095)(2.54/d)} \qquad (2.3)$$
$$If\,(-0.24T + 134) > 100,\ \ use\,100\ \ for\ this\ term$$

$$RS_{COM} = RS_{1350}(STR_{1350} / STR_T) + 109(STR_{ST} / STR_T) \quad (2.4)$$

Note that this model was derived for the ACSR conductors. It assumes that the loss of tensile strength of stranded conductors is dependent on the diameter of the strand wires. The factor 1.09 in the ACSR model accounts for the increased load carried by the steel core as a result of conductor elongation due to the high temperature operation [44]. Therefore, this factor can be adjusted for other conductors accordingly. In applying these equations, the cumulative strength reduction for multiple exposures at the same conductor temperature may be found by simply adding up all the hours and calculating the residual strength. For multiple exposures at different conductor temperatures, all exposures should be expressed as an orderly series of temperatures and times and converted to an equivalent time at the highest temperature. Finally, they can be added all together to determine the cumulative loss of strength.

Morgan et al. [46] proposed that the percentage reduction in cross-sectional area during wire drawing has more effect on the loss of tensile strength than its diameter. The loss of strength in his method is expressed as follows, and the constants A, B, C, and m can be evaluated for each conductor type. Such constants and comparison with IEEE standard method are given in [46].

$$W = W_a\{1 - \exp[-\exp(A + m\ln t + BT + C\ln(R/80))]\} \quad (2.5)$$

Note that methods that have been previously proposed for calculating the long-term loss of tensile strength require the thermal history of the conductor. In addition, such temperature information should be expressed as an orderly series of temperatures. Therefore, the resultant cumulative loss of tensile strength due to annealing at each time is still uncertain.

2.5 High Temperature Low Sag (HTLS) Overhead Conductor

It The Alloy Aluminum Conductor Steel Reinforced (ACSR) is mainly used in the existing transmission system. Those conductors have thermal limits due to either the maximum sag or the loss of tensile strength. The High Temperature Low Sag (HTLS) conductors are developed to overcome such limits by improving thermal expansion characteristic and tensile strength with temperature. Therefore, the HTLS conductor can dissipate more heat, without incurring excessive sag and this increases the thermal power rating of the line typically by a factor of two. For limited time emergencies, the ACSR may be operated at temperatures as high as 125◦C. At a same time, the HTLS conductor with the same diameter as the ACSR could be operated at temperatures as high as 240◦C with less thermal elongation than ACSR [47]. In addition, HTLS conductors can replace conventional conductors without extensive alteration of existing structures and new ROWs [48].

Low conductor sags is another advantage of HTLS conductors. As mentioned in section 2.2, not all the congested lines reach their thermal limits. Many times the line flow is

limited by other security limits. HTLS conductors can also improve the security restrictions such as sag limits. If the HTLS lines operated below the thermal rating due to such security limits, they will incur lower sag than similar lines that are not HTLS [49].
HTLS conductors have similar configuration with ACSR. Most of the electrical current flows in aluminum wires that are stranded over a reinforcing core. The reinforcing core supports most of the tension load at high temperatures and under high loads. So the performance of HTLS conductors depends on the mechanical and electrical properties of the aluminum strand and reinforcing cores.

There are many commercially available HTLS conductors. Aluminum Conductor Steel Supported (ACSS) has fully annealed aluminum strands over a conventional steel core. Gap-type (Super) Thermal resistant Aluminum alloy Conductor Steel Reinforced (GZTACSR or GTACSR) has high-temperature aluminum alloy strands (TAL or ZTAL) over a low-thermal elongation steel alloy. (Super) Thermal resistant Aluminum alloy conductor Invar Reinforced (ZTACIR or TACIR) has an oil-filled gap between TAL wires and a conventional steel core. Aluminum Conductor Composite Core (ACCC) has ZTAL wires over a low-thermal elongation metal matrix composite core. Aluminum Conductor Composite Reinforced (ACCR) has fully annealed aluminum strands over a low-thermal elongation polymer matrix composite core. Also, Carbon fiber reinforced aluminum (ACCFR) and Composite Reinforced Aluminum Conductors (CRAC) are in a stage of development [47], [50].

2.6 Piecewise Loss Approximation

It Power flow analysis is an essential part of studying the TEP. The ACOPF is non-linear and non-convex problem. Thus, linear approximations of the ACOPF, the DCOPF, have been applied widely in TEP to avoid a computational complexity [12], [51]. The traditional DCOPF approximates a lossless system. However, it is clear that the dispatch and power flow solutions obtained from a lossless DCOPF do not reflect the effect of real power losses. In the TEP, the cost savings of line investment highly depends on the more efficient dispatch, as well as the power flow. Therefore, investigating on the lossy DCOPF model is preferred to capture more precise line power flow in this study.

Diverse loss approximation methods have been studied. Reference [52] presents the Taylor Series expansion to linearize the loss formulation. Losses are represented as fictitious loads in [53]. One can intrinsically capture the real power losses by using the piecewise linear loss approximation as well [54]-[55]. The line loss between bus n and m can be expressed as a mathematical form in (2.6). By applying one of the assumptions used in the DCOPF approximation, i.e., by assuming all voltages are 1 pu, one can simplify this equation to be (2.7). The non-linear part of (2.6), along with a piecewise linear curve approximation, is shown in Figure 2.3.

$$P_{loss} = G_k(V_n^2 + V_m^2) - 2G_k V_n V_m \cos(\theta_n - \theta_m) \tag{2.6}$$

$$P_{loss} = 2G_k(1 - \cos(\theta_n - \theta_m)) \tag{2.7}$$

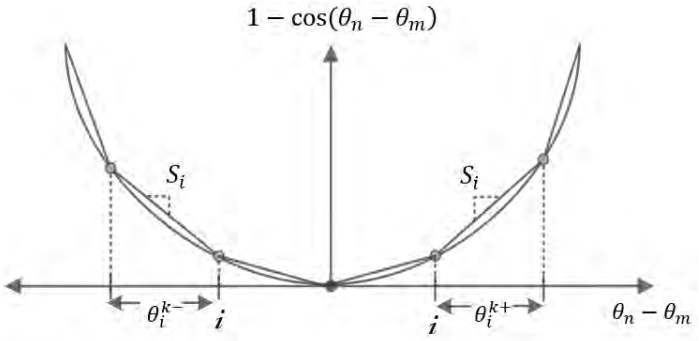

Figure 2.3 Piecewise linearized loss approximation

In order to linearize the simplified loss equation, the bus angle difference can be expressed as a sum of multiple segments θ_i^{k+} and θ_i^{k-} in (2.8). The slope of segments used to represent the non-linear part, i.e., $1-\cos(\theta_n-\theta_m)$ accordingly in (2.9). Finally, $2G_k$ is multiplied to fully approximate the line loss equation (2.7) in (2.10). The length of bus angle difference segments is limited by (2.11) and (2.12). Note that the number and the length of segments may affect accuracy of the approximation and computational complexity. Additional information on the lossy DCOPF and the alternative way to model it using MIP to avoid fictitious losses can be found in [54]-[55].

$$\left(\theta_n-\theta_m\right)=\left(\sum_{\forall i}\theta_i^{k+}-\sum_{\forall i}\theta_i^{k-}\right) \tag{2.8}$$

$$1-\cos(\theta_n-\theta_m)=\left(\sum_{\forall i}S_i\theta_i^{k-}\right)+\left(\sum_{\forall i}S_i\theta_i^{k+}\right) \tag{2.9}$$

$$P_{loss}=\sum_{\forall k(n,:)}2G_k\left(\sum_{\forall i}S_i\theta_i^{k-}\right)+\sum_{\forall k(:,n)}2G_k\left(\sum_{\forall i}S_i\theta_i^{k+}\right) \tag{2.10}$$

$$0\le\theta_i^{k+}\le\theta_i^{\max}\qquad\forall i \tag{2.11}$$

$$0\le\theta_i^{k-}\le\theta_i^{\max}\qquad\forall i \tag{2.12}$$

2.7 The Lagrange Relaxation and Decomposition

The LR solves problems by relaxing certain constraints and adding these relaxed constraints with a 'penalty factor' in the objective function [56]. For example, the second constraint in the original problem (2.13) can be dualized with the Lagrangian multiplier, λ, in (2.14).

$$\begin{aligned}&\text{Min}: c^T x\\ &\quad A_1x=b_1\\ &\quad A_2x=b_2\\ &\quad x\ge 0\end{aligned} \tag{2.13}$$

$$
\begin{aligned}
L(\lambda) = \min\ & c^T x + \lambda^T (b_2 - A_2 x) \\
& A_1 x = b_1 \\
& x \geq 0
\end{aligned}
\tag{2.14}
$$

The Lagrangian, $L(\lambda)$, is a relaxation of the original problem. Based on optimization theory, the Lagrangian is a lower bound (LB) to the solution of (2.13). Note that Lagrange Relaxation provides a lower bound when the original problem is a minimization problem and it provides an upper bound when the original problem is a maximization problem; for this work and this discussion, we are focused on minimization problems. Instead of solving the primal problem (2.14), one can solve the Lagrangian dual by maximizing the Lagrangian function with respect to the Lagrangian multipliers in (2.15). The Lagrangian dual finds the Lagrangian multipliers with the tightest LB that enforce $(b_2 - A_2 x)$ term into zero at optimality. However, the tightest LB may be below the optimal solution for non-convex problems. The gap between the LB and the optimal solution is known as a duality gap. Thus, the Lagrangian relaxation does not guarantee an optimal solution for non-convex problems, but LR generally can provide a decent LB. However, this LB solution is infeasible whenever the duality gap is not zero. To achieve a feasible solution, one can repair the infeasibility or find a possible feasible solution with proper techniques. Thus, the LB can still be used to provide a path to find a "good" feasible solution.

$$
\begin{aligned}
\max_{\lambda} L(\lambda) = \max_{\lambda} \Big[\min\ & c^T x + \lambda^T (b_2 - A_2 x) \Big] \\
& A_1 x = b_1 \\
& x \geq 0
\end{aligned}
\tag{2.15}
$$

Lagrangian decomposition is one special case of LR, which is based on the dual optimization theory. That is, one can decompose the original problem into several independent sub-problems by choosing proper coupling constraints and relax them using LR. Then, one can solve the sub-problems independently while sharing the same Lagrangian multiplier during each iteration. In addition, parallel computing techniques can be applied to solve independent sub-problems. In [57], generator outputs are treated as coordination variables to form coupling constraints. In [58], the coupling constraints contain the voltage and bus angle variables along with tie-lines to decompose operating areas into independent sub-areas. Choosing the coupling constraints vary on how to model the problem as well as different situations. Reference [59] shows that relaxing two kinds of constraints were more beneficial.

The performance of Lagrangian decomposition is dependent on the parameter tuning process. For example, the initialization and updating strategies of the Lagrangian multipliers influence algorithm efficiency in the optimization process. Reference [60] introduced three algorithms in determining of the Lagrangian multipliers: the sub-gradient method, various versions of the simplex-based method, and multiplier

adjustment methods. In addition, The Lagrangian Relaxation and Genetic Algorithms (LRGA) method is introduced in [56].

3. The Degradation Model

The operation of overhead conductors at elevated temperatures can cause loss of tensile strength, as well as a reduction in the expected service life of the conductor. Therefore, there is a cost associated with overloading operations. This cost can be captured by introducing the degradation model in this report. As a beginning process, calculating the line temperature should be conducted to capture the loss of strength due to the overheated operation. The piecewise linear approximation of line temperature calculation is introduced in Section 3.1. The chapter proposes the degradation model in Section 3.2. The simulation results of the Monte Carlo Simulations, conducted to get a flattening factor as well as compare the proposed degradation model and the IEEE standard model, are given in Section 3.3.

3.1 The Piecewise Linearized Temperature Model

The simplified current-temperature equation in Section 2.3 still has a nonlinearity in terms of the line current (3.1). If the environmental factors can be assumed as fixed values throughout the planning horizon, one can approximate the line temperature using a piecewise linearized model. Figure 3.1 shows the non-linear trends of the current-temperature equation (3.1) and overview of its piecewise linearization.

$$T_k = \frac{I_k^{\,2}(A + BT_\infty) + \alpha_s D Q_S}{\pi h D + \alpha_f D \sigma E - I_k^{\,2} B} + T_\infty \tag{3.1}$$

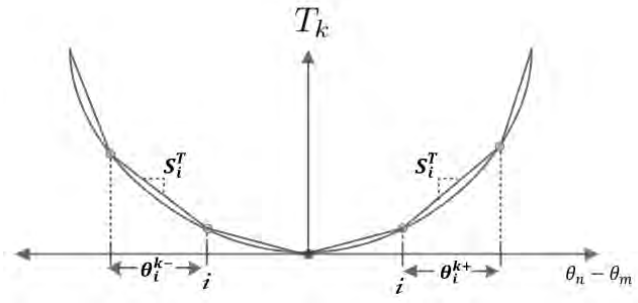

Figure 3.1 Piecewise linearized current-temperature approximation

In order to apply the piecewise linear approximation, the bus angle difference along the line can be represented as a summation of linear blocks in (3.2). The line conductance is multiplied to obtain line power flow, which can be interpreted as the line current in the linearized DCOPF (3.3) model. Finally, one can obtain the piecewise approximation of line temperature equation (3.1) by multiplying the proper slope of segments (3.4). Note that the bus angle difference segments θ_i^{k+} and θ_i^{k-} can be shared with a loss approximation formulation, but it is not necessary. That is, one can eliminate the equations limiting the length of segments (3.5) and (3.6) based on conditions and assumptions.

$$(\theta_n - \theta_m) = \left(\sum_{\forall i} \theta_i^{k+} - \sum_{\forall i} \theta_i^{k-} \right) \tag{3.2}$$

$$I_k = \left(\sum_{\forall i} 2G_k \theta_i^{k-} \right) + \left(\sum_{\forall i} 2G_k \theta_i^{k+} \right) \tag{3.3}$$

$$T_k = \left(2G_k \sum_i S_i^T \theta_{it}^{k+} \right) + \left(2G_k \sum_i S_i^T \theta_{it}^{k-} \right) \tag{3.4}$$

$$0 \le \theta_i^{k+} \le \theta_i^{\max} \qquad \forall i \tag{3.5}$$

$$0 \le \theta_i^{k-} \le \theta_i^{\max} \qquad \forall i \tag{3.6}$$

The difference between a line temperature and the steady state temperature rating is captured in (3.7) with two slack variables T^{b+} and T^{b-}. The maximum operating temperature is limited to the emergency line temperature to prevent permanent line damage in (3.8) and (3.9) [50]. Thus, allowable overloading of each line is limited in the region between the steady state operating temperature and the emergency line temperature.

$$T_k - T^{rating} = T_k^{b+} - T_k^{b-} \qquad \forall k \tag{3.7}$$

$$0 \le T_k^{b+} \le T^{max} \tag{3.8}$$

$$0 \le T_k^{b-} \le T^{max} \tag{3.9}$$

3.2 The Linearized Degradation Model

The method to approximate the residual conductor strength for high-temperature operation, which was introduced in Section 2.4, shows the exponential characteristic of consecutive high temperature operation and the residual conductor tensile strength. Figure 3.2 presents the loss of the tensile strength trends due to the different operating temperatures.

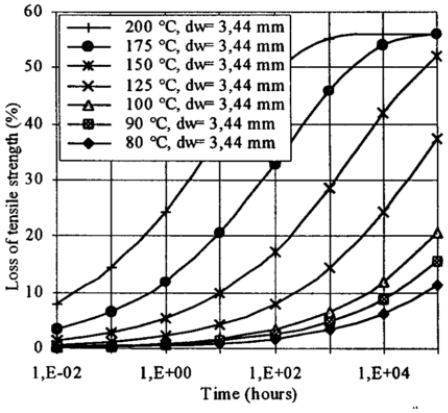

Figure 3.2 Loss of the tensile strength of 3.44mm aluminum wire [61]

However, those methods aim to approximate the final accumulated loss of conductor tensile strength in a planning horizon based on an ordered series of temperature history. There-fore, such methods alone cannot provide the degradation contributions and overloading costs at each operation time interval. In addition, the non-linearity in the equations makes it difficult to be applied in the optimization model directly.

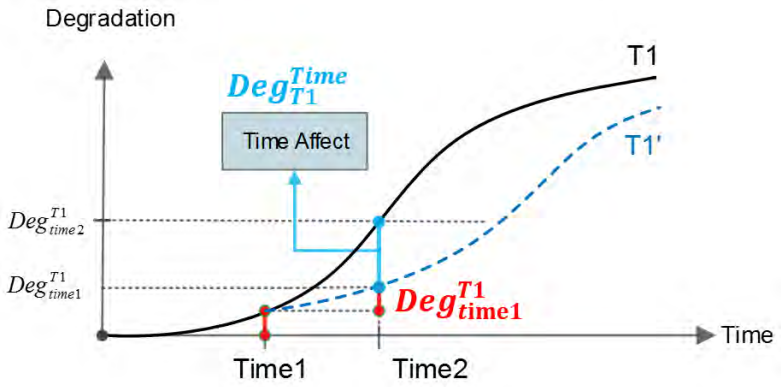

Figure 3.3 Decomposition of degradation effect

The main goal of the proposed degradation model is capturing the degradation costs associated with the reduced residual life that is due to overloading operations at each time interval in the linearized manner. This is done by decomposing the degradation effect properly into two terms. Figure 3.3 presents an overview of the proposed approximation. That is, the degradation of the conductor can be represented by the temperature effect term, Deg_{kt}^{Temp}, and the additional term, Deg_{kt}^{Time}, due to the consecutive overheating operation as follows,

$$Deg_{kt} = Deg_{kt}^{Temp} + Deg_{kt}^{Time} \qquad \forall k,t \tag{3.10}$$

To carry the analysis further, several assumptions can be made at this point. First the degradation effect is assumed to be proportional to the temperature at the same time interval. That is, one can approximate the degradation level based on the ratio of the certain temperature and the predefined maximum allowable overheating temperature. However, if the allowable maximum temperature is above the temperature, which incurs the permanent loss of tensile strength, then the first assumption will become less accurate and the nonlinear relationship between each temperature and degradation effect should be considered. A second assumption is that only a specific number of consecutive overheating operations are considered. It is clear that considering a longer span of time will provide a better approximation and more computational complexity. Since the marginal effect of additional degradation due to consecutive operation decreases as time increases, one can obtain a more conservative approximation within a shorter time span.

By applying these assumptions, the temperature effect term can be obtained using the IEEE standard residual conductor strength prediction equations for each conductor type [45]. The maximum temperature, e.g., the emergency temperature, is considered to prevent permanent damage to the line. The additional effect due to the consecutive time

operation of each type of conductors can be obtained by taking the gap between the accumulated temperature effect term and the degradation in a following consecutive time interval, which can also be obtained using the IEEE standard equation. All of the above values can be utilized as parameters and can be determined initially. At the end, the loss of tensile strength of the conductor at each moment in time, as well as the cost of such degradation, can be expressed in the following mathematical form.

$$LoS_{kt} = \frac{T_{kt}^{b+}}{fT^{max}} LS^{Temp} + \frac{T_{k,t-1}^{b+}}{fT^{max}} LS^{time} \qquad \forall k,t \tag{3.11}$$

$$C_{kt}^{deg} = Cost^{deg} LoS_{kt} \qquad \forall k,t \tag{3.12}$$

Here, the amount of overheated temperature can be obtained by taking the gap between the line temperature and the steady state temperature rating for that line. Then, the ratio of the obtained value and the maximum allowable overheating temperature is multiplied by the temperature effect term at each time. The additional effect term is only applied when there is a consecutive overloading operation. For simplicity, only one consecutive overloading operation is considered here. Additionally, the flattening factor is applied to avoid the overestimation. The approximated loss of strength obtained by proposed method should be overestimated without such flattening factor since the marginal degradation effect is reduced with time increases. Such flattening factor can be obtained by comparing the final degradation obtained from proposed linearized method and IEEE standard equations initially. Figure 3.4 shows the overview of the proposed degradation approximation model.

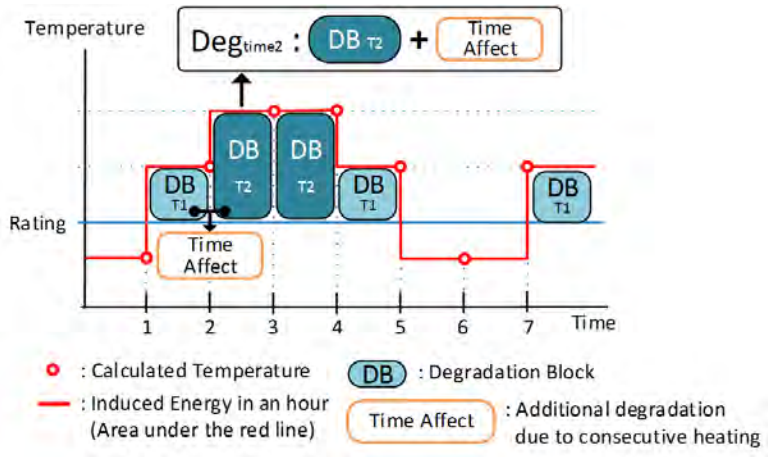

Figure 3.4 Overview of the linearized degradation approximation model

The end of service time of transmission conductor should be assumed to calculate the degradation cost in (3.12). The manufacturers of ACSR and ACCR conductor roughly mentioned that each conductor can be operated 1000 hours and 1500 hours at the emergency temperature in the whole service life time respectively [62]-[63]. Such operation may result in about 10% loss of strength, which can be obtained from the IEEE standard equations [45]. Therefore, 10% loss of strength is assumed as an end of service life of each conductor. That is, one should replace the specific line if the loss of strength

has reached 10%; at such a point, it is assumed that the line is replaced at the additional capital cost of that line. Thus, 10% loss of strength can be interpreted as a capital cost of the line.

The main advantage of the proposed method is that the degradation cost of each operation time interval can be obtained. However, there are two drawbacks of this approach. First, the loss of tensile strength is measured every time when the line temperature exceeds its steady state limits. This may be inaccurate in some cases, for example, when the temperature is close to the steady state limits, actual degradation occurs after several consecutive operations. Second, this method requires a tuning process, the flattening factor. The level of the flattening factor depends on the length of the planning horizon.

3.3 Monte Carlo Simulation

Monte Carlo Simulations are conducted to compare the final degradation with the proposed method and IEEE standard equations as well as to obtain the flattening factor values. The random line temperature ranges from room temperature to the emergency temperature are generated and the final degradation level obtained from the proposed method and IEEE standard equations are compared. From the 10,000 times simulation, the average difference between those two methods is 1.76%. Therefore, the authors conclude that the proposed method can approximate the degradation effect well in the linearized manner.

4. Transmission Expansion Planning Model

As discussed in Section 2.2, there are many different means of increasing the transmission system ampacity without the construction of new lines. In section 4.1, the optimal long-term TEP model in terms of preserving current ROWs is proposed. Reconductoring with the HTLS conductors, parallel line addition (with a traditional conductor, e.g., ACSR), and HTLS parallel line addition are considered as possible investment options. Note that any other alternatives described in Section 2.2 can be utilized as a possible option by modifying the formulation accordingly.

The cost savings by changing the system topology may depend on more efficient generation dispatch. Thus, one can analyze such cost savings more precisely by using the more accurate network model, but it brings more computational complexity. The proposed TEP model adopted the lossy DCOPF, which is mentioned in Section 2.7. In addition, the model incorporated a SCUC formulation to approximate the system commitment decisions more precisely.

It is clear that the proposed TEP problem is difficult to solve as is. Therefore, several assumptions can be made at this point. First, one can observe a similarity of load patterns for weekdays in a same season. Thus, single weekdays can be aggregated into a typical weekday for each season. The same approach can be applied to weekends. For simplicity, the spring and fall are also aggregated into a one typical season in this study. Therefore, a total of six day types, which represent weekdays and weekends in the spring/fall, summer, and winter, are used in this study. Note that the proposed formulation can easily accommodate additional characteristic days.

Second, the unit commitment decisions are identical for days of the same type. In addition, the investment status variables, which are the only variables that connect the investment decision and system operating conditions, are treated with coupling constants. By relaxing these coupling constraints along with these assumptions, the original TEP problem can be decomposed using LR. The investment decision and corresponding investment status are determined in the investment sub-problem, which is indexed by *st1*. In addition, the production cost model, which is indexed by *st2*, can be decomposed again into each day type over the planning horizon. The detailed information of the decomposition approach is described in Section 4.2.

4.1 Transmission Expansion Planning Model Formulation

The In this section, the proposed formulation of the transmission expansion planning problem is represented as a mixed integer programming (MIP) problem. The direct current optimal power flow (DCOPF) is adopted as a linear approximation of the alternating current optimal power flow (ACOPF). Furthermore, the DCOPF is modified to incorporate a piecewise linear approximation of the losses in order to create a lossy DCOPF.

$$\text{Minimize}: \sum_{y=1}^{Y} \frac{1}{(1+ir)^{y-1}}(OC + IC - SV) \tag{4.1}$$

$$\text{OC}: \sum_{d=1} Day_d \{\sum_{t=1}^{T}\Big(\sum_{g}(C_g P_{gtdy} + C_g^{SU} v_{gtdy} + C_g^{SD} w_{gtdy} + NL_g u_{gtdy}) + \sum_{k}(C_{ktdy}^{degO} + C_{ktdy}^{degA} + C_{ktdy}^{degR} + C_{ktdy}^{\deg AH})\} \tag{4.2}$$

$$\text{IC}: \sum_{k} \{Line_k^{mile}(re_{ky} I^{HTLS} + ad_{ky} I^{Add} + ah_{ky} I^{AH})\} \tag{4.3}$$

$$\text{SV}: \sum_{y=1}^{Y} \kappa_y (re_{ky} I^{HTLS} + ad_{ky} I^{Add} + ah_{ky} I^{AH}) Line_k^{mile} \tag{4.4}$$

The objective function in (4.1) minimizes system costs throughout the planning horizon and is evaluated in terms of discounted costs, i.e., the cost function takes into consideration the time value of money. Operating costs include typical generator costs (fuel costs, start up and shut down costs, and no load costs) and degradation costs of overheated transmission lines (4.2). Investment costs consist of the HTLS reconductoring costs, the cost of parallel line addition, and the HTLS parallel line addition cost (4.3). The salvage value is considered as a percentage of depreciation of the initial capital cost at the end of the planning horizon (4.4).

4.1.1 System Operation Constraints

The load balance constraint (4.5) ensures that the net power injection over all lines connected to a node n equal the summation of the demands, losses, and power withdrawn from that node. The active power flows are determined by the product of the line susceptance associated with the line investment status and the voltage phase angle difference (4.6)-(4.9). The big-M reformulation is applied to avoid non-linearities as well as to ensure that only one of those constraints will be binding at each time according to the line investment status; while the use of this big-M reformulation is common for disjunctive constraints, there are computational setbacks due to this mathematical reformulation. Theoretically, the value of this large multiplier, the big-M value, needs to be large enough such that only one set of the disjunctive constraints are active for a particular solution. If the big-M value is too large, the likely result is a substantially increased solution time as the value of the big-M multiplier significantly influences the relaxation of the mixed integer program, which generally results in the branch-and-bound algorithm being required to search many more nodes in the branch-and-bound tree. If the big-M value is too small, the solution time is generally less but then the resulting solution may not be the true optimal solution. The definition of the term “sufficiently large” is dependent upon the problem and requires some judgment for implementation [64]. In here, the value of big-M value should be a large number greater than or equal to the biggest production value of the line susceptance and the bus angle difference. For simplicity, 120% of maximum power flow for each line is chosen for the value of big-M in this study. The bus voltage angle difference constraint (4.10) proxies the angle stability. It is of note that, this constraint would be redundant in the DCOPF model since

one can implicitly put angle difference constraint in the power flow constraint properly [65]. However, in the presented formulation, employing bus angle limit is easier than determining each line's power flow limits considering the angle difference between two connected buses for every investment option. The chosen maximum bus angle values are 0.6 radians.

$$\sum_{\forall k(n,;)} P_{ktdy} - \sum_{\forall k(;,n)} P_{ktdy} + \sum_{g \in g_{(n)}} P_{gtdy} - P^{L}_{ntdy} = d_{ntdy} \qquad \forall n,t,d,y \qquad (4.5)$$

$$-(rs^{st2}_{kdy} + as^{st2}_{kdy} + ahs^{st2}_{kdy})M^{2}_{k} \le P_{ktdy} - B^{O}_{k}(\theta_{ntdy} - \theta_{mtdy}) \le (rs^{st2}_{kdy} + as^{st2}_{kdy} + ahs^{st2}_{kdy})M^{2}_{k} \qquad \forall k,t,d,y \qquad (4.6)$$

$$-(1 - as^{st2}_{kdy})M^{2}_{k} \le P_{ktdy} - B^{A}_{k}(\theta_{ntdy} - \theta_{mtdy}) \le (1 - as^{st2}_{kdy})M^{2}_{k} \qquad \forall k,t,d,y \qquad (4.7)$$

$$-(1 - rs^{st2}_{kdy})M^{2}_{k} \le P_{ktdy} - B^{R}_{k}(\theta_{ntdy} - \theta_{mtdy}) \le (1 - rs^{st2}_{kdy})M^{2}_{k} \qquad \forall k,t,d,y \qquad (4.8)$$

$$-(1 - ahs^{st2}_{kdy})M^{2}_{k} \le P_{ktdy} - B^{AH}_{k}(\theta_{ntdy} - \theta_{mtdy}) \le (1 - ahs^{st2}_{kdy})M^{2}_{k} \qquad \forall k,t,d,y \qquad (4.9)$$

$$-\theta^{max} \le \theta_{ntdy} - \theta_{mtdy} \le \theta^{max} \qquad \forall n,t,d,y \qquad (4.10)$$

4.1.2 Thermal Constraints Relaxation

The thermal limit constraints in (4.11) and (4.12) are relaxed to add flexibility to a line operation by allowing the line's flow to exceed the steady state operating level. The line thermal limits are picked up according to their investment status. As mentioned in Section 2.4, there is a cost associated with exceeding the steady state operation level since this can cause the loss of tensile strength of a conductor and reduce the lifespan of the asset. The penalty price for overloading is determined based on a positive value of P^{over}_{ktdy} by line temperature calculation and the proposed degradation model. The objective is to minimize total cost, which includes the production cost, the investment cost, and the cost accrued by degradation of the line due to exceeding steady state operation level. Thus, the model optimizes the tradeoffs between cost savings from a better generation dispatch by allowing flexible line operation and the cost associated with this action. The authors assume that the thermal constraint relaxation is only allowed when there is no negative effect on reliability, stability, or no excess sagging. The only effect of the short term overloading is assumed to be an associated cost based on a reduced lifetime for the line, additional required maintenance, etc.

$$P^{min,O}_{k}(1 - rs^{st2}_{kdy} - as^{st2}_{kdy} - ahs^{st2}_{kdy}) + P^{min,R}_{k} rs^{st2}_{kdy} + P^{min,A}_{k} as^{st2}_{kdy} + P^{min,AH}_{k} ahs^{st2}_{kdy} \le P_{ktdy} + P^{over}_{ktdy} \qquad \forall k,t,d,y \qquad (4.11)$$

$$P^{max,O}_{k}(1 - rs^{st2}_{kdy} - as^{st2}_{kdy} - ahs^{st2}_{kdy}) + P^{max,R}_{k} rs^{st2}_{kdy} + P^{max,A}_{k} as^{st2}_{kdy} + P^{max,AH}_{k} ahs^{st2}_{kdy} \ge P_{ktdy} - P^{over}_{ktdy} \qquad \forall k,t,d,y \qquad (4.12)$$

4.1.3 Security Constrained Unit Commitment Constraints

Note that the SCUC formulations have adopted the one presented in [65]. The minimum and maximum operating capacity (4.13), minimum up and down time constraints (4.14)-(4.17), ramp rate constraints (4.18)-(4.21), and reserve requirement constraints (4.22)-(4.25) for the generators are modeled. The generator's commitment state is represented by a binary variable, U_{gt}, which has a value of one only when the unit is on; otherwise, it has a value of zero. The startup variable, V_{gt}, equals zero except when the unit commitment status is changed from zero to one in period *t*. Similarly, the shutdown variable, W_{gt}, equals one only when the unit is shut down in period *t*. Reference [65] shows that integrality constraints of the startup and shutdown variables could be relaxed by including constraints (4.29) and (4.30). Therefore, only U_{gt} variables are modeled as binary variables (4.26), while V_{gt} and W_{gt} variables are modeled as continuous variables (4.27) and (4.28). The minimum up and down time constraints, (4.14)-(4.17), employ facet defining valid inequalities. This formulation was analyzed by Hedman et al. [66] as the use of valid inequalities and facets of the minimum up and down time constraints within the generation unit commitment problem. The ramp rate constraints, (4.18)-(4.21), represent the limited flexibility of generators to ramp up or down based on their commitment status. The spinning reserves are included as proxies to enforce N-1 of generators (4.22)-(4.25).

$$P_g^{min} u_{gtdy} \le P_{gtdy} \le P_g^{max} u_{gtdy} \qquad \forall g,t,d,y \qquad (4.13)$$

$$\sum_{q=t-UT_g+1}^{t} v_{gqdy} \le u_{gtdy} \qquad \forall g, t \ge UT_g, d, y \qquad (4.14)$$

$$\sum_{q=T+t-UT_g+1}^{T} v_{gqdy} + \sum_{q=1}^{t} v_{gqdy} \le u_{gtdy} \qquad \forall g, t \le UT_g - 1, d, y \qquad (4.15)$$

$$\sum_{q=t-DT_g+1}^{t} w_{gqdy} \le 1 - u_{gtdy} \qquad \forall g, t \ge DT_g, d, y \qquad (4.16)$$

$$\sum_{q=T+t-DT_g+1}^{T} w_{gqdy} + \sum_{q=1}^{t} w_{gqdy} \le 1 - u_{gtdy} \qquad \forall g, t \le DT_g - 1, d, y \qquad (4.17)$$

$$P_{gtdy} - P_{g,t-1,dy} \le R_g^{hr} u_{g,t-1,dy} + R_g^{SU} v_{gtdy} \qquad \forall g, t \ge 2, d, y \qquad (4.18)$$

$$P_{g,1,dy} - P_{g,T,dy} \le R_g^{hr} u_{g,T,dy} + R_g^{SU} v_{g,1,dy} \qquad \forall g, d, y \qquad (4.19)$$

$$P_{g,t-1,dy} - P_{gtdy} \le R_g^{hr} u_{gtdy} + R_g^{SD} w_{gtdy} \qquad \forall g, t \ge 2, d, y \qquad (4.20)$$

$$P_{g,T,dy} - P_{g,1,dy} \le R_g^{hr} u_{g,1,dy} + R_g^{SU} w_{g,1,dy} \qquad \forall g, d, y \qquad (4.21)$$

$$r_{gtdy} \le P_g^{max} u_{gtdy} - P_{gtdy} \qquad \forall g,t,d,y \qquad (4.22)$$

$$r_{gtdy} \le R_g^{10} u_{gtdy} \qquad \forall g,t,d,y \qquad (4.23)$$

$$max(P_{gtdy} + r_{gtdy}) \le \sum_{\gamma \in g} r_{\gamma,tdy} \qquad \forall t,d,y \qquad (4.24)$$

$$\alpha \sum_{n} d_{ntdy} \le \sum_{\gamma \in g} r_{\gamma,tdy} \qquad \forall t,d,y \qquad (4.25)$$

$$u_{gtdy} \in \{0,1\} \qquad \forall g,t,d,y \qquad (4.26)$$

$$0 \le v_{gtdy} \le 1 \qquad \forall g,t,d,y \qquad (4.27)$$

$$0 \le w_{gtdy} \le 1 \qquad \forall g,t,d,y \qquad (4.28)$$

$$v_{gtdy} - w_{gtdy} = u_{gtdy} - u_{g,t-1,dy} \qquad \forall g,t \ge 2,d,y \qquad (4.29)$$

$$v_{g,1,dy} - w_{g,1,dy} = u_{g,1,dy} - u_{g,T,dy} \qquad \forall g,d,y \qquad (4.30)$$

4.1.4 Piecewise Linearized Losses Approximation

The piecewise linearized real power losses are modeled within the standard DCOPF formulation as mentioned in Section 2.6. The real power losses for line *k*, which is determined as $2G_k(1-\cos(\theta_n - \theta_m))$ where G_k is line conductance, can be approximated by a series of linear blocks in terms of designated sending end and receiving end bus (4.31). Equation (4.40) replaces the angle difference across a line *k* by slack variables θ^+ and θ^-. Since the line conductance varies according to the conductor type and the transmission system structure, the big-M method is applied again to capture those linearized loss terms, P^{L+}_{ktdy} and P^{L-}_{ktdy}, based on the line investment status (4.32)-(4.39). Again, this approach ensures that only two equations of each linearized loss term will be binding.

$$P^L_{ntdy} - \sum_{\forall k(n,;)} P^{L-}_{ktdy} - \sum_{\forall k(n,;)} P^{L+}_{ktdy} = 0 \qquad \forall n,t,d,y \qquad (4.31)$$

$$-(rs^{st2}_{kdy} + as^{st2}_{kdy} + ahs^{st2}_{kdy})M^1_k \le P^{L-}_{ktdy} - 2G^O_k(\sum_{\forall i} S^L_i \theta^{k-}_{itdy}) \le (rs^{st2}_{kdy} + as^{st2}_{kdy} + ahs^{st2}_{kdy})M^1_k \qquad \forall k,t,d,y \qquad (4.32)$$

$$-(rs^{st2}_{kdy} + as^{st2}_{kdy} + ahs^{st2}_{kdy})M^1_k \le P^{L+}_{ktdy} - 2G^O_k(\sum_{\forall i} S^L_i \theta^{k+}_{itdy}) \le (rs^{st2}_{kdy} + as^{st2}_{kdy} + ahs^{st2}_{kdy})M^1_k \qquad \forall k,t,d,y \qquad (4.33)$$

$$-(1-rs^{st2}_{kdy})M^1_k \le P^{L-}_{ktdy} - 2G^R_k(\sum_{\forall i} S^L_i \theta^{k-}_{itdy}) \le (1-rs^{st2}_{kdy})M^1_k \qquad \forall k,t,d,y \qquad (4.34)$$

$$-(1-rs^{st2}_{kdy})M^1_k \le P^{L+}_{ktdy} - 2G^R_k(\sum_{\forall i} S^L_i \theta^{k+}_{itdy}) \le (1-rs^{st2}_{kdy})M^1_k \qquad \forall k,t,d,y \qquad (4.35)$$

$$-(1-as^{st2}_{kdy})M^1_k \le P^{L-}_{ktdy} - 2G^A_k(\sum_{\forall i} S^L_i \theta^{k-}_{itdy}) \le (1-as^{st2}_{kdy})M^1_k \qquad \forall k,t,d,y \qquad (4.36)$$

$$-(1-as^{st2}_{kdy})M^1_k \le P^{L+}_{ktdy} - 2G^A_k(\sum_{\forall i} S^L_i \theta^{k+}_{itdy}) \le (1-as^{st2}_{kdy})M^1_k \qquad \forall k,t,d,y \qquad (4.37)$$

$$-(1-ahs^{st2}_{kdy})M^1_k \le P^{L-}_{ktdy} - 2G^{AH}_k(\sum_{\forall i} S^L_i \theta^{k-}_{itdy}) \le (1-ahs^{st2}_{kdy})M^1_k \qquad \forall k,t,d,y \qquad (4.38)$$

$$-(1-ahs^{st2}_{kdy})M^1_k \le P^{L+}_{ktdy} - 2G^{AH}_k(\sum_{\forall i} S^L_i \theta^{k+}_{itdy}) \le (1-ahs^{st2}_{kdy})M^1_k \qquad \forall k,t,d,y \qquad (4.39)$$

$$(\theta_{ntdy} - \theta_{mtdy}) - (\sum_{\forall i} \theta^{k+}_{ktdyi} - \sum_{\forall i} \theta^{k-}_{ktdyi}) = 0 \qquad \forall k,t,d,y \qquad (4.40)$$

4.1.5 Current-Temperature Approximation

The linearized current-temperature equations, which were presented in Section 3.1, can be rewritten as in (4.41)-(4.47). The Big-M method is used again to capture the different conductor type and structure based on their investment status. The series of linear blocks representing the angle difference along the line k, which is obtained in (4.40), are shared here to approximate line temperature. The environmental factors assumed to be fixed throughout the planning horizon; therefore, each slope of the segment can be determined initially. The variance of line temperature from the steady state temperature rating captured in (4.45) with two slack variable T^{b+} and T^{b-}. The maximum operating temperature is limited to the emergency line temperature to prevent permanent line damage in (4.46) and (4.47). Thus, allowable overloading of each line in (4.11) and (4.12) is limited in the region between the steady state operating temperature and the emergency line temperature. Note that the steady state temperature rating and the maximum allowable operating temperature are picked up according to the line investment status.

$$-(rs_{kdy}^{st2}+as_{kdy}^{st2}+ahs_{kdy}^{st2})M_k^3 \le T_{ktdy}-\sum_i S_i^{TO}\theta_{itdy}^{k+}-\sum_i S_i^{TO}\theta_{itdy}^{k-} \le (rs_{kdy}^{st2}+as_{kdy}^{st2}+ahs_{kdy}^{st2})M_k^3 \quad \forall k,t,d,y \quad (4.41)$$

$$-(1-as_{kdy}^{st2})M_k^3 \le T_{ktdy}-\sum_i S_i^{TA}\theta_{itdy}^{k+}-\sum_i S_i^{TA}\theta_{itdy}^{k-} \le (1-as_{kdy}^{st2})M_k^3 \quad \forall k,t,d,y \quad (4.42)$$

$$-(1-rs_{kdy}^{st2})M_k^3 \le T_{ktdy}-\sum_i S_i^{TR}\theta_{itdy}^{k+}-\sum_i S_i^{TR}\theta_{itdy}^{k-} \le (1-rs_{kdy}^{st2})M_k^3 \quad \forall k,t,d,y \quad (4.43)$$

$$-(1-ahs_{kdy}^{st2})M_k^3 \le T_{ktdy}-\sum_i S_i^{TAH}\theta_{itdy}^{k+}-\sum_i S_i^{TAH}\theta_{itdy}^{k-} \le (1-ahs_{kdy}^{st2})M_k^3 \quad \forall k,t,d,y \quad (4.44)$$

$$T_{ktdy}-T^{rating_O}(1-as_{kdy}^{st2}-rs_{kdy}^{st2}-ahs_{kdy}^{st2}) - T^{rating_A}as_{kdy}^{st2}-T^{rating_R}rs_{kdy}^{st2}-T^{rating_{AH}}ahs_{kdy}^{st2}=T_{ktdy}^{b+}-T_{ktdy}^{b-} \quad \forall k,t,d,y \quad (4.45)$$

$$0 \le T_{ktdy}^{b+} \le T^{max_O}(1-as_{kdy}^{st2}-rs_{kdy}^{st2}-ahs_{kdy}^{st2}) + T^{max_A}as_{kdy}+T^{max_R}rs_{kdy}+T^{max_{AH}}ahs_{kdy} \quad \forall k,t,d,y \quad (4.46)$$

$$0 \le T_{ktdy}^{b-} \le T^{max_O}(1-as_{kdy}^{st2}-rs_{kdy}^{st2}-ahs_{kdy}^{st2}) + T^{max_A}as_{kdy}+T^{max_R}rs_{kdy}+T^{max_A}ahs_{kdy} \quad \forall k,t,d,y \quad (4.47)$$

4.1.6 Loss of Tensile Strength Prediction

The method to approximate the residual conductor strength for high-temperature operation was investigated in Section 3.2. First, the loss of strength due to the maximum operation temperature, e.g., the emergency temperature within one operation interval, LS^{Temp}, is obtained using the IEEE standard residual conductor strength prediction equations [45] for each conductor type. Second, the additional effect due to the consecutive time operation, LS^{Time}, can be defined by taking the gap between the accumulated temperature effects and the loss of strength in a next consecutive time interval. For simplicity, only two consecutive time operations are considered in this

study. The only positive temperature segments in (4.45) are utilized to approximate the loss of tensile strength in (4.48)-(4.55). The ratio of the positive temperature segments and the maximum operating temperature is multiplied by the loss of strength block at each time. The additional effect block is only applied when there is consecutive overloading operation. In addition, the flattening factor, f, was applied to make the each loss of strength proportional to the temperature.

$$LoS^{O}_{ktdy} = \frac{LS^{TempO}}{fT^{max_O}} T^{b+}_{ktdy} + \frac{LS^{timeO}}{fT^{max_O}} T^{b+}_{k,t-1,dy} \qquad \forall k, t \geq 2, d, y \quad (4.48)$$

$$LoS^{A}_{ktdy} = \frac{LS^{TempA}}{fT^{max_A}} T^{b+}_{ktdy} + \frac{LS^{timeA}}{fT^{max_A}} T^{b+}_{k,t-1,dy} \qquad \forall k, t \geq 2, d, y \quad (4.49)$$

$$LoS^{R}_{ktdy} = \frac{LS^{TempR}}{fT^{max_R}} T^{b+}_{ktdy} + \frac{LS^{timeR}}{fT^{max_R}} T^{b+}_{k,t-1,dy} \qquad \forall k, t \geq 2, d, y \quad (4.50)$$

$$LoS^{AH}_{ktdy} = \frac{LS^{TempAH}}{fT^{max_{AH}}} T^{b+}_{ktdy} + \frac{LS^{timeAH}}{fT^{max_{AH}}} T^{b+}_{k,t-1,dy} \qquad \forall k, t \geq 2, d, y \quad (4.51)$$

$$LoS^{O}_{k,1,dy} = \frac{LS^{TempO}}{fT^{max_O}} T^{b+}_{k,1,dy} + \frac{LS^{timeO}}{fT^{max_O}} T^{b+}_{k,T,dy} \qquad \forall k, d, y \quad (4.52)$$

$$LoS^{A}_{k,1,dy} = \frac{LS^{TempA}}{fT^{max_A}} T^{b+}_{k,1,dy} + \frac{LS^{timeA}}{fT^{max_A}} T^{b+}_{k,T,dy} \qquad \forall k, d, y \quad (4.53)$$

$$LoS^{R}_{k,1,dy} = \frac{LS^{TempR}}{fT^{max_R}} T^{b+}_{k,1,dy} + \frac{LS^{timeR}}{fT^{max_R}} T^{b+}_{k,T,dy} \qquad \forall k, d, y \quad (4.54)$$

$$LoS^{AH}_{k,1,dy} = \frac{LS^{TempAH}}{fT^{max_{AH}}} T^{b+}_{k,1,dy} + \frac{LS^{timeAH}}{fT^{max_{AH}}} T^{b+}_{k,T,dy} \qquad \forall k, d, y \quad (4.55)$$

4.1.7 Degradation Cost

The non-linear degradation costs in Section 3.2 can be linearized by introducing new variables and inequality constraints in (4.56)-(4.63). This optimization trick to avoid the nonlinear term in the objective function is introduced in [67].

$$C^{degO}_{ktdy} \geq Cost^{degO} LoS^{O}_{ktdy} - Cost^{degO}(1 - rs_{ky} - as_{ky} - ahs_{ky}) \qquad \forall k, t, d, y \quad (4.56)$$

$$C^{degA}_{ktdy} \geq Cost^{degA} LoS^{A}_{ktdy} - Cost^{degA} as_{ky} \qquad \forall k, t, d, y \quad (4.57)$$

$$C^{degR}_{ktdy} \geq Cost^{degR} LoS^{R}_{ktdy} - Cost^{degR} rs_{ky} \qquad \forall k, t, d, y \quad (4.58)$$

$$C^{\deg AH}_{ktdy} \geq Cost^{\deg AH} LoS^{AH}_{ktdy} - Cost^{\deg AH} ahs_{ky} \qquad \forall k, t, d, y \quad (4.59)$$

$$C^{degO}_{ktdy} \geq 0 \qquad \forall k, t, d, y \quad (4.60)$$

$$C^{degA}_{ktdy} \geq 0 \qquad \forall k, t, d, y \quad (4.61)$$

$$C^{degR}_{ktdy} \geq 0 \qquad \forall k, t, d, y \quad (4.62)$$

$$C^{\deg AH}_{ktdy} \geq 0 \qquad \forall k, t, d, y \quad (4.63)$$

4.1.8 Investment Variable Constraints

The investment decisions are treated as integer variables and each decision is made annually (4.64)-(4.66). Only one of those investment decisions can be made in a whole planning time horizon for each line (4.67). The investment status variables, rs_{kdy}^{st1}, as_{kdy}^{st1}, and ahs_{kdy}^{st1}, have a value of one after each investment decision is made; otherwise, they have a value of zero (4.68)-(4.70).

$$re_{ky} = \begin{cases} 1: \text{if the reconductoring is made} \\ 0: \text{Otherwise} \end{cases} \qquad \forall k, y \qquad (4.64)$$

$$ad_{ky} = \begin{cases} 1: \text{if the adding twin circuit is made} \\ 0: \text{Otherwise} \end{cases} \qquad \forall k, y \qquad (4.65)$$

$$ah_{ky} = \begin{cases} 1: \text{if the adding HTLS parallel line using is made} \\ 0: \text{Otherwise} \end{cases} \qquad \forall k, y \qquad (4.66)$$

$$\sum_{y} (re_{ky} + ad_{ky} + ah_{ky}) \le 1 \qquad \forall k \qquad (4.67)$$

$$rs_{kdy}^{st1} = \sum_{q \le y} re_{kq} \qquad \forall k, d, y \qquad (4.68)$$

$$as_{kdy}^{st1} = \sum_{q \le y} ad_{kq} \qquad \forall k, d, y \qquad (4.69)$$

$$ahs_{kdy}^{st1} = \sum_{q \le y} ah_{kq} \qquad \forall k, d, y \qquad (4.70)$$

4.1.9 Coupling Constraints

One can observe that only investment status variables connect the investment decision and the system operating conditions. The coupling constraints (4.71)-(4.73) imply that the investment decision made in the investment model, which is indexed by '*st1*', should be consistent with the production model, which is indexed by '*st2*'.

$$rs_{kdy}^{st1} = rs_{kdy}^{st2} \qquad \forall k, d, y \qquad (4.71)$$

$$as_{kdy}^{st1} = as_{kdy}^{st2} \qquad \forall k, d, y \qquad (4.72)$$

$$ahs_{kdy}^{st1} = ahs_{kdy}^{st2} \qquad \forall k, d, y \qquad (4.73)$$

4.2 Decomposition Approach

The proposed TEP formulation in Section 4.1 is well structured for the use of the Lagrangian decomposition algorithm, which is introduced in Section 2.7. The figure 4.1 shows the overview of applied Lagrangian relaxation.

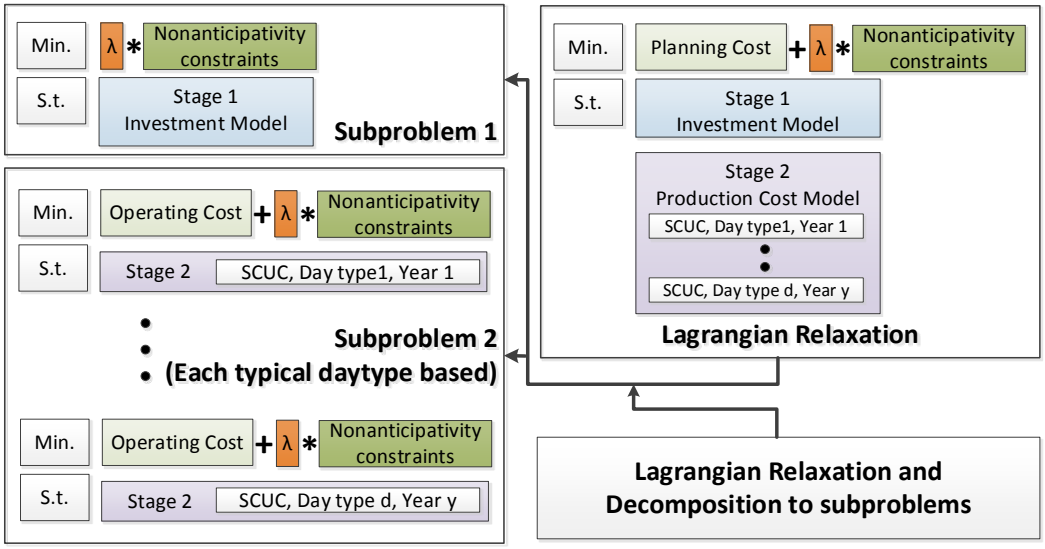

Figure 4.1 Overview of Lagrange relaxation algorithm

First, the Lagrangian can be obtained by dualizing the coupling constraints (4.71)-(4.73) as in (4.74). As mentioned above, only the coupling constraints link the investment model and the production cost model. Thus, relaxing the coupling constraints makes the investment model and the production cost model independent.

$$\begin{aligned} \mathrm{L} \equiv & \sum_{y}^{Y} \frac{1}{(1+ir)^{y-1}}(OC + IC - SV) \\ & + \sum_{y}\sum_{d}\sum_{k}(\alpha_{kdy}(rs_{kdy}^{st1} - rs_{kdy}^{st2}) + \beta_{kdy}(as_{kdy}^{st1} - as_{kdy}^{st2}) + \gamma_{kdy}(ahs_{kdy}^{st1} - ahs_{kdy}^{st2})) \end{aligned} \tag{4.74}$$

Therefore, the Lagrangian can be decomposed into a single investment sub-problem, which determines the optimal investment decision and associated investment status:

$$\begin{aligned} (SP1) \quad Minimize: \quad & \sum_{y}^{Y} \frac{1}{(1+ir)^{y-1}}(IC - SV) \\ & + \sum_{y}\sum_{d}\sum_{k}(\alpha_{kdy} rs_{kdy}^{st1} + \beta_{kdy} as_{kdy}^{st1} + \gamma_{kdy} ahs_{kdy}^{st1}) \end{aligned} \tag{4.75}$$

s.t. (4.64), (4.65), (4.66), (4.67), (4.68), (4.69), (4.70).

The production cost model can be decomposed into one sub-problem for each day type over the planning time horizon, which determines the optimal dispatch solution:

$$(SP2)\quad Minimize: \quad \sum_{y}^{Y} \frac{1}{(1+ir)^{y-1}}(OC) - \sum_{y}\sum_{d}\sum_{k}(\alpha_{kdy} rs_{kdy}^{st2} + \beta_{kdy} as_{kdy}^{st2} + \gamma_{kdy} ahs_{kdy}^{st2}) \tag{4.76}$$

s.t. (4.5) - (4.63).

The dual variables are updated based on optimal investment status solution of (*SP1*) and (*SP2*) at iteration *k* as follows:

$$\alpha_{kdy}^{k+1} = \alpha_{kdy}^{k} + \lambda_k (rs_{kdy}^{st1,k} - rs_{kdy}^{st2,k}) \tag{4.77}$$

$$\beta_{kdy}^{k+1} = \beta_{kdy}^{k} + \lambda_k (as_{kdy}^{st1,k} - as_{kdy}^{st2,k}) \tag{4.78}$$

$$\gamma_{kdy}^{k+1} = \gamma_{kdy}^{k} + \lambda_k (ahs_{kdy}^{st1,k} - ahs_{kdy}^{st2,k}) \tag{4.79}$$

The method to choose the step size at each iteration is adopted based on the one presented in [68] and is given by follows,

$$\lambda_k = \frac{\rho(UB^k - LB^k)}{\sum_{y,d,k} ((rs_{kdy}^{st1} - rs_{kdy}^{st2})^2 + (as_{kdy}^{st1} - as_{kdy}^{st2})^2 + (ahs_{kdy}^{st1} - ahs_{kdy}^{st2})^2)} \tag{4.80}$$

Note that the investment solutions of the (*SP1*) can be used for generating a feasible solution to the original problem. That is, one can solve the original problem with a fixed investment solution of (*SP1*) and get an upper bound at each step. The gap between the obtained lower bound and the upper bound can used for terminating criteria. Figure 4.2 shows the overall flow chart of the Lagrangian decomposition algorithm applied in this study.

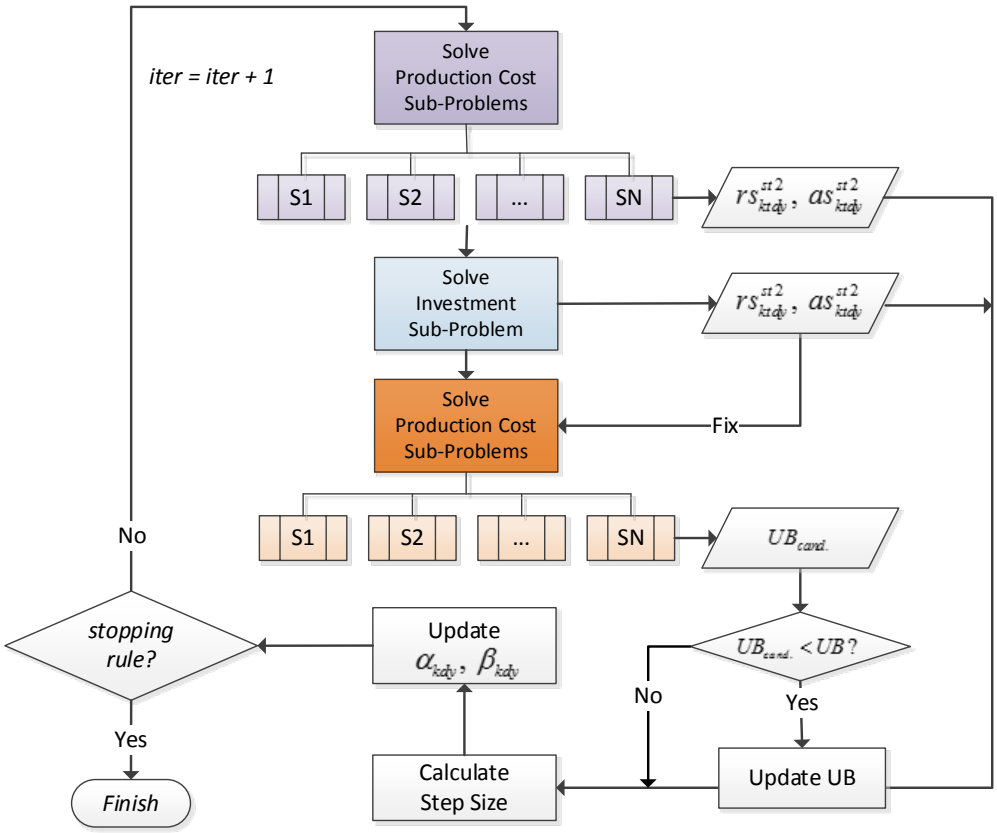

Figure 4.2 Flow chart of the Lagrangian decomposition algorithm

5. Numerical Result

The proposed TEP formulation in Chapter 4 is used for the modified IEEE 24 bus Reliability Test System (RTS) in this chapter. The modification of the test system is presented in Section 5.1. The method for choosing investment candidate lines is described in Section 5.2. The simulations are conducted for: (1) a traditional TEP model, which do not allow for line overloads and (2) the proposed TEP model that includes the degradation model with and without considering line losses. A summary of the simulations, along with results, are presented in Section 5.3.

5.1 IEEE 24 Bus Reliability Test System (RTS)

The chosen case study includes a modified version of the IEEE 24 bus Reliability Test System (RTS) [69]. The original system has 24 nodes, 35 transmission lines, and 32 generators providing 3,405 MW of capacity to 2,850MW of total peak load. The transmission capacity of this system is redundant; therefore, system modifications need to be made to carry out further TEP studies. First, three generators and two loads shown in Table 5.1 are added into the system. Second, the parallel lines have been removed, and remaining line data are shown in Table 5.2. Thus, the modified IEEE 24 bus reliability test system has 4,310MW of generation capacity and 3,110MW of total peak load. Figure 5.1 represents the modified IEEE 24 bus reliability test system. Note that the modified system is still reliable but may not be efficient. Thus, system expansion will be conducted only if net cost savings from the investment exceeds its capital cost; as a result, this study is aimed primarily at making an investment decision in HTLS based on economics (operational cost savings versus capital investment).

Table 5.1 Modification of IEEE 24 bus RTS

Gen Bus	Number	Type	Capacity (MW)	Load Bus	Load (MW)
13	1	Coal/Steam	350	15	160
21	1	Nuclear	400	16	100
23	1	Coal/Steam	155		

Table 5.2 Line data for the IEEE 24 bus RTS

Line No.	Bus From	Bus To	Susceptance (S)	Conductance (S)	Capacity (MW)
1	1	2	-68.30	14.64	175
2	1	3	-4.44	1.16	175
3	1	5	-11.03	2.85	175
4	2	4	-7.38	1.92	175
5	2	6	-4.88	1.27	175
6	3	9	-7.87	2.05	175
7	3	24	-11.90	0.28	400
8	4	9	-9.01	2.34	175
9	5	10	-10.64	2.78	175
10	6	10	-15.57	3.57	175
11	7	8	-15.34	4.02	175
12	8	9	-5.68	1.48	175
13	8	10	-5.68	1.48	175
14	9	11	-11.90	0.28	400
15	9	12	-11.90	0.28	400
16	10	11	-11.90	0.28	400
17	10	12	-11.90	0.28	400
18	11	13	-20.51	2.56	500
19	11	14	-20.51	2.56	500
20	12	13	-23.48	2.80	500
21	12	23	-20.51	2.56	500
22	13	23	-10.15	1.26	500
23	14	16	-13.10	1.75	500
24	15	16	-16.83	1.43	500
25	15	21	-58.02	6.83	500
27	15	24	-20.11	2.46	500
28	16	17	-18.89	2.54	500
29	16	19	-37.96	4.38	500
30	17	18	-42.75	5.58	500
31	17	22	-70.00	10.00	500
32	18	21	-93.58	1.25	500
34	19	20	-37.96	4.38	500
36	20	23	-24.62	3.08	500
38	21	22	-44.63	6.09	500

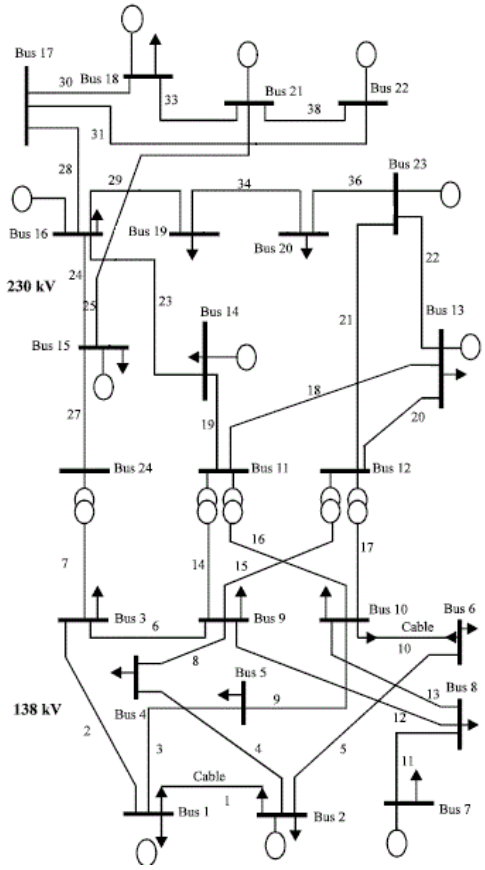

Figure 5.1 Modified IEEE 24 bus RTS

The test system includes startup costs and no-load costs; shutdown costs are assumed to be zero. In addition, it is assumed that the generator cost information is an average cost based on the heat rate data presented in [69] and the fuel cost provided in [70]-[71], as shown in Table 5.3 and Table 5.4, respectively. Hourly loads presented in [69] were aggregated into six typical days representing a typical weekday and weekend day for each of three seasons, as shown in Table 5.5 and Table 5.6.

Table 5.3 Generator data

Gen Group	Size (MW)	Type	Fuel Costs ($/MWh)	Startup Costs ($)	No-load Costs ($)
U12	12	Oil/Steam	219.38	1322.65	168.29
U20	20	Oil/CT	280.98	130.74	1962.63
U50	50	Hydro	N/A	N/A	N/A
U76	76	Coal/Steam	26.09	1409.05	173.50
U100	100	Oil/Steam	174.42	10963.55	1935.75
U155	155	Coal/Steam	20.61	2261.82	336.90
U197	197	Oil/Steam	174.10	15162.04	2701.52
U350	350	Coal/Steam	21.33	10676.86	480.92
U400	400	Nuclear	8.66	3806.37	341.11

Table 5.4 Fuel costs (Energy Information Administration, 2013 prices)

Fuel Type	#2 Oil	#6 Oil	Coal	Uranium
Costs [$/MBtu]	23.08	19.33	2.35	0.95

Table 5.5 Typical day types

Day Type	Season	Day	Number of days
1	Winter	Week	85
2	Winter	Weekend	34
3	Summer	Week	65
4	Summer	Weekend	26
5	Spring/Fall	Week	110
6	Spring/Fall	Weekend	44

Table 5.6 Hourly load percent levels for each day type

Time		1	2	3	4	5	6	7	8	9	10	11	12
Day Type	1	67	63	60	59	59	60	74	86	95	96	96	95
	2	78	72	68	66	64	65	66	70	80	88	90	91
	3	64	60	58	56	56	58	64	76	87	95	99	100
	4	74	70	66	65	64	62	62	66	81	86	91	93
	5	63	62	60	58	59	65	72	85	95	99	100	99
	6	75	73	69	66	65	65	68	74	83	89	92	94
Time		13	14	15	16	17	18	19	20	21	22	23	24
Day Type	1	95	95	93	94	99	100	100	96	91	83	73	63
	2	90	88	87	87	91	100	99	97	94	92	87	81
	3	99	100	100	97	96	96	93	92	92	93	87	72
	4	93	92	91	91	92	94	95	95	100	93	88	80
	5	93	92	90	88	90	92	96	98	96	90	80	70
	6	91	90	90	86	85	88	92	100	97	95	90	85

Two types of conductors have been considered, ACSR and ACCR. The 2 kcmil 1/6 (Sparrow) and 336 kcmil 18/1 (Merlin) Southwire® ACSR conductors are used for parallel line addition according to the line rating of the test system. The 300 kcmil 26/7 (Ostrich) and 336 kcmil 26/7 3M™ ACCR (Linnet) conductors are used for HTLS reconductoring and HTLS parallel line addition. It is assumed that the line resistance and reactance after parallel line addition decreased by 50% and 26%, respectively [72]. In addition, the ampacity of HTLS conductor assumed to be increased by a factor of two while other electrical properties unaltered. Note that the comparison of different type of

HTLS conductors is out of scope of this report. Electrical characteristic of each conductor is presented in Table 5.7 and 5.8 [73]-[74].

Table 5.7 Conductor electrical properties (ACSR)

	Southwire® ACSR (Sparrow)	Southwire® ACSR (Merlin)	Unit
Resistance (25°C)	0.25	0.05	Ohms/mile
Resistance (75°C)	0.05	0.06	Ohms/mile
Ampacity (Steady state)	184	519	Amps
Ampacity (Emergency)	211	596	Amps

Table 5.8 Conductor electrical properties (ACCR)

	3M™ ACCR (Ostrich)	3M™ ACCR (Linnet)	Unit
Resistance (25°C)	0.3004	0.2568	Ohms/mile
Resistance (75°C)	0.3597	0.3144	Ohms/mile
Resistance (240°C)	0.5555	0.4855	Ohms/mile
Ampacity (Steady state)	864	944	Amps
Ampacity (Emergency)	926	1012	Amps

The capital cost of HTLS reconductoring, parallel line addition, and HTLS parallel line addition are assumed to be 126%, 160%, and 576% more expensive than typical ACSR conductors, respectively [75]. Also, the cost of conductor itself is assumed to be 30% of total capital cost for 138 kV lines, and 35% for 230 kV lines, respectively. Table 5.9 presents the capital costs for each investment option based on the line length.

Table 5.9 Capital costs of investment

Line Length	138 kV	230 kV	138 kV	230 kV
	Typical ACSR line [$/Mile]		HTLS Reconductoring [$/Mile]	
> 10	630,200	927,000	794,052	1,168,020
3 ~ 10	756,240	945,300	952,862	1,401,624
< 3	1,112,400	1,390,500	1,191,078	1,752,030
Line Length	Parallel Line Addition [$/Mile]		HTLS Parallel Line Addition [$/Mile]	
> 10	1,009,600	1,484,00	3,634,560	5,342,400
3 ~ 10	1,211,520	1,780,800	4,361,472	6,410,880
< 3	1,514,400	2,226,000	5,451,840	8,013,600

The weather conditions that affect the conductor temperature are assumed to be fixed during the whole planning horizon. Note that the conductor thermal dynamics analysis under various weather conditions is not conducted in this study. Specific parameters have adapted the one presented in [37], as listed in Table 5.10.

Table 5.10 Weather conditions

Ambient Temperature	40 °C
Wind Speed	2 ft/s
Wind Direction	90°
Atmosphere	Clear
Elevation	328 ft
Latitude	30° North
Sun Time	11:00 am
Emissivity	0.5
Solar absorptivity	0.5

Four cases have been considered, namely, case A, case B, case C, and case D in addition to a base case. In the base case, transmission expansion is not allowed. That is, only total production costs for the entire planning horizon are examined in the base case. In case A, all alternatives, HTLS reconductoring, parallel line addition, and HTLS parallel line addition are considered together in a model. In case B, only HTLS reconductoring can be applied as an investment option. In case C, only parallel line addition is considered as an investment option. In case D, HTLS parallel line addition is considered as an investment option. Thus, one can analyze the economic benefits of each alternative as well as the combination of alternatives to increase transmission system ampacity without requiring new ROWs. It is important to note that these case studies assume that there is the option to add a new parallel line within the existing ROW. This is not always the case and, when this is not the case, the economic argument for HTLS increases since it is a viable option in regards to reconductoring an existing transmission path.

As mentioned above, the modified test system can meet all of the required demand but it may not be efficient. Thus, as a first step, TEP studies are conducted only for one year horizon in order to investigate whether and how the system expansion can enhance economic efficiency. Then, a load growth scenario for a 15-year planning, 3-years per each stage, horizon was created as a hypothetical in order to create a long-term planning problem. It is assumed that the load grows at a rate of 0.9% each year [76], the discount rate is 3% [77], and fuel costs as well as other fixed costs are assumed to be fixed for the simplicity. The salvage value is assumed to be the value of invested resource at the end of the planning horizon. The spinning reserve requirement is set to be 7% of the total load of each day type [78].

In all cases, the expansion strategies are obtained with and without the degradation model for comparison. The purpose of this comparison is to point out the impact of modeling the degradation effects in the optimal long-term expansion plan. Also, the lossy DCOPF

and lossless DCOPF models are compared in all cases in order to investigate the impact of capturing the change in system losses. A summary of the studies in this chapter is presented in Table 5.11. The model is implemented in the C++ callable library of CPLEX 12.6 and parallelized using the Message Passing Interface (MPI). All of the simulations are conducted on Intel® Xeon® 3.60 GHz CPU with 48GB memory. Lastly, a 0.1% mipgap is applied as a terminate criteria.

Table 5.11 Summary of case study

	Case	HTLS Reconductoring	Parallel Line Addition	HTLS Parallel Line Addition	Losses	TCR	Planning Horizon
1	Base	N/A	N/A	N/A	N/A	N/A	1 year
2	A	Yes	Yes	Yes	N/A	N/A	1 year
3	B	Yes	N/A	N/A	N/A	N/A	1 year
4	C	N/A	Yes	N/A	N/A	N/A	1 year
5	D	Yes	N/A	Yes	N/A	N/A	1 year
6	Base	N/A	N/A	N/A	Yes	N/A	1 year
7	A	Yes	Yes	Yes	Yes	N/A	1 year
8	B	Yes	N/A	N/A	Yes	N/A	1 year
9	C	N/A	Yes	N/A	Yes	N/A	1 year
10	D	Yes	N/A	Yes	Yes	N/A	1 year
11	Base	N/A	N/A	N/A	Yes	Yes	1 year
12	A	Yes	Yes	Yes	Yes	Yes	1 year
13	B	Yes	N/A	N/A	Yes	Yes	1 year
14	C	N/A	Yes	N/A	Yes	Yes	1 year
15	D	Yes	N/A	Yes	Yes	Yes	1 year
16	Base	N/A	N/A	N/A	N/A	N/A	15 year
17	A	Yes	Yes	Yes	N/A	N/A	15 year
18	B	Yes	N/A	N/A	N/A	N/A	15 year
19	C	N/A	Yes	N/A	N/A	N/A	15 year
20	D	Yes	N/A	Yes	N/A	N/A	15 year
21	Base	N/A	N/A	N/A	Yes	N/A	15 year
22	A	Yes	Yes	Yes	Yes	N/A	15 year
23	B	Yes	N/A	N/A	Yes	N/A	15 year
24	C	N/A	Yes	N/A	Yes	N/A	15 year
25	D	Yes	N/A	Yes	Yes	N/A	15 year
26	Base	N/A	N/A	N/A	Yes	Yes	15 year
27	A	Yes	Yes	Yes	Yes	Yes	15 year
28	B	Yes	N/A	N/A	Yes	Yes	15 year
29	C	N/A	Yes	N/A	Yes	Yes	15 year
30	D	Yes	N/A	Yes	Yes	Yes	15 year

5.2 Choice of the Candidate Lines

The proposed model is a mixed integer linear program. Two independent factors may influence difficulties in solving the problem. First, the consideration of multiple time periods creates a problem that is very large and difficult to solve since the variables are linked across the periods. Second, the large number of integer variables generate a combinatorial number of different problems, which increases the computational difficulty and slows down the convergence of the Lagrange decomposition algorithm. The first factor can be resolved by introducing a proper decomposition technique. For the second factor, one possible approach, to improve the computational efficiency, is to reduce the number of integer variables. There are two types of integer variables, unit commitment status variables and line investment decision variables. Thus, instead of investigating the option of new lines across all existing corridors, it is preferable (in order to reduce the computational burden) to determine potential candidate lines before solving the problem.

Different type of criteria could be conducted to choose candidate lines. S. Z. Moghaddam et al. [79] introduced several parameters related to Locational Marginal Price (LMP) to determine candidate lines and selected the best candidate lines based on Analytical Hierarchy Process (AHP). Since the proposed model in this paper preserve the ROWs, a simplified method can be applied. First, the congested lines, which impede more efficient generation dispatch, could be candidate lines. Uprating those congested lines could release congestion and improve power delivery efficiency. However, it is important to carefully investigate whether such congestion is due to thermal limits. If the line flow is limited due to other stability constraints, increasing line thermal limits cannot resolve the problem. In the DCOPF, bus angle difference limits are proxies for stability limitations. Thus, for simplicity, only specific lines with thermal limits below the product of line susceptance and the maximum bus angle difference can be considered as a candidate line. Second, lines that have large LMP difference between two connecting buses could be treated as candidate lines. A location with high LMP indicates that cheap energy cannot access this location. In addition, the low LMP value shows that excessive cheap energy is available, which is not utilized [80]. Thus, one can conclude that the large LMP difference could lead to low delivery efficiency. Note, however, that looking at the LMP difference is only a heuristic way to identify candidates since LMPs are based on dual variables, which do not directly reflect how the overall cost would change if that large LMP difference between the nodes could be alleviated. Since transmission lines are lumpy assets, indicators that are based on the *marginal* value to deliver a MW of energy to a particular location (i.e., LMPs) are not always preferred.

The MATPOWER is used to obtain LMPs and the congested lines by solving ACOPF. All the candidate lines are shown in Table 5.12. There is a lack of reference to determine a specific value of a LMP gap. Thus, in this report, the LMP difference of all branches is compared first and the lines that have relatively large LMP gaps are chosen as candidates. Then, verification of thermal congestion is conducted.

Table 5.12 Predetermined candidate lines

Branch Number	From Bus	To Bus
21	12	23
23	14	16
25	15	21
28	16	17

5.3 Simulation Results for Single Period Planning Horizon

5.3.1 Network Investment Results (Lossless, No Degradation, 1 Year)

The proposed TEP model is first solved without considering line losses and degradation effect in a one year horizon. Table 5.13 presents the investment decisions along with the resulting planning costs. In cases A and B, the lines 25 and 28 are replaced by an HTLS conductor. On the other hand, only line 28 is invested in case C and case D. In this case study, the HTLS reconductoring option gives better cost savings than other options since it can provide higher thermal capacity with the lowest investment cost. Note that the total production cost of each case is slightly different but the gap is within the mipgap. Therefore, one can infer that the optimal solution depends on the investment cost when losses are ignored. In addition, the results of case A and case B are identical. That is, there are no additional benefits by taking any combination of alternatives.

Figure 5.2 presents the average line power flow for each line and figure 5.3 shows the maximum line power flows. Note that the maximum power flow of lines 21, 25, and 28 reached its maximum limits in the base case. That is, a more economical system operation may be restricted due to the thermal limits of those lines. However, line 21 is not invested in all cases. It is important to note that the average power flow of line 21 is below its maximum limits. That is, line congestion is not occurring frequently. Thus, accumulated cost savings for this line does not exceeds the investment cost.

Table 5.13 Investment results when losses and degradations are ignored (1 year)

	Base	Case A	Case B	Case C	Case D
Options	-	All	HTLS Reconductoring	Parallel Line Addition	HTLS Parallel Line Addition
HTLS Reconductored	-	25 28	25 28	-	-
Parallel Line Added	-	-	-	28	-
HTLS Parallel Line Added	-	-	-	-	28
Total Planning Cost [$M]	409.85	398.20	398.20	398.36	405.91
Production Cost [$M]	409.85	391.59	391.59	395.46	395.44
Reconductoring Cost [$M]	-	60.74	60.74	-	-
Parallel Line Cost [$M]	-	-	-	26.71	-
HTLS Parallel Line Cost [$M]	-	-	-	-	96.16
Salvage Cost [$M]	-	54.13	54.13	23.80	85.70
Investment Cost [$M]	-	6.61	6.61	2.91	10.46
Cost Saving [%]	-	2.84	2.84	2.80	0.96

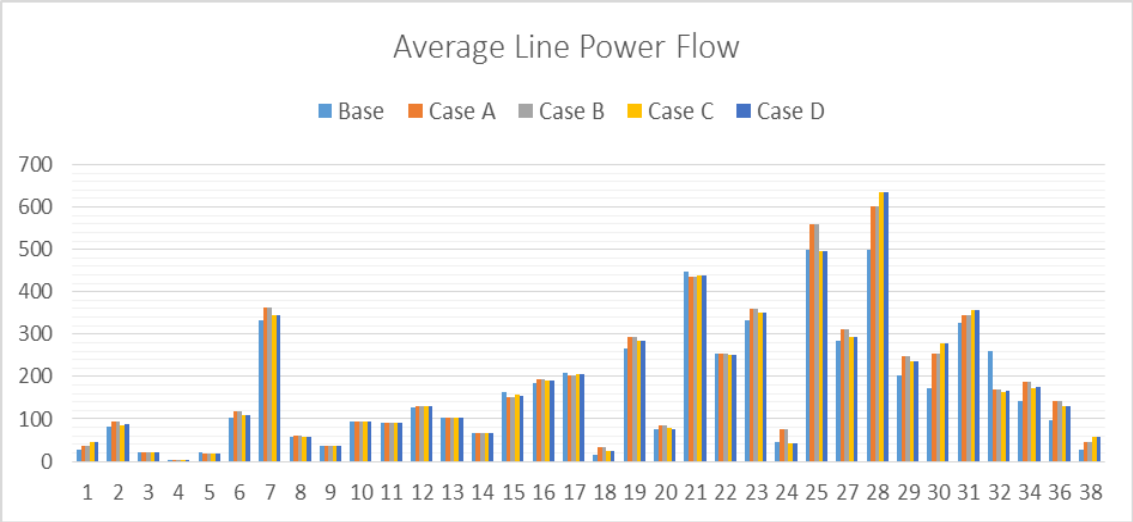

Figure 5.2 Average line power flow
(1 year, losses and degradations are ignored, MW)

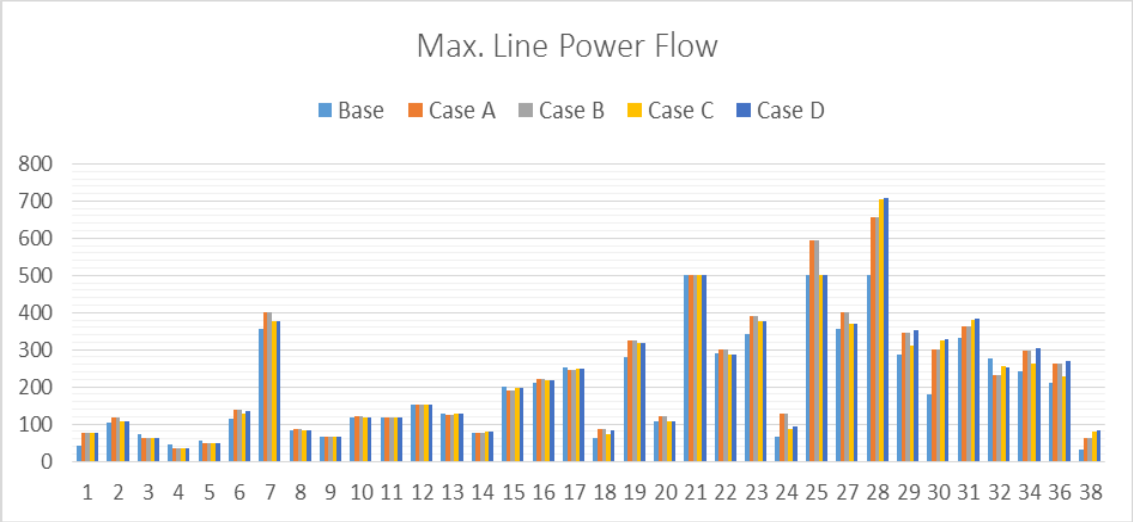

Figure 5.3 Maximum line power flow
(1 year, losses and degradations are ignored, MW)

5.3.2 Network Investment Results (Lossy, No Degradation, 1 Year)

The proposed TEP model is solved considering line losses, while ignoring the degradation effect in a one year time horizon in this section. Table 5.14 presents the investment decisions along with the resulting planning costs. Total production cost of the base case is increased since the total generation should be increased in order to supply additional power due to the line losses.

Table 5.14 Investment results
when losses are considered and degradations are ignored (1 year)

	Base	Case A	Case B	Case C	Case D
Options	-	All	HTLS Reconductoring	Parallel Line Addition	HTLS Parallel Line Addition
HTLS Reconductored	-	-	25 28	-	-
Parallel Line Added	-	23 28	-	23 28	-
HTLS Parallel Line Added	-	-	-	-	28
Total Planning Cost [$M]	471.27	454.75	458.90	454.75	463.09
Production Cost [$M]	472.27	447.49	452.29	447.49	452.63
Reconductoring Cost [$M]	-	-	60.74	-	-
Parallel Line Cost [$M]	-	66.78	-	66.78	-
HTLS Parallel Line Cost [$M]	-	-	-	-	96.16
Salvage Cost [$M]	-	54.13	59.52	54.13	85.70
Investment Cost [$M]	-	7.26	6.61	7.26	10.46
Cost Saving [%]	-	3.51	2.63	3.51	1.74

When losses are considered, parallel line addition is favored since additional line losses are less than the HTLS reconductoring option and the investment cost is less than HTLS parallel line addition option. HTLS reconductoring does not alter electrical properties of the transmission system; the addition of a parallel line alters both resistance and reactance of the transmission path. As mentioned above, it is assumed that parallel line addition reduces line resistance and reactance by half and 26%, respectively. Therefore, the conductance of the parallelized lines is decreased, which gives less additional line losses. Table 5.15 shows the summary of total line losses for each scenario. Note that the losses are average values of whole day type. Parallel line addition reduces the line losses in cases A, C, and D while HTLS reconductoring add more line losses in case B.

Parallel lines are added to the lines 23 and 28 in both cases A and C. One can observe that considering parallel line addition as a possible option gives lower total planning cost than the HTLS reconductoring option and the HTLS parallel line addition option. Although the capital cost of HTLS reconductoring is less than the addition of parallel

lines, the additional production costs of the reconductored line due to the line losses exceeds the cost savings from the capital cost. Again, the result of cases A and C are identical. That is, there is no additional benefit by taking any combination of alternatives. Figure 5.4 presents the average line power flow for each line and figure 5.5 shows the maximum line power flows. Note that the line 23, which is not invested when losses are ignored, is invested in cases A and C. That is, additional overloading due to the line losses gives more production cost savings that exceed the investment cost of line 23.

Table 5.15 Summary of the line losses (Daily Avg.)

	Base	Case A	Case B	Case C	Case D
Losses (MW)	2622.85	2678.09	3109.55	2678.09	2754.02
Losses (%)	4.23	4.32	5.02	4.32	4.45

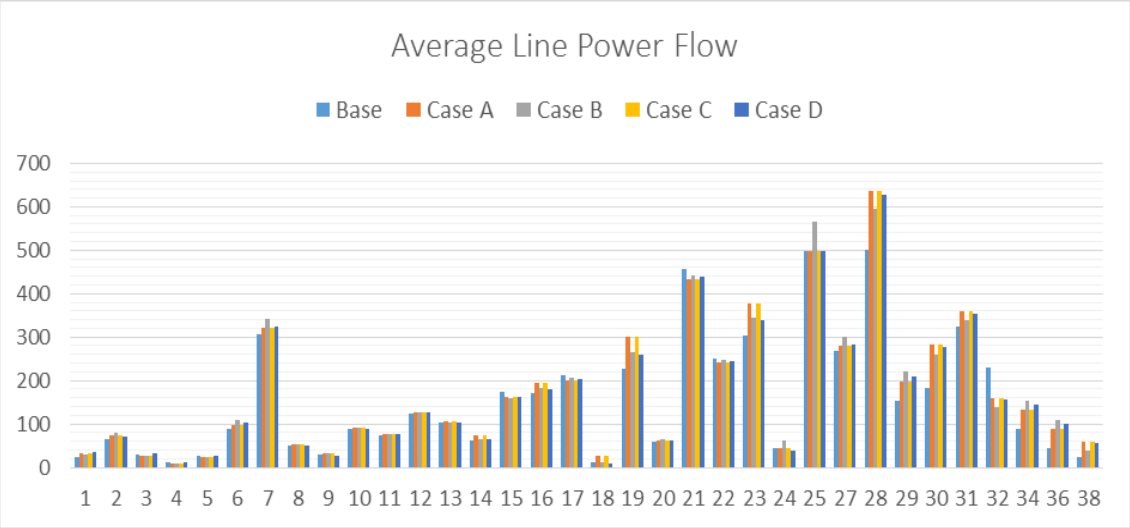

Figure 5.4 Average line power flow
(1 year, losses are considered and degradations are ignored, MW)

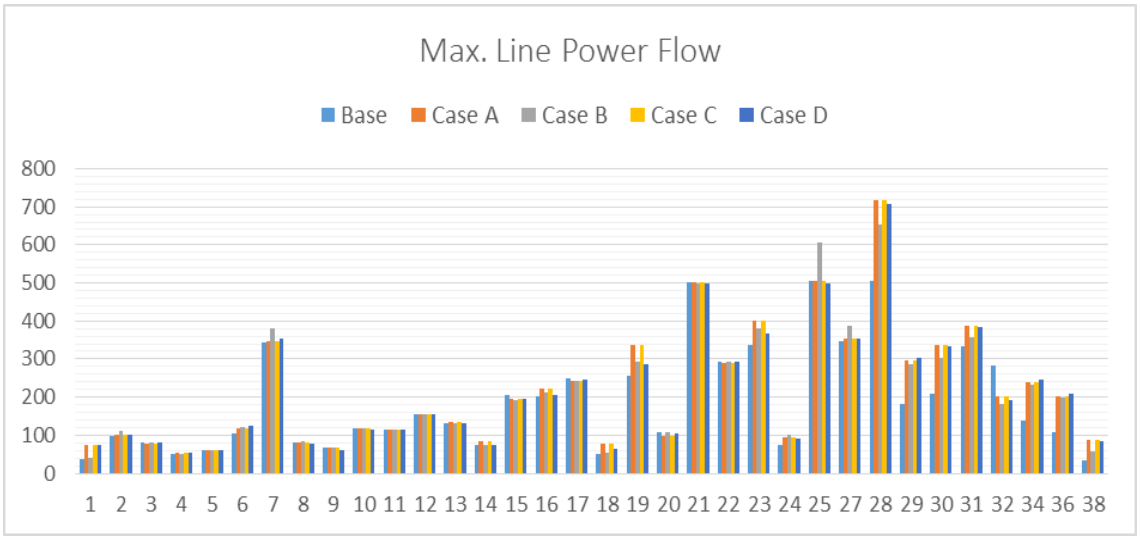

Figure 5.5 Maximum line power flow
(1 year, losses are considered and degradations are ignored, MW)

5.3.3 Network Investment Results (Lossy, Degradation, 1 Year)

The case study results considering both line losses and degradation effect in a one year planning horizon are presented in this section. Table 5.16 shows the investment decisions and associated costs. The network planning solutions are identical with the ones when losses and degradation effects are ignored in Section 5.4. That is, cost savings from investments exceed the cost savings from TCR. Figure 5.6 presents the average line power flow for each line and figure 5.7 shows the maximum line power flows.

Table 5.16 Investment results
when degradations and losses are considered (1 year)

	Base	Case A	Case B	Case C	Case D
Options	-	All	HTLS Reconductoring	Parallel Line Addition	HTLS Parallel Line Addition
HTLS Reconductored	-	-	25 28	-	-
Parallel Line Added	-	23 28	-	23 28	-
HTLS Parallel Line Added	-	-	-	-	28
Total Planning Cost [$M]	471.27	454.75	458.90	454.75	463.09
Production Cost [$M]	472.27	447.49	452.29	447.49	452.63
Reconductoring Cost [$M]	-	-	60.74	-	-
Parallel Line Cost [$M]	-	66.78	-	66.78	-
HTLS Parallel Line Cost [$M]	-	-	-	-	96.16
Salvage Cost [$M]	-	54.13	59.52	54.13	85.70
Investment Cost [$M]	-	7.26	6.61	7.26	10.46
Degradation Cost [$M]	0.01	-	-	-	-
Cost Saving [%]	-	3.51	2.63	3.51	1.74

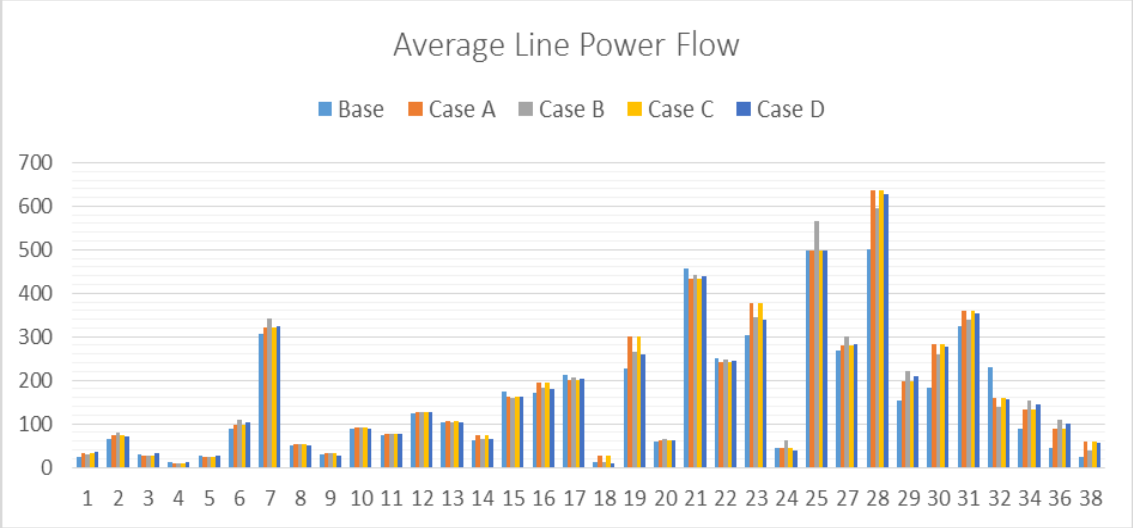

Figure 5.6 Average line power flow
(1 year, degradations and losses are considered, MW)

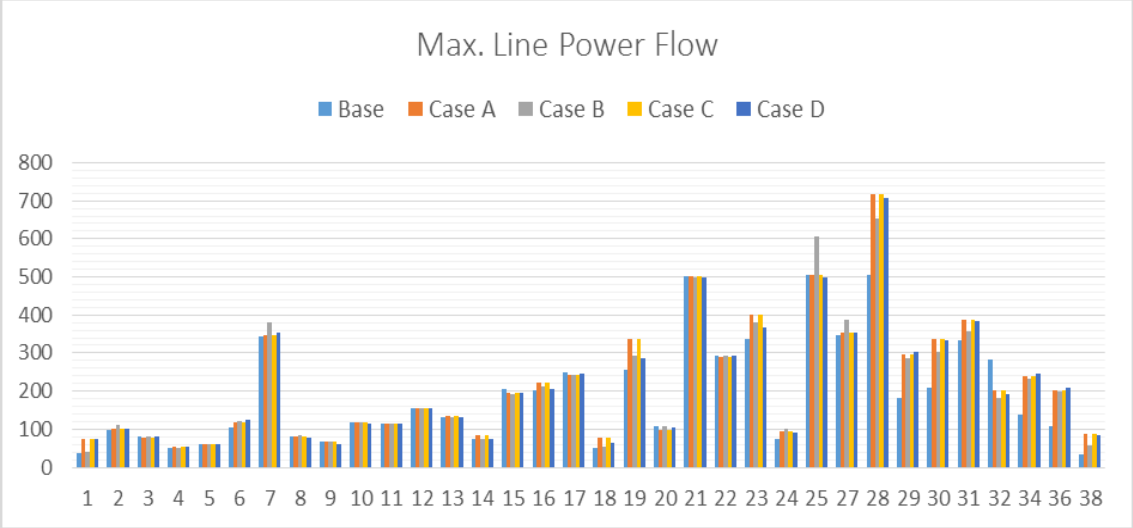

Figure 5.7 Maximum line power flow
(1 year, degradations and losses are considered, MW)

5.4 Simulation Results for Multi Period Planning Horizon

The load increasing case studies are conducted to see a long-term effect of network reinforcement. As mentioned in section 5.1, a total 15-year planning horizon is aggregated into multiple stages, each incorporating 3-years, and the load growth rate and the interest rate are assumed to be 0.9% and 3%, respectively. Note that the modified test system is still reliable even for the increased load in the future. The difference between a single period and a multi period planning problem is determining the timing of the investment. In the single period planning problem, investment decisions do not consider the time of investment. That is, the problem decides only whether or not to invest. On the

other hand, the multi period planning problem provides investment strategy, which includes the investment time. Thus, in this section, the purpose of the planning problem is to find a transmission expansion strategy considering the timing of the investment, as well as an investment decision of three types of investment options and the location. Table 5.17 shows the investment decision along with the resulting planning costs when losses and degradation effect are ignored. The investment strategy is identical with the result of a single period cases except case C. Note that the line 21 is still not invested in all cases.

Table 5.17 Investment results
when losses and degradations are ignored (15 year)

	Base	Case A	Case B	Case C	Case D
Options	-	All	HTLS Reconductoring	Parallel Line Addition	HTLS Parallel Line Addition
HTLS Reconductored	-	25(1) 28(1)	25(1) 28(1)	-	-
Parallel Line Added	-	-	-	25(3) 28(1)	-
HTLS Parallel Line Added	-	-	-	-	28(1)
Total Planning Cost [$M]	2,122.75	2,027.53	2,027.53	2,209.83	2,072.21
Production Cost [$M]	2,122.75	2,000.71	2,000.71	2,008.87	2,029.74
Reconductoring Cost [$M]	-	60.74	60.74	-	-
Parallel Line Cost [$M]	-	-	-	68.87	-
HTLS Parallel Line Cost [$M]	-	-	-	-	96.16
Salvage Cost [$M]	-	33.91	33.91	47.92	53.69
Investment Cost [$M]	-	26.82	26.82	20.95	42.47
Cost Saving [%]	-	4.49	4.49	4.38	2.38

Table 5.18 presents the investment decision along with the resulting planning costs when losses are considered and degradation effects are ignored. In this case, more lines are invested in case A and C than single period cases. The parallel line addition is still most

favored when losses are considered; thus, the result of the case A and case C are identical.

Table 5.18 Investment results
when losses are considered and degradations are ignored (15 year)

	Base	Case A	Case B	Case C	Case D
Options	-	All	HTLS Reconductoring	Parallel Line Addition	HTLS Parallel Line Addition
HTLS Reconductored	-	-	25(1) 28(1)	-	-
Parallel Line Added	-	23(1) 25(1) 28(1)	-	23(1) 25(1) 28(1)	-
HTLS Parallel Line Added	-	-	-	-	28(1)
Total Planning Cost [$M]	2,464.77	2,337.53	2,373.83	2,337.53	2,401.45
Production Cost [$M]	2,464.77	2,285.75	2,347.01	2,285.75	2,358.98
Reconductoring Cost [$M]	-	-	60.74	-	-
Parallel Line Cost [$M]	-	117.24	-	117.24	-
HTLS Parallel Line Cost [$M]	-	-	-	-	96.16
Salvage Cost [$M]	-	65.46	33.91	65.46	53.69
Investment Cost [$M]	-	51.78	26.82	51.78	42.47
Cost Saving [%]	-	5.16	3.69	5.16	2.57

Table 5.19 presents the investment decision along with the resulting planning costs when losses and degradation effects are considered. The addition of a parallel line is still most favored when losses are considered; thus, the result of case A and case C are identical. Note that the cost savings from the network reinforcement is less than other case studies. The reason is that the TCR allows more flexible system operation; thus, the total planning cost of the base case is reduced. Therefore, even the total planning cost of each case is below the costs when the degradation effects are ignored, the percentage of the cost savings are relatively small.

Table 5.19 Investment results
when losses and degradations are considered (15 year)

	Base	Case A	Case B	Case C	Case D
Options	-	All	HTLS Reconductoring	Parallel Line Addition	HTLS Parallel Line Addition
HTLS Reconductored	-	-	25(1) 28(1)	-	-
Parallel Line Added	-	23(2) 28(1)	-	23(2) 28(1)	-
HTLS Parallel Line Added	-	-	-	-	28(1)
Total Planning Cost [$M]	2,378.17	2,333.09	2,366.01	2,333.09	2,368.91
Production Cost [$M]	2,374.20	2,308.31	2,327.02	2,263.88	2,317.18
Reconductoring Cost [$M]	-	-	60.74	-	-
Parallel Line Cost [$M]	-	63.34	-	63.34	-
HTLS Parallel Line Cost [$M]	-	-	-	-	96.16
Salvage Cost [$M]	-	39.21	33.91	39.21	53.69
Investment Cost [$M]	-	24.13	26.82	24.13	42.47
Degradation Cost [$M]	3.97	0.65	0.30	0.65	1.03
Cost Saving [%]	-	1.90	0.51	1.90	0.39

In this case, the investment strategy is different with the result of the single period planning problem. That is, the investment of line 25 does not occur in all cases. Instead, more line overflow occurs and the degradation cost increases. Fig 5.8 and Fig. 5.9 shows the line overflow history along with the line temperature of the line 25 at the stage 1 in day type 2 and stage 5 in day type 2, respectively. The line overflow is activated according to the network topology and demand at each time. Since more line is constructed at stage 5, the frequency of the line overflow at stage 5 is reduced in comparison to stage 1. Note that the line thermal limit is 500MW and 75°C. Table 5.20 presents the accumulated degradation effect for each line.

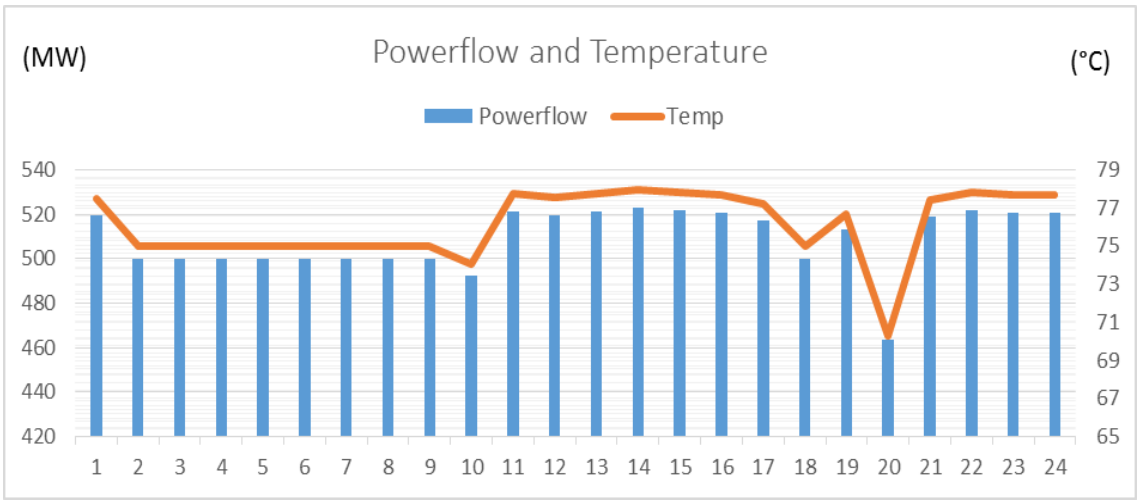

Figure 5.8 Power flow and temperature of the line 25
(Stage 1, Day type 2, Case A, degradations and losses are considered)

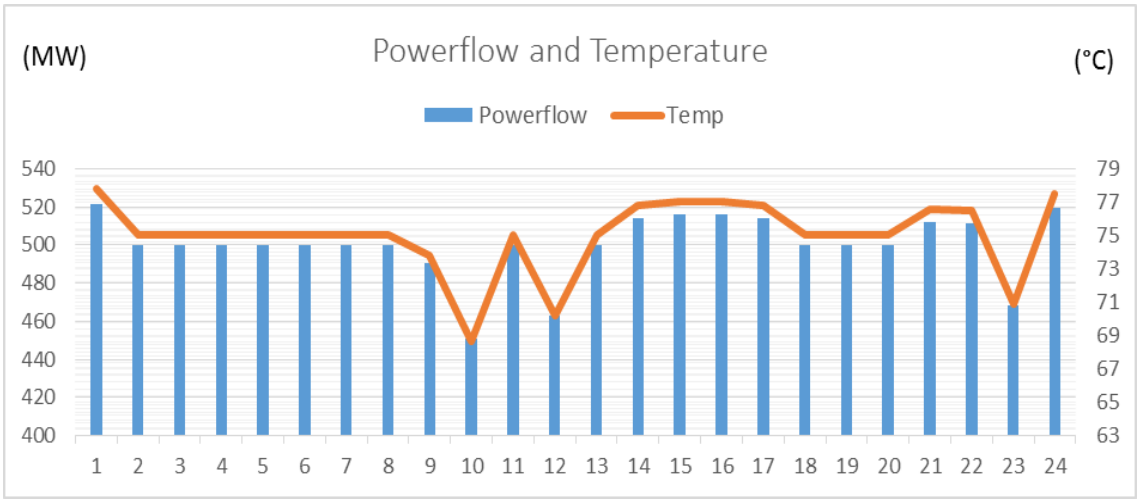

Figure 5.9 Power flow and temperature of the line 25
(Stage 5, Day type 2, Case A, degradations and losses are considered)

Table 5.20 Accumulated loss of strength for each line (15 years, Case A)

Line No.	Average Overflow (MW)	Average Temp. (°C)	Loss of Strength (%)	Line No.	Average Overflow (MW)	Average Temp. (°C)	Loss of Strength (%)
1	0	52.12	0	18	0	47.91	0
2	0	52.40	0	19	0	57.69	0
3	0	48.76	0	20	0	48.37	0
4	0	48.16	0	21	0.3	71.41	0.015
5	0	48.60	0	22	0	53.93	0
6	0	55.74	0	23	0	51.58	0
7	0	47.85	0	24	0	47.97	0
8	0	50.53	0	25	5.66	77.03	0.21
9	0	48.96	0	27	0	59.45	0
10	0	47.85	0	28	0	58.55	0
11	0	52.43	0	29	0	52.35	0
12	0	63.15	0	30	0	55.42	0
13	0	58.37	0	31	0	62.45	0
14	0	47.85	0	32	0	48.90	0
15	0	47.85	0	34	0	49.31	0
16	0	47.85	0	36	0	48.61	0
17	0	47.85	0	38	0	47.85	0

6. Conclusion and Future Work

6.1 Conclusion

The economic case of HTLS conductor is investigated in this report. First, the long-term TEP model considers an HTLS reconductoring option, a parallel line addition (with a traditional conductor), an HTLS parallel line addition option, and thermal constraint relaxation options to increase the transmission system ampacity without needing new ROWs. The proposed TEP model is formulated using mixed integer programming and the network model is approximated by the DCOPF coordinated with the SCUC problem along with a piecewise linear loss approximation. The work also proposed a degradation model to capture the cost associated with the operation of overhead conductors at elevated temperatures. The degradation model is applied in the proposed TEP model. A parallelization algorithm, along with the use of Lagrangian relaxation, is developed to improving the computational time of this complex combinatorial problem.

The purpose of the proposed TEP model is to provide clear information to planners when and where existing overhead conductors should be invested to enhance the system efficiency and reliability. It is shown on the test cases that HTLS reconductoring is usually preferred when real power losses are ignored. It has also been shown that HTLS is a valuable economic option when existing right of ways cannot accommodate a parallel line and, thus, reconductoring with HTLS is the preferred option. Also, allowing thermal constraint relaxations reduces total planning costs by utilizing the flexibility in the system more appropriately. On the other hand, the parallel line addition (with traditional conductors) was generally favored when taking into consideration losses. However, there is no guarantee that the addition of a parallel line always dominates other options. HTLS reconductoring may be favored when additional line losses are small and the length of the path is short. As expected, system condition such as overloading magnitude and frequency and the relative cost of each investment option is shown to be key factors that may affect long-term solutions for transmission expansion planning.

6.2 Future Work

While this report discussed the potential benefits and the optimal investment strategy of the HTLS conductors, additional work is required to fully develop the economic case of the HTLS conductors. First, additional research regarding the degradation modeling is preferred, by incorporating further studies on the breakdown of the conductor over its lifecycle due to operating the conductor at elevated temperatures. For instance, the actually degradation effects for HTLS conductors are expected to accumulate more slowly than what occurs for typical ACSR conductors in a same overloading operation. Such additional extensive information on the degradation impacts for HTLS in comparison to alternative conductor types would further facilitate the analysis being conducted when determining the best conductor for a transmission investment option. Further work is also necessary to find other cases when HTLS reconductoring is favored.

In particular, future work should look into the benefit of HTLS conductors when large renewable farms are being integrated into the grid.

References

[1] B. Dewani, M. B. Daigavane, and A. S. Zadgaonkar, “A review of various computational intelligence techniques for transmission network expansion planning,” IEEE International Conference on Power Electronics Drives and Energy Systems, pp. 1-5, 16-19, Dec. 2012.

[2] R. Hemmati, R.-A. Hooshmand, and A. Khodabakhshian, “Comprehensive review of generation and transmission expansion planning,” IET Generation, Transmission and Distribution, vol. 7, no. 9, pp. 955-964, Sept. 2013.

[3] D. Chattopadhyay and J. Momoh, “A multiobjective operations planning model with unit commitment and transmission constraints,” IEEE Transactions on Power Systems, vol. 14, no. 3, pp. 1078-1084, Aug. 1999.

[4] Western Electricity Coordinating Council, “Transmission expansion planning,” [Online]. Available: http://www.wecc.biz/committees/BOD/TEPPC/

[5] C. W. Lee, S. K. Ng, J. Zhong, and F. F. Wu, “Transmission expansion planning from past to future,” in Proc. 2006 Power Systems Conf. Expo. (PSCE), pp. 257-265

[6] PJM Overhead Conductor Ad Hoc Committee, “Bare overhead transmission conductor rating,” [Online]. Available: http://www.pjm.com/~/media/planning/design-engineering/maac-standards/bare-overhead-transmission-conductor-ratings.ashx

[7] G. Latorre, R. D. Cruz, J. M. Areiza, and A. Villegas, "Classification of publications and models on transmission expansion planning," IEEE Transactions on Power Systems, vol. 18, no. 2, pp. 938-946, May 2003.

[8] G. Latorre, R. D. Cruz, J. M. Areiza, and A. Villegas, "Classification of publications and models on transmission expansion planning," IEEE Transactions on Power Systems, vol. 18, no. 2, pp. 938-946, May 2003.

[9] A. H. El-Abiad and Y. P. Dusonchet, “Discrete optimization and the planning of electric power networks,” IEEE Transactions on Circuit Theory, vol. CT-20, no.3, pp. 230-238, May 1973.

[10] M. El-Metwally and A. Harb, “Transmission planning using admittance approach and quadratic programming,” Electric Machines and Power Systems, vol. 21, no.1, pp. 69-83, Jan. 1993.

[11] Z. M. Al-Hamouz and A. S. Al-Faraj, “Transmission expansion planning using nonlinear programming,” in Proc. 2002 IEEE Power Eng. Soc. Transmission and Distribution Conf., vol 1, pp. 50-55, Oct. 2002

[12] N. Alguacil, A. L. Motto, and A. J. Conejo, “Transmission expansion planning: a mixed-integer LP approach,” IEEE Transactions on Power Systems, vol. 18 no. 3, pp. 1070–1077, Aug. 2003

[13] A. Khodaei, M. Shahidehpour, L. Wu, and Z. Li, “Coordination of short-term operation constraints in multi-area expansion planning,” IEEE Transactions on Power Systems, vol. 27, no. 4, pp. 2242-2250, Nov. 2012.

[14] I. G. Sanchez, R. Romero, J. R. S. Mantovani, and A. Garcia, “Interior point algorithm for linear programming used in transmission network synthesis,” Electric Power Systems Research, vol. 76, no. 1, pp. 9-16, Sep. 2005.

[15] E. J. de Oliveira, I. C. da Silva, J. L. R. Pereira, and S. Carneiro, “Transmission system expansion planning using a sigmoid function to handle integer investment variables,” IEEE Transaction on Power Systems, vol. 20, no.3, pp. 1616-1621, Aug. 2005.

[16] S. Binato, M. V. F. Pereira, and S. Granville, “A new Benders decomposition approach to solve power transmission network design problems,” IEEE Transactions on Power Systems, vol. 16, no. 2, pp. 235-240, May 2001.

[17] S. Haffner, A. Monticelli, A. Garcia, J. Mantovani, and R. Romero, “Branch and bound algorithm for transmission system expansion planning using a transportation model,” IEE Proceedings-Generation, Transmission and Distribution, vol. 147, no. 3, pp.149-156, May 2000.

[18] R.C. Leou, “A multi-year transmission planning under a deregulated market,” International Journal of Electrical Power & Energy Systems, vol. 33, no. 3, pp. 708–714, Mar. 2011.

[19] S. Binato, G. C. de Oloveira, and J. de Araujo, “A greedy randomized adaptive search procedure for transmission expansion planning,” IEEE Transactions on Power Systems, vol. 16, no. 2, pp. 247-253, May 2001.

[20] E. L. da Silva, J. M. A. Ortiz, G. C. de Oliveira, and S. Binato, “Transmission network expansion planning under a tabu search approach,” IEEE Transactions on Power Systems, vol. 16, pp. 62-68, Feb. 2001.

[21] H. Kim, S. Moon, J. Choi, C. Lee, J. Wang, and R. Billinton, “Transmission system expansion planning of KEPCO system (Youngnam area) using fuzzy set theory,” IEEE Power Engineering Society Summer Meeting 2002, vol. 1, pp. 535-540, Jul. 2002.

[22] F. F. Wu, F. L. Zheng, and F.S. Wen, “Transmission investment and expansion planning in a restructured electricity market,” Energy, vol. 31, no. 7, pp. 954-966, Jun. 2006.

[23] California Independent System Operator, “Transmission economic assessment methodology (TEAM),” Jun. 2004. [Online]. Available: http://www.caiso.com/docs/2004/06/03/2004060313241622985.pdf

[24] J. Chan, B. Clairmont, D. Rueger, D. Childs, and S. Karki, "Demonstration of advanced conductors for overhead transmission lines," Electric Power Research Institute, Palo Alto, CA, Tech. Rep. CEC-500-2013-030, July. 2008.

[25] F. F. Wu, F. L. Zheng, and F. S. Wen, “Transmission investment and expansion planning in a restructured electricity market,” Energy, vol. 31, no. 7, pp. 954-966, Jun. 2006.

[26] J.S. Engelhardt, and S.P. Basu, “Design, installation, and field experience with an overhead transmission dynamic line rating system,” in Proc. 1996 IEEE Transmission and Distribution Conf., pp. 366-370.

[27] B. Clairmont, D. A. Douglass, E. C. Bascom, III, and T. C. Raymond, “Increased power flow guidebook: increasing power flow on transmission and substation circuits,” Electric Power Research Institute, Palo Alto, CA, Tech. Rep. 1010627, Nov. 2005.

[28] A. G. Exposito, J. R. Santos, and P. C. Romero, “Planning and operational issue arising from the widespread use of HTLS conductors,” IEEE Transactions on Power Systems, vol. 22, no. 4, pp. 1446-1455, Nov. 2007.

[29] S. Uski-Joutsenvuo and R. Pasonen, “Maximising power line transmission capability by employing dynamic line ratings–technical survey and applicability in Finland,” VTT Technical Research Centre, Finland, Tech. Rep. VTT-R-01604-13, Feb. 2013.

[30] G. Brennan, "Refurbishment of existing overhead transmission lines," CIGRE, Tech. Rep. B2-203, 2004.

[31] S. L. Chen, W. Z. Black, and H. W. Loard Jr., “High-temperature ampacity model for overhead Conductors,” IEEE Transactions on Power Delivery, vol. 17, no. 4, pp. 1136-1141, Oct. 2002.

[32] CAISO, “Price inconsistency market enhancements – revised straw proposal,” [Online]. Available: http://www.caiso.com/Documents/RevisedStrawProposal-PriceInconsistencyMarketEnhancements.pdf

[33] Y. M. Al-Abdullah, M. Abdi-Khorsand, and K. W. Hedman, "The role of out-of-market corrections in day-ahead scheduling," IEEE Transactions on Power Systems, submitted for publication.

[34] Y. Yang, R. G. Harley, D. Divan, and T. G. Havetler, "Overhead conductor thermal dynamics identification by using echo state networks," International Joint Conference on Neural Networks, 2009.

[35] IEEE Standard for Calculating the Current-Temperature of Bare Overhead Conductors, IEEE Standard 738-2006, Jan. 2006.

[36] "Thermal Behavior of Conductors," CIGRE, ELECTRA No. 144, October 1992.

[37] N. P. Schmidt, "Comparison between IEEE and CIGRE ampacity standards," IEEE Transactions on Power Delivery, vol. 14, no. 4, pp. 1155-1159, Oct. 1999.

[38] W. Z. Black and R. L. Rehberg, "Simplified model for steady state and real-time ampacity of overhead conductors," IEEE Transactions on Power Apparatus and Systems, vol. PAS-104, no. 10, pp. 2942-2953, Oct. 1985.

[39] H. A. Smolleck and J. P. Sims, "Guidelines for the selection and operation of bare ACSR conductors with regard to current-carrying capacity," Electric Power Systems Research, vol. 5, no. 3, pp. 179-190, Sep. 1982.

[40] M. M. I. Bhuiyan, P. Musilek, J, Heckenbergerova, and D. Koval, "Evaluating thermal aging characteristics of electric power transmission lines," 23rd IEEE Canadian Conference on Electrical and Computer Engineering (CCECE), 2010.

[41] D. A. Douglass, "Coping with aging distribution and transmission conductors," IEEE Power Engineering Society Summer Meeting, 2002, vol. 2. pp. 704-709, Jul 2002.

[42] M. M. I. Bhuiyan, P. Musilek, and J. Hecken, "Evaluating thermal aging characteristics of electric power transmission lines," 23rd IEEE Canadian Conference on Electrical and Computer Engineering (CCECE), pp. 1-4, 2010.

[43] "ACCC conductor," Wikipedia: The Free Encyclopedia. Wikimedia Foundation, Inc., [Online]. Available: http://en.wikipedia.org/wiki/ACCC_conductor, Sep. 3. 2013.

[44] J. R. Harvey, "Effect of elevated temperature operation on the strength of aluminum conductors," IEEE Transactions on Power Apparatus and Systems, vol. PAS-91, no. 5, pp. 1769–1772, Sept./Oct. 1972.

[45] IEEE Guide for Determining the Effects of High-Temperature Operation on Conductors, Connectors, and Accessories, IEEE Std 1283-2013, Aug. 2013.

[46] V. T. Morgan, "The loss of tensile strength of Hard-Drawn conductors by annealing in service," IEEE Transactions on Power Apparatus and Systems, no. 3, pp. 700-709, May 1979.

[47] D. Douglass, "High-temperature, low-sag transmission conductors," Electric Power Research Institute, Palo Alto, CA, Tech. Rep. 1001811, June. 2002.

[48] A. Gomez-Exposito, J. R. Santos, and P. C. Romero, "Planning and operational issues arising from the widespread use of HTLS conductors," IEEE Transactions on Power Systems, no. 4, pp. 1446-1455, Nov. 2007.

[49] B. J. Pierre and G. T. Heydt, "Increased ratings of overhead transmission circuits using HTLS and compact designs," North American Power Symposium (NAPS), 2012.

[50] R. Gorur, B. Mobasher, and R. Olsen, "Characterization of composite cores for high temperature-low sag (HTLS) conductors: final project report," [Online]. Available: http://www.pserc.wisc.edu/documents/publications/reports/2009_reports/gorur_pserc_report_t-33_july2009.pdf

[51] A. Khodaei, M. Shahidehpour, and S. Kamalinia, "Transmission switching in expansion planning," IEEE Transactions on Power Systems, vol. 25, no. 3, pp. 1722-1733, Aug. 2010.

[52] H.-T. Yang, P.-C. Yang, and C.-L. Huang, "Evolutionary programming based economic dispatch for units with non-smooth fuel cost functions," IEEE Transactions on Power Systems, vol. 11, no. 1, pp. 112-118, 1996.

[53] F. Li and R. Bo, "DCOPF-based LMP simulation: algorithm, comparison with ACOPF, and sensitivity," IEEE Transactions on Power Systems, vol. 22, no. 4, pp. 1475-1485, 2007.

[54] O. W. Akinbode and K. W. Hedman, "Fictitious losses in the DCOPF with a piecewise linear approximation of losses," IEEE Power and Energy Society General Meeting, pp. 1-5, 2013.

[55] R. S. M. A. Ramos and P. Sanchez, "Modeling transmission ohmic losses in a stochastic bulk production cost model," Institute for Research in Technology, Madrid 1997. [Online]. Available: http://www.iit.upcomillas.es/~aramos/papers/losses.pdf

[56] C.-P. Cheng, C.-W. Liu, and C.-C. Liu, "Unit commitment by Lagrangian relaxation and genetic algorithms," IEEE Transactions on Power Systems, vol. 15, no. 2, pp. 707-714, 2000.

[57] T. Mitani, et al., “Security constrains unit commitment by Lagrangian decomposition and tabu search,” Proceedings of the 13th International Conference on Intelligent Systems Application to Power Systems, 2005.

[58] X. Wang, Y. H. Song, and Q. Lu, “Lagrangian decomposition approach to active power congestion management across interconnected regions,” IEE Proceedings on Generation, Transmission, and Distribution, vol. 148, no. 5, 2001.

[59] A. Papavasiliou and S. S. Oren, “Multiarea stochastic unit commitment for high wind penetration in a transmission constrained network,” Operations Research, vol. 61, no. 3, pp. 578-592, 2013.

[60] M. L. Fisher, “The Lagrangian relaxation method for solving integer programming problem,” Management Science, vol. 27, no. 1, pp. 1-18, 1981.

[61] F. Jakl and A. Jakl, “Effect of elevated temperatures on mechanical properties of overhead conductors under steady state and short-circuit conditions,” IEEE Transactions on Power Delivery, vol. 15, no. 1, pp. 242-245, 2000.

[62] ALCAN, “Aluminum Conductor Steel Reinforced (ACSR) Cables,” [Online]. Available: ece.citadel.edu/mckinney/elec403/ACSR.pdf

[63] 3M, “3M™ Aluminum Conductor Composite Reinforced (ACCR),” [Online]. Available: http://solutions.3m.com/wps/portal/3M/en_US/EMD_ACCR/ACCR_Home/TechnicalInfo/ProductDataSpecs/

[64] Business Management Courses, “The Big M Method,” [Online]. Available: http://businessmanagementcourses.org/Lesson09TheBigMMethod.pdf

[65] K. W. Hedman, M. Ferris, R. P. O'Neill, E. Fisher, and S. S. Oren, “Co-optimization of generation unit commitment and transmission switching with N-1 reliability,” vol. 25, no. 2, pp. 1052-1063, May 2010.

[66] K. W. Hedman, R. P. O'Neill, and S. S. Oren, "Analyzing valid inequalities of the generation unit commitment problem," 2009 IEEE/PES Power Systems Conference and Exposition, pp. 1-6, 15-18, Mar. 2009.

[67] R. Fourer, D. M. Gay, and B. W. Kernighan. AMPL. Boyd & Fraser, 1993.

[68] A. Papavasiliou, S. S. Oren, and R. P. O'Neill, “Reserve requirements for wind power integration: a scenario-based stochastic programming framework,” IEEE Transactions on Power Systems, vol. 26, pp. 2197-2206, Nov. 2011.

[69] C. Grigg, et al., “The IEEE reliability test system-1996. A report prepared by the reliability test system task force of the application of probability methods

subcommittee," IEEE Transactions on Power Systems, vol. 14 no. 3 pp. 1010-1020, 1999.

[70] Energy Informative Administration, "Short-term energy outlook," [Online]. Available: http://www.eia.gov/forecasts/steo/tables/pdf/2tab.pdf

[71] Energy Informative Administration, "Uranium marketing annual report," [Online]. Available: http://www.eia.gov/uranium/marketing/?src=Nuclear-f1

[72] M. Anvari, F. Razavi, and A. A. Nazari, "Electiral and economic study of applying the ACSS conductor in TREC subtransmission network," Indian Journal of Science & Technology vol. 6, no. 1, 2013.

[73] Southwire Company, "ACSR," [Online]. Available: http://www.southwire.com/products/ACSR.htm

[74] 3M, "3M Aluminum Conductor Composite Reinforced," [Online]. Available: http://solutions.3m.com/wps/portal/3M/en_US/EMD_ACCR/ACCR_Home/TechnicalInfo/ProductDataSpecs/

[75] M. Tim, C. Trevor, and W. Dan, "Capital costs for transmission and substations - recommendations for WECC transmission expansion planning," Black and Veatch, Phoenix, AZ, Tech. Rep. 176322, Oct. 2012.

[76] Energy Informative Administration, "Annual energy outlook 2014," [Online]. Available: http://www.eia.gov/forecasts/aeo/MT_electric.cfm

[77] Trading Economics, "US interest rate," [Online]. Available: http://www.tradingeconomics.com/united-states/interest-rate

[78] California ISO, "Spinning Reserve and Non-Spinning Reserve," [Online]. Available: ttp://www.caiso.com/Documents/SpinningReserveandNonSpinningReserve.pdf

[79] S. Z. Moghaddam, H. Monsef, and M. Jafari, "A new heuristic method for transmission expansion planning using AHP," 2011 10th International Conference on Environment and Electrical Engineering, pp. 1-4, May 2011.

[80] M. O. Buygi, G. Balzer, H. M. Shanechi, and M. Shahidehpour, "Market-based transmission expansion planning," IEEE Transactions on Power Systems, vol. 19, pp. 2060-2067, Nov. 2004.